Faculty of Science and Engineering
Department of Civil Engineering

Durability properties of high volume fly ash concretes containing nano particles

Steve Wilben Macquarie Supit

This thesis is presented for the Degree of
Doctor of Philosophy
of
Curtin University

December 2014

Declaration

To the best of my knowledge and belief this thesis contains no material previously published by any other person except where due acknowledgment has been made.

This thesis contains no material which has been accepted for the award of any other degree or diploma in any university.

Signature:

Date:

ABSTRACT

As a by-product of industrial process, the utilization of high volume fly ash in concrete addresses the challenges of sustainable construction. However, their mechanical and durability properties are inferior to those containing low volume fly ash. Recently, the use of nano-size particles on blended cements has been extended in order to utilize the innovation on the area of high volume fly ash system. The most common reasons are the beneficial effect due to its fineness and chemical composition for producing more strong and durable concrete.

The main aim of this study is to evaluate the effectiveness of nano silica and nano calcium carbonate particles on the enhancement of early age compressive strength and chloride induced corrosion resistance and related durability properties of HVFA concretes and compare with those of OPC concrete. The compressive strength of concretes is measured at 3, 7, 28, 56 and 90 days. The 2% nano silica (NS) and 1% nano-$CaCO_3$ (NC) are selected as an optimum quantities and used to evaluate their effectiveness on accelerated corrosion and related durability properties including water sorptivity, porosity, volume of permeable voids, rapid chloride permeability and chloride diffusion of high volume fly ash concretes.

According to the results, the concretes containing NS and NC led to an improvement in compressive strength and durability properties of ordinary Portland cement (OPC) and HVFA concretes. Results also clearly indicate that the high surface area of the nanoparticles and its reactivity accelerate the hydration process and improves the microstructure of the OPC and HVFA concretes to better mechanical and durability properties. For example, the results show that among different NS contents ranging from 1% to 6%, the cement mortar containing 2% NS exhibited highest 7 and 28 days compressive strength. Moreover, the addition of 2% NS to the HVFA mortars improved the early age (7 days) compressive strength of mortars containing 40% and 50% fly ash by 5% and 7%, respectively. In HVFA concretes, the significant improvement of early age (3 days) compressive strength is also noticed due to addition of 2% NS. Besides improvement in compressive strength, the addition of 2% NS also significantly reduced the water sorptivity, volume of permeable voids, chloride permeability, chloride diffusion and porosity of HVFA concretes. It is also revealed that the above durability properties of concretes containing 38% class F fly ash and

2% NS as partial replacement of cement are superior than ordinary concrete containing 100% cement.

With regard to the nano-$CaCO_3$, the results show that 1% $CaCO_3$ nanoparticles exhibited the highest compressive strength among all nano-$CaCO_3$ contents and about 22% higher than that of cement mortar. The results also showed that, the HVFA concretes containing 1% $CaCO_3$ nanoparticles have reasonably higher compressive strength (146-148% higher than the ordinary concrete at early ages), lower volume of permeable voids, porosity, higher resistance to water sorptivity, chloride permeability and chloride ion diffusivity than the counterpart HVFA concretes. It is also found that 1% $CaCO_3$ nanoparticles improves the microstructure by forming additional calcium silicate hydrate gels and decreases the calcium hydroxide and calcium silicates of HVFA concretes. It is also revealed that the addition of $CaCO_3$ nanoparticles not only led to much denser microstructure in HVFA matrix but also changed the formation of hydration products, hence contributed to the improvement of early-age compressive strength and durability properties of HVFA concretes. Furthermore, the chloride-induced corrosion resistance of cement and high volume fly ash concrete are found improved by inclusion of nano particles. According to the mass loss measurement of rebars in corrosion test, the steel loss of HVFA concrete specimens containing 2% NS and 1% NC is lower than concretes containing 40% and 60% fly ash, respectively. The scanning electron microscopy, x-ray diffraction, thermal analysis (TGA/DTA) and nano indentation results also support the above findings.

Keywords: High volume fly ash, nano silica, nano-$CaCO_3$, compressive strength, durability properties.

ACKNOWLEDGMENT

First of all, I am grateful to The Almighty God, Jesus Christ, for establishing me during my research until the completion of this thesis. I thank for the gift of life, health, knowledge and all life opportunities.

I am incredibly indebted to Dr. Faiz U.A Shaikh as my research and thesis supervisor for his continuous support, thoughtful advice and encouragement throughout my doctoral program. Without his guidance and persistent help this thesis would not have been accomplished.

I also express my deep gratitude to Dr. Prabir Sarker and Dr. Ranjan Sarukkalige, for their input to serve as the thesis committee and also Dr. Salim Barbhuiya and Mr. Pengloy Chow for the valuable guidance regarding to nano indentation test. I also extend my thanks to the head of civil engineering department, and the secretary of civil engineering department, for their assistance during my study. Sincere thanks are also extended to Ashley Hughes, Mick Elliss, Joe, Andy and all technicians for their kind support on the successful completion of my experimental works in concrete laboratory at Curtin University. I am also grateful to Centre for Materials Research and Department of Chemistry at Curtin University for microstructure and phase identification analysis.

I would also like to acknowledge the financial support provided through the Indonesian Directorate General of Higher Education (DIKTI) scholarships. My thanks also extended to Private High Education Coordinator (KOPERTIS) region IX for granting valuable contribution and support for the funding.

Last but not least, I would express a deep sense of gratitude to my beloved parents for all the moral supports, their confidence, prayer and their love during all these years. And also all friends for their kind support at various points during my study and life at Curtin University.

TABLE OF CONTENTS

	Page
Abstract	iii
Acknowledgment	v
Table of contents	vi
List of acronyms	x
List of notations	xi
List of tables	xii
List of figures	xiii
List of publications	xvi
Chapter I Introduction	1
1.1 Background	1
1.2 Research significance	4
1.3 Research objectives	5
1.4 Scope of work	5
1.5 Thesis structure	6
Chapter II Literature review	7
2.1 Introduction	7
2.2 Portland cement	7
2.2.1 Cement hydration	7
2.2.2 Hydration of silicates (C_3S and C_2S)	8
2.2.3 Hydration of aluminates (C_3A and C_4AF)	10
2.2.4 Calcium hydroxide (CH)	10
2.2.5 Pozzolanic reaction	10
2.3 Fly ash	11
2.3.1 Characteristics of fly ash	11
2.3.2 High volume fly ash (HVFA)	13
2.4 Nano materials	16
2.4.1 Nano silica (SiO_2)	18
2.4.1.1 Properties of concrete containing nano silica	19
2.4.2 Nano calcium carbonate ($CaCO_3$)	21
2.4.2.1 Properties of concrete containing nano calcium carbonate	22
2.4.3 Dispersion of nanoparticles	23
2.5 Durability properties of concrete	25
2.5.1 Permeability	25
2.5.2 Chloride diffusion	26
2.5.3 Corrosion of steel in concrete	28
2.6 Microstructure and phase identification techniques	30
2.6.1 Scanning electron microscopy	30
2.6.2 X-ray diffraction	30
2.6.3 Thermogravimetric analysis	30
2.6.4 Nano indentation	31
2.6.4.1 Principle of nanoindentation	32
2.6.4.2 Oliver and Pharr method	35
2.7 Summary	37

Chapter III Methodology 39
3.1 Introduction 39
3.2 Properties of materials 39
3.2.1 Ordinary Portland cement 40
3.2.2 Class F fly ash 41
3.2.3 Nano silica 41
3.2.4 Nano calcium carbonate 42
3.2.5 Fine aggregates 43
3.2.6 Coarse aggregates 44
3.2.7 Water 44
3.2.8 Superplasticizer 44
3.3 Mix proportions 44
3.4 Experimental method 47
3.4.1 Mixing methods 47
3.4.1.1 Mortar (Part I) 47
3.4.1.2 Concrete (Part II) 47
3.4.1.3 Paste (Part III) 47
3.4.1.4 Dispersion of nano silica 48
3.4.2 Workability measurements 48
3.4.2.1 Flow table test 48
3.4.2.3 Slump test 49
3.4.3 Compressive strength 49
3.4.4 Water sorptivity 50
3.4.5 Volume of permeable voids 51
3.4.6 Porosity 52
3.4.7 Rapid chloride permeability test 52
3.4.8 Chloride diffusion 53
3.4.9 Accelerated corrosion test 54
3.5 Microsturucture and phase identification analysis 57
3.5.1 Backscattered electron (BSE) image 57
3.5.2 X-ray diffraction (XRD) 57
3.5.3 Thermal analysis (DTA/TGA) 58
3.5.4 Nano indentation 58

Chapter IV Results and discussions 62
4.1 Introduction 62
4.2 Workability of mortars and concretes containing nano silica and nano-$CaCO_3$ 62
4.2.1 Effect of nano silica on workability 62
4.2.2 Effect of nano-$CaCO_3$ on workability 64
4.3 Compressive strength of mortars containing nano silica and nano-$CaCO_3$ (Part I) 66
4.3.1 Effect of nano silica on the compressive strength of cement and HVFA mortars 66

4.3.2 Effect of nano-$CaCO_3$ on compressive strength of cement and HVFA mortars 71
4.4 Compressive strength of concretes containing nano silica and nano- $CaCO_3$ (Part II) 73
4.4.1 Effect of nano silica on compressive strength of OPC concrete and HVFA concretes 73
4.4.2 Effect of nano-$CaCO_3$ on compressive strength of OPC concrete and HVFA concretes 76
4.5 Durability properties of cement concrete and HVFA concretes containing nano silica and nano-$CaCO_3$ 79
4.5.1 Water sorptivity 79
4.5.1.1 Effect of nano silica on water sorptivity of OPC concrete and HVFA concretes 79
4.5.1.2 Effect of nano-$CaCO_3$ on water sorptivity of OPC concrete and HVFA concretes 82
4.5.2 Volume of permeable voids 87
4.5.2.1 Effect of nano silica on volume of permeable voids of OPC concrete and HVFA concretes 87
4.5.2.2 Effect of nano-$CaCO_3$ on volume of permeable voids of OPC concrete and HVFA concretes 88
4.5.3 Mercury intrusion porosimetry (MIP) 89
4.5.3.1 Porosity of cement and HVFA pastes containing nano silica 90
4.5.3.2 Porosity of cement and HVFA pastes containing nano-$CaCO_3$ 95
4.5.4 Chloride permeability 98
4.5.4.1 Effect of nano silica on chloride permeability of ordinary OPC and HVFA concretes 98
4.5.4.2 Effect of nano-$CaCO_3$ on chloride permeability of OPC concrete and HVFA concretes 99
4.5.5 Chloride diffusion 101
4.5.5.1 Effect of nano-silica on chloride diffusion OPC concrete and HVFA concretes 101
4.5.5.2 Effect of nano-$CaCO_3$ on chloride diffusion of OPC concrete and HVFA concretes 104
4.5.6 Accelerated corrosion 107
4.5.6.1 Effect of nano silica on corrosion of steel in OPC concrete and HVFA concretes 107
4.5.6.2 Effect of nano-$CaCO_3$ on corrosion of steel in OPC concrete and HVFA concretes 112
4.6 Microstructural analysis and phase identification of OPC and HVFA pastes containing nano silica and nano-$CaCO_3$ (Part III) 116
4.6.1 Scanning electron microscopy (SEM) 116
4.6.1.1 Micro- and nano-structural analysis of OPC and HVFA pastes containing nano silica 116
4.6.1.2 Micro- and nano-structural analysis of OPC and HVFA pastes containing nano-$CaCO_3$ 118
4.6.2 X-ray diffraction (XRD) 120
4.6.2.1 XRD results of OPC and HVFA pastes containing nano silica 120
4.6.2.2 XRD results of OPC and HVFA pastes containing nano-$CaCO_3$ 125

4.6.3 DTA/TGA analysis 129
4.6.3.1 Thermogravimetric analysis results of OPC and HVFA pastes containing nano silica 129
4.6.3.2 Thermogravimetric analysis results of OPC and HVFA pastes containing nano-$CaCO_3$ 132
4.7 Nano indentation analysis 137
4.7.1 Nano indentation results of HVFA pastes containing 2% nano silica 137
4.7.2 Nano indentation results of HVFA pastes containing 1% nano-$CaCO_3$ 144
4.8 Effect of ultrasonic mixing on dispersion of amorphous nano silica 148
4.9 Summary 149

Chapter V Conclusions and recommendations 151
5.1 Review of the work 151
5.2 Summary of findings 151
5.2.1 Effect of nano silica addition on mortar and concrete properties 151
5.2.2 Effect of nano-$CaCO_3$ addition on mortar and concrete properties 153
5.3 Summary of main achievements 154
5.4 Recommendations for further studies 155

References 157
Appendix A 174

LIST OF ACRONYMS

ACI	American Concrete Institute
ASTM	American Society of Testing Materials
BSE	Backscattered Electron
C_2S	Dicalcium Silicate
C_3A	Tricalcium Aluminate
C_3S	Tricalcium Silicate
C_4AF	Tetracalcium aluminoferrite
CH	Calcium Hydroxide
CSH	Calcium Silicate Hydrate
DTA	Differential Thermal Analysis
HVFA	High Volume Fly Ash
MIP	Mercury Intrusion Porosimetry
NC	Nano $CaCO_3$
NS	Nano Silica
OPC	Ordinary Portland Cement
RCPT	Rapid Chloride Permeability Test
SCM	Supplementaty Cementitious Materials
SEM	Scanning Electron Microscopy
TGA	Thermogravimetric Analysis
VPV	Volume of Permeable Voids
XRD	X-Ray Diffraction

LIST OF NOTATIONS

$C(x,t)$ = the chloride ion concentration at a depth x in mm from the exposed surface for an elapsed time t in years since the start of chloride exposure

C_s = the chloride concentration at the surface, expressed as a % of concrete mass

C_i = the initial (or background) chloride concentration of the concrete, expressed as a % of concrete mass

erf = the error function (a special function related to the integral of a normal probability function)

D_a = the chloride diffusion coefficient in mm^2/year

ρ = density of water = 1 g/cm^3

Q = charge passed (coulombs)

I_o = current (amperes) immediately after voltage is applied, and

I_t = current (amperes) at t min after voltage is applied

M_{th} = theoretical mass of rust per unit surface area of the bar (g/cm^2)

W = equivalent weight of steel which is taken as the ration of atomic weight of iron to the valency of iron (27.925 g)

I_{app} = applied current density (Amp/cm^2)

T = duration of induced corrosion (sec)

F = Faraday's constant (96487 Amp-sec)

M_{ac} = actual mass of rust per unit surface area of the bar (g/cm^2)

W_i = initial weight of the bar before corrosion (g)

W_f = weight after corrosion (g) for a given duration of induced corrosion (T)

D = diameter of the rebar (cm)

L = length of the rebar sample (cm)

WL_{CH} = weight loss during the dehydration of CH as percentage of the ignited weight (%)

MW_{CH} = the molecular weight of CH

MW_{HO} = the molecular weight of H_2O

LIST OF TABLES

2.1 Approximate oxide composition limits of ordinary Portland cement
2.2 The composition of major compounds in typical Portland cement
2.3 Production methods of nano silica
2.4 Classification of pores in hardened Portland cement paste
2.5 Limits for water-soluble chloride-ion content in concrete (ACI 318)
2.6 Nanoindentation modulus and hardness of different phases of cement paste
3.1 Physical properties and chemical compositions of Ordinary Portland cement (OPC), class F fly ash (FA), nano silica (NS) and nano calcium carbonate (NC)
3.2 Part I: Mix proportions of mortars containing nano silica, fly ash and nano $CaCO_3$
3.3 Part II: Mix proportions of concrete and HVFA concretes containing optimum nano silica and nano $CaCO_3$
3.4 Mixture proportions of mortars containing NS to study the effect of ultrasonic mixing on dispersion of nano silica
3.5 Chloride ion penetrability based on charge passed (ASTM C1202)
4.1 Phase abundance of combined NS with fly ash paste samples based on quantitative XRD analysis
4.2 Quantitative XRD analysis of cement and nano-$CaCO_3$ pastes at 28 days
4.3 Quantitative XRD analysis of HVFA with and without nano-$CaCO_3$ pastes at 7 and 28 days
4.4 Weight-loss measurement of rebar from concretes containing nano silica
4.5 Weight-loss measurement of rebar from concretes containing nano calcium carbonate
4.6 Elastic modulus and hardness of HVFA pastes containing 2% nano silica after 28 days of water curing
4.7 Elastic modulus and hardness of HVFA pastes containing 1% nano-$CaCO_3$ after 28 days of water curing

LIST OF FIGURES

2.1 Image of Portland cement hydration products
2.2 Typical shape of fly ash
2.3 Approaching methods in nanotechnology
2.4 Particle size and specific surface area of concrete materials
2.5 Chloride-induced reinforcement corrosion phases
2.6 Pitting on a corroded rebar
2.7 Schematic diagram of nano indentation equipment
2.8 Typical representation of the indentation load versus depth curves
2.9 Images of different indenter tip
2.10 Cross-section through an indenter
3.1 Physical appearance of cement, fly ash, nano silica and nano calcium carbonate
3.2 XRD spectra of Portland cement
3.3 XRD spectra of Class F fly ash
3.4 SEM image of nano silica
3.5 XRD spectra of nano silica
3.6 SEM image of nano calcium carbonate
3.7 XRD spectra of nano calcium carbonate
3.8 Ultrasonic processor type UP400S
3.9 Workability measurement
3.10 Compressive strength test setup
3.11 Water sorptivity test setup
3.12 Rapid chloride permeability test setup
3.13 Chloride diffusion analysis
3.14 Accelerated corrosion test
3.15 Schematic diagram of accelerated corrosion test
3.16 SEM investigation
3.17 Nano indentation technique
3.18 Example of load-displacement curves in nano indentation test
4.1 Workability of cement and HVFA mortars containing NS
4.2 Effect of nano silica on workability of concrete and high volume fly ash concretes
4.3 Workability of cement and HVFA mortars containing NC
4.4 Effect of nano-$CaCO_3$ on workability of concrete and high volume fly ash concretes
4.5 Compressive strength of mortars containing NS and fly ash
4.6 Strength activity index of mortars containing NS
4.7 Effects of 2% NS on compressive strength of mortars containing HVFA
4.8 Strength activity index of HVFA mortars containing 2% NS at 7 and 28 days
4.9 Compressive strength of control mortar containing NC and HVFA mortars containing NC at 7 and 28 days
4.10 Compressive strength of cement and nano silica concrete
4.11 Effects of 2% NS on compressive strength of HVFA concretes containing 40% and 60% fly ash
4.12 Gain or loss of compressive strength of HVFA mortars measured at different ages due to addition of 2% NS
4.13 Compressive strength of concretes containing NC and HVFA concretes containing NC at 3, 7, 28, 56 and 90 days

4.14 Water absorption of cement concrete mixes containing nano silica at 28 and 90 days
4.15 Water absorption of HVFA concrete mixes containing 2% nano silica at 28 and 90 days
4.16 Sorptivity value of concretes containing 2% nano silica at 28 and 90 days
4.17 Water absorption of cement concrete mixes containing nano-$CaCO_3$ at 28 and 90 days
4.18 Water absorption of HVFA concrete mixes containing 1% nano-$CaCO_3$ at 28 and 90 days
4.19 Sorptivity value of various concretes containing NC measured after 28 and 90 days of curing
4.20 Volume of permeable voids of different types of concrete mixtures containing 2% nano silica at 28 and 90 days
4.21 Volume of permeable voids of different types of concrete mixtures containing 1% nano-$CaCO_3$ at 28 and 90 days
4.22 Cumulative pore volume of cement and HVFA concretes containing 2% nano silica
4.23 Change in intruded pore volume of cement and HVFA concretes containing 2% nano silica
4.24 Cumulative pore volume of cement and HVFA concretes containing 1% nano-$CaCO_3$
4.25 Change in intruded pore volume of cement and HVFA concretes containing 1% nano-$CaCO_3$
4.26 Charge passed in concretes containing 2% nano silica measured after 28 and 90 days of curing
4.27 Charge passed in concretes containing 1% nano-$CaCO_3$ measured after 28 and 90 days of curing
4.28 The acid-soluble chloride ion content profile of different mixes of concretes containing 2% nano silica
4.29 Chloride diffusion coefficient of the variation of concrete mixes containing nano silica after 60 days exposure in NaCl solution
4.30 The acid-soluble chloride ion content profile of different mixes of concretes containing nano-$CaCO_3$ after 60 days exposure in NaCl solution
4.31 Chloride diffusion coefficient of the variation of concrete mixes containing 1% nano-$CaCO_3$
4.32 Corrosion current-time relationships of concretes containing nano silica after 28 days of curing
4.33 Corroded concrete specimens containing NS after accelerated corrosion test
4.34 Typical deterioration of rebars taken from concretes containing nano silica after accelerated corrosion test
4.35 Corrosion current-time relationships of concretes containing nano-$CaCO_3$ after 28 days of curing
4.36 Corroded concrete specimens containing nano calcium carbonate after accelerated corrosion test
4.37 Typical deterioration of rebars taken from concretes containing nano calcium carbonate after accelerated corrosion test

4.38 Secondary electron (SE) images of paste samples after 28 days of curing
4.39 Backscattered electron (BSE) images of polished surface of paste samples after 28 days of curing
4.40 Backscattered electron images of cement and NC1 pastes after 28 days of curing
4.41 Backscattered electron images of HVFA and combined HVFA with 1% NC pastes cured at 28 days
4.42 XRD analysis of cement paste samples after 28 days of curing
4.43 XRD analysis of FA40 paste samples after 3 and 28 days of curing
4.44 XRD analysis of FA60 paste samples after 3 and 28 days of curing
4.45 XRD analysis of cement and 1% nano-$CaCO_3$ pastes at 28 days
4.46 XRD analysis of FA40 paste samples with and without nano-$CaCO_3$ at 7 and 28 days
4.47 XRD analysis of FA60 paste samples with and without nano-$CaCO_3$ at 7 and 28 days
4.48 DTA/TGA analysis of cement pastes containing NS after 28 days of curing
4.49 DTA/TGA analysis of cement pastes containing HVFA, NS and HVFA with NS after 28 days of curing
4.50 Calcium hydroxide content in pastes containing 2% nano silica after 28 days of curing
4.51 DTA/TGA analysis of cement pastes containing NC after 28 days of curing
4.52 DTA/TGA analysis of HVFA cement pastes containing NC at 7 days
4.53 DTA/TGA analysis of HVFA cement pastes containing NC at 28 days
4.54 Calcium hydroxide content in pastes containing 1% nano-$CaCO_3$ after 28 days of curing
4.55 Modulus and hardness of FA40 paste after 28 days of curing
4.56 Modulus and hardness of FA60 paste after 28 days of curing
4.57 Modulus and hardness of FA38.NS2 paste after 28 days of curing
4.58 Modulus and hardness of FA58.NS2 paste after 28 days of curing
4.59 Modulus and hardness of FA39.NC1 paste after 28 days of curing
4.60 Modulus and hardness of FA59.NC1 paste after 28 days of curing
4.61 Effect of ultrasonic mixing of NS and its time on the strength development of mortars containing different NS contents

LIST OF PUBLICATIONS

1. Faiz U.A Shaikh and Steve W.M Supit. (2014). Mechanical and durability properties of high volume fly ash (HVFA) concrete containing calcium carbonate ($CaCO_3$) nanoparticles. *Construction and Building Materials,* Volume 70, pp. 309-321.
2. Steve W.M Supit, and Faiz U.A Shaikh. (2014). Effect of nano-$CaCO_3$ on compressive strength development of high volume fly ash mortars and concretes. *Journal of Advanced Concrete Technology,* Volume 12, pp. 178-186.
3. Steve W.M Supit, and Faiz U.A. Shaikh. (2014). Durability properties of high volume fly ash concrete containing nano-silica. *Material and Structures.* DOI 10.1617/s1 1527-014-0329-0.
4. F.U.A. Shaikh, S.W.M. Supit, and P.K. Sarker. (2014). A study on the effect of nano silica on compressive strength of high volume fly ash mortars and concretes. *Materials and Designs,* Volume 60, pp. 433-442.
5. Supit, W.M.S., Shaikh, A.A.U, and Sarker, P.K. (2013). Effect of Nano Silica and Ultrafine Fly Ash on Compressive Strength of High Volume Fly Ash Mortar. *Applied Mechanics and Materials,* Vol. 368-370, pp. 1061-1065.
6. Supit, S.W.M. and Shaikh, F.U.A. (2014). Chloride induced corrosion durability of high volume fly ash concretes containing nano particles. *Cement and Concrete Composites*. (under review)
7. Shaikh, F.U.A. and Supit, W.M.S. (2015). Mechanical properties and durability of high volume fly ash concrete reinforced with calcium carbonate nano particles. Dong et al. (eds.) *Fillers and reinforcements for advanced nanocomposites*. Woodhead publications, UK. (in Press)

CHAPTER I

INTRODUCTION

1.1 Background

Concrete is one of the most widely used construction materials in the world. Due to increasing population and urbanisation the increase in the use of concrete is unavoidable in near future. The demand of cement increased to 3.6% in 2013 and forecast to increase by 4% in 2014 – 2016 (http://www.cement.org). Ordinary Portland cement (OPC) production, however, is a highly energy intensive and releases approximately one tonne of carbon-di-oxide to produce one tonne of OPC during calcination process which has a crucial effect on global warming (Malhotra and Mehta, 2002). In another estimate, it is also shown that the production of cement contributes approximately 5-7% of global carbon-di-oxide emission (Benhalal et al, 2012). Therefore, it is important to reduce the consumption of OPC in concrete by incorporating industrial by-product materials which can be disposed at low economic and environmental costs. This concern has led the use of various industrial by-products such as fly ash, blast furnace slag, silica fume, etc. as supplementary cementitious materials (SCM) as partial replacement of low to moderate amount of OPC in the concrete.

Among various SCM, fly ash as by-product of coal fired power station has long been used as partial replacement of OPC in concrete for many decades. In year 2012, the utilization of fly ash was approximately 55.8% in construction application and become a commercial product which is available in bulk quantities (Fly ash utilisation, 2013). Fly ash acts as pozzolanic material which reacts with Calcium Hydroxide (CH) of cement hydration due to the presence of amorphous SiO_2 and Al_2O_3. However, the reaction of fly ash in the hydration reaction is slow and affects the early age properties of concrete (Thomas et al, 1999; Shi and Shao, 2002). Moreover, its use in concrete is also limited to approximately 15-25% by mass (ACI 226.4R). In view of sustainability of concrete the maximisation of the use of fly ash or other SCMs in concrete is the key priority and also researched extensively specially on high volume fly ash (HVFA) concrete. Generally, if 50% or more OPC is replaced by fly ash the concrete is termed as HVFA concrete (Siddique, 2004). Previous studies have shown that the substitution of OPC by high volume fly ash

improved the workability, mechanical properties and various durability properties of concrete. Malhotra and Mehta (2002) reported that up to 20% reduction of water in the concrete can be achieved if high volume fly ash is used. This phenomenon is attributed to the spherical shape and the smooth surface of fly ash particles in reducing the inter-particle friction and thus facilitates the mobility of aggregates in the concrete (Mehta, 2004). Further, fly ash particles act as fillers for the voids within the aggregate in making dense concrete and improve the resistance to sulphate attack (Bendapudi, 2011). In addition, the high volume fly ash concretes, when properly cured, are able to provide excellent water-tightness which can contribute in improving the permeability and durability of concrete exposed to severe environmental conditions (Mehta, 2004). However, although the use of fly ash shows improvement of properties of concrete, yet its low early age strength development is still a limitation due to slow pozzolanic reaction especially in the high volume fly ash (HVFA) concrete. For instance, Naik et al. (1994) reported about 40% and 18% reduction in 7 days compressive strength and modulus of elasticity, respectively of concrete due to addition of 40% fly ash as partial replacement of cement. HVFA concretes containing more than 40% fly ash also exhibited reduction in early age mechanical properties in above study. This view is also supported by Guo-qiang and Juan-hong (2010) who reported about 75% and 77% reduction in compressive strength of HVFA concrete containing 40% fly ash at 3 and 7 days, respectively.

Several researchers have studied the use of silica fume on improvement of early age properties of concretes containing fly ash, however in low to moderate amount. Mehta and Gjorv (1982) reported about 22% increase in 7 days compressive strength of concrete containing 12.5% fly ash due to addition of 12.5% silica fume., In another study, Carette and Malhotra (1983) also evaluated the effect of addition of 10% silica fume on the early age compressive strength of concrete containing 30% fly ash and reported that the silica fume compensated the low early age compressive strength development. In this study, the 7 days compressive strength of cement concrete containing 30% fly ash with 10% silica fume was 45% higher than the concrete without silica fume. Nochaiya et al. (2010) also evaluated the compressive strength development of ternary blended cement system containing 60% OPC, 30% fly ash and 10% silica fume by weight. The early age (7 days) compressive strength of above concrete was increased up to 35% when silica fume was used at 10 wt%.

Thomas et al., (1999) and Barbhuiya et al. (2009) also reported superior durability properties of concrete containing both fly ash and silica fume.

In recent years, the use of nano materials has received particular attention in the application of construction materials especially in cement mortar and concrete. Nano materials appear to be potentially better than micro-size supplementary cementitious materials because of high specific surface area, extremely small particle size and more amorphous nature of particles. Various manufactured nano materials have been used in concrete such as nano alumina (Behfarnia and Salemi, 2013), nano titanium (Jayapalan et al., 2009), nano carbon tubes (Konsta-Gdoutos et al., 2008) nano silica (Givi et al., 2010; Elkady and Serag, 2013) and nano calcium carbonate (Camiletti, 2013). These materials influence the development of strength and enhance the durability properties of concrete. For example, nano silica due to its high specific surface area reacts with calcium hydroxide to form additional calcium silicate hydrate (CSH) within the hydration system (Sobolev et al., 2006). It also forms dense microstructure and reduces the capillary pores in the matrix. On the other hand, the presence of nano-$CaCO_3$ as partial replacement of cement leads to increase the hydration degree of the binder and accelerates the setting time thus compensates the low early age strength (Goergescu, 2009). Chemically, the presence of nano-$CaCO_3$ increases the rate of hydration reaction of tricalcium aluminate (C_3A) to form carboaluminate compound (Pera et al., 1999). The reaction of nano-$CaCO_3$ with tricalcium silicate (C_3S) is also found as another factor in accelerating the setting time and early strength development of concrete (De Weerdt et al., 2011).

The beneficial effect of the use of nano silica and nano calcium carbonate on the mechanical properties of HVFA system is reported in limited studies. For instance, Li (2004) studied the effect of 4% NS (by wt.) on the compressive strength of HVFA concrete containing 50% fly ash and observed improvement in both short-term and long-term compressive strength of HVFA concretes. Improved early age compressive strength of HVFA mortars due to addition of NS are also reported by Hou et al. (2013). With regard to the addition of nano calcium carbonate in HVFA concrete, Sato and Beaudoin (2011) carried out an investigation on the incorporation of micro- and nano-$CaCO_3$ materials with high volume of supplementary cementitious materials. In this experiment, the cement was replaced with 50% of fly ash and 50% of slag and incorporated with 10 and 20% of micro- and nano-$CaCO_3$

by weight of binders. It was found that the replacement of cement with nano-$CaCO_3$ accelerated the early hydration of cement and enhanced the early development of modulus of elasticity with increase in nano-$CaCO_3$ contents.

1.2 Research significance

While the existing research shows that the addition of nano silica and nano calcium carbonate as partial replacement of cement improve the compressive strength of OPC and HVFA mortars, no thorough research in terms of critical amount of nano silica and nano calcium carbonate in HVFA concretes is reported. Moreover, in most of the studies on HVFA system, only the effect of nano silica and nano calcium carbonate on compressive strength is reported. Although the durability properties of concrete is partly related to compressive strength, however, the effect of nano silica and nano calcium carbonate on the durability properties of HVFA concretes also need to be evaluated for the structural application of this eco-friendly material. The use of nano silica and nano calcium carbonate in HVFA concrete is expected to provide dual benefits. First, they will improve the low early age compressive strength and other related mechanical properties of HVFA concrete thus significantly shorten the formwork removal time of such concrete in the field, which will provide significant savings of the construction project. Secondly, due to their extremely small size and very high specific surface area the durability of HVFA concretes will also be improved significantly, which will increase the service life and reduce the maintenance cost. Despite the benefits of using nano silica and nano calcium carbonate on the compressive strength of ordinary and HVFA mortars, no results are available of their roles on chloride induced corrosion and related durability properties of HVFA concretes. Therefore, it will be useful to evaluate the effect of nano silica and nano calcium carbonate as partial replacement of cement on the compressive strength development and on chloride induced corrosion and related durability properties of HVFA concretes.

The results of this research will provide better understanding on the potential structural application of HVFA concretes by incorporating nanoparticles particularly in the marine environment. The development of such eco-friendly durable concrete will also produce excellent environmental benefits due to the maximization of the use of fly ash and reduction of CO_2 associated with ordinary Portland cement production.

1.3 Research objectives

The main aim of this study is to evaluate the effectiveness of nano silica (SiO_2) and nano calcium carbonate ($CaCO_3$) particles on the enhancement of early age compressive strength and chloride induced corrosion and related durability properties of HVFA concretes and compare with those of OPC concrete. In order to achieve the above aim, the specific objectives are:

1) To evaluate the optimum nano silica and nano calcium carbonate contents in OPC concrete based on compressive strength development.
2) To evaluate the effects of optimum nano silica and nano calcium carbonate contents on the development of early age as well as later ages compressive strength of high volume fly ash concretes.
3) To evaluate the effectiveness of optimum nano silica and nano calcium carbonate contents on chloride induced corrosion of HVFA concretes and associated durability properties such as chloride permeability, water sorptivity, permeable voids, chloride diffusion and porosity.
4) To investigate the micro- and nano-structural changes of above HVFA concretes due to addition of optimum nano silica and nano calcium carbonate contents.

1.4 Scope of work

Among different nano silica (NS) and nano calcium carbonate (NC) contents, the optimum content that exhibited the highest compressive strength in OPC mortar is used to evaluate the compressive strength development of HVFA concretes containing 40% and 60% fly ash as partial replacement of cement at 3, 7, 28, 56 and 90 days. The durability properties of concrete including chloride permeability, volume of permeable voids, water sorptivity, porosity, chloride diffusivity and chloride induced corrosion of above HVFA concretes containing optimum NS and NC are evaluated. All durability properties are measured after 28 and 90 days of wet curing in accordance with American Society for Testing and Materials (ASTM) and Australian standards. The microstructure and changes in hydration phases of HVFA pastes due to incorporation of optimum nano silica and nano calcium carbonate are investigated through backscattered electron (BSE) microscopy, x-ray diffraction (XRD), thermogravimetric analysis (DTA/TGA) and nano-indentation techniques.

1.5 Thesis structure

The thesis is composed of five chapters as follows:

Chapter 1: This chapter contains relevant sections including the background, objectives and scope of this research.

Chapter 2: This chapter identifies the issues based on the previous researches related to the properties of cement and high volume fly ash and the development of nano materials in mortar and concrete application. This chapter also clarifies the research techniques used in determining the microstructure and phase analysis and discusses some of the outlines of durability properties of concrete including water permeability, chloride diffusion and corrosion mechanism of steel in concrete.

Chapter 3: This chapter explains the experimental methods including mixture proportions and testing methods used to measure the compressive strength and durability properties of HVFA concretes in order to achieve the objectives of this study.

Chapter 4: This chapter presents and discusses the results of the experimental works including workability, compressive strengths and durability properties of OPC and HVFA concretes containing nano silica and nano calcium carbonate. The results from micro- and nano-structural analysis of the HVFA matrix are also used to explain the better behaviour of HVFA concretes obtained in this study.

Chapter 5: This chapter concludes the results of the experimental work and provides recommendations for future work.

CHAPTER II

LITERATURE REVIEW

2.1. Introduction

This chapter provides a review of the properties of cement, Class F fly ash, and nano materials (nano silica and nano calcium carbonate) that used as replacement of cement in this study. An attempt has been made based on the relevant literatures to summarize and discuss the general studies pertaining to the main objectives of the current thesis. This chapter also clarifies the research techniques used in determining the microstructural analysis (SEM, XRD, DTA/TGA, nano indentation) and discusses with respect to durability properties of concrete including chloride permeability, porosity, chloride diffusion and corrosion mechanism of steel in concrete.

2.2 Portland cement

2.2.1 Cement hydration

Cement has been the main ingredient used in making concrete. As shown in Table 2.1, the raw materials of ordinary Portland cement (OPC) consist principally of limestone (CaO) and clay as the principal source of SiO_2, Al_2O_3 and Fe_2O_3. The other constituents or impurities including magnesia, sodium and potassium oxide (the alkalies), titania, phosphorous and manganese oxides (Popovics, 1992). Although these constituents exist in relatively small amount, the proportions of the oxide compositions are responsible for influencing the hydration process and the properties of cement concrete.

Table 2.1 Approximate oxide composition limits of ordinary Portland cement (Shetty, 1982)

Oxide	Content (%)
CaO	60-67
SiO_2	17-25
Al_2O_3	3.0-8.0
Fe_2O_3	0.5-6.0
MgO	0.1-4.0
Alkalies (K_2O, Na_2O)	0.4-1.3
SO_3	1.3-3.0

During the manufacture of cement, the oxides interact with one another at high temperature to form more complex compounds (Shetty, 1982). The four constituents of major compounds in typical Portland cement clinker which are silicate (C_3S, C_2S) and aluminate (C_3A and C_4AF) minerals have been recognized after the publication of Le Chatelier's research in 1905 (see Table 2.2). The silicate minerals (C_2S and C_3S) contribute the strength development of cement paste while the stiffening and setting of Portland cement paste is generally attributed to the aluminate minerals (C_3A and C_4AF) (Mehta, 2003).

The results of a series of simultaneous and consecutive reactions between the water and the major compounds of the cement are known as hydration of Portland cement. When cement mixes with water, the different cement compounds start to react with some part of mixing water so the cement starts to hydrate then produces solid structure and creates a dense material. Cement hydration stops when there is no more anyhydrous phase or when water can no longer reach the unhydrated phases or when there is no water available (Aitcin, 1998). However, the hydration of Portland cement is a complex process and influenced by many factors such as the phase composition of cement, the fineness and particle size distribution, the presence of chemical admixtures, the water/binder ratio and the presence of additives. The next section separately describes the hydration reactions of the silicate and aluminate minerals.

Table 2.2 The composition of major compounds in typical Portland cement

Name of compound	Formula	Mineral name	Abbreviated formula
Tricalcium silicate	$3\ CaO.SiO_2$	Alite	C_3S
Dicalcium silicate	$2\ CaO.SiO_2$	Belite	C_2S
Tricalcium aluminate	$3\ CaO.Al_2O_3$	Aluminate	C_3A
Tetracalcium aluminoferrite	$4\ CaO.Al_2O_3.Fe_2O_3$	Ferrite	C_4AF

2.2.2 Hydration of silicates (C_3S and C_2S)

Generally, the two calcium silicate minerals, tricalcium silicate (C_3S) and dicalcium silicate (C_2S), make up 75-80% of Portland cement and have significant role in the strength development and the long-term structural properties of Portland cement (Ramachandran, 1995). When compared, the reactivity between C_3S and C_2S, half of the C_3S formation is effectively complete by 3 days and 80% by 28 days. By

contrast, the presence of C_2S in the clusters hydrates until approximately 14 days and has minor impact in the early hydration (Newman and Choo, 2003). Normally, the reaction of C_3S and C_2S with water produces an amorphous calcium silicate hydrate or known as CSH gel or also called tobermorite gel (see Eq. 2.1 and 2.2). The following equations approximately summarize the hydration reactions:

$2C_3S$	+ 6H	⟶	$C_3S_2H_3$	+ 3CH
(2.1)				
Tricalcium silicate	Water		CSH gel	Calcium hydroxide
$2C_2S$	+ 4H	⟶	$C_3S_2H_3$	+ CH
(2.2)				
Dicalcium silicate	Water		CSH gel	Calcium hydroxide

Figure 2.1 shows an electron micrograph of the products formed in hydrated Portland cement. The CSH makes up 50 to 60% of the volume of solids in a completely hydrated Portland cement paste (Mehta and Monteiro, 2006). It has a very fine texture and high specific surface (Mehta, 2003). It binds the aggregates and the other crystalline phases and increases the volume of solids within the boundaries of paste specimen resulting in reducing the overall porosity and high density (Kosmatka et al, 2003). The CSH is, therefore, become the most important phase determining the properties of the paste.

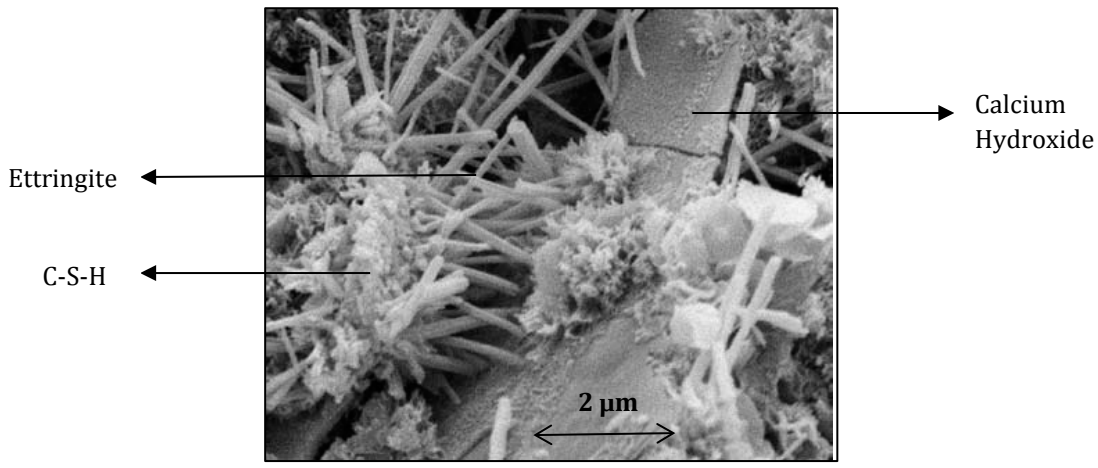

Figure 2.1 Image of Portland cement hydration products (Alizadeh, 2009)

2.2.3 Hydration of aluminates (C_3A and C_4AF)

The other chemical compounds in ordinary Portland cement are C_3A and C_4AF. The amount of C_3A and C_4AF on the cement usually ranges between 6 to 8% and react with water rapidly to form crystalline products, with liberation of large amount of heat of hydration (Mehta and Monteiro, 2006). The aluminate phase reacts with water and gypsum to form ettringite. When the gypsum is consumed, the ettringite starts to react with the remaining aluminate to form monosulphate (see Equations 2.3 and 2.4). However, their presence is harmful to the durability of concrete particularly in sulphates attack. It is because of the reaction of C_3A with water takes place in presence of sulphate ions supplied by dissolution of gypsum present in Portland cement (Mehta, 2003).

$$\underset{\text{Tricalcium alluminate}}{C_3A} + \underset{\text{gypsum}}{3\,(CSH_2)} + \underset{\text{water}}{26H} \longrightarrow \underset{\text{ettringite}}{C_3A(CS)_3H_{32}} \qquad (2.3)$$

$$C_3A + CSH_2 + 10H \longrightarrow \underset{\text{monosulphoaluminate hydrate}}{C_3ACSH_{12}} \qquad (2.4)$$

2.2.4 Calcium Hydroxide (CH)

Calcium hydroxide (also called portlandite) is a compound produced from the hydration of C_3S and C_2S. It constitutes 20 to 30% of the solid volume of the hydrated paste with distinctive hexagonal prism morphology (Popovics, 1992). In contrast to the CSH gel, calcium hydroxide is soluble in water, has lower surface area and gets leached out making the hydraulic structures of concrete porous, develop micro-cracks, weakening the bond with aggregate and thus affect the durability properties of concrete (Mehta, 1991). The calcium hydroxide also reacts with sulphates present in soils or water to form calcium sulphate which further reacts with C_3A and cause deterioration of concrete (Prasad et al., 2006). Therefore, its present is not expected in the concrete mass. In order to reduce the quantity of CH in concrete, the use of cementitious materials such as fly ash, silica fume and such other pozzolanic materials becomes important as it influences to overcome the bad effect of CH in concrete (Weng et al., 1997).

2.2.5 Pozzolanic reaction

Pozzolanicity is defined as the capacity of certain materials to enter into reaction with CaO or CH in the presence of water at room temperature, to form solid and

water-insoluble masses (Wesech, 1991). According to ASTM C 618 standard, the composition of pozzolanic material is siliceous and aluminous with a minimum of 70-75% of the pozzolan to be composed of SiO_2+Al_2O_3+Fe_2O_3. Examples of some pozzolan materials are fly ashes, silica fumes, and raw or calcined natural pozzolans such as metakaolin, volcanic ashes, calcined shales and clays, and diatomaceous earths. Their benefits derived include higher early strength, higher later age strength, reduced permeability, control of alkali-aggregate reactivity, lower heat of hydration, and reduced costs (Russell, 2002).

In the pozzolan-lime reaction, OH^- and Ca 2+ react with the SiO_2 or Al_2O_3-SiO_2 framework to form calcium silicate hydrate (CSH), calcium aluminate hydrate (CAH) and calcium aluminate ferrite hydrate (see Equations 2.5, 2.6 and 2.7) that have binding properties (Bendapudi, 2011). The calcium silicate hydrates are the most important product of cement and responsible for setting and hardening of cement and cement composites materials (Jozic, 2010). It is also the essence that determines the good properties of concrete.

Tobermorite gel:

$$CH + SiO_2 + H_2O \longrightarrow CaO.SiO_2.H_2O \quad (2.5)$$

Calcium aluminate hydrate:

$$CH + H_2O + Al_2O_3 \longrightarrow CaO.Al_2O_3.CH.H_2O \quad (2.6)$$

Calcium aluminate ferrite hydrate:

$$CH + Fe_2O_3 + Al_2O_3 + H_2O \longrightarrow CH.Al_2O_3.Fe_2O_3.H_2O \quad (2.7)$$

2.3 Fly ash

2.3.1 Characteristics of fly ash

According to ASTM C 618, fly ash is a finely divided residue that results from the combustion of ground or powdered coal. As a fuel coal combustion product which composed of glassy particles, processed fly ashes effective in acting as pozzolan materials and contribute concrete performance with better resistance to durability concerns such as water absorption, chloride diffusion and corrosion resistant (Saraswathy and Song, 2006). In addition, it also increases sustainability and appropriate for producing high mechanical strength with low cost.

In the fly ash generation process, particle size is controlled by removing the coarse particles from powdered products in mechanical or electrostatic separators. The material has variation in size and shape depending on the nature of the coal burned and the combustion conditions (see Figure 2.2). The final shape will form mostly solid spheres and some are hollow spheres at high combustion temperature whereas irregular shape can be originated when the combustion temperature is low. From a size point of view, the particle size of fly ash may vary from 0.2 to 200 μm and composed by glassy compound of Si, Al and Fe and crystalline minerals such as quartz, mullite, hematite, magnetic, free calcium oxide, etc (Wesche, 1991). The chemical composition, particle size and reactivity are some important variables which affect the concrete performances.

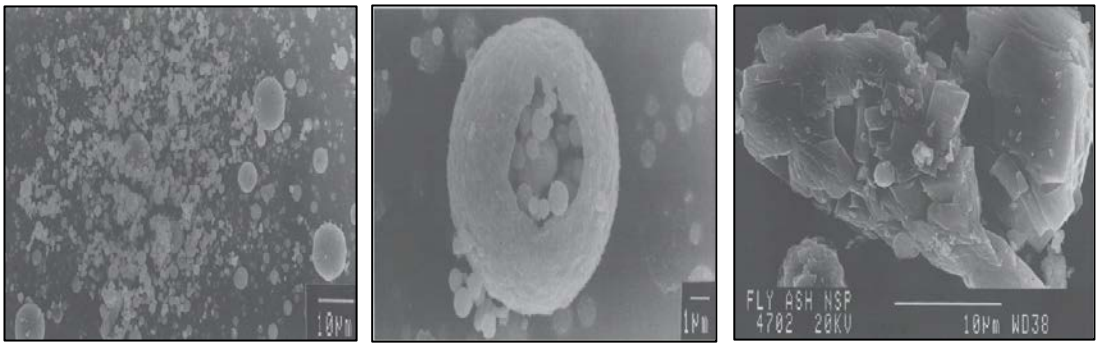

(a) (b) (c)

Figure 2.2 Typical shape of fly ash: a) Spherical particles, b) Hollow spheres, c) Angular-shaped particles (Wesche, 1991)

In general, typical fly ashes may be Classified into Class F and Class C. Class F is produced from coals by burning bituminous and anthracite at higher heat. On the other hand, Class C is processed by burning lignite and sub-bituminous coal and contains a higher amount of carbon compared to that belonging to Class F. ASTM C 618 Classified Class F fly ash if the (SiO_2+Al_20_3+Fe_20_3) > 70% and Class C fly ash if 70%>(SiO_2+Al_20_3+Fe_20_3)>50%. Although Class F fly ashes have no cementitious properties with low CaO but it is considered as a better ingredient in cement mortar or concrete due to its versatility especially in mitigating alkali-silica reaction and sulphate attack (Caldarone, 2009).

The utilization of fly ash has made some progress in addressing the challenges of sustainable construction. Due to the spherical shape and the glassy particles of fly ash, water content can be reduced thus offsetting the early age strength reduction. In addition, fly ash has pozzolanic activity which is attributed to the presence of SiO_2 and Al_2O_3 (Bendapudi, 2011). In pozzolanic reaction, it reacts with calcium hydroxide thus reducing the risk of leaching calcium hydroxide during cement hydration, to form additional Calcium Silicate Hydrate (CSH) and Calcium Aluminate Hydrate (CAH) which are effective in forming denser matrix leading to higher strength and better durability, for example, on sulphate attack and alkali silica reaction resistance (Tahir and Sabir, 2005; Malvar and Lenke, 2006; Bendapudi, 2011). However, pozzolanic reaction between lime and fly ash is a slow process. This results in low early strength development and inadequate strength at the time of loading. Therefore, some attempts have been made through the grinding of fly ash, elevated temperature curing of cement or concrete containing fly ashes and the addition of chemical activators to activate the potential pozzolanic reactivity of fly ashes (Shi and Shao, 2002).

2.3.2 High volume fly ash (HVFA)

In practice, the quantity of fly ash to replace cement is limited to 15-20% by mass of the total cementitious material (Aggarwal et al., 2010; Bendapudi, 2011) which is not adequate to make the concrete more sustainable. In addition, the small percentage is beneficial in optimizing workability and low cost but it may not improve durability to any considerable extent. Moreover, the optimization of high volume fly ash has raised many arguments and limitations regardless of the fact that the variation of constituent in fly ash such as alkalis, sulphates, lime and organics may affect the crystallization and slow down the pozzolanic reaction (Sarath and Saha, 2011). Therefore, some studies have been developed on the use of high volume fly ash to determine whether or not cement can be replaced by fly ash above the limited quantity. A literature review on the mechanical and durability properties of high volume fly ash mortar and concrete mixtures has been carried out and reported in the following discussions.

Thangaraj and Thenmozhi (2012) evaluated the strength properties of fly ash concrete using a cement replacement level of 50%, 55% and 60%. The compressive strength at 7 and 14 days were found slightly improved with 50% cement

replacement by fly ash. The addition of 1.5% of superplasticizer was found effective in increasing the strength development of concrete with 50% fly ash at early ages even more after 28 days.

Murali (2012) have studied the effect of fly-ash replacement levels (10 to 60%) for their 28 days compressive strength of concrete. Replacement levels of 10% to 20% fly ashes showed improved mechanical properties of blended cement concrete. However, at higher percentage of replacement (above 20%) a decrease in compressive strength values was observed irrespective of the period of curing and the nature of activation. It has also been observed that, when fly ash was used as an addition of cement (i.e. 50% and 60% by weight of cement) in concrete, there were a 23% and 27% decrease in strength at 28 days testing. Shrivastara (2012) also found that the compressive strength, flexural strength, modulus of rigidity and toughness of cement concrete increased with the increase of fly ash content up to 35% replacement by weight of cement but the strength decreased with further increase in fly ash contents.

Bazzar (2013) studied the mechanical properties and durability results of mortar containing high volume fly ash. In this study, cement was replaced by two percentages (25% and 50%) of Class F fly ash. The development of compressive strength at 7 days was 70% and 40% lower for 50% and 25% fly ash than ordinary Portland cement concrete, respectively.

Soni and Saini (2014) on the other hand, reported that the compressive strength of concrete mixtures with 30%, 40% and 50% fly ash as cement replacement was lower than the control mixture at all ages and the strength of all mixtures continued to increase with the age. Similarly, splitting tensile strength and modulus of elasticity were also increased with the increase in age at each replacement level of cement with fly ash up to 50% but they were decreased with increase in volume of fly ash.

Recent work from Soman (2014) studied the fresh and hardened properties of high volume fly ash concrete with 50% replacement of cement and ordinary Portland cement. Addition of 50% fly ash reduced 7 day strength by about 20% when compared to control mix. But it acquired strength almost equal to that of control mix at 28 days and attained higher strength thereafter.

From the experimental work under marine environment, Chalee et al. (2009) developed a model for predicting chloride diffusion of cement and fly ash concretes (up to 50% replacement of cement). It was found that concrete with high fly ash replacement with low water binder ratio significantly gain better chloride resistance than ordinary concrete under long term exposure in a marine environment.

Burden (2006) has studied the effect of high volume fly ash on the rate of carbonation of concrete mixture. The concrete mixtures were produced at range of water to cement ratios (0.3, 0.4 and 0.5) and fly ash replacement levels (0%, 30%, 40% and 50%). It was reported that the rate of carbonation increases with increase in fly ash contents. However, it can offset by specifying lower w/c ratio, extending the period of moist curing and increasing the depth of concrete's cover.

Guo-qiang and Juan-hong (2010) have investigated the compressive strength, carbonation and steel corrosion resistance when the mixing amount of fly ash was 30% and 40% and the water binder ratio was below 0.4. It was reported that the early strength (3 and 7 days) decreased as the fly ash increased but better strength at later age i.e. 28 days. Considering the carbonation and steel corrosion resistance of HVFA concrete, the use of lower water binder ratio followed by good compactness are recommended.

In a recent study Balakrishnan and Awal (2014) experimentally evaluated the effect of high volume fly ash concretes with 0, 40, 50 and 60% fly ash when exposed to chloride, acid and sulphate solutions. They reported that among the four mixes, the highest compressive strength value was obtained for 0% fly ash concrete, while samples containing 40, 50 and 60% replacements made up 85, 72 and 63%, respectively of the control sample strength at 28 days. In addition, it was also revealed that the penetration depth of chloride ions at 7 days was highest for 0% fly ash concrete with a value of 7.05 mm. However, at 28 and 90 days, the penetration depth for 0% fly ash concrete increased significantly to 13.10 mm and 19.20 mm. In the high volume fly ash concrete chloride penetration was only about half and quarter of the value. The lowest penetration depth was obtained for concrete with 60% fly ash with a penetration depth of 4.89 and 5.02 mm for 28 and 90 days, respectively. The increased resistance of the high volume fly ash concrete was also noticed on the acid attack and sulphate resistance. It is suspected mainly due to consumption of the

CH which leads to reduced porosity and increased impermeability that prevented the migration of the detrimental chemical ions inside the concrete.

Based on the previous researches, it can be concluded that although the use of HVFA improves the workability and some of mechanical and durability properties of mortar and concrete, it also possess some draw backs in terms of inferior mechanical and durability properties particularly at early ages.

2.4 Nano materials

The concept of nanotechnologies was first introduced in 1959 by the physicist Richard Feynman, in his lecture 'There's plenty of room at the bottom' (Feynman, 1960). Feynman explored the possibility of manipulating material at the scale of individual atoms and molecules. There are two ways to approach the nano scale. Figure 2.3 provides an illustrative approach of methods that have been used to obtain nanoparticles. First is top-down method which also known as physical approach where the materials are characterized by reducing its actual size by using reduction techniques (machining and etching techniques) (Zhu et al., 2004). The second method is bottom-up or also called "molecular nanotechnology" which includes chemical approach where the materials are built from their atom or molecular components (Rahman and Padabettan, 2012). This method produces significant breakthroughs in number of applications, including materials and manufacturing electronics, medicine and healthcare, energy, biotechnology, information technology, and many engineering disciplines (Sanchez and Sobolev, 2010).

In the construction sector, nano materials refer to materials with nano scale dimension containing nano sized particles. The dimension of materials ranged from 100nm down to approximately 0.1nm (see Figure 2.4). This characteristic can increase surface area (per unit mass) and result in a corresponding increase in chemical reactivity (Carmichael and Arulraj, 2012). As the strength of concrete is based on its nanometre size crystal structure, the usage of nano materials as additives has provided a unique opportunity for the improvement of cement based materials.

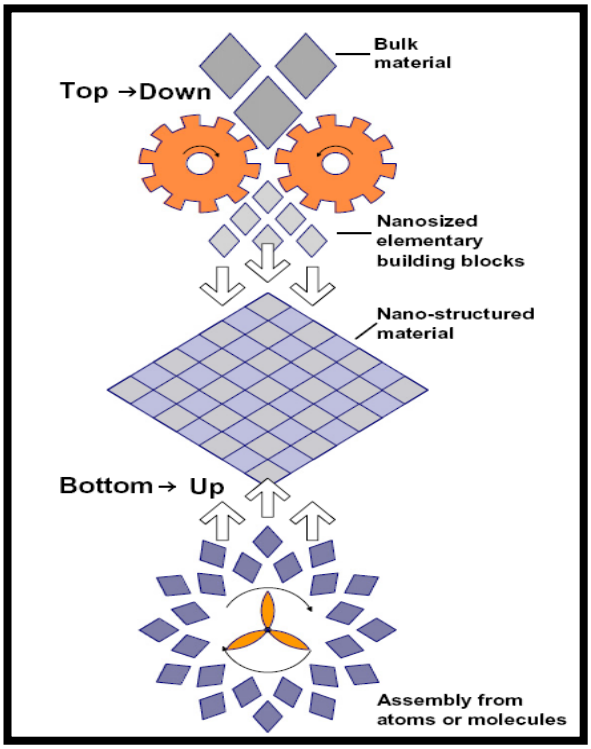

Figure 2.3 Approaching methods in nanotechnology (Sobolev et al. 2006)

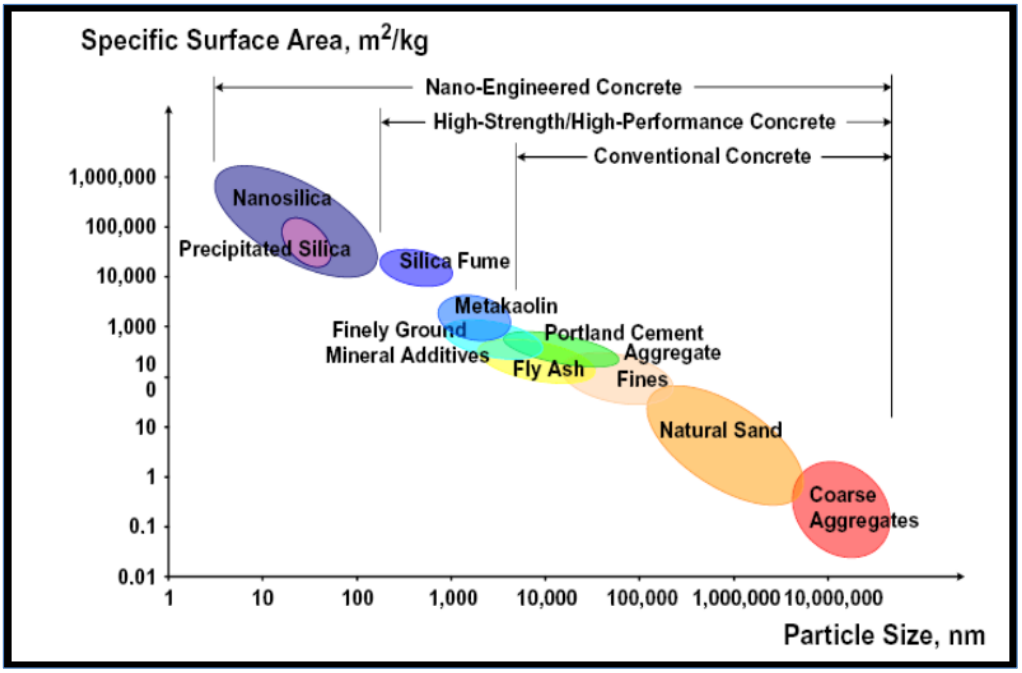

Figure 2.4 Particle size and specific surface area of concrete materials (Sobolev et al., 2006)

2.4.1 Nano silica (SiO_2)

Development of new techniques to characterise materials at the nanoscale has brought many ideas to study the properties of concrete due to the addition of nanoparticles. One of the advancement made is the discovery that addition of silica (in nano-size) can improve the particle packing of the concrete matrix resulting in improved mechanical properties (Qing et al., 2007). It also reduces the permeability, refined pore structure, leading to a reduction in the diffusion of harmful ions, reduces calcium hydroxide content which results in a higher resistance to sulphate attack (Siddique and Khan, 2011).

With regard to the production of nano silica, various methods have been used to obtain silica particles based on physical and chemical approach (see Table 2.3). One of the widely applied methods in producing nano silica particles is sol-gel process due to its ability to form pure and homogenous products at mild conditions (Rahman and Padabettan, 2012). The sol-gel process is a wet-chemical techniques or chemical solution deposition used recently in the fields of materials science and ceramic engineering (Nik et al., 2011). In the market, two types of nano silica are available and are studied by the researchers, namely the colloidal nano silica and powder dry grains nano silica. In most of the studies on nano silica concrete, colloidal NS is used (Hosseini et al., 2009; Nili et al., 2010) and only few researchers reported their studies using powder nano silica.

Table 2.3 Production methods of nano silica

Methods	Production route	References
Sol-gel process	Na_2SiO_4 and organometallics like TMOS/TEOS are added in solvent, and the pH of the solution is changed, reaching the precipitation of silica gel. The reaction kinetics of the process can be controlled by varying the composition of the reaction mixture.	Quercia et al., 2012; Singh et al., 2012; Rahman and Padabettan, 2012; Lazaro and Brouwers, 2010
Vaporization of silica	Reducing SiO_2 in an electric arc furnace with under temperature 1500 to 2000^{o}C.	Quercia, 2010
By-product manufacture	Nano silica with high specific surface area (15 to 25 m^2/g) and main diameter of 150 nm is produced as a by-product of the manufacture of silicon metals and ferro-silicon alloys.	Quercia, 2010
Precipitation method	Nano silica is precipitated from a solution at temperature between 50 to 100^{o}C	Sobolev et al., 2006; Lieftink, 1997; Iler, 1955.

2.4.1.1 Properties of concrete containing nano silica

Nano silica (NS) has recently been introduced as an advanced pozzolan to improve the microstructure and stability of cement-based system (Kawashima et al., 2013). Based on some available results, the beneficial action of the nanoparticles on the microstructure and performance of cement based materials can be explained by the following factors:

1. Nano silica due to its high fineness and reactivity participates in the pozzolanic reactions, resulting in the consumption of CH and formation an "additional" CSH condensed gel. (Sobolev, et al., 2006; Li, 2004; Sadrmomtazi and Fasihi, 2011; Singh, et al., 2012; Gaitero et al., 2006). The reaction process between SiO_2 and CH may be as follows (Qing et al,, 2007):

   $\equiv Si{-}O{-} + H{-}OH \rightarrow \equiv Si{-}OH$ (react quickly)

   $\equiv Si{-} + OH \rightarrow \equiv Si{-}OH$ (react quickly)

   $\equiv Si{-}OH + CH \rightarrow C{-}S{-}H$

   The reaction makes the microstructure denser and very effective in decreasing the permeability of concrete (Bahadori and Hosseini, 2013).
2. Nanoparticles contribute to formation of a dense structure of the aggregates' contact zone, resulting in a better bond between aggregates and cement paste (Sobolev et al., 2006). This matter can be originated from the crystallization effect of nanoparticles which can control the growth of CH and AFm crystals and resulted in making the homogeneous matrix (Bahadori and Hosseini, 2013).
3. Nanoparticles fill the voids between cement grains, resulting in the immobilization of "free" water (Sobolev et al., 2006). The nano silica fills the interstitial spaces of the hardened microstructure skeleton of cement paste and provide denser microstructure, reduced porosity and improved strength (Gaitero et al., 2006; Sadrmomtazi and Fasihi, 2011; Stefanidou and Papayianny, 2012).

There are many studies that have been conducted to investigate the effect of incorporating nanoparticles to mortar and concrete on enhancing its properties. From some conducted experiments, Zhang and Islam (2012) and Jo et al, (2007) reported better performance of concrete containing NS than that containing silica fume. Li

(2004) studied the effect of NS (4% by wt.) on compressive strength of HVFA concrete containing 50% fly ash and observed improvement in both short-term and long-term compressive strength of HVFA concrete. Improved early age compressive strength of HVFA mortars due to addition of NS are also reported by Hou et al. (2013). On the other hand, (Said et al., 2012) reported that at 28 days, the compressive strength was considerably improved for mixtures incorporating 30% Class F fly ash and 6% nano silica. Significant improvement was also observed in terms of reactivity, refinement of pore structure and densification of interfacial transition zone. The chloride permeability and the total porosity results were found significantly lower for mixture containing nano silica.

In another study on durability properties of concrete with nano silica particles have found that nano silica has a very reactive performance in making the binding paste matrix dense and improved the water permeability resistant capacity of concrete (Ji, 2005). Jalal et al. (2012) also found that adding silica fume combined with nano silica in concrete mixtures decreased the chloride ion penetration which could be as a result of more refined microstructure and smaller pores. This view is supported by Ammar (2012) who reported that incorporating both nano silica and silica fume to cement mortar mixtures generally enhanced their mechanical properties. Nano silica mortar also exhibited relatively high early age compressive strength than silica fume when added to cement mortar mixtures.

Some authors have also reported the effect of nano materials on permeability and microstructure improvement of concrete. He and Shi (2008) examined the chloride permeability and microstructure of Portland cement mortar with nano materials admixed at 1% by weight of cement. The results showed that the incorporation of nanoparticles and nanoclay improved the chloride penetration resistance of the mortar, as indicated by the reduced apparent diffusion coefficient by 61.7% when compared to the control specimen.

Khanzadi et al. (2010) also studied the influence of nano silica particles on compressive strength, tensile strength, water absorption and the depth of chloride ion penetration. It was found that both the compressive and splitting strengths of concrete can be enhanced by about 10-16% at 7, 28 and 91 days. In addition, the

microstructure of the nano silica concrete was found uniform and denser than that of reference concrete thus increased the permeability resistance.

Givi, et al. (2010) investigated the particle size effect on the permeability properties of nano silica blended Portland cement concrete. It was concluded that the relative permeability reduction is higher for coarser nano silica after 90 days of moisture curing. However, finer nano silica particles showed better effects in early ages. Similarly, Nik et al. (2011) also found that the incorporation of nano silica particles also improved the water penetration resistance and changed the morphology of cement hydration products.

The shrinkage performance of cementitious binders made with NS, compared to other traditional concreting technologies, is still not known in greater depth at this time. Shrinkage in the concrete matrix is a main contributor of cracks and therefore reduced durability. Robertson (2013) reported about 2–46% lower autogenous shrinkage of cement paste containing NS than control paste. The autogenous shrinkage of paste containing fly ash is also reduced by about 10–45% due to addition of NS this that study. On the other hand, ordinary mortar containing NS showed higher drying shrinkage, compared to the control mortar. This effect was more for high NS addition. However, it can be controlled by carefully adding superplasticizer and by appropriate curing methods (Bjornstrom et al., 2004; Senff et al., 2010)

2.4.2 Nano calcium carbonate ($CaCO_3$)

In recent years nano-$CaCO_3$ has also been introduced in concrete. In general, calcium carbonate can be found in limestone, marble, chalk or produced artificially by combining calcium with CO_2 (Camiletti, 2013). It can also be produced by precipitation from saturated sodium carbonate and calcium nitrate aqueous solutions (Babou-Kammoe et al., 2012). Although the use of calcium carbonate was first considered as filler to partially replace cement or gypsum, some studies have shown some advantages of using $CaCO_3$ in terms of strength gain, accelerating effect and economic benefits as compared to cement and other supplementary cementitious materials.

2.4.2.1 Properties of concrete containing nano calcium carbonate

Some studies have suggested a potential benefit of physical properties of calcium carbonate on the development of cementitious system. In terms of durability properties, it was revealed that replacement of PC with limestone had significant effect on the resistance of sulphate attack and water absorption which related to the filler effect, heterogeneous nucleation and the dilution effect of limestone powder (Ramezanianpour et al., 2010). Elsewhere, Sato and Beaudoin (2011) carried out a number of investigations on the incorporation of micro- and nano-$CaCO_3$ materials with high volume of supplementary cementitious materials. In this experiment, cement was replaced with 50% of fly ash (series one) and 50% of slag (series two) and incorporated with 10 and 20% of micro- and nano-$CaCO_3$ by weight of binders. It was found that replacement of cement with nano-$CaCO_3$ accelerated the early hydration of cement and enhanced the early development of modulus elasticity as the amount of nano-$CaCO_3$ was increased. The presence of nano-$CaCO_3$ particles has been suggested to have a significant effect on the hydration kinetics of C_3A and C_3S which may cause acceleration of setting and early strength development.

In another study, Sato and Diallo (2010) reported the seeding effect of nano-$CaCO_3$ where the rapid growth of CSH can be obtained by the access of nano-$CaCO_3$ on the surface of the C_3S particles. As a consequence of the formation of a higher volume of hydrates, the increase in hydration degree compensates the dilution effect of the binder thus develops higher initial strengths (Goergescu, 2009). This view is supported by Kawashima et al., (2013) who provided a basis for understanding the mechanical properties of high volume fly ash when incorporated with calcium carbonate nanoparticles. It was shown that the 5% $CaCO_3$ with 30% fly ash-cement paste samples tested at 1, 3 and 7 days showed progressive development in the compressive strength compared to control fly ash-cement paste. It is also suggested that fly ash with high aluminate content can introduce addition aluminates to the system thereby decreased the SO_3/Al_2O_3 ratio and amplified the impact of the limestone powder on the hydration products (De Weerdt et al., 2011).

Early work by Camiletti et al. (2013) investigated the research on ultra-high-performance concrete containing single and combination of micro- and nano-$CaCO_3$. These concretes have 0, 2.5, 5, 10 and 15% micro-$CaCO_3$ and 0, 2.5 and 5% nano-$CaCO_3$ as partial replacement of cement. From this study, it was reported that

$CaCO_3$ particles in blended cement concrete exploited the beneficial characteristics in producing higher density and "well-formed" microstructure. The compressive strength of concrete with 2.5 or 5% nano- and 0% micro $CaCO_3$ gained highest 24-h compressive strength results compared to other mixes. However, the highest 28 days compressive strength was achieved by 0% nano- and 2.5% micro-$CaCO_3$ and indicated the extent of hydration at early ages was influenced by the finer particles of $CaCO_3$. In a study related to the performance of limestone in high volume fly ash concretes, it was found that the limestone provided additional surfaces for the nucleation and growth of reaction product thus accelerated and amplified the early age hydration. At later ages it participates in the reaction of the aluminate phases, leading to the production of carboaluminate hydrates (Tanesi et al., 2013). This supports the results found by Guemmadi et al (2009) who reported the fineness of limestone fines plays a considerable role in the improvement of mechanical performances of the concrete due to the formation the new compounds such as carboaluminates.

2.4.3 Dispersion of nanoparticles

Method of applying the nanoparticles as a supplementary cementitious material has been an issue, as they are highly agglomerated when mixed with water. This is mainly because of nano particle has a very high surface area, therefore, has a tendency to form agglomeration when it cannot be dispersed uniformly. The excessive amount of nano silica particles could deteriorate its efficiency and block the surface to react with other hydration products, thus low compressive strength is expected (Morsy et al., 2010). The forces that form permanent attachment when two particles come into close contact with one another are known as Van der Waal's forces (Venkataraman, 2002). These forces must be broken to break the particles in an aggregate part. Sobolev et al. (2006) in his study commented the positive effect of well-dispersed nanoparticles as follows:

1. Well-dispersed nanoparticles may exhibit relatively high viscosity then becomes important in improving good resistance to segregation and workability of the system.
2. Well-dispersed nanoparticles compensates for the acceleration of hydration.

In order to obtain better dispersion of nanoparticles, some methods from previous study have been proposed. Konsta-Gdoutos et al. (2008) found that the application of ultrasonic energy with the use of surfactant were effectively dispersed the nanoparticles on cement paste reinforced with carbon nanotubes. The ratio of surfactant to carbon nanotubes was suggested to lie within the range from 4.0 to 6.25.

Another study by Elkady and Serag (2013) also found that the use of sonication and superplasticizer as dispersing agent on nano silica particles helped increasing the concrete workability and showed significant performance in increasing the compressive strength of concrete by 26%. When the de-agglomeration method was evaluated, it was reported that the use of 5 minute sonication showed as significant effect on dispersion nano silica particles. The compressive strength of nano silica concrete was reached 23% higher compared to control concrete. In the same view, Arefi et al. (2011) studied the homogenous dispersion of nano- and micro-silica particles on mechanical properties of cement mortar. The nano silica was prepared by mixing the distilled water and stirred for 6-10 hours by rotational speed of 250-300rpm. The superplasticizer was mixed with the silica particles and the cement was added to the mixture simultaneously. Based on the mechanical properties (tensile, compressive and flexural strengths) of mortar, it was concluded that the homogenous dispersion of the smaller nanoparticles sizes is more difficult than the larger nanoparticles. This is resulted from the fact that smaller nanoparticles have higher specific surface area compared to the larger nanoparticles.

On the other hand, previous study from Martinez-Velandia et al. (2011) showed the results on the effect variation of the sonication power level on the mechanical properties of silica fume mortars. It was observed that the compressive strength of cement mortars substituted with 10% silica fume increased as the sonication power level was increased at the constant sonication time of 20 min. Moreover, the effect of sonication times between 5 and 25 min was also observed based on the thermogravimetric analysis. The increased of sonication time was found effective in increasing the percentage of hydrated lime fixation from 29.4% to 48.1%. While some previous studies reported the advantage in using sonication method (Islam, 2011), there are still some major barriers to overcome in finding the best method for proper dispersion of nanoparticles.

2.5 Durability properties of concrete

Durability of cement concrete is defined as the ability of concrete to resist from any deterioration including chemical attack, abrasion, moisture movement, internal volume change etc. In this process, it is important to determine the basic requirement to limit the degradation to acceptable levels during the design life of structure.

In concrete, the durability characteristics are greatly influenced by the quality of the hydrated cement paste including the influence of w/c ratio, total porosity, the structure of the interfacial transition zone and the presence of supplementary cementing materials. A brief description of durability properties such as permeability, chloride diffusion and the corrosion of steel in concrete are given below.

2.5.1 Permeability

Permeability is defined as the property that governs the rate of flow of a fluids into a porous solid (Mehta and Monteiro, 2006). It also refers to the ability of concrete to resist penetration by water or other substances (liquid, gas, or ions) (Kosmatka et al, 2003). In the water transport process, water will move in the pore and crack systems of concrete due to pressure difference. When cracks occur, the deterioration process is accelerated due to the increase of the formation of transport properties of concretes. In concrete, the higher water/cement ratio becomes the fundamental cause of higher permeability (Shetty et al., 2011). Moreover, the permeability of concrete also depends on mix proportions, proper compaction, curing and on microcracks caused by the ambient temperature and humidity cycles (Mehta and Monteiro, 2006).

The most important parameter that influence the water and ion transport is the structures of the pores particularly the pore volume, pore size distribution, connectivity and shape of the pores in the microstructure of the concrete (Ma et al., 2013). Generally, the pores in hardened Portland cement paste can be Classified into two categories as shown in Table 2.4 (Mindess et al., 2003). It can be seen that capillary voids larger than 50 nm, referred to as macropores which is more influential in determining the strength and impermeability characteristics, whereas voids smaller than 50 nm, referred to as micropores, play an important part in drying shrinkage and creep. A reduction in the volume of large capillary voids (e.g., >100 nm) in the paste matrix is necessary to reduce the permeability (Mehta and Monteiro, 2006).

The most widely used for the study of pore structure characteristics of cement-based materials is mercury intrusion porosimetry (MIP). This analysis is used to determine the quantity of mercury that is forced into the pores of the material at different pressures. This technique then measures the pore system whether continuous or discontinuous by applying pressures and intrusion volume during the experiment. If the pore system is continuous, a pressure may be achieved at which mercury can penetrate the smallest pore necks of the system and penetrate the bulk sample volume. If the pore system is not continuous, mercury may penetrate the sample volume by breaking through pore walls (Cook, 1999). Through the MIP analysis, the decrease in total capillary porosity can be determined and the porosity of cementitious systems can be correlated with the strength and the resistance of concrete to durability concerns.

Table 2.4 Classification of pores in hardened Portland cement paste (Mindess et al., 2003)

Category	Size	Description	Effect on the concrete properties
Capillary pores	50 nm - 10µm 10 – 50 nm	Macropores Large mesopores	Permeability, diffusivity Permeability in the absence of macropores, shrinkage above 80% RH (relative humidity)
Gel pores	2.5 – 10 nm 0.5 – 2,5 nm < 0.5 nm	Small mesopores Micropores Interlayer spaces	Shrinkage between 80% RH and 50% RH Shrinkage at all RH, creep

2.5.2 Chloride diffusion

Another important factor of permeation capacity in concrete involves measurement of chloride ions. Chlorides can diffuse into concrete as a result of sea salt spray and direct sea water wetting, deicing salts and use to chemicals (structure used for salt storage, brine tanks, aquaria, etc) (Broomfield, 1997). When chloride ions penetrate into the interstitial solution, the ions can be chemically bounded by unhydrated C_3A to form Friedel's salt or monochloroaluminates ($3CaO.Al_2O_3.CaCl_2.10H_2O$) and modify the microstructure of concrete (Aitcin, 1998). While most of the chloride ions in hardened concrete are chemically combined, a smaller number are soluble in water and free to contribute corrosion (Bola, 2000). However, chloride transport in concrete is a rather complicated process, which involves ion diffusion, capillary

suction and convective flow with flowing water, accompanied by physical and chemical binding. In addition, changes in temperature and weather condition introduce different process of chloride transport. From previous studies, the safe limits on the chloride content of concrete members are determined, and are presented in Table 2.5. It is defined as the concentration at which corrosion is initiated, independent from any damage to the structure.

Table 2.5 Limits for water-soluble chloride-ion content in concrete (ACI 318)

Type of concrete member	Maximum water-soluble chloride ion content, percent by weight of cement
Prestressed concrete	0.06
Reinforced concrete exposed to chloride	0.15
Reinforced concrete that will be dry of protected from moisture	1.00
Other reinforced concrete construction	0.30

Diffusion is the predominant transport mechanism of chloride in concrete. It is the movement of a substance under a gradient of concentration or, more strictly speaking, chemical potential, from an area of high concentration to an area of low concentration (Luping et al., 2012). The diffusion of chloride will be through the water in the capillary pores, therefore, the denser the pores, the slower the chloride diffusion rate. Its theory is mainly according to the mathematical models by Adolph Eugen Fick or also known as Fick's law (Poulsen and Mejlbro, 2006). Fick's second law of diffusion is a differential equation that describes how the concentration of a diffusing species varies with time. It simply says that the change in chloride content per unit time is equal to the change of flux per unit length. For one-dimensional diffusion, the differential equation is as follows:

$$\frac{\partial C\ (x,t)}{\partial t} = D_a\ \frac{\partial^2 C(x,t)}{\partial x^2} \tag{2.9}$$

From a dimensional analysis, it can be shown that the diffusion coefficient, $D_{a,}$ has units of length^2/time. The chloride penetration distance is measured in mm and exposure time in in terms of years. If it is assumed that there is one-dimension diffusion and that the chloride ion content at the surface is constant, a solution to Fick's second law is as follows (Luping et al., 2012).

$$C\,(x,t) = C_s - (C_s - C_i)\; erf\left[\frac{x}{2\sqrt{D_a t}}\right] \quad (2.10)$$

Where,

$C(x,t)$ = the chloride ion concentration at a depth x in mm from the exposed surface for an elapsed time t in years since the start of chloride exposure

C_s = the chloride concentration at the surface, expressed as a % of concrete mass

C_i = the initial (or background) chloride concentration of the concrete, expressed as a % of concrete mass

erf = the error function (a special function related to the integral of a normal probability function)

D_a = the chloride diffusion coefficient in mm^2/year

The model for chloride ingress due to diffusion as mentioned in Equation 2.10 is used to predict diffusion of chlorides into concrete and to estimate the depth of cover of concrete that will prevent the critical concentration of chloride ions diffusion to the depth of the reinforcing steel during the design life of the structure.

2.5.3 Corrosion of steel in concrete

The chloride content, the access of oxygen to the steel and the resistivity of the environment are some factors influencing the corrosion rate. Due to the porosity of concrete, O_2 can easily diffuse into concrete, becoming dissolved in the pore solution and finally reaching the surface of steel (Song and Shayan, 1998). The process of corrosion-induced deterioration starts with the loss of protection by the concrete cover and then followed by corrosion initiation and propagation.

Chen and Mahadevan (2008) described the chloride-induced reinforcement corrosion process in reinforced concrete into three phases as seen in Figure 2.5. The first phase is characterized by the chloride penetration, during which the chloride diffuses gradually from the concrete surface through the concrete cover towards the reinforcement. Chloride acts as catalyst to corrosion where it breaks down the passive layer of oxide on the steel rebars and corrodes them rapidly. When the chloride content at reinforcement reaches a threshold value to initiate the corrosion process at time ($t_{initiation}$), the second phase is assumed to begin. The second phase is dominated by the reinforcement rust expansion, during which the rust (i.e., the corrosion products) accumulated in the concrete-steel ITZ. Once voids in ITZ are

occupied completely with the rust at time (t_{stress}), further rust accumulation will trigger expansive stress and then cracking in the surrounding concrete, which indicates the start of the third phase. During the third phase, the rust expansion-induced cracks propagate in concrete surrounding the reinforcing steels (see Figure 2.6) until some critical failure mode, such as the spalling or delamination of concrete cover, occurs at time ($t_{spalling}$). The accelerated corrosion process ends up by the spalling of concrete cover resulting from the expansive forces from the formation of rust.

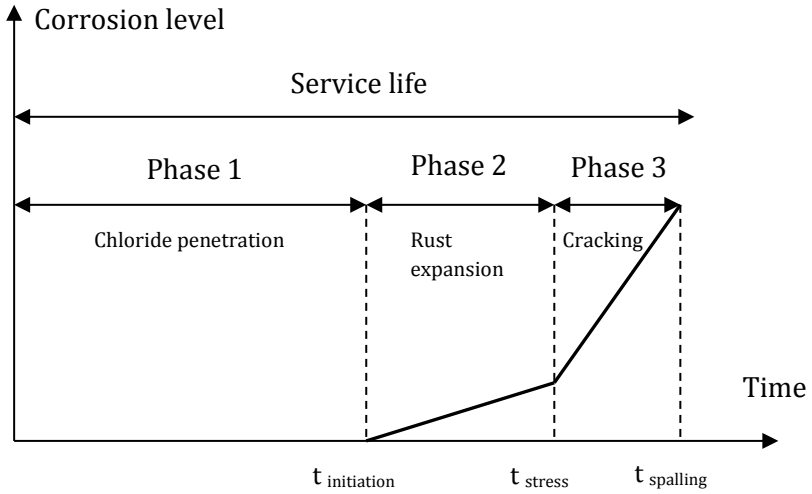

Figure 2.5 Chloride-induced reinforcement corrosion phases

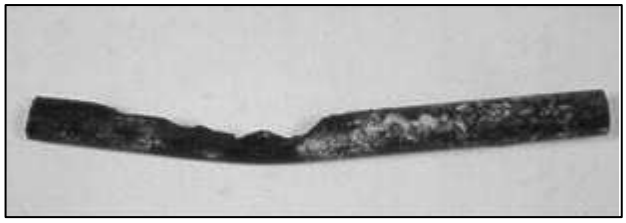

Figure 2.6 Pitting on a corroded rebar (Page, 2007)

In order to increase the resistance of concrete to chloride or carbon dioxide, some methods have been considered such as using of low water-cement ratio, at least seven days moist curing, and the use of supplementary cementitious materials to limit the initiation of corrosion for no significant damage to occur (Shi, 2011; Guneyisi et al., 2013). Increasing the concrete cover over the steel also helps down the migration of chlorides (Liu, 1996). Other methods of reducing steel corrosion include the use of corrosion inhibiting admixtures (Goodwin et al., 2000), epoxy-

coated reinforcing steel (ASTM D 3963 or AASHTO M 284), surface treatments (Lisa et al., 2008), concrete overlays, and cathodic protection (Kepler et al., 2000) have been intensively discussed.

2.6 Microstructure and phase identification techniques

2.6.1 Scanning electron microscopy

Scanning electron microscopy is commonly used to investigate the microstructure of the materials. This technique is capable in producing images of various samples and the chemical composition of hydration phases. Three commonly used types of images are secondary electron imaging which generally provides topographical information, backscattered electron imaging which gives compositional contrast based primarily on atomic mass and X-ray mapping which provides information regarding to the compositional analysis in terms of the amounts of the specific elements present (Detwiller et al., 2001). The high resolution of the SEM can be used to study the hydrated cement paste in concrete or mortar.

2.6.2 X-ray diffraction

X-ray diffraction is one of the established methods in determining, estimating and quantifying the structure of unhydrated and hydrated phases of cement based on the diffraction pattern. In the analysis, diffraction methods is used to determine the crystalline structures, the phase quantitative and qualitative analysis and the study of phase transformation, the study of crystallographic texture, the size of the crystallites, the internal stresses in the sample (Elena and Manea, 2012). The various hydration products such as quartz, ettringite, calcium silicate, monosulfoaluminate, portlandite, calcite, larnite, etc., can be determined by using this analysis.

2.6.3 Thermogravimetric analysis

Differential thermal analysis (DTA) and thermogravimetric analysis (TGA) have been used for both qualitative and quantitative work in cement chemistry. The DTA/TGA methods allow for the performance of the following studies: exothermic or endothermic reactions caused by reactions such as crystal inversion, dehydration, decomposition, oxidation, reduction, chemical reactions, and destruction of lattice (Ramachandran, 1995). Basically, the sample for this technique is prepared isothermally with respect to an inert material by supplying heat to the sample or inert material from ambient ~ 1000°C. The heat energy required to maintain isothermal

conditions is recorded as a function of time or temperature. The quantitative analysis on the proportion of some phases present such as ettringite and calcium hydroxide can be determined.

2.6.4 Nano indentation

Nano indentation analysis is used for the determination of mechanical properties of homogenous and heterogeneous materials. In the area of cement phase, the main of the analysis is to obtain the hardness, elasticity and volume fractions of the various phases which are responsible for the strength and durability of cement paste. The phases are grouped into anhydrous particles and three forms of calcium silicate hydrate (CSH) – namely, low stiffness (LS), medium stiffness (MS), and high stiffness (HS) of C-S-H (Jha et al., 2012). It was suggested that the low density and high density C-S-H exist in hydrated Portland cement with a volume of fraction of 30 and 70%, respectively (Alizadeh, 2009). Moreover, the nano indentation of the cement paste can result in identifying another cement paste phases including calcium hydroxide (CH), ettringite, pores and un-hydrated cement. Based on the various nano indentation results from previous studies, the means stiffness of each phase is reported in Table 2.6. It is critical to note that the mechanical properties of LD C-S-H and HD C-S-H are independent of the mix design, they are inherent properties of the C-S-H phases themselves (Dejong, 2005).

Table 2.6 Nanoindentation modulus and hardness of different phases of cement paste

Phase	M (GPa)	H (GPa)	Volume fraction	Comment	Reference
LD C-S-H	20 ± 2	-	-	-	Acker (2001)
	21.7 ± 2.2	-	0.66	w/c=0.5; 1 year	Constantinides et al, 2003; Constantinides and Ulm, 2004
	19.7 ± 2.5	0.55 ± 0.03	-	w/c=0.5	Sorelli et al (2008)
	15 to 20	-	-	w/c=0.5; 28 days	Shah et al, 2009
	23.7 ± 5.9	0.68 ± 0.18	-	w/c=0.3; 28 days	Vandamme, M, and Ulm, F.-J, (2009)
	16.5 ± 4.7	-	0.63	w/c=0.5; 1 month	Mondal et al, 2010
	24.84 ± 3.62	0.88 ± 0.13	0.68	w/c=0.4; 7 days	Howind et al, 2014
HD C-S-H	31 ± 4	-	-	-	Acker (2001)
	29.4 ± 2.4	-	0.33	w/c=0.5; 1 year	Constantinides et al, 2003; Constantinides and Ulm, 2004
	34.2 ± 5.0	1.36 ± 0.35	-	w/c=0.5	Sorelli et al (2008)
	20 to 25	-	-	w/c=0.5; 28 days	Shah et al, 2009
	36.1 ± 3.4	1.01 ± 0.16	-	w/c=0.3; 28 days	Vandamme, M, and Ulm, F.-J, (2009)
	27.1 ± 3.5	-	0.19	w/c=0.5; 1 month	Mondal et al, 2010
	32.92 ± 3.36	1.21 ± 0.20	0.17	w/c=0.4; 7 days	Howind et al, 2014
CH	36 ± 3	-	-	-	Acker, 2001
	38 ± 5	-	-	Indentation on single CH crystal	Constantinides et al, 2003; Constantinides and Ulm, 2004
	36.9 ± 3.5	-	0.08	w/c=0.5; 1 month	Mondal et al, 2010
	40.52 ± 2.14	1.66 ± 0.08	0.02	w/c=0.4; 7 days	Howind et al, 2014

2.6.4.1 Principle of nanoindentation

In nano indentation, force and displacement (i.e. penetration depth) are monitored in the apparatus. During the process, an indenter is pushed into a sample while force applied by the indenter is plotted continuously with the displacement of the indenter into the sample (load-indentation plot or also called p-h plot) with a prescribed loading and unloading profile (Schuh, 2006). Miller et al. (2007) defines the nano indentation techniques as a process of making contact between a sample and an indenter tip of known geometry and mechanical properties, followed by a continuously applied and recorded change in load (P) and depth (h). The schematic diagram of nano indentation equipment is shown in Figure 2.7.

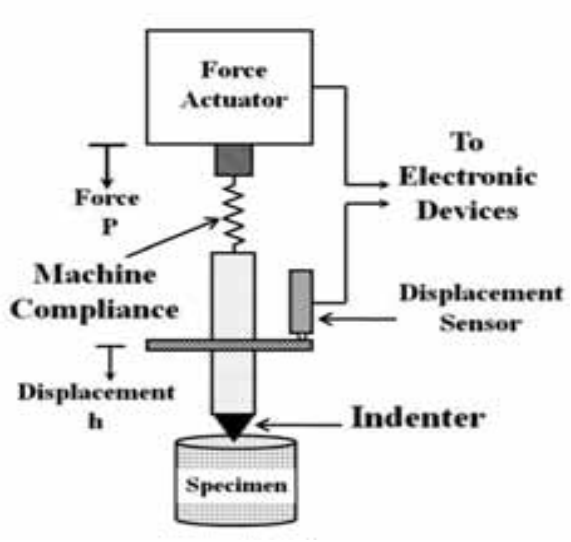

Figure 2.7 Schematic diagram of nano indentation equipment (Jha et al., 2012)

Figure 2.8 shows a typical representation of the indentation load versus depth curves. It is composed of a loading and unloading response (Constantinides et al., 2003). In Figure 2.8, $P_{\max}$ is the maximum indentation load and h_t and h are nanoindentation depths corresponding to the applied load obtained from the nanoindentation test. The slope of the unloading curve can be used as a measure of the elastic properties of the material. The analysis of the *P-h* curve proceeds by applying a continuum scale model to derive an indentation modulus (*M*) and hardness (*H*) based on the equation (2.11) and (2.12).

$$M = \frac{\sqrt{\pi}}{2}\frac{S}{\sqrt{A_C}} \tag{2.11}$$

$$H = \frac{P_{max}}{A_c} \tag{2.12}$$

Where S $(dP/dh)_{h=hmax}$ is the unloading indentation stiffness or the slope of the upper portion of the unloading curve during the initial stages of unloading (Oliver and Pharr, 2003) and A_c is the projected contact area estimated from the maximum penetration depth (h_{max}) using the Oliver and Pharr method, which is described in the next section.

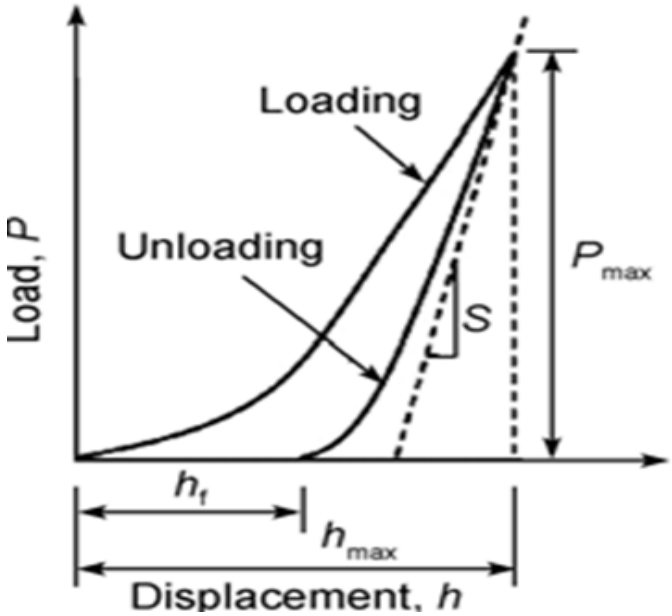

Figure 2.8 Typical representation of the indentation load versus depth curves (Jiande et al., 2012)

The most common types of indenters which are more commonly applied in nano indentation technique are pyramidal indenters, which are the four-sided Vickers indenter and the three-sided Berkovich indenter. Pyramidal indenters are generally treated as conical indenters with a cone angle that provides the same area to depth relationship as the actual indenter in question (Mondal, 2008). This allows the use of convenient axisymmetric elastic solution. The images of different indenter tip are shown in Figure 2.9.

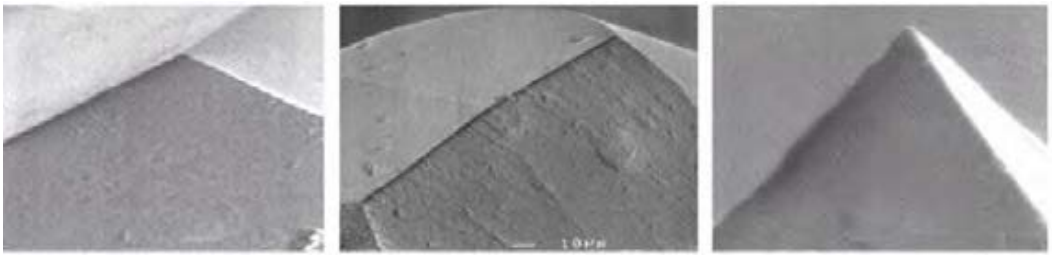

(a) (b) (c)

Figure 2.9 Images of different indenter tip: (a) Berkovich (b) Cono-Spehrical (c) Flat-Ended (Fischer-Cripps and Anthony, 2002)

2.6.4.2 Oliver and Pharr method

The method of the indentation analysis is based on analytical solutions proposed by Oliver and Pharr in 1992. This accounts the procedure to determine the contact area based on the depth of indentation and indenter shape function. Figure 2.10 shows the cross-section through an indenter during indentation testing.

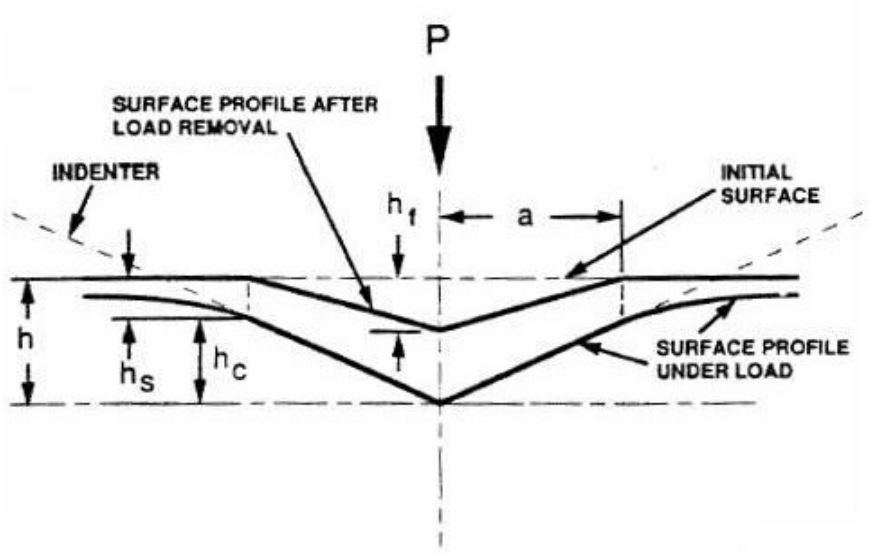

Figure 2.10 Cross-section through an indenter (Nemecek, 2005)

During loading the total displacement h is written as $h = h_c + h_s$ where h_c is the vertical distance along which contact is made (contact depth), h_s is the displacement of the surface at the perimeter of the contact. At the peak load (P_{max}), displacement is h_{max} and the radius of contact circle is α. During unloading, elastic displacement is recovered and the final depth of the residual hardness impression once the indenter is fully withdrawn is h_f.

The projected contact area, A is determined as a function of the contact depth (h_c):

$$A = F\,(h_c) \tag{2.13}$$

where the form of the function F has to be established prior to the analysis of data on the sample of interest.

From Figure 2.9, $$h_c = h_{max} - h_s \tag{2.14}$$

and for conical indenter

$h_s = \frac{(\pi - 2)}{\pi}\ (h - h_f)$ and $(h - h_f) = 2\,\frac{P}{S}$

(2.15)

Combining these two equations at peak load, one can obtain:

$h_s = \varepsilon \frac{P_{max}}{S}$ and $\varepsilon = \frac{2}{\pi}(\pi - 2) = 0.72$ (2.16)

where ε is the geometric constant. From similar analysis, ε = 1 for a flat punch and ε = 0.75 for a paraboloid of revolution. So, for flat punch, $h_s = \frac{P_{max}}{S}$ and the contact depth h_c is obtained by the intercept of the initial unloading slope with the displacement axis. Once the contact area is determined, the modulus and hardness as mentioned on Equations 2.11 and 2.12 are obtained.

2.6.4.3 Grid indentation

Due to the high heterogeneity of cement paste at the nano- and micro-scale, applying the grid indentation technique is a challenge, as it is difficult to choose to indent on a specific material phase with sufficient repeatability (Miller et al., 2008). Therefore, it is necessary to perform large grids of indentation on heterogeneous samples, such as cement paste (Jha et al., 2012).

The deconvolution technique consists of fitting the experimental probability density function (PDF) of the measured indentation modulus (M) and indentation hardness (H), to the sum of model-phase PDFs (Sorelli et al, 2008):

$$\min P(x) = \sum_{i=1}^{N} \sum_{\mathrm{X=(M,H)}} \left(\sum_{j=1}^{n} f_j D\,(X_i; \mu_j^X, S_j^X) - P(x_i) \right)^2$$

subjected to

$\sum_{j=1}^{n} f_j = 1$ (2.17)

Where μ_j and S_j are the mean and standard deviation of $x = (M, H)$ of the phase $J = 1, n; f_J$ is the volume fraction of the phase composing the heterogeneous material; $P(X_i)$ is the measured value of the normalized frequency; m is the number of intervals (bins) by which the problem is discretised; and P_j is the value of the theoretical probability density function of the single phase, which is assumed to be a normal distribution:

$$P_j = \frac{2}{\sqrt{2\pi S_{j^2}}} \exp\left(\frac{-(x-\mu_j)^2}{2S_{j^2}}\right) \quad (2.18)$$

Where μ_j and $S_j(H)$ stand for mean and standard deviation, respectively. The minimization of Equation 2.17 is done simultaneously for the frequency distribution of the indentation modulus *M* and the hardness *H*. The results of the deconvolution technique are the mean and standard deviation of the indentation modulus and hardness, and the volume fraction for each phase, i.e., $\{\mu_j(x), S_j(x), f_j\}$, of $x = (M, H)$, for $j = 1, n$. In addition, to identify statistically relevant phase properties with a sufficient contrast, the overlap of successive Gaussian curves representative of two phases is constrained by:

$$\mu_j^x + S_j^x < \mu_{j+1}^x + S_{j+1}^x \qquad x = (M, H) \quad (2.19)$$

The results of the deconvolution technique are estimates of the *n* x 5 unknowns $\{\mu_j^M, S_j^M, \mu_j^H, S_j^H, f_j\}, j = 1, n$; that is, the mean and standard deviation of indentation modulus and hardness for each mechanical phase, and the volume fractions.

2.7 Summary

Due to the new potential uses of nano silica and nano calcium carbonate, there is a growing global interest in the investigation of their influence in construction materials especially in short-term and long-term properties of concrete. According to the literature reviews, several experimental results on the use of nano particles in OPC concrete have been reported. However, little laboratory data exists on the effects of nano silica and nano calcium carbonate in high volume fly ash mortar and concrete. In addition, in the above studies the use of the amount of nano silica and nano calcium carbonate varied significantly among researchers and no optimum content of those nano particles are also reported. Moreover, the effect of nano silica and nano $CaCO_3$ on durability properties of HVFA concretes are not thoroughly studied. Therefore, in order to promote the sustainability of HVFA concrete by incorporating nano particles thorough investigation on the performance of HVFA concretes containing nano particles on mechanical and durability properties is needed. The

results obtained can lead to contribute the application of nano silica and nano CaC03 particles including the optimum dosage and their effectiveness to overcome the deficiency of the use of high volume fly ash in concrete, and also confirm that nano particles is adequate for design purposes and has major advantage over other supplementary cementitious materials.

CHAPTER III

METHODOLOGY

3.1 Introduction

This chapter describes the type of materials, mix proportions and the methods used to measure various properties of concrete. Details of various tests methods based on the objectives of each investigation are also included in this chapter. This chapter also describes the test methods and analysis for compressive strength of mortars and concretes containing nano silica and nano calcium carbonate and the durability properties of concretes such as water sorptivity, volume of permeable voids, porosity, chloride permeability, chloride diffusion and accelerated corrosion tests. The test methods and analysis confirmed to those specified by American Society for Testing and Materials (ASTM) standards. A brief description of the concept for microstructure and phase identification techniques such as backscattered electron (BSE) image analysis, x-ray diffraction (XRD), thermogravimetric (DTA/TGA) analysis and nano indentation technique is also explained.

3.2 Properties of materials

Ordinary Portland cement type I (PC), Class F fly ash (FA), nano silica (NS) and nano calcium carbonate (NC) are used in this study. Figure 3.1 shows the physical appearance of cement, fly ash, nano silica and nano calcium carbonate. The chemical analysis and physical properties of all used materials are listed in Table 3.1.

Figure 3.1 Physical appearance of cement, fly ash, nano silica and nano calcium carbonate

Table 3.1 Physical properties and chemical compositions of Ordinary Portland cement (OPC), Class F fly ash (FA), nano silica (NS) and nano calcium carbonate (NC)

Chemical Analysis	OPC (wt. %)	Class F Fly Ash (wt. %)	Nano Silica (wt. %)	Nano $CaCO_3$ (wt. %)
SiO_2	20.2	51.80	99	-
Al_2O_3	4.9	26.40	-	-
Fe_2O_3	2.8	13.20	-	0.02
CaO	63.9	1.61	-	97.8
MgO	2.0	1.17	-	0.5
MnO	-	0.10	-	-
K_2O	-	0.68	-	-
Na_2O	-	0.31	-	-
P_2O_5	-	1.39	-	-
TiO_2	-	1.44	-	-
SO_3	2.4	0.21	-	-
Physical Properties				
Particle size	25 - 40% ≤ 7 µm	40% of 10 µm	25 nm	15 – 40 nm
Specific gravity	2.7 to 3.2	2.6	2.2 to 2.6	-
Surface area (m^2/g)	-	-	160	40
Loss on ignition (%)	2.4	0.5	-	-

3.2.1 Ordinary Portland cement

In this research, the ordinary Portland cement type I, manufactured by Swan Cement was used to produce the mortar and concrete. As shown in Table 3.1, the specific gravity of cement was 2700 – 3200 kg/m^3 and 25 – 40% of particles are ≤ 7µm size. Based on the XRD spectra, cement consists mainly of calcium silicate (Ca_3SiO_5), calcite ($CaCO_3$) and larnite (Ca_2SiO_4) (see Figure 3.2).

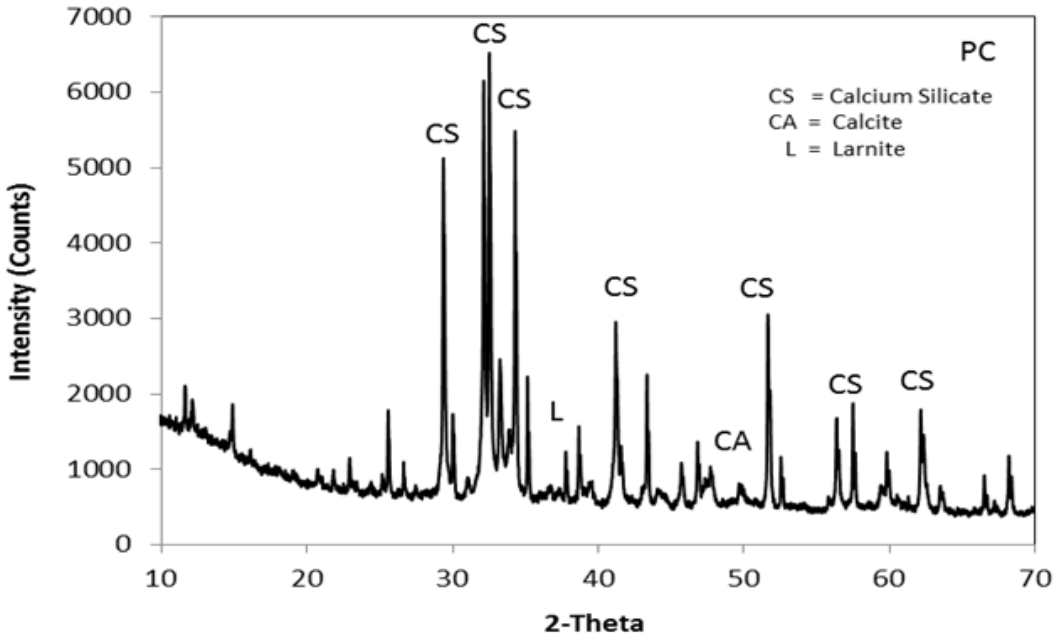

Figure 3.2 XRD spectra of Portland cement

3.2.2 Class F fly ash

The fly ash was sourced from Collie power station of Western Australia. It is classified as Class F as it has low lime content and the total sum of the silica, alumina and iron oxide is greater than 70% and satisfied the ASTM C618 standard. This product contains 100% fly ash (approximately 40% of particles in the bulk material are in the respirable dust fraction), consisting of 10-30% mullite, 9% crystalline silica (as Quartz-SiO_2) and 30-60% amorphous silica.

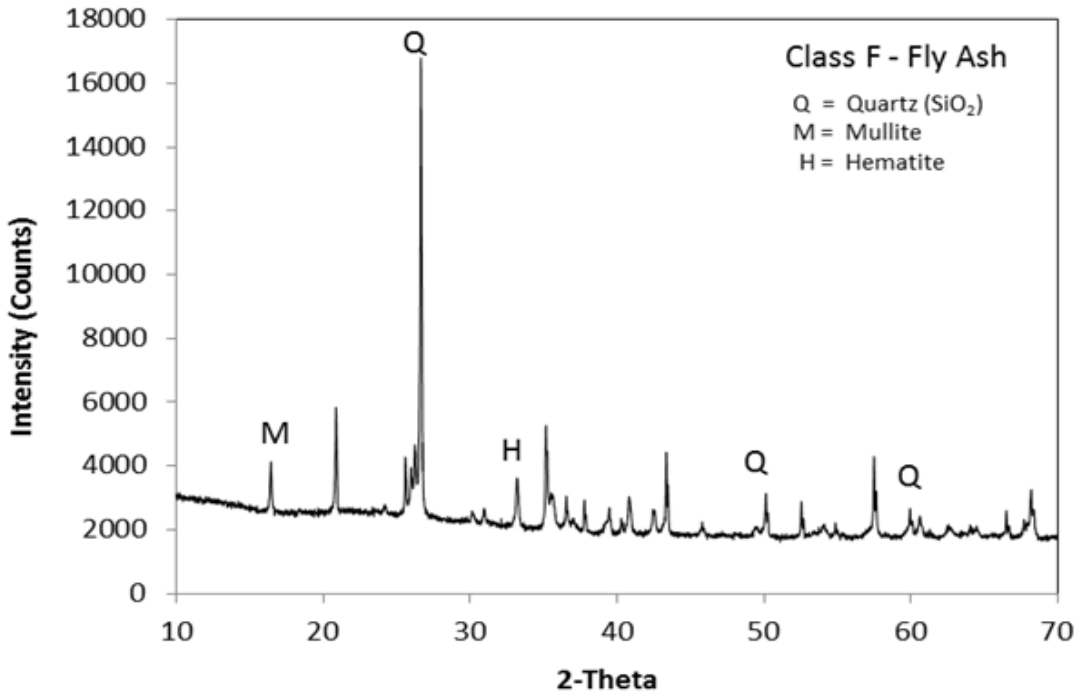

Figure 3.3 XRD spectra of Class F fly ash

3.2.3 Nano silica

The nano silica is obtained from Nanostructured and Amorphous Materials, Inc. of USA with average particle diameter of 25 nm and of spherical morphology (see Figure 3.4). Chemically, nano silica is composed mainly of SiO_2 (99%). The XRD spectra of nano silica indicates that the NS is amorphous material and is relatively less crystal than PC and FA (see Figure 3.5).

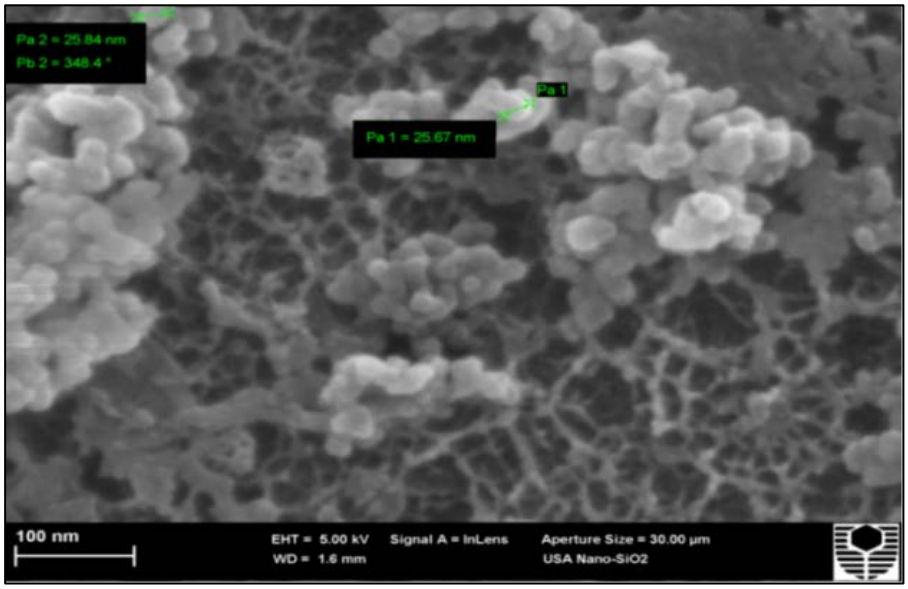

Figure 3.4 SEM image of nano silica

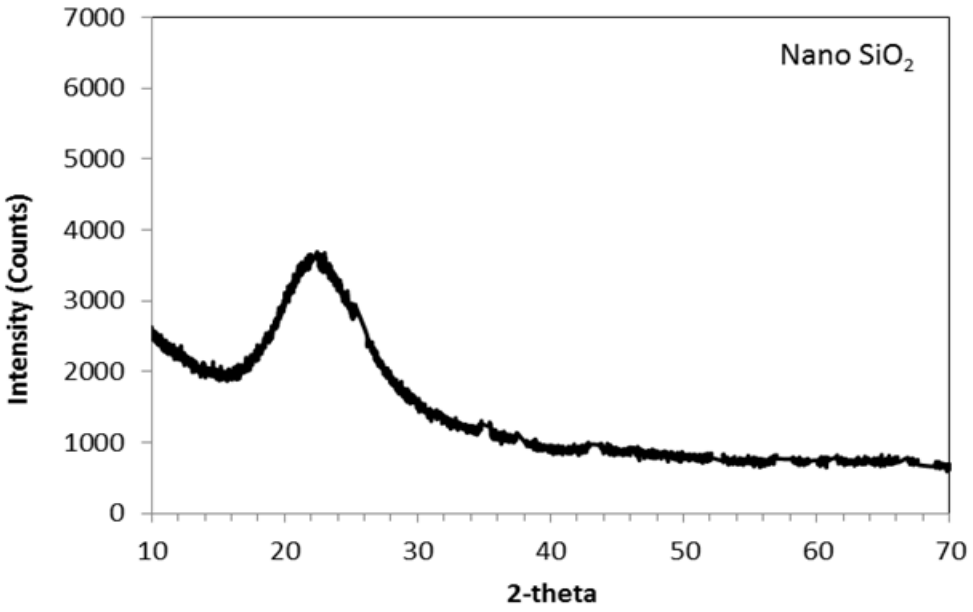

Figure 3.5 XRD spectra of nano silica

3.2.4 Nano calcium carbonate

The commercially available dry nano-$CaCO_3$ powder was used. Figures 3.6 and 3.7 show the SEM image and XRD spectra of nano-$CaCO_3$, respectively. The nano-$CaCO_3$ is white in color with size of 40-50 nm and has cubical morphology (see Figure 3.6). It also contains mainly 97.8% CaO as can be seen in Figure 3.7.

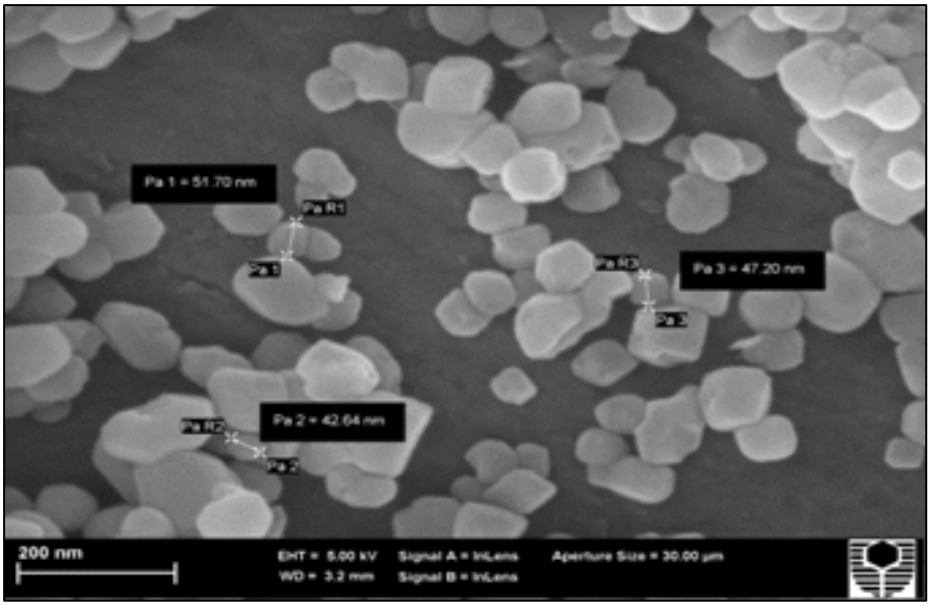

Figure 3.6 SEM image of nano calcium carbonate

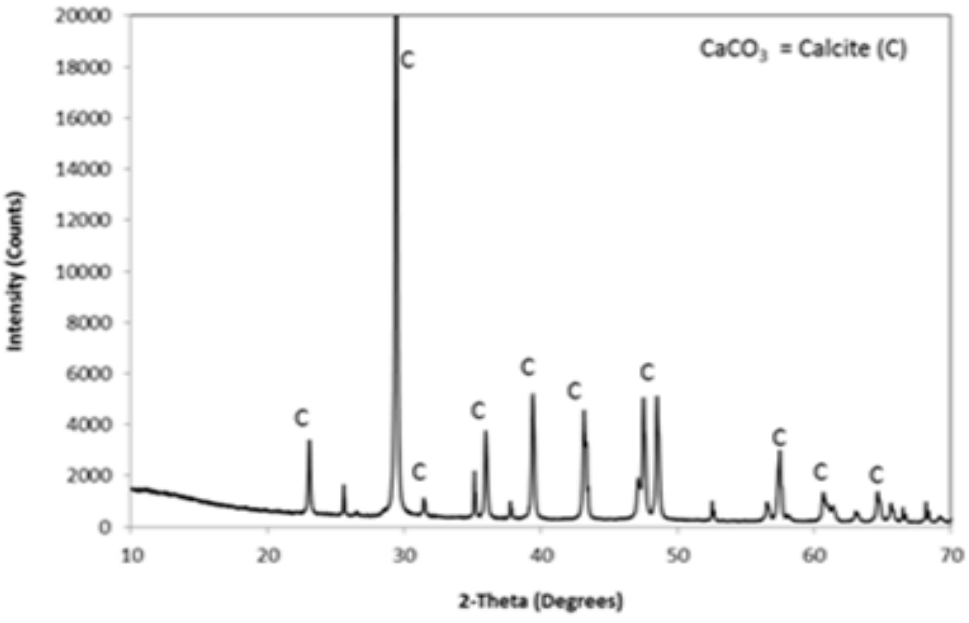

Figure 3.7 XRD spectra of nano calcium carbonate

3.2.5 Fine aggregates

Natural sand with fineness modulus of 1.9 and specific gravity of 2.2 g/cm^3 according to ASTM C128 standard was used as a fine aggregate for mortar and

concrete mixtures. The fine aggregates were treated to achieve a saturated and surface dry (SSD) condition.

3.2.6 Coarse aggregates

Crushed granite stone in the laboratory with maximum size of 20 mm and specific gravity 2.9 g/cm^3 according to ASTM C127 standard was used as coarse aggregate. The coarse aggregates were also treated to achieve a saturated and surface dry (SSD) condition.

3.2.7 Water

The tap water from concrete laboratory at Curtin University was considered for mixing mortar and concrete. Water should not contain materials or impurities in quantities large enough to produce harmful coating on the surface of aggregate particles.

3.2.8 Superplasticizer

In this study, a naphthalene sulphonate based superplasticizer type Rheobuild 1000 was used to maintain the workability of mixtures. The superplasticizer dosage was calculated as a percentage by mass of total binders and used to maintain the consistency and workability of mortars and concretes.

3.3 Mix Proportions

The experimental work was divided into three parts. The first part determined the optimum nano silica and nano-$CaCO_3$ contents based on compressive strength development of ordinary cement mortar. In the second part the effect of optimum nano silica and nano calcium carbonate contents on the compressive strength development from 3 days to 90 days of high volume fly ash concretes containing 40% and 60% (by wt.) Class F fly ash as partial replacement of cement was evaluated. The effects of optimum nano silica and nano-$CaCO_3$ contents on chloride induced corrosion resistance of above HVFA concretes and related durability properties affecting chloride induced corrosion were also evaluated in the second part. The third part evaluated the effects of nano silica and nano-$CaCO_3$ on micro- and nano-structural changes of HVFA matrix in pastes samples. In all parts a constant water/ binder ratio of 0.4 was considered. Superplasticizer was added to the mixes containing nano silica and nano $CaCO_3$ to maintain adequate workability.

The mix proportions of first part (Part I) of this study are presented in Table 3.2. The first series is the control mortar containing 100% OPC without any nano particles. The second series is the mortars containing different HVFA contents of 40, 50, 60 and 70% as partial replacement of cement. In third and fourth series, mortars contained different nano silica contents of 1, 2, 4 and 6% (by wt.) and nano $CaCO_3$ contents of 1, 2, 3 and 4% (by wt.) as partial replacement of cement, respectively are considered. The optimum nano silica and nano $CaCO_3$ contents that exhibited the highest compressive strength in Part I is then used to investigate their effects on the compressive strength development and chloride induced corrosion and durability properties of HVFA concretes containing 40% and 60% Class F fly ash as partial replacement of cement in the second part, whose mix proportions is shown in Table 3.3.

Due to extremely high specific surface area, small particle sizes and amorphous nature, the nano particles have a tendency to agglomerate more than other micro size cementitious materials in the concrete. Unless the individual nano particles are well dispersed, the agglomeration reduces the exposed particle surface area leading to inferior concrete properties. The ultrasonication technique is commonly used to disperse nano particles in surfactant solution. In this study the effect of different mixing times in ultrasonic mixer on the dispersion of nano silica is also evaluated. Three different ultrasonic mixing times of 30, 60 and 120 minutes are used to disperse 2, 4 and 6% nano silica in the water containing superplasticizer. Table 3.4 presents the mix proportions of mortars containing nano silica to evaluate the effect of ultrasonic mixing time on the compressive strength development of mortars containing nano silica. The 28 days compressive strength of mortars containing nano silica is considered as the benchmark of dispersion of NS, where higher compressive strength indicates better dispersion of NS in the system and vice versa. The compressive strength of mortars containing ultrasonically mixed nano silica is also compared with dry mixing of nano silica with cement prior to addition of water and superplasticizer in the first part of this study.

Table 3.2 Part I: Mix proportions of mortars containing nano silica, fly ash and nano $CaCO_3$

Series	Mix designation	Cement (kg/m^3)	Class F Fly Ash (kg/m^3)	Nano Silica (kg/m^3)	Nano $CaCO_3$ (kg/m^3)	Sand (kg/m^3)	Water (kg/m^3)	Super-plasticizer (%*)
1	PC	400	-	-	-	1100	160	-
2	FA40	240	160	-	-	1100	160	-
	FA50	200	200	-	-	1100	160	-
	FA60	160	240	-	-	1100	160	-
	FA70	120	280	-	-	1100	160	-
3	NS1	396	-	4	-	1100	160	1.1
	NS2	392	-	8	-	1100	160	1.3
	NS4	384	-	16	-	1100	160	1.5
	NS6	376	-	24	-	1100	160	1.8
4	NC1	396	-	-	4	1100	160	-
	NC2	392	-	-	8	1100	160	-
	NC3	388	-	-	12	1100	160	
	NC4	384	-	-	16	1100	160	

*Superplasticizer dosages are added as percentage of binder (Cement+fly ash+nano silica)

Table 3.3 Part II: Mix proportions of concrete and HVFA concretes containing optimum nano silica and nano $CaCO_3$

Mix designation	Cement (kg/m^3)	Class F Fly Ash (kg/m^3)	Nano Silica (kg/m^3)	Nano $CaCO_3$ (kg/m^3)	Sand (kg/m^3)	Coarse Aggregate (kg/m^3)	Water (kg/m^3)	Super-plasticizer (%*)
PC	400	-	-	-	684	1184	163	-
NS2	392	-	8	-	684	1184	163	1.3
NC1	396	-	-	4	684	1184	163	-
FA40	240	160	-	-	684	1184	163	-
FA60	160	240	-	-	684	1184	163	-
FA38.NS2	264	128	8	-	684	1184	163	-
FA58.NS2	160	232	8	-	684	1184	163	-
FA39.NC1	240	156	-	4	684	1184	163	-
FA59.NC1	160	236	-	4	684	1184	163	-

* Superplasticizer dosages are added as percentage of binder (Cement + nano silica or nano CaCO3)

Table 3.4 Mixture proportions of mortars containing NS to study the effect of ultrasonic mixing on dispersion of nano silica

Mix designation	Cement (kg/m^3)	Nano silica (kg/m^3)	Sand (kg/m^3)	Water (kg/m^3)	Superplasticizer (%*)	Ultrasonic mixing time (minutes)
NS2(U-30)	392	8	1100	160	1.3	30
NS4(U-30)	384	16	1100	160	1.5	30
NS6(U-30)	376	24	1100	160	1.8	30
NS2(U-60)	392	8	1100	160	1.3	60
NS4(U-60)	384	16	1100	160	1.5	60
NS6(U-60)	376	24	1100	160	1.8	60
NS2(U-120)	392	8	1100	160	1.3	120
NS4(U-120)	384	16	1100	160	1.5	120
NS6(U-120	376	24	1100	160	1.8	120

* Superplasticizer dosages are added as percentage of binder (Cement + nano silica)

3.4 Experimental method

3.4.1 Mixing methods

3.4.1.1 Mortar (Part I)

All mortars are mixed in a Hobart mixer at an ambient temperature of approximately 25°C using water/binder ratio of 0.4 and sand/binder ratio of 2.75. Dry sand, cement, fly ash and nanoparticles are mixed in high speed Hobart mixer for approximately 2-3 minutes. Water is added thereafter and mixed for another 2-3 minutes. The 50mm mortar cubes are cast and demolded after 24 hour. The mortar specimens are cured in water at room temperature for 7 and 28 days.

3.4.1.2 Concrete (Part II)

The concrete mixes are prepared in a pan mixer with the same water/binder ratio used for mortars. Similar to the mortar mixing, dry mixing time of cement, fly ash, nanoparticles and aggregates are extended to 4-5 minutes due to higher volume of mix and presence of coarse aggregate. Standard cylinder having diameter of 100mm and height of 200mm are cast and cured in water at room temperature. The compressive strengths of concretes are determined at 3, 7, 28, 56 and 90 days according to ASTM C873 standard.

3.4.1.3 Paste (Part III)

The mix proportions of pastes were similar to those of mortars except the exclusion of sand. The water/binder ratio of paste was same as that of mortar. The 50 mm cube

samples were also cast for pastes and followed similar curing to those of mortars. Small portions were cut from the cubes to perform scanning electron microscope (SEM), x-ray diffraction (XRD), mercury intrusion porosimetry (MIP), and thermal (TGA/DTA) analysis of pastes containing nanoparticles, fly ash and combined fly ash and nanoparticles.

3.4.1.4 Dispersion of nano silica

The ultrasonic processor type UP400S was used to disperse nano silica particles (see Figure 3.8). The ultrasonic transducers use electric excitation to generate ultrasound, which is transferred to the liquid medium via sonotrode. The vibrations are amplified by the sonotrode fitted to the horn and formed as a λ/2 vibrator and transferred via its end face to the medium to be sonically irradiated. The amplitude of the oscillatory system was adjusted to 20% and remained constant under all operating conditions.

Figure 3.8 Ultrasonic processor type UP400S

3.4.2 Workability measurements

3.4.2.2 Flow table test

The flow values of mortars were determined according to ASTM C1437 standard. The flow test is conducted by placing the mortar in the mini conical mold and tamp 20 times with the tamper rod. The tamping pressure was just sufficient to endure uniform filling of the mold. The mold was then filled with mortar and tamped as

specified in the first layer. The excess mortar on top of the mold was removed. Then the mold was lifted vertically from the mortar and immediately dropped the table 25 times in 15 sec and recorded the diameter of the mortar (see Figure 3.9a).

Figure 3.9 Workability measurement: (a) flow table (b) slump test

3.4.2.3 Slump test

The workability of concrete was measured in terms of slump measurement according to ASTM C143 standard. In this test, concrete was poured into the mold in three layers. Each layer was tamped 25 times throughout its depth with the rounded end of tamping rod. The excess concrete was strike off from the top surface of mold with the tamping rod. The mold was lifted vertically and the drop of the subsided wet concrete was measured slump value as shown in Figure 3.9b.

3.4.3 Compressive strength

The compression tests of mortar and concrete specimens were carried out using multifunctional control console machine (MCC8). Compressive strength of mortar specimens were tested according to ASTM C109 standard using a loading rate of 0.7 MPa/s, while the compressive strength of concretes was determined at 3, 7, 28, 56 and 90 days according to ASTM C39 standard using a loading rate of 0.33 MPa/s. For each age, three specimens were tested and the mean value of these measurements is reported. The specimen setup is shown in Figure 3.10.

(a) (b)

Figure 3.10 Compressive strength test setup: (a) mortar specimen (b) concrete specimen

3.4.4 Water sorptivity

The rate of water absorption (sorptivity) of concrete was measured on specimens of 100mm in diameter and 50 mm in thick disks and was determined after 28 and 90 days wet curing according to ASTM C1585 standard. The principle of the method is that a specimen has one surface in free contact with water (no more than 5 mm above the base of the specimen) while the others are sealed (see Figure 3.11). This test determines the rate of absorption of water by hydraulic cement concrete by measuring the increase in the mass of a specimen resulting from absorption of water as a function of time. In this study, the mass of the concrete specimen is regularly measured to determine the initial absorption from 1 min to first 6 hours. The absorption (I) is the change in mass divided by the product of the cross-sectional area of the test specimen and the density of water. The initial rate of water absorption value ($mm/s^{1/2}$) is calculated as the slope of the line that is the best fit to *I* plotted against the square root of time ($s^{1/2}$). The $I\text{-}t^{0.5}$ plot has to be linear with a regression coefficient (r^2), of less than an arbitrary value of 0.98.

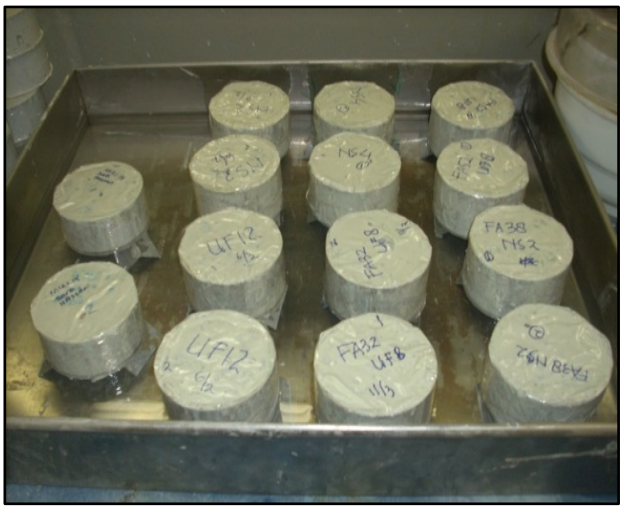

Figure 3.11 Water sorptivity test setup

3.4.5 Volume of permeable voids

This test was conducted to estimate the percentage of voids present in the concrete specimens after curing at 28 and 90 days, based on ASTM C642 standard. Volume of permeable voids (VPV) is determined by boiling the 50 mm cut concrete specimens for at least 5 hours in a water tank at 105°C, weighing the samples in water, then measuring the percentage of boiled specimen with dried mass and mass in the water. The values for mass determined during the tests are described as follows:

Absorption after immersion (%) = [(B-A)/A] x 100 (3.1)

Absorption after immersion and boiling (%) = [(C-A)/A) x 100 (3.2)

Bulk density (dry) = [A/C-D)].ρ = g1 (3.3)

Bulk density after immersion = [B/(C-D)].ρ (3.4)

Bulk density after immersion and boiling = [C/(C-D)].ρ (3.5)

Apparent density = [A/(A-D)].ρ = g2 (3.6)

The volume of permeable voids of concrete specimens was calculated by using equation:

$$VPV = \left(\frac{g2-g1}{g2}\right) x\ 100 \quad (3.7)$$

Where:

A = mass of oven-dried sample in air (g)

B = mass of surface-dry sample in air after immersion (g)

C = mass of surface-dry sample in air after immersion and boiling (g)

D = apparent mass of sample in water after immersion and boiling (g)

g1 = bulk density, dry (x 10^3 kg/m^3)

g2 = apparent density (x 10^3 kg/m^3)

ρ = density of water = 1 g/cm^3

3.4.6 Porosity

The porosity of cementitious systems influenced the strengths and durability properties of concrete. The mercury intrusion porosimetry (MIP) test was performed to measure the pore volumes and their distribution in the matrix. This measurement was performed with a PoreMaster series - Quantachrome instruments, with a pressure ranged between 0.0083 and 207 MPa, and the pore diameter and intrusion mercury volume were recorded at each pressure point. Some researchers used the maximum pressure of 200 – 230 MPa during MIP analysis (Poon and Wong, 2000; Aligizaki, 2006; Krakowak et al., 2015). The pressures were converted to equivalent pore diameter using the Washburn equation, as expressed in Equation (3.8):

$$d = \frac{-2\gamma\cos\theta}{\mathrm{P}} \tag{3.8}$$

Where d is the pore diameter (μm), γ is the surface tension (mN/m), θ is the contact angle between mercury and the pore wall (°), and P is the net pressure across the mercury meniscus at the time of the cumulative intrusion measurement (MPa).

3.4.7 Rapid chloride permeability test

Rapid chloride permeability test (RCPT) was conducted to investigate the performance of concrete against chloride ingress. The penetration of chloride ions can reach reinforcing steel bars and corrode them rapidly. The lower the total charge passed through the concrete matrix, the higher the resistance to chloride penetration. ASTM C1202 specifies the rating of chloride permeability of concrete based on the charge passed through the specimen during 6 hours of testing period. A RCPT value of less than 2000 Coulombs is characterized as low chloride permeability, 2000-4000

Coulombs is in medium level while higher than 4000 Coulombs is defined as high chloride permeability (see Table 3.5).

The specimens from each series were tested at the ages of 28 and 90 days. After curing, the specimens of 100 mm in diameter and 50 mm in thickness was first prepared by coating the dry surface with a sealer and then vacuum conditioning it as per the ASTM C1202 procedures (see Figure 3.12a). Afterwards, the specimen which had been conditioned were placed on the cells and subjected to a 60-V potential for 6-h (see Figure 3.12b). One of the cells was filled with 0.3 N NaOH solution and the other cell was with 3% NaCl solution. The amount of electrical current passing through the slices of concrete cylinder is measured and the total charge passed (in Coulombs) is used as an indicator of the resistance of the concrete to chloride ion penetration. The total charge passed through the concrete specimens was calculated using the following formula in Equation (3.9):

$$Q = 900 (I_o + 2I_{30} + 2I_{60} + \ldots + 2I_{300} + 2I_{330} + 2I_{360}) \quad (3.9)$$

Where:

Q = charge passed (Coulombs)

I_o = current (amperes) immediately after voltage is applied, and

I_t = current (amperes) at t min after voltage is applied

Table 3.5 Chloride ion penetrability based on charge passed (ASTM C1202)

Charge passed	Chloride ion penetrability
>4,000	High
2,000 – 4,000	Moderate
1,000 – 2,000	Low
100 – 1,000	Very low
<100	Negligible

Figure 3.12 Rapid chloride permeability test setup: (a) vacuum dessicator (b) specimens ready for test

3.4.8 Chloride diffusion

In order to evaluate the chloride content and chloride diffusion coefficient of the concrete mixtures, 100/200 mm cylinder specimens were cast and cured. After 28 days of water curing, two specimens with size of 50 mm thick of each sample were prepared and placed in the exposure container containing NaCl solution prepared with a concentration of 165 ± 1 g NaCl per L of solution. The specimens were coated by epoxy paint except the test surface to ensure that chloride will be penetrated in one direction to the concrete. In this study, the specimens are remained in the exposure liquid for 60 days. Profile grinding is applied to collect concrete powder samples (see Figure 3.13a) at depth increments ranging between 1 mm to 16 mm, according to ASTM C1556 standard. In order to determine the acid soluble Cl^- ion contents, the powder samples are measured using CL-2000, Chloride Test System, James instruments (see Figure 3.13b). An accurately weighed 3 gram sample is dissolved in 20 ml of extraction liquid consisting of a precise, measured concentration of acid. The chloride ions react with the acid of the liquid in an electrochemical reaction. An electrode, with an integral temperature sensor, is inserted into the liquid and the electrochemical reaction measured. The percentage of chlorides is displayed directly on LCD readout. Chloride diffusion coefficient for each sample is determined by fitting the data obtained in the chloride profile analysis to Fick's diffusion second law equation (as discussed in section 2.5.2).

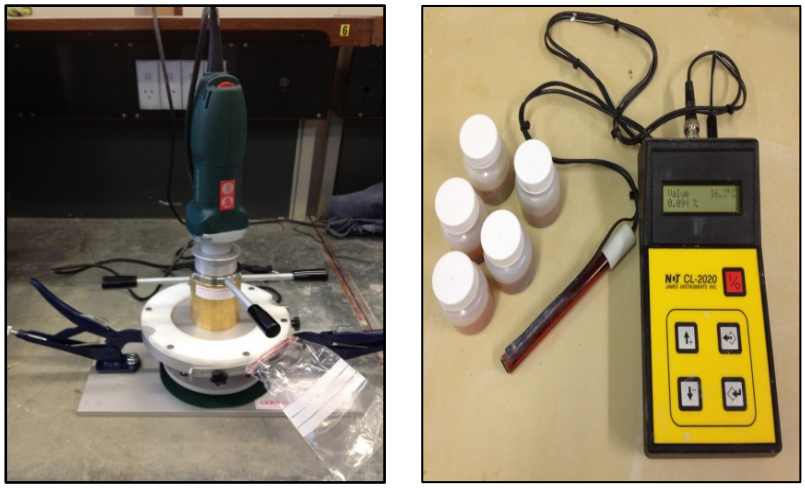

(a) (b)

Figure 3.13 Chloride diffusion analysis: (a) Profile grinder to obtain concrete powder (b) Acid-soluble chloride ion test instrument

3.4.9 Accelerated corrosion test

Accelerated corrosion test or impressed voltage test is conducted for simulating the corrosion of steel reinforcement in concrete. The corrosion process is accelerated by impressing an anodic potential between rebar (anode) and steel plate (cathode) to record the variation of current with time. Concrete with size of 100x200 mm cylinder specimens are used for the study after curing in water for 28 days. Deformed steel bars of 16mm diameter and 250mm in length are used and fixed in the centre of the specimens after being cleaned and accurately weighed (see Figure 3.14a). The steel bar has an effective cover of 50mm at the bottom. The reinforced concrete specimens were immersed in a 3.5% sodium chloride solution under a “3 days wet” and “4 days dry” cyclic regime to simulate the tide environment. Readings for each type of mixes were taken from two specimens tested at the age of 28 days, and recorded every hour using an automatic data acquisition system. The average was calculated to compute the time of corrosion for the reinforced steel bar. The photographic view of the test configuration is shown in Fig 3.14b. The schematic of the accelerated corrosion test is presented in Figure 3.15. The steel bars of the sample are connected to a 10-volt DC power supply. The negative terminal of the DC power source is connected to the stainless steel plate. The impressed current flow is measured regularly and testing is stopped when the initiation of corrosion is detected. A rapid increase in current flow

indicates the formation of cracks in concrete samples. In order to measure the weight loss measurement, the corroded steel is retrieved from the broken samples and weight to be compared with the initial weight after accelerated corrosion test.

In this study, the theoretical mass of rust and the actual mass loss per unit surface area are theoretically calculated according to Faraday's law as follows:

$$M_{th} = \frac{W\, I_{app}\, T}{F} \tag{3.10}$$

Where:

M_{th} = theoretical mass of rust per unit surface area of the bar (g/cm^2)

W = equivalent weight of steel which is taken as the ration of atomic weight of iron to the valency of iron (27.925 g)

I_{app} = applied current density (Amp/cm^2)

T = duration of induced corrosion (sec)

F = Faraday's constant (96487 Amp-sec)

The actual mass of rust per unit surface area is calculated by gravimetric test (Equation 3.11) in accordance with ASTM G1 standard on rebars extracted from the concrete by breaking the specimens after the accelerated corrosion test.

$$M_{ac} = \frac{W_i - W_f}{\pi DL} \tag{3.11}$$

Where:

M_{ac} = actual mass of rust per unit surface area of the bar (g/cm^2)

W_i = initial weight of the bar before corrosion (g)

W_f = weight after corrosion (g) for a given duration of induced corrosion (T)

D = diameter of the rebar (cm)

L = length of the rebar sample (cm)

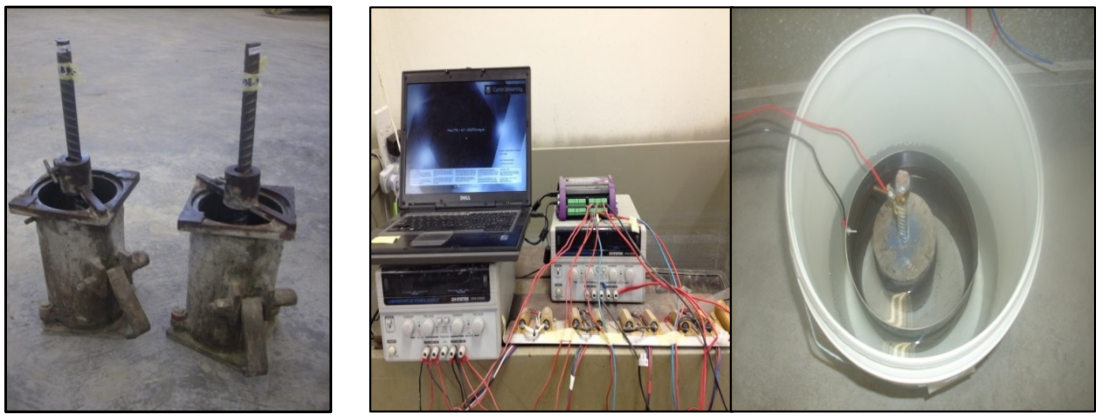

(a) (b)

Figure 3.14 Accelerated corrosion test: (a) lollipop moulds (b) photographic view of test configuration

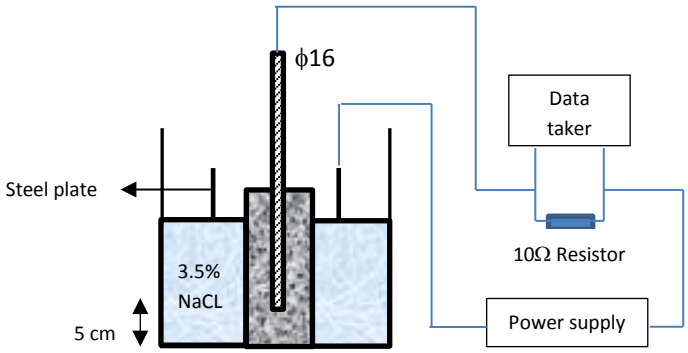

Figure 3.15 Schematic diagram of accelerated corrosion test

3.5 Microstructure and phase identification analysis

3.5.1 Backscattered electron (BSE) image

The microstructure of different paste samples were examined on a Zeiss EVO40XVP (Carl-Zeiss, Germany) using backscattered electron (BSE) detector. The BSE detector is ideal for analysing samples that have a wide range of atomic numbers. The small cut paste samples were polished using silicon carbide paper, mounted on the stubs and coated with platinum before imaging in the SEM. In this analysis, the electron microscope images the sample surface by scanning it with a high-energy beam of electrons. The electrons then interact with the atoms that make up the sample producing signals that contain information about the sample's surface

topography, composition and other properties such as electrical conductivity (Stultzman, 2004).

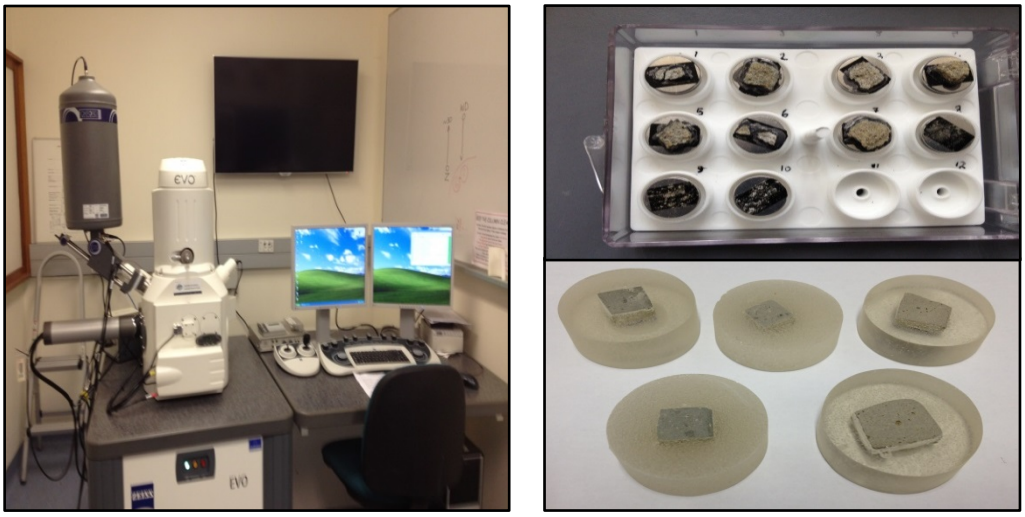

(a) (b)

Figure 3.16 SEM investigation: (a) SEM apparatus (b) samples preparation

3.5.2 X-ray diffraction (XRD)

The powder of cement paste samples of about 3 g were prepared and submitted for XRD analysis. XRD patterns were acquired on a D8 Advance Diffractometer (Bruker-AXS) using copper radiation a LynxEye position sensitive detector. Operating conditions were set a 40 kV and 30 mA using a Cu$k\alpha$ X-ray source (λ = 1.5406 Å). An analysis from 5^0 to 70^0 (2θ) is carried out at a speed of 0.5^0/min. The Quantitative X-ray Diffraction Analysis (QXDA) with Rietveld refinement was done with Bruker *DIFFRAC*^{plus} EVA software associated with the International Centre for Diffraction Data PDF-4 2013 database.

3.5.3 Thermal analysis (DTA/TGA)

DTA/TGA analysis measures both heat flow and weight changes in a material as a function of temperature of time in a controlled atmosphere. DTA figures the thermal decompositions of different phases in paste, while TGA simultaneously measures the weight loss due to the decomposition of phases. About 50 mg of well-powdered sample in a 110 µL platinum crucible was heated from ambient to 1000°C at 20°C

per minute in a nitrogen atmosphere flowing at 100 ml per minute. Mass and differential temperature data were acquired with respect to furnace temperature. Generally the amount of bound water is determined by the weight loss between 105 and 1000°C. It was decided to use the weight loss between 40 and 550°C, as at 105°C the decomposition of ettringite and CSH has already started, and in the temperature interval 550-900°C the weight loss is mainly due to the decomposition of carbonates. The analysis also allows the estimation of the content of CH from the weight losses in all of the different paste samples.

The calcium hydroxide (CH) content can be calculated according to Taylor formula (Taylor, 1990):

$$CH\ (\%) = WL_{CH}\ (\%).\frac{MW_{CH}}{MW_{H_2O}} \tag{3.12}$$

Where:

WL_{CH} is the weight loss during the dehydration of CH as percentage of the ignited weight (%)

MW_{CH} is the molecular weight of CH

MW_{HO} is the molecular weight of H_2O

3.5.4 Nano indentation

Nanoindentation analysis is used for the determination of mechanical properties of homogenous and heterogeneous materials. In the area of cement phase, the main of the analysis is to obtain the hardness, elasticity and volume fractions of the various phases which are the chemical compound responsible for the strength and durability of cement paste.

In this study, the cement paste samples with different type of mixes were prepared after 28 days of curing. In order to protect the samples from damage during grinding and polishing, the 10mm cube of cut samples were cast in the mixture of epoxy resin and hardener in cylindrical resin moulds. The samples were then placed in a vacuum to remove the entrapped air from the mixture. After 24 hours, the samples were demolded and prepared for the process of grinding and polishing. All samples were sanded using sandpapers of gradations 52.2 µm, 35.0µm, 21.8µm, 15.3µm, and then polished using diamond suspension solutions ranged from 9µm, 6µm, 3µm, 1µm, 0.25µm, 0.1µm. The rotation speed was maintained at 150 revolutions per minute

(rpm) with polishing was done for approximately 30 minutes in each step. After polishing, samples were cleaned with running water to remove all dust and diamond particles away from the surface.

(a)

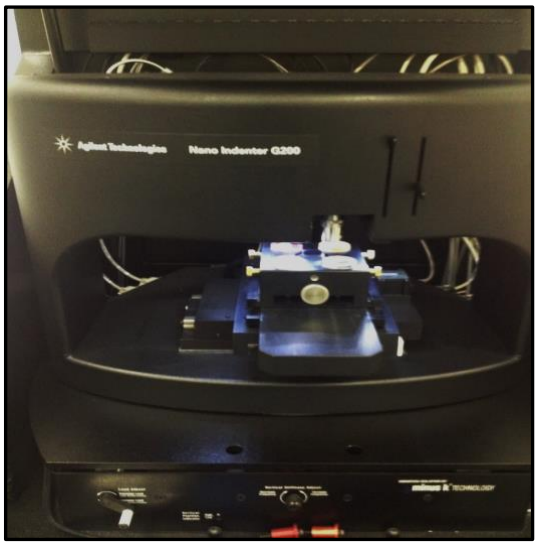

(b)

Figure 3.17 Nano indentation technique: (a) polishing samples
(b) nano indenter set-up

The samples were tested with a Nano Indenter G200 fitted with a Berkovich indenter diamond tip (three-sided pyramid) with an indentation load of 0.5 and 1 mN, where a progressive multistep indentation testing with two load-unload cycles were performed at each test point (see Figure 3.18). In each cycle, maximum load was

held constant for a period of 10 s. The unloading data of the second cycle were used to determine the modulus and hardness values.

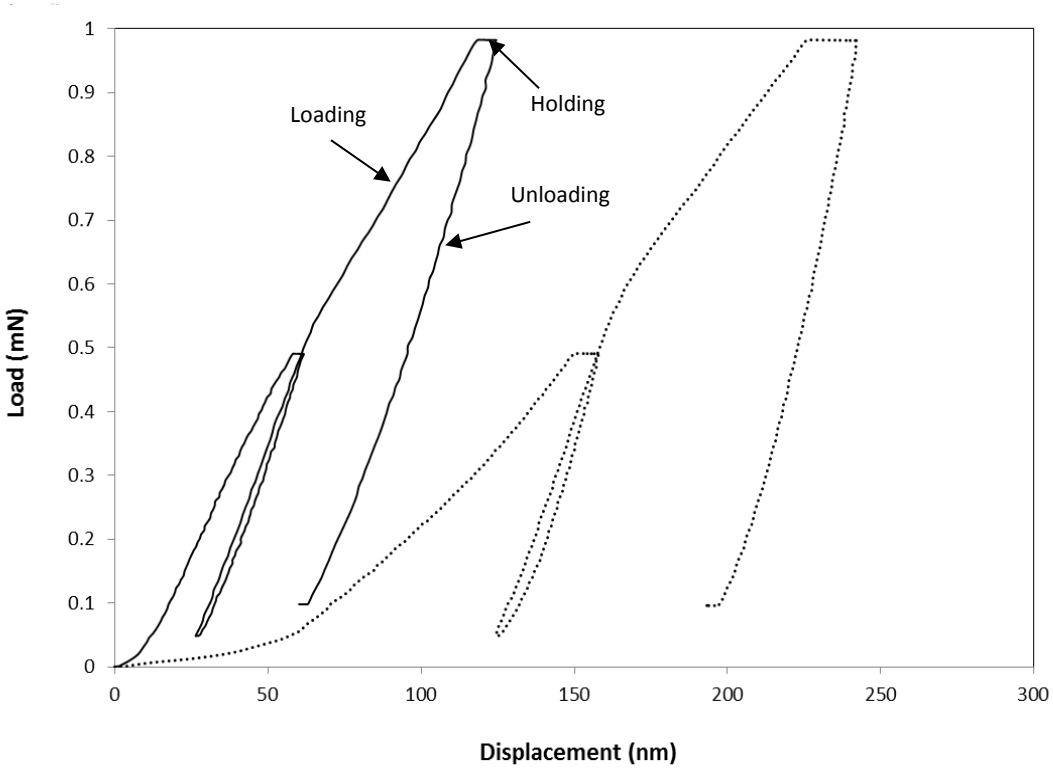

Figure 3.18 Example of load-displacement curves in nano indentation test

Before applying the load, the cement paste sample was scanned by optical microscopes to select a suitable place for indentation with minimum roughness and a representative unhydrated cement particle and large amount of well-hydrated phases. During the test, the indenter tip is pressed into the surface of the samples where the force (P) and displacement (h) are recorded. In order to determine the hardness and elastic modulus from the indentation data, the Oliver and Pharr method was used (see section 2.6.4.2). Moreover, grid indentation was conducted to determine the volume fractions of different phases in the paste samples. In this technique, grid system of 40 points (4 rows by 10 columns, evenly spaced by 10 μm) was performed in which 8 arrays were made on each samples and the data collected was analysed statistically where the distribution of the mechanical properties of each phase is assumed to follow a normal distribution (also known as Gaussian distribution).

CHAPTER IV

RESULTS AND DISCUSSION

4.1 Introduction

This chapter presents the compressive strength and durability properties on the effect of nano silica and nano calcium carbonate as partial replacement of cement on mortars and concretes containing high volume fly ash. The results are divided into three main parts. The first part presents the results on the optimum nano silica and nano-$CaCO_3$ contents based on compressive strength development of ordinary cement mortar. The results on the effect of optimum nano silica and nano-$CaCO_3$ contents on the compressive strength at 3, 7, 28, 58 and 90 days of OPC and HVFA concretes containing 40% and 60% (by wt.) Class F fly ash as partial replacement of cement are reported in the second part of this chapter. Additionally, the results on accelerated corrosion and related durability properties including water sorptivity, porosity, volume of permeable voids, chloride permeability and chloride diffusion of HVFA concretes and those containing nano silica and nano calcium carbonate are also presented in this part. The third part reports the results on microstructure and phase identification of HVFA pastes due to incorporation of nano silica and nano calcium carbonate based on backscattered electron (BSE), x-ray diffraction (XRD), thermal (DTA/TGA) analysis and nano-indentation results.

4.2 Workability of mortars and concretes containing nano silica and nano $CaCO_3$

4.2.1 Effect of nano silica (NS) on workability

The effects of nano silica on the workability of mortars and concretes are shown in Figures 4.1 and 4.2, respectively. The workability of mortars and concretes is measured in terms of flow and slump values, respectively according to ASTM-standards. Since the nano silica has a higher specific surface, a naphthalene sulphonate superplasticizer was used to maintain the workability of cement mortar and concrete containing NS. At water to binder ratio of 0.4 the addition of NS in mortar mixtures exhibited slightly higher workability while in concrete mixtures the NS addition significantly decreased the slump as the dosage increased from 2% to 4%. It was found that the NS showed strong influence on the workability of the concrete, due to its high specific surface. In HVFA mortars and concretes, the similar

trend on workability due to the addition of NS particles is also observed. In this case, the slump of HVFA concretes was found decreased indicating the effect of NS particles in providing excellent water-tightness on concretes containing HVFA. For example, the slump of FA38.NS2 concrete was decreased from 160 mm to 140 mm and had the same initial slump as Portland cement concrete while in FA58.NS2 concrete, the slump dropped from 200 mm to 160 mm (see Figure 4.2). The flow values of mortar samples also show a similar trend. With its characteristics as an ultrafine pozzolan material which comprises essentially of amorphous silica and greater surface area, the NS is very effective in controlling the workability of HVFA concrete mixtures. By controlling the excessive water in HVFA concretes, NS particles are able to enhance the resistance of HVFA concretes to permeability and durability.

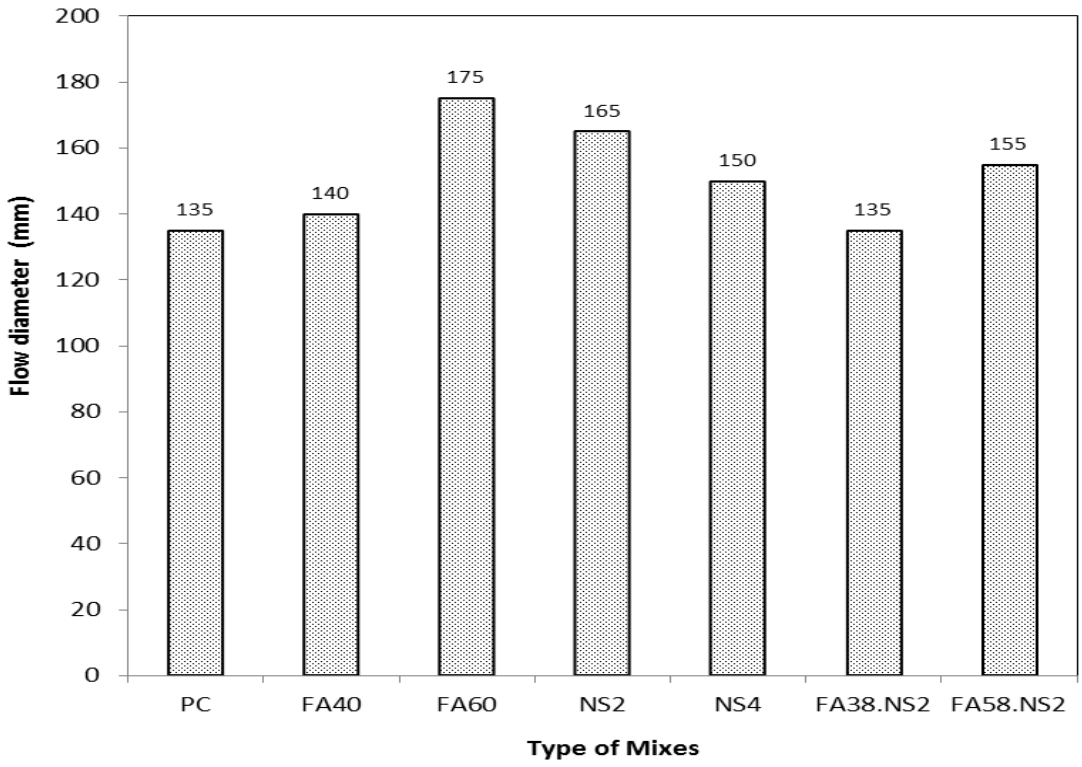

Figure 4.1 Workability of cement and HVFA mortars containing NS

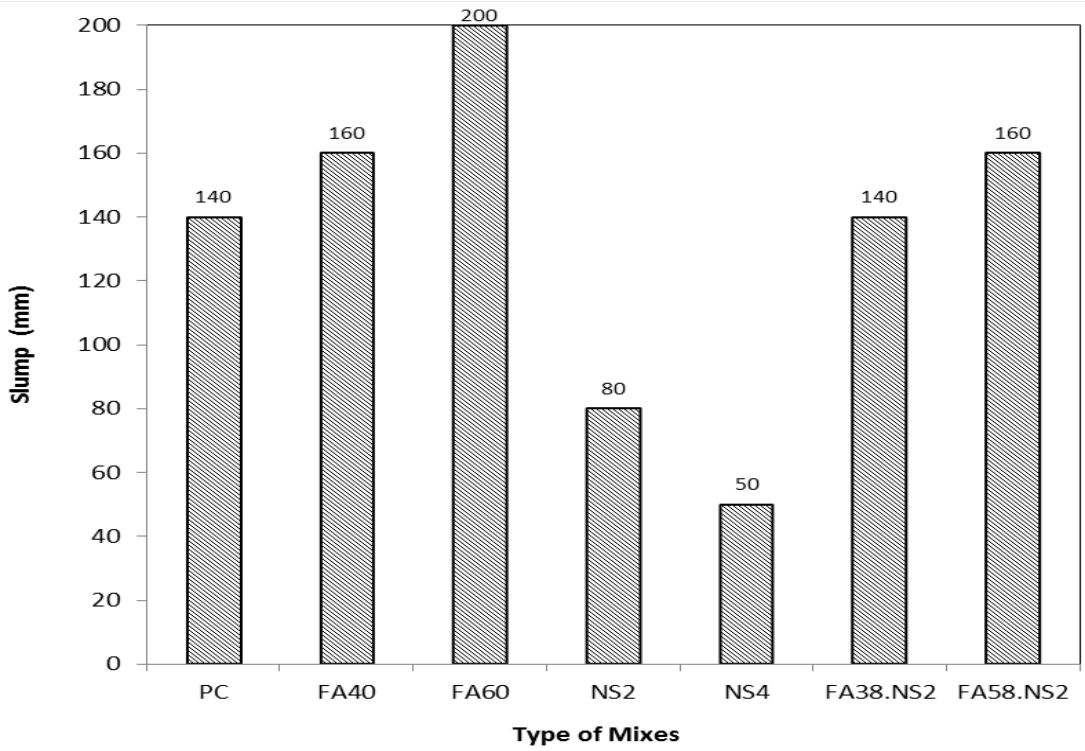

Figure 4.2 Effect of nano silica on workability of concrete and high volume fly ash concretes

4.2.2 Effect of nano-$CaCO_3$ on workability

The effect of nano-$CaCO_3$ on workability of cement and HVFA mortars using the flow table test (ASTM C1437 standard) is also investigated. It can be seen from Figure 4.3 that the high volume fly ash mixtures have recorded higher workability than the control cement mixture. In nano-$CaCO_3$ mortars, it is noticeable that the flow values decrease with the increase in the nano-$CaCO_3$ contents. Liu et al. (2012) also found the similar results. However, the presence of nano-$CaCO_3$ is found to have a plasticizing effect in maintaining the consistency of mortars thus does not need extra water and/or superplasticizer to provide sufficient fluidity. When nano-$CaCO_3$ was combined in HVFA mortars and concretes, the flow and slump were also decreased. For instance, the FA40 mortar and concrete yielded a flow diameter and slump of 140 mm and 160 mm, respectively while these results reduced to 135 mm and 160 for FA39.NC1 mortar and concrete, respectively (see Figures 4.3 and 4.4). This similar observation is also found in FA60 and FA59.NC1 mortars and concretes. This can be explained that due to its high specific surface area and smaller

particle sizes, the incorporation of nano-$CaCO_3$ considerably offsets the high water amount of HVFA.

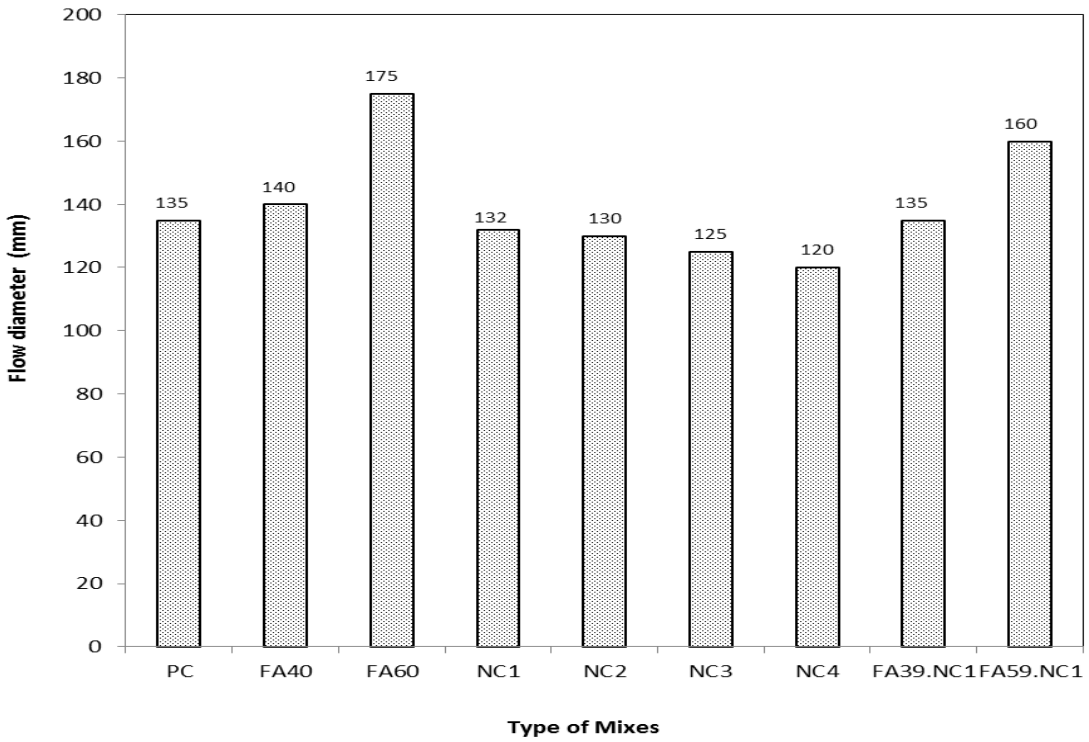

Figure 4.3 Workability of cement and HVFA mortars containing NC

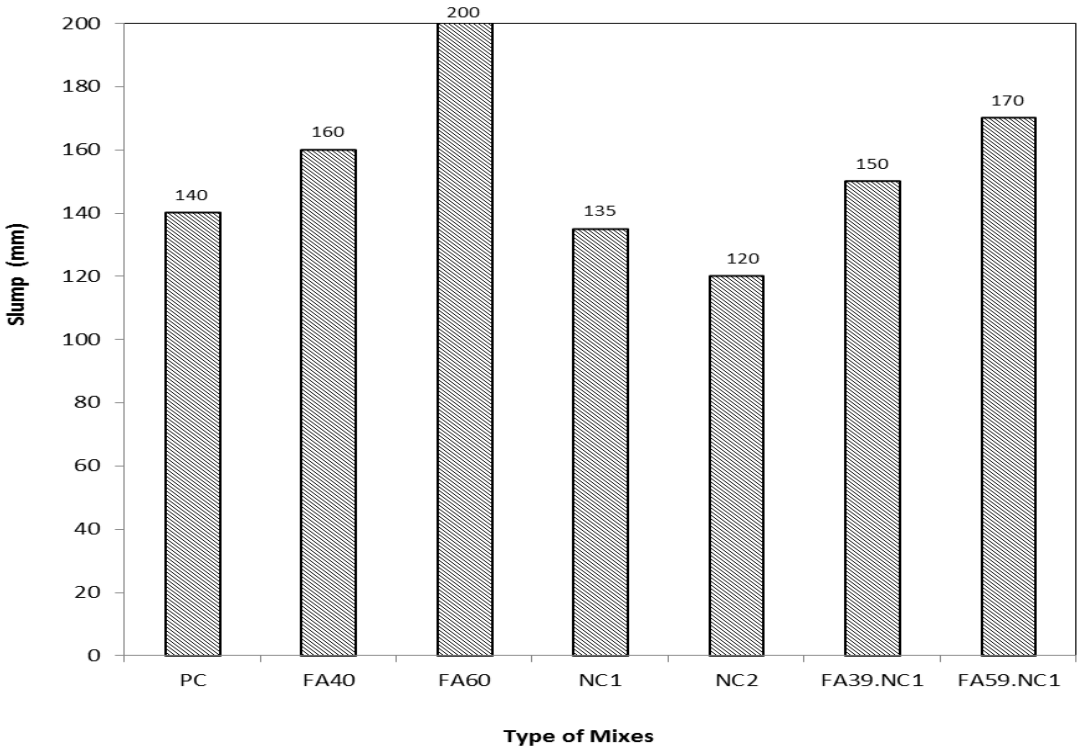

Figure 4.4 Effect of nano-$CaCO_3$ on workability of concrete and high volume fly ash concretes

4.3 Compressive strength of mortars containing nano silica and nano $CaCO_3$ (Part I)

4.3.1 Effect of nano silica on the compressive strength of cement and HVFA mortars

The effect of different nano silica (NS) contents on 7 and 28 days compressive strength of cement mortar is shown in Figure 4.5. In the same figure the effect of high volume fly ash as partial replacement of cement on 7 and 28 days compressive strength of cement mortar is also shown. A clear decreasing trend in compressive strength at both ages can be seen with increase in fly ash contents from 40% to 70%. This usual behaviour is also observed by several researchers (e.g. Siddique, 2004) and is believed to be due to slow pozzolanic reaction of fly ash with calcium hydroxide at early age. However, the compressive strength of mortar containing 40% fly ash is slightly higher than the control cement mortar. This confirms that the optimum fly ash content in this mixes is to be 40% of cement. The result from Islam (2010) also showed that the 28 days compressive strength of FA40 mortar was only lower by 1% than OPC mortar strength. It can be suggested that a properly-proportioned with well-cured condition affected the compressive strength of fly ash mortar. For this reason, mortar made with 40% fly ash will have slightly higher strength than cement mortar up to 28 days.

On the other hand, it can be seen that the compressive strength of mortars containing NS increases with increase in NS content up to 2% (by wt.), and decreases with further increase in NS contents (e.g. at 4% and 6%). The highest improvement is observed in mortar containing 2% NS, where 16% and 14% improvement in compressive strength are noticed at 7 and 28 days, respectively (see Figure 4.6). The addition of high NS contents e.g. 6% did not show any improvement in the compressive strength development at both ages. It seems that the 2% is the optimum content of NS used in this study. The slightly lower compressive strength of mortar containing 6% NS can be attributed to the agglomeration of NS in wet mix. Due to its higher van der Waal's forces, the NS agglomerate more than other pozzolans e.g. silica fume, metakaolin, etc (Senff et al, 2009; Quercia et al, 2012). The effect of NS on the compressive strength of mortar and concrete is also reported by several researchers. Hou et al. (2012 and 2013) studied the effect of colloidal NS on the compressive strength of mortar and reported higher compressive strength

(approximately 16% increase) of mortar containing 2.25% colloidal NS than 5%. They also observed higher amount of un-hydrated cement particles in mortar containing 5% colloidal NS than that containing 2.25% colloidal NS. This clearly indicates that large portion of NS did not participate in the secondary hydration reaction in the case of mortar containing 5% colloidal NS in their study, which is attributed to the possible agglomeration of NS in that mix due to its higher amount. Li et al. (2004) reported compressive behaviour of mortar containing 3, 5 and 10% NS. They observed increase in compressive strength of mortars at both 7 and 28 days with increase in NS contents. They reported from 5.7 to 20% and from 13.8 to 26% increase in compressive strength of mortars at 7 and 28 days, respectively due to NS addition.

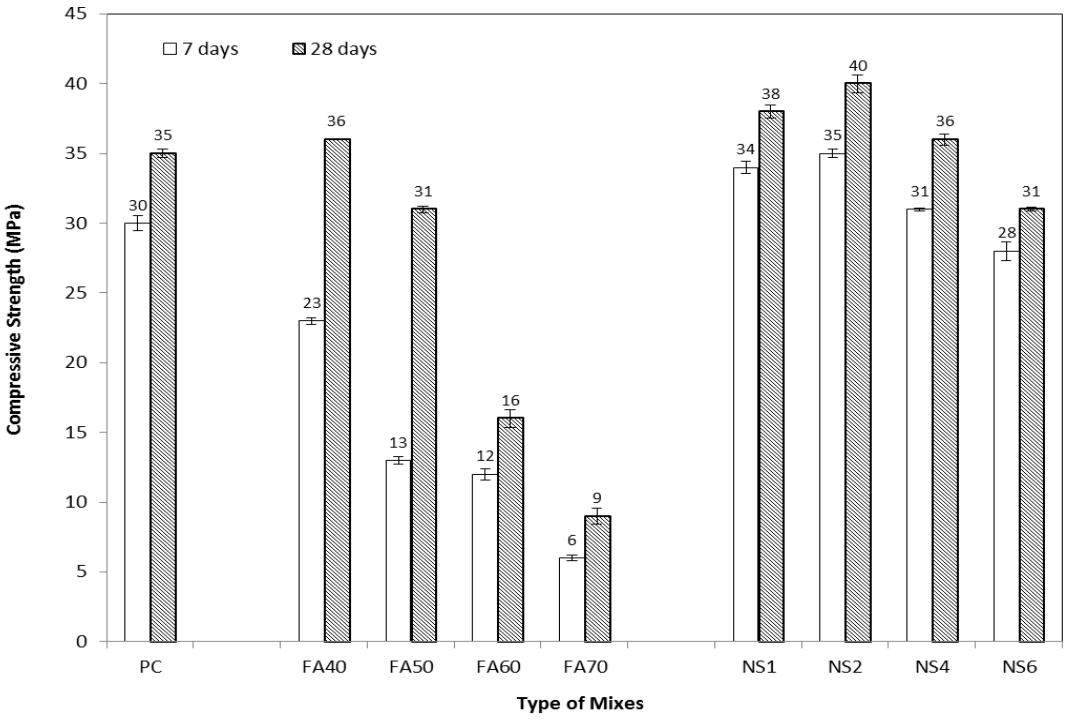

Figure 4.5 Compressive strength of mortars containing NS and fly ash

It is also observed in this study that the improvement of compressive strength of mortar containing NS is higher at 7 days than that at 28 days (see Figure 4.6). This can be attributed to the faster pozzolanic reaction of NS with calcium hydroxide (CH) in the hydration reaction of cement. Due to extremely high surface area and small particle size, the NS reacts more quickly with CH in the hydration reaction than fly ash and formed additional C-S-H gel and filled the micro pores in the matrix. The quantitative XRD analysis (see Table 4.2) also shows that the cement paste

containing 2% NS exhibited about 20% less CH (free lime) than the control cement paste. This clearly indicates the effectiveness of NS in consuming calcium hydroxide (CH) and formation of additional C-S-H in the system. The improvements in early age compressive strength of concrete due to addition of NS are also reported by several researchers e.g. Jo et al. (2007) observed about 2% improvement in 7 days compressive strength due to addition of 3% NS compared to no improvement in mortar containing 5% silica fume; Li et al. (2004) noticed about 5.7% improvement in 7 days compressive strength of cement mortar containing 3% NS.

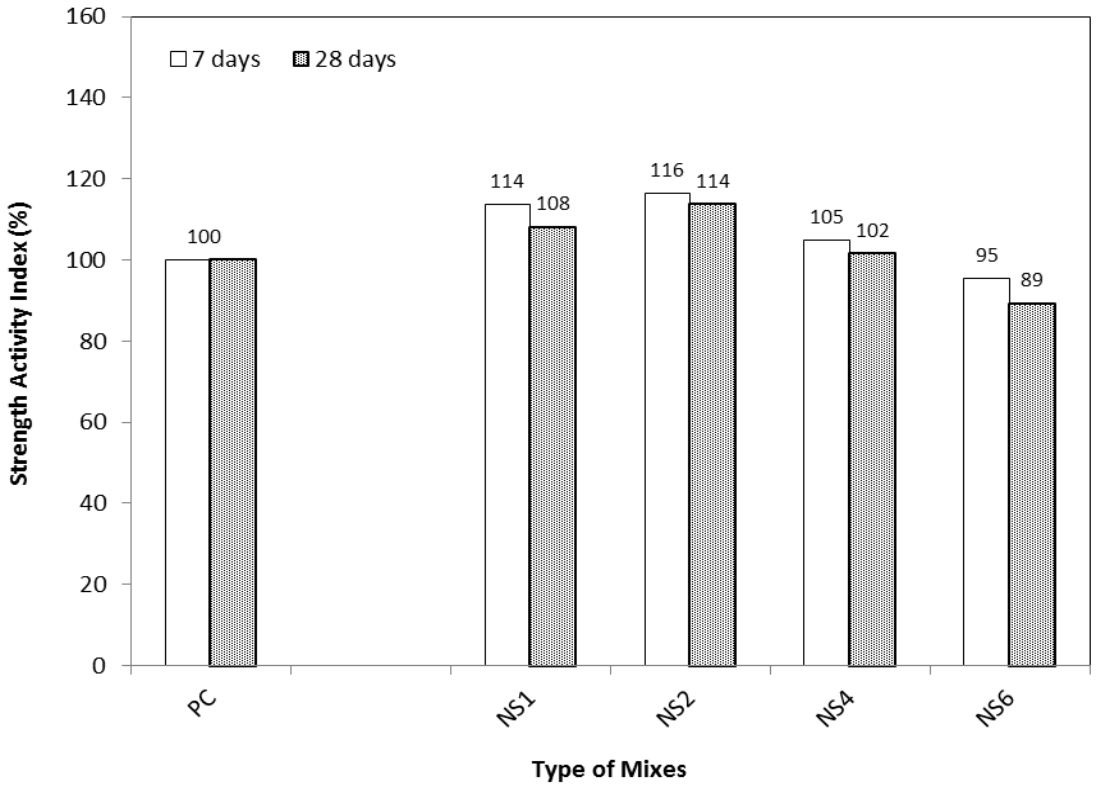

Figure 4.6 Strength activity index of mortars containing NS

Among different NS contents studied in the previous section, the 2% NS exhibited the highest compressive strength at both ages and is used in HVFA mortars containing different fly ash contents as partial replacement of cement. Figure 4.7 shows the effect of 2% NS on the compressive strength of HVFA mortar at 7 and 28 days. The compressive strengths of HVFA mortars and control cement mortar without NS are also shown in the same figure for comparison purpose. Results show that the addition of 2% NS slightly improved (between 5 and 9%) the 7 and 28 days compressive strengths of mortars containing 40% and 50% fly ash. The scenario is different in the case of mortars containing 60% and 70% fly ash, where 33% and

48% improvement in 28 days compressive strengths are observed, respectively with no improvement at 7 days (see Figure 4.8). In a separate study, Hou et al. (2013) also reported similar increase (approximately 33%) in 28 days compressive strength of mortar containing 60% fly ash than that containing 40% fly ash (approximately 11% increase) due to addition of 5% colloidal NS. However, they observed improvement in 7 days compressive strength in both mortars (40% and 60% fly ash) due to addition of colloidal NS. In another study, Zhang and Islam (2012), however, did not observed such huge improvement in 28 days compressive strength of mortar containing 50% fly ash. They observed about 17% and 6.8% improvement in 7 and 28 days compressive strengths, respectively and those improvements are at NS content of 1% only. It can be seen that the amount of improvement in compressive strength of HVFA mortars observed in this study and reported by others due to addition of NS varies significantly and could be attributed to the NS content, its sizes, physical properties and the mixing methods. For example, the mixing of colloidal NS in mortar or concrete is relatively easy, and dispersion of NS particles compared to powder NS. Its dispersion is wet cement matrix is an important issue which significantly affects the compressive strength of concrete or mortar. Therefore, it is difficult to compare the results among different studies considering NS. Nevertheless, based on this study and the results reported by others, it can be seen the beneficial effect of using NS in early age as well as later age (e.g. 28 days) compressive strength of HVFA mortars.

In this study two distinct scenarios are also observed, one is HVFA mortars containing up to 50% fly ash and the other containing more than 50% fly ash. In the former, the addition of 2% NS improved the early age compressive strength (7 days) and in latter case the improvement is observed at 28 days. The quantitative XRD analysis results, shown in Table 4.1, also support this observation where the addition of 2% NS consumed about 58% CH in mortar containing 40% fly ash. On the other hand, in mortar containing 60% fly ash this reduction in CH content is 50%. This clearly shows that the reactivity of NS is higher in HVFA mortar containing less than 50% fly ash than that containing more than 50% fly ash.

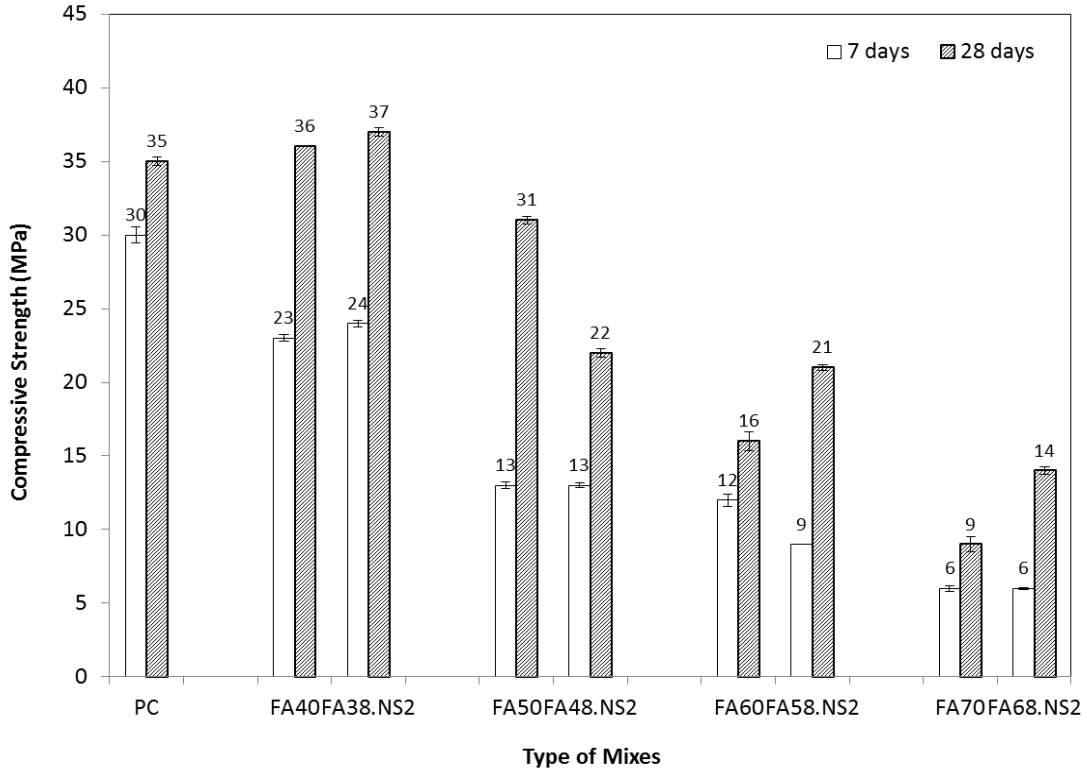

Figure 4.7 Effects of 2% NS on compressive strength of mortars containing HVFA

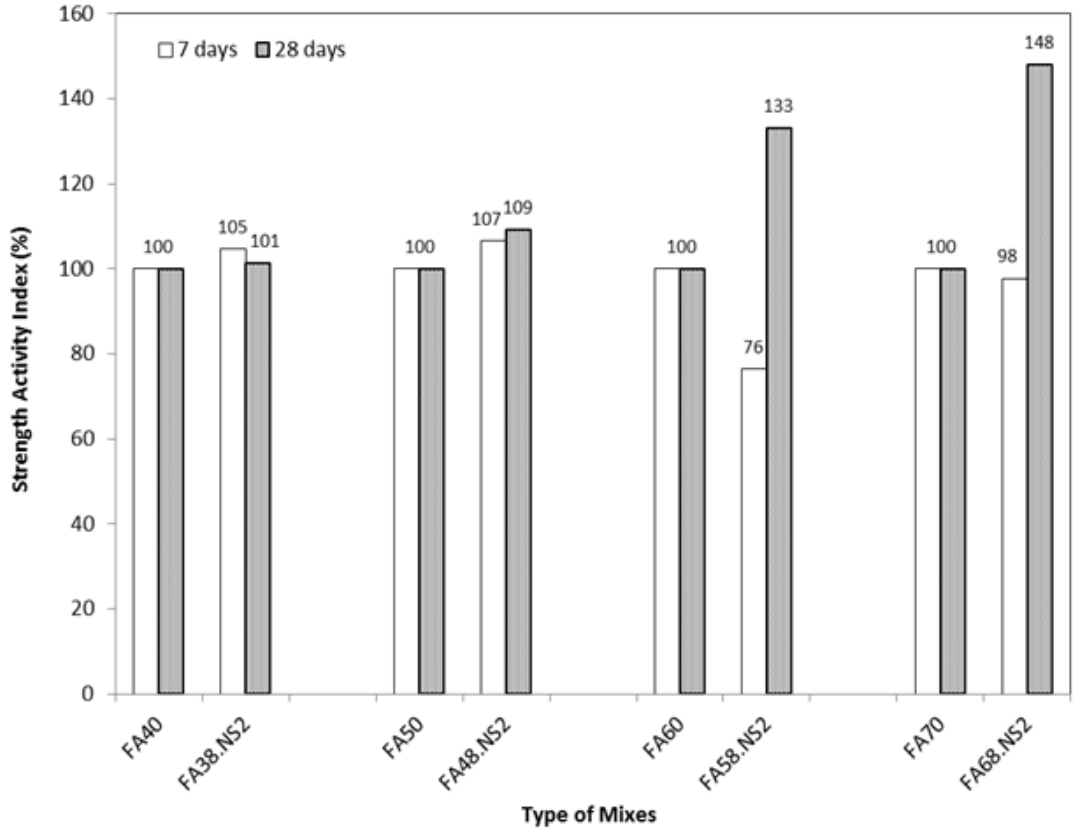

Figure 4.8 Strength activity index of HVFA mortars containing 2% NS

Table 4.1 Phase abundance of combined NS with fly ash paste samples based on quantitative XRD analysis

Phases	3 days curing				28 days curing					
	Weight %				Weight %					
	FA40	FA60	FA38. NS2	FA58. NS2	PC	NS2	FA40	FA60	FA38. NS2	FA58. NS2
Dicalcium Silicate – C_2S	9.5	9.7	9.3	6.1	16.6	16.8	8.7	15.1	6.5	9.5
Tricalcium Silicate – C_3S	2.6	1.7	2.0	-	5.0	4.1	2.9	3.2	0.6	1.4
Calcite - $CaCO_3$	2.7	2.4	2.4	3.6	5.0	4.7	2.9	4.3	2.4	3.6
Ettringite – $Ca_6Al_2(SO_4)_3(OH)_{12}.26H_2O$	-	-	1.4	0.6	0.5	0.4	-	0.4	0.4	1.2
Portlandite - $Ca(OH)_2$	7.5	4.1	6.6	3.2	15	12.1	7.2	13.0	3.0	6.5
Quartz - SiO_2	6.6	9.7	6.2	8.7	-	0.4	6.5	0.9	9.1	5.5
Amorphous content	57	59	59	60	54	52	63	58	62	59

4.3.2 Effect of nano-$CaCO_3$ on compressive strength of cement and HVFA mortars

The effects of nano-CaCO3 on the compressive strength of cement mortars are shown in Figure 4.9. It can be seen that 1% nano-$CaCO_3$ exhibited the highest compressive strength at both 7 and 28 days among all four nano-$CaCO_3$ contents and the compressive strength is decreased gradually with increase in nano-$CaCO_3$ contents. Based on the results, it can be seen that the NC1 mortar exhibited about 22 % and 18% higher compressive strengths at 7 and 28 days, respectively than the control mortar (PC). The lower compressive strength of mortars containing higher nano-$CaCO_3$ contents can be attributed to the poor dispersion due to agglomeration of nano-$CaCO_3$ in wet mix due to its higher van der Waal's forces than cement. On the other hand, in mortars containing high volume fly ash, common trend can be identified with lower compressive strength at higher fly ash contents.

The effect of nano-$CaCO_3$ on the compressive strength of high volume fly ash cement mortars is also shown in Figure 4.9. The results revealed that the compressive strength increased at all ages when nano-$CaCO_3$ is added in HVFA mortars containing 40 and 60% fly ash. It also can be seen that the 7-day compressive strength of mortar containing 40% fly ash is increased by about 21% due to addition of 1% nano-$CaCO_3$ and at 28 days this improvement is ceased, indicating the effectiveness of nano-$CaCO_3$ in compensating the low compressive strength at early age of HVFA system. A similar increase (approximately 21%) in 7-days compressive

strength of paste containing 30% fly ash and 5% nano-$CaCO_3$ is also reported by Kawashima et al. (2013). By comparing the 7 days compressive strength of FA39.NC1 with that of control cement mortar in the same figure, it can be seen that the addition of 1% nano-$CaCO_3$ significantly reduced the gap in 7 days compressive strength between the HVFA mortar and the control mortar. The results also show significant improvement of both 7 and 28 days compressive strengths of mortar containing 59% fly ash and 1% nano-$CaCO_3$. As an example, the compressive strength of FA60 mortar is increased from 12 to 24 MPa at 7 days and from 16 to 33 MPa at 28 days, which are about 100% and 111% improvement at 7 and 28 days, respectively. From the results in this study, it is apparent that the blending of nano-$CaCO_3$ with fly ash is effective in compensating the low early age compressive strength of HVFA mortars at 40% and 60% of cement replacement levels.

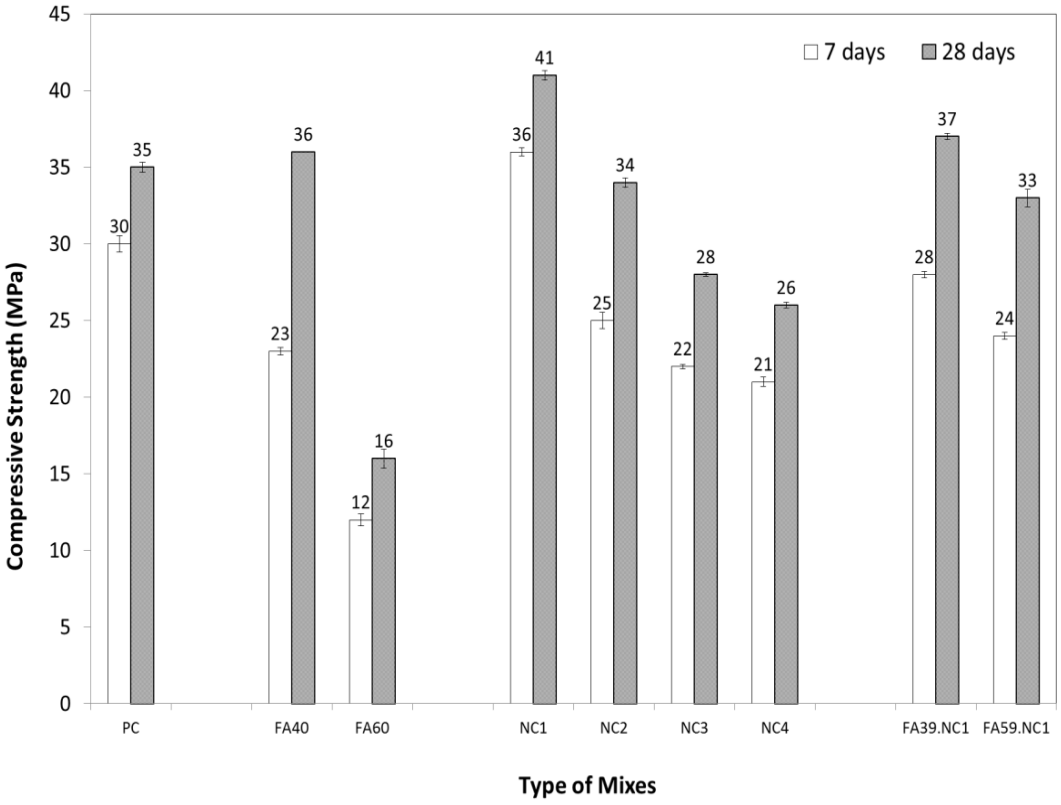

Figure 4.9 Compressive strength of control mortar containing NC and HVFA mortars containing NC at 7 and 28 days

4.4 Compressive strength development of concretes containing nano silica and nano $CaCO_3$ (Part II)

4.4.1 Effect of nano silica on compressive strength of OPC concrete and HVFA concretes

The compressive strength of all concrete measured after 3, 7, 28, 56 and 90 days of water curing is presented in Figure 4.10. It can be seen from the results that the addition of NS increases the compressive strength of ordinary concrete at all ages. For instance, the concrete containing 2% NS (Mix NS2) exhibited an enhancement in compressive strength from 13 to 31 MPa and from 17 to 44 MPa at 3 and 7 days, respectively. For mix NS4, the compressive strength reached 37 and 45 MPa at 3 and 7 days, respectively. It is about 150% higher than the compressive strength of ordinary concrete. At later ages including 28, 56 and 90 days, the NS2 and NS4 concretes led to an improvement in compressive strength between 45 and 75 %. However, there is no significant difference between NS2 and NS4 on the compressive strength development at later ages. The increase in compressive strength of NS concrete indicates that the NS particles take part in accelerating the process of pozzolanic reaction and densified the microstructure of the matrix (Li, 2004). Due to extremely high surface area and small particle size, the NS reacts more quickly with free lime in the hydration reaction than fly ash and produced secondary C-S-H gel and filled the capillary pores in the matrix. This improvement is also believe to be effective in enhancing the quality of the interfacial transition zone between the cement paste and aggregate.

The quantitative XRD analysis (see Table 4.1) also confirms that the cement paste containing 2% NS and 4% NS exhibited about 20% and 28% respectively, less calcium hydroxide, than control cement paste. This clearly indicates the effectiveness of NS in consuming calcium hydroxide (CH) and formation of additional C-S-H in the system. Furthermore, the improvements in early age compressive strength of concrete due to addition of NS are also reported by Nili et al., (2010). This author observed about 7% improvement in 7 days compressive strength due to addition of 1.5% NS compared to cement concrete.

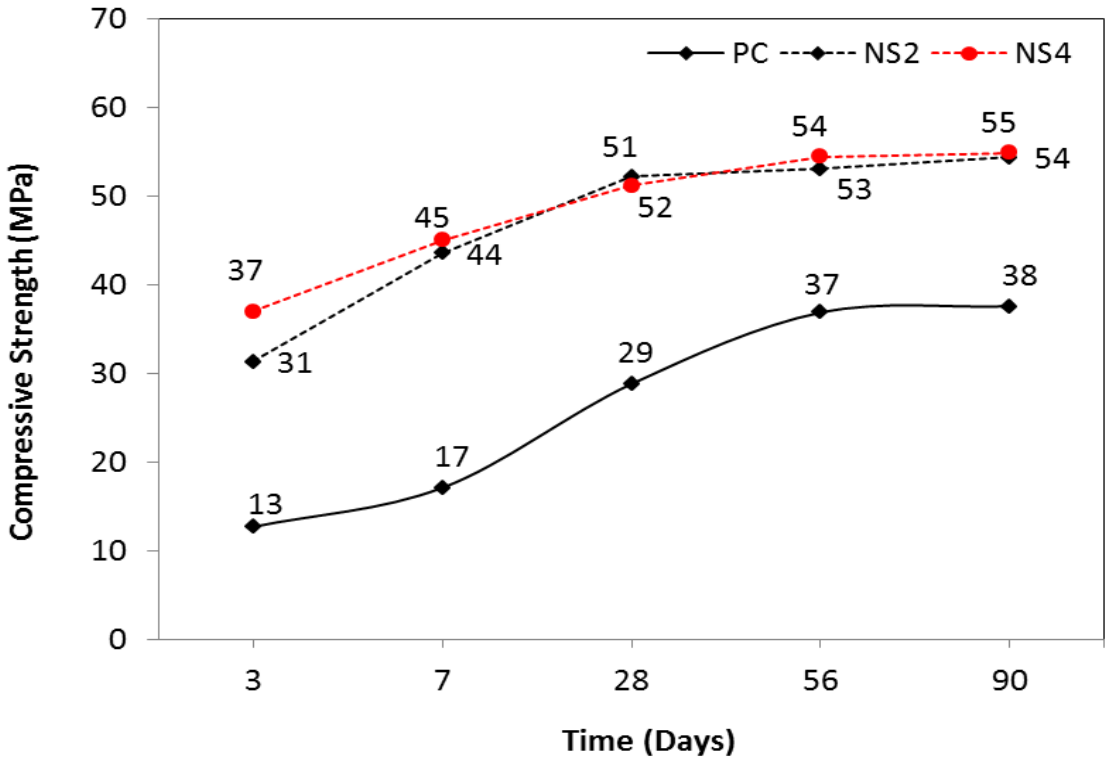

Figure 4.10 Compressive strength of cement and nano silica concrete

The study of the effect of NS on the compressive strength development of HVFA mortar is also extended to HVFA concretes. The 2% NS, which exhibited the highest compressive strength in part one is considered in the HVFA concretes containing 40% and 60% fly ash. These two fly ash contents are considered as the addition of 2% NS exhibited improvement in 7 days compressive strength in mortar containing 40% fly ash and in 28 days compressive strength in mortar containing 60% fly ash. Figure 4.11 shows the effect of 2% NS on 3, 7, 28, 56 and 90 days compressive strength of HVFA concretes containing 40% and 60% fly ash. It can be seen that the 2% NS significantly improved the 3 days compressive strength of both HVFA concretes, especially in concrete containing 60% fly ash, where about 95% improvement is observed. At later ages no such improvement is observed in that concrete, but the concrete containing 40% fly ash maintained the improvement between 15% and 21% at later ages (see Figure 4.11). In addition, it also can be seen that the addition of 2% NS performed better in improving the 7 and 28 days compressive strength of HVFA concrete containing 40% fly ash than its mortar counterpart. However, the slight reduction in 7 days compressive strength of HVFA concrete containing 60% fly ash is also consistent with its mortar counterpart. The effect of NS on the compressive strength development of HVFA concrete containing

50% fly ash is also studied by few researchers (e.g. Li et al., 2004; Zhang and Islam, 2012) and the improvements in 3 days compressive strength due to addition of 2-3% NS in their studies are very similar to that observed in this study of HVFA concrete containing 40% fly ash. However, the compressive strength development at later ages in their concretes is slightly higher than those observed in this study and can be attributed due to 10% more fly ash and different types and contents of NS.

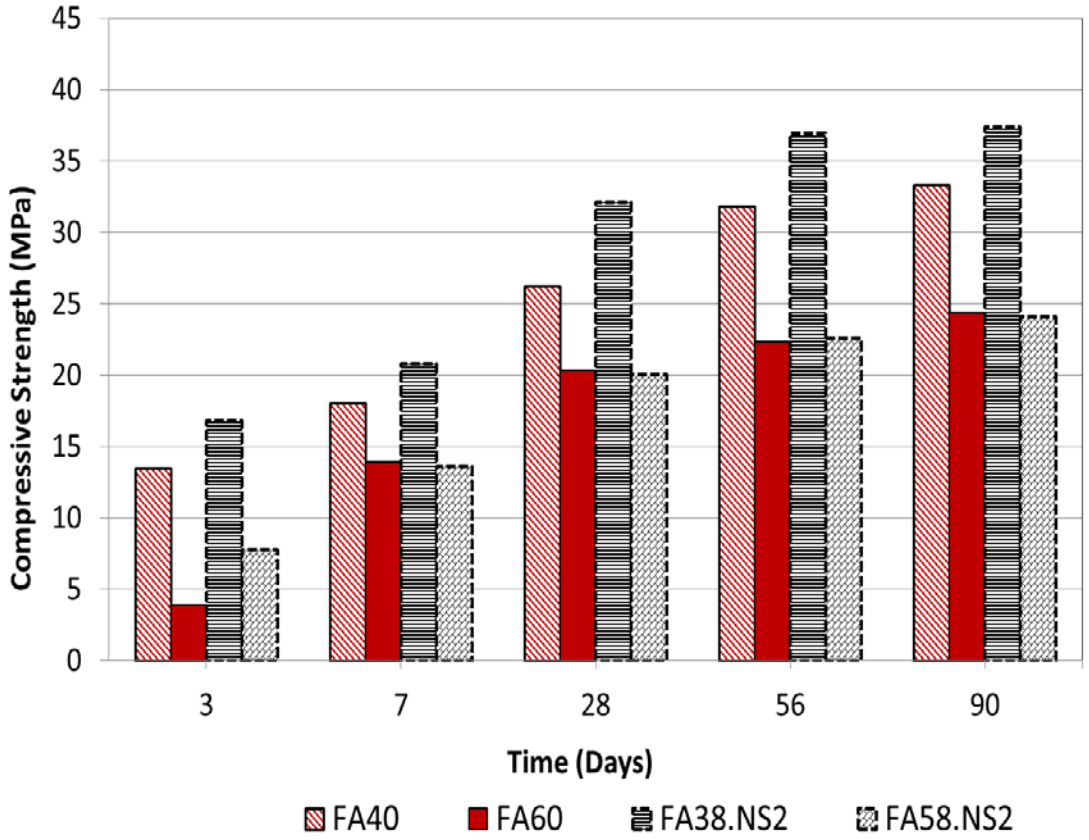

Figure 4.11 Effects of 2% NS on compressive strength of HVFA concretes containing 40% and 60% fly ash

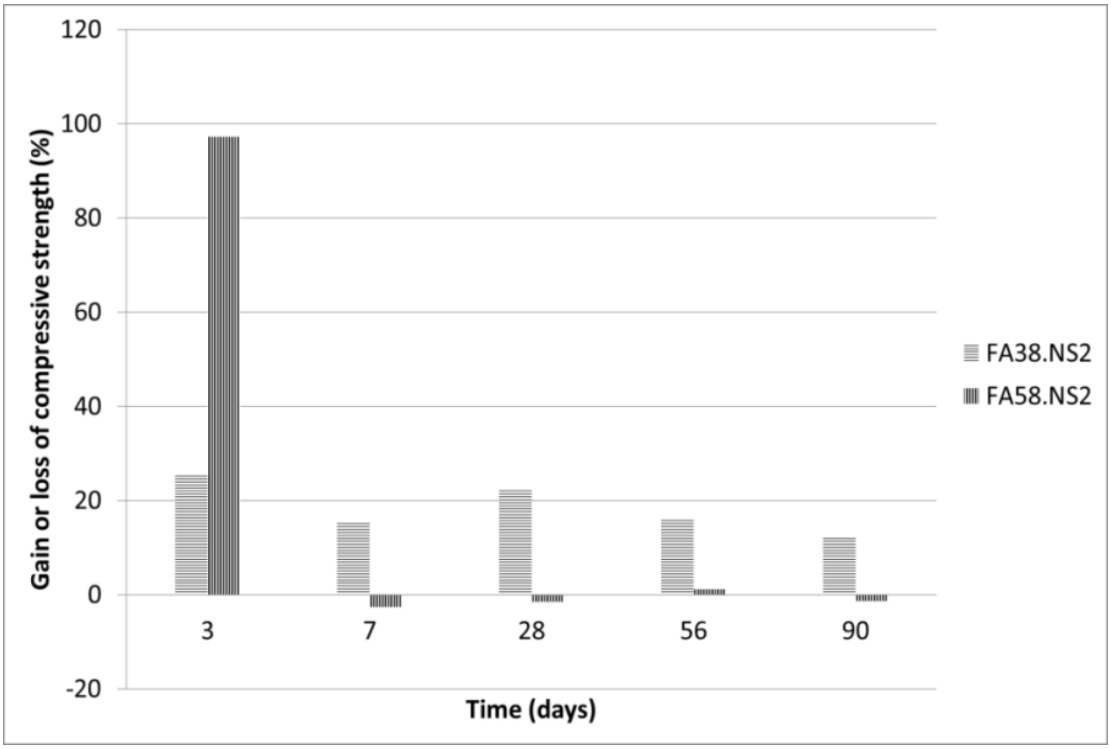

Figure 4.12 Gain or loss of compressive strength of HVFA mortars measured at different ages due to addition of 2% NS

4.4.2 Effect of nano-$CaCO_3$ on compressive strength of OPC concrete and HVFA concretes

The study of the effect of nano-$CaCO_3$ on the compressive strength development of OPC and HVFA mortars is also extended to OPC and HVFA concretes. The 1% nano-$CaCO_3$ which exhibited the highest compressive strength in mortar mixtures is considered as a replacement of cement in concrete mixes. Figure 4.13 shows the effect of 1% nano-$CaCO_3$ on compressive strength of cement concrete. Similar to that observed in mortar, the concrete containing 1% nano-$CaCO_3$ also exhibited higher compressive strength at all ages than the ordinary concrete. It can be observed that the 1% nano-$CaCO_3$ significantly improved the 3 and 7 days compressive strength by about 146% and 141%, compared to control cement mortar. At 28 days, the strength was recorded of about 41 MPa or 62% higher than control concrete and increased at all curing ages up to 90 days. However, replacing the cement with 2% of nano-$CaCO_3$ produced lower compressive strength than 1% of nano-$CaCO_3$, but still higher than the compressive strength of the control cement concrete, ranging between 22 and 44 MPa.

Table 4.2 shows the quantitative XRD analysis of cement pastes and nano-$CaCO_3$ pastes at 28 days. It is revealed that C_3S contents on NC1 and NC2 paste samples are lower compared to cement paste sample, indicates the rapid reaction between $CaCO_3$ particles and C_3S, resulted in an increase of Ca/Si ratio in C-S-H formation. Considering the CH consumption in pastes containing nano-$CaCO_3$ addition, it is clearly identified that there is no significant difference to CH content in cement pastes. However, it is assumed that an improvement in strength is also due to the physical nano-packing effect of nano-$CaCO_3$. Furthermore, the amorphous content is found to be at 58 and 57% in NC1 and NC2 paste samples, respectively greater than the cement paste. It can be explained that as the amorphous content increases, the volume of solids within the paste increases, therefore, improves the interlocking effect and reduces the overall porosity.

Figure 4.13 also shows the influence of 1% nano-$CaCO_3$ on the compressive strength of HVFA concretes containing 39 % and 59 % of fly ash as replacement of cement at the age of 3, 7, 28, 56 and 90 days. It is clearly seen that the addition of 1% nano-$CaCO_3$ significantly improved the compressive strength of HVFA concretes at all ages. It can also be observed that the addition of 1% nano-$CaCO_3$ significantly improved the 3 and 7 days compressive strength of HVFA concrete containing 39% fly ash, where about 47% and 44% improvements are observed, respectively. At 28, 56, and 90 days, the improvements are even higher (between 53% and 58%) for the concrete containing 39% fly ash and 1% nano-$CaCO_3$. However, the improvement in compressive strength of HVFA concrete containing 59% fly ash due to addition of 1% nano-$CaCO_3$ is not as great as that containing 39% fly ash and 1% nano-$CaCO_3$. Although due to limited published results the above results on early age as well as later age compressive strengths of HVFA concretes containing nano-$CaCO_3$ cannot be compared, the above trend, however, is very similar to that of HVFA concretes containing fine limestone powder reported by Tanesi et al. (2013).

The effect of 1 % nano-$CaCO_3$ addition in HVFA mortars and concretes are also evaluated based on the quantitative XRD analysis as shown in Table 4.3. The results indicate that the HVFA pastes containing 1% nano-$CaCO_3$ significantly reduced the CH, C_2S and C_3S amounts and increased the C-S-H amount. For example, at 7 and 28 days, the CH of FA40 paste sample was reduced from 6.6% to 6.1% and from 7.2% to 6.1%, respectively. Similar trend is also observed in FA59NC1 paste. The

reduction was very significant at both 7 and 28 days. For example, at 7 days the percentage of CH was 4.5% and reduced to 1.9% after 1% nano-$CaCO_3$ addition. Moreover, at 28 days, the CH was reduced from 13% to 3%. In addition, the amount of C_3S indicates the cement hydration level particularly at early-age of compressive strength. The lesser the amount of C_3S the higher the degree of cement hydration thus the higher early strength of concrete (Xu et al., 2012). As shown in Table 4.4, the presence of C_3S could not be identified in HVFA pastes containing 1% nano-$CaCO_3$ compared to FA40 and FA60 pastes, that means the higher degree of cement hydration is accelerated thus the higher early strength can be expected.

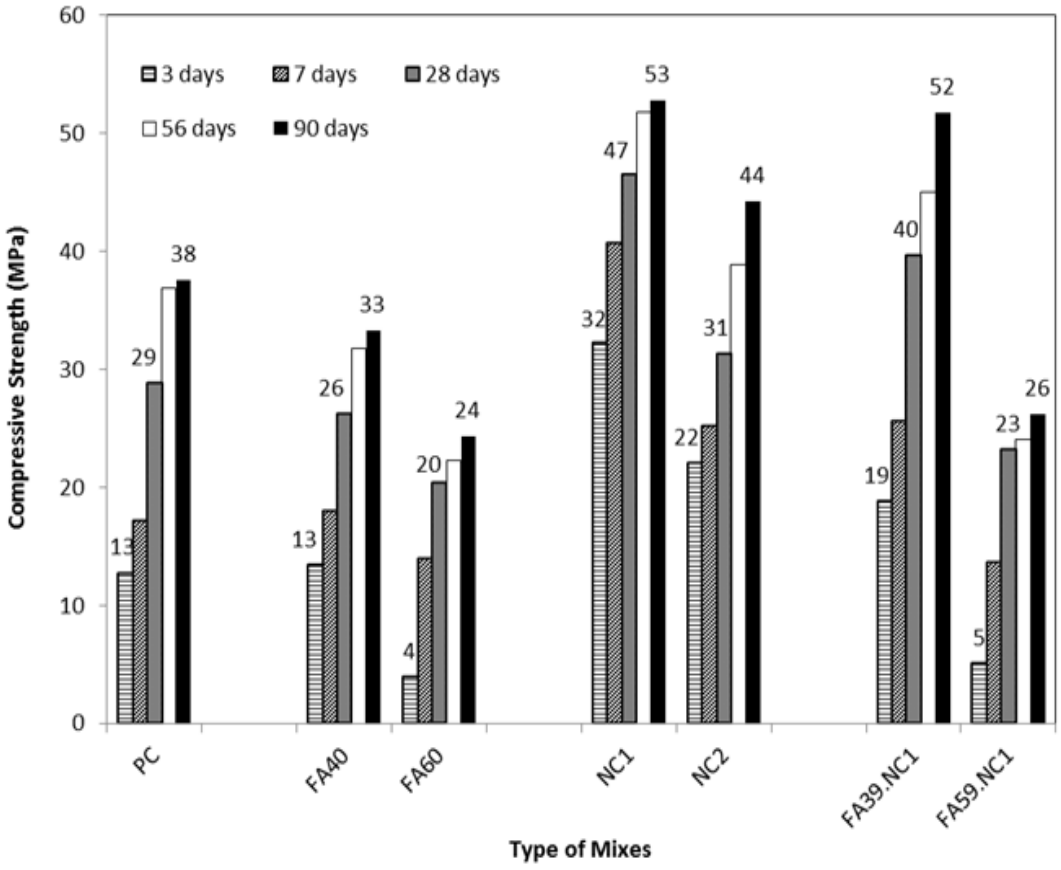

Figure 4.13 Compressive strength of concretes containing NC and HVFA concretes containing NC at 3, 7, 28, 56 and 90 days

Table 4.2 Quantitative XRD analysis of cement and nano-$CaCO_3$ pastes at 28 days

Phase	Weight %		
	PC	**NC1**	**NC2**
Dicalcium Silicate - Ca_2SiO_4	16.6	9.6	10.6
Tricalcium Silicate - Ca_3SiO_5	4.5	1.7	2.5
Calcite - $CaCO_3$	5.0	7.4	5.9
Ettringite - $Ca_6Al_2(SO_4)_3(OH)_{12}.26H_2O$	0.5	3.6	3.2
Portlandite - $Ca(OH)_2$	12.1	12.4	12.8
Quartz - SiO_2	-	0.4	0.5
Amorphous content	54	58	57

Table 4.3 Quantitative XRD analysis of HVFA with and without nano-$CaCO_3$ pastes at 7 and 28 days

Phase	Weight (%)							
	FA40		**FA60**		**FA39.NC1**		**FA59.NC1**	
	7days	***28 days***	***7days***	***28 days***	***7days***	***28 days***	***7 days***	***28 days***
Dicalcium Silicate - C_2SiO_4	9.0	8.7	5.5	15.1	5.8	6.3	3.4	4.3
Tricalcium Silicate - C_3SiO_5	2.7	2.9	1.5	3.2	-	-	-	-
Calcite - $CaCO_3$	3.8	2.9	2.7	4.3	5.9	5.6	6.1	5.5
Ettringite - $Ca_6Al_2(SO_4)_3(OH)_{12}.26H_2O$	-	-	-	0.4	2.5	1.3	1.7	0.6
Portlandite - $Ca(OH)_2$	6.6	7.2	4.5	13.0	6.1	6.1	1.9	3.0
Quartz - SiO_2	6.8	6.5	9.7	0.9	4.7	5.4	5.8	6.0
Amorphous content	58	63	45	58	60	61	64	62

4.5 Durability properties of cement concrete and HVFA concretes containing nano silica and nano-$CaCO_3$

4.5.1 Water sorptivity

4.5.1.1 Effect of nano silica on water sorptivity of OPC concrete and HVFA concretes

The rate of absorption of all types of concretes at 28 and 90 days are presented in Figures 4.14 and 4.15. The best-fit lines in the figures as based on coefficient of determination (r^2) values greater than 0.98 for all mixes. It can be seen that the cumulative volume of water absorbed in the concrete increased with the square root of time. The slope of the obtained line defines the sorptivity of different concretes

during the initial 6 hour of testing. It can be clearly seen that the rate of water absorption of ordinary concrete is reduced at 28 and 90 days due to addition of NS. It is due to fineness, high pozzolanic activity and the formation of secondary C-S-H due to reaction of nano silica particles with CH. According to the summarised sorptivity values in Figure 4.16, the minimum water sorptivity at 28 and 90 days were 28 and 21 ($x10^{-4}$ $mm/sec^{1/2}$), respectively for NS4 concrete. The values are 2-3 times lower when compared to ordinary concrete without NS. In addition, the NS2 concrete also shows comparable results with NS4 concrete mix.

Figures 4.15a and b show that the sorptivity of HVFA concretes is higher than those containing 2% NS with similar w/b ratio because of high fly ash content. In HVFA concretes containing NS, it can generally be seen that the FA38.NS2 concrete exhibits higher resistance to water absorption by capillary suction than FA40 concrete. Based on the sorptivity values in Figure 4.16, the water sorptivity of FA38.NS2 concrete at 28 and 90 days reveals 27% - 32% lower than that of FA40 concrete. In addition, in FA58.NS2 concrete, the influence of NS addition was found more pronounced in reducing the water absorption due to the capillary pores suction after 90 days of water curing, since the mature concrete has a more discontinuous pore system. The results also shows that the addition of 2% NS reduced the sorptivity of HVFA concrete containing 38% fly ash below the sorptivity values of OPC concrete at both 28 and 90 days.

The results show that by combining NS in HVFA concrete, the capillary absorption of water can be reduced. The reduction in water sorptivity can be explained as the rapid reaction of NS with CH, thus accelerating the hydration products and improving the bonding effect between cement paste and aggregate. This process, therefore, improves the density of concrete due to reduction of pore volume, which is also observed in mercury intrusion porosity tests discussed in section 4.5.3. This finding corroborates the ideas of Sadrmomtazi and Fasihi, (2011) who suggested that the nano silica particles generate large amount of nucleation sites for precipitation of hydration products and block the passages connecting capillary pores and water channels in cement paste.

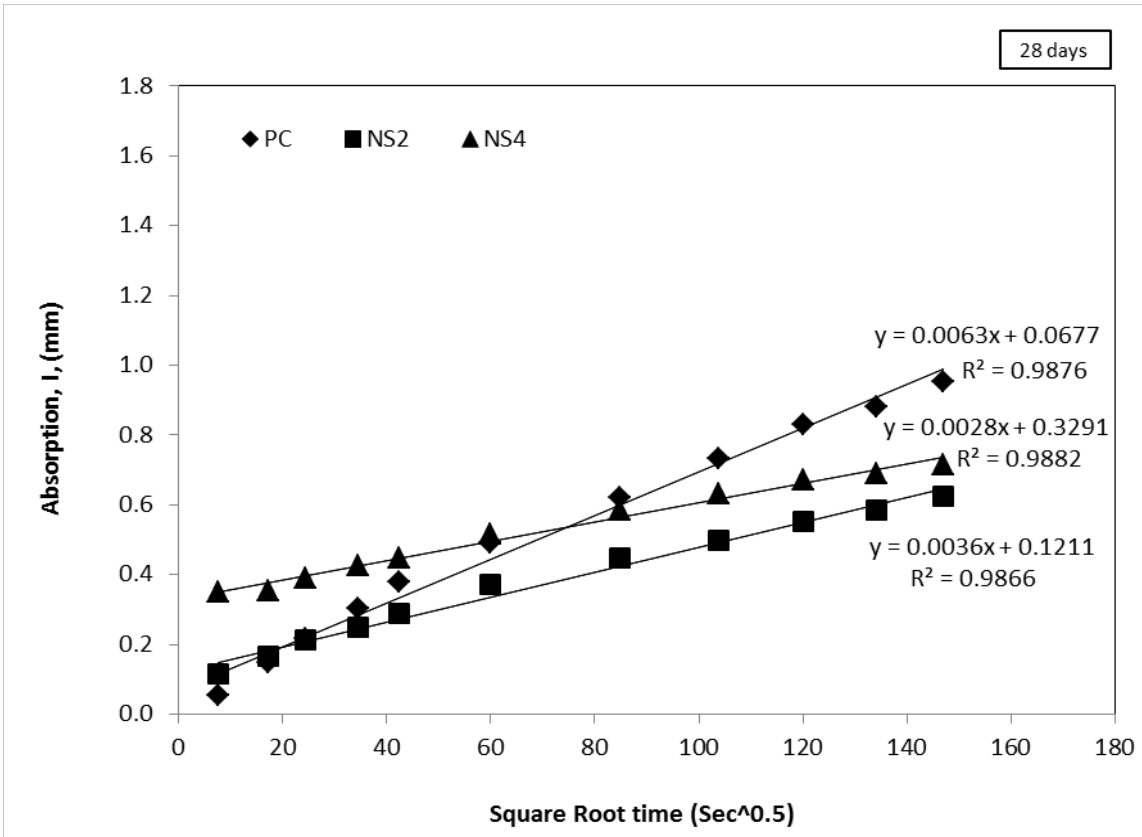

(a)

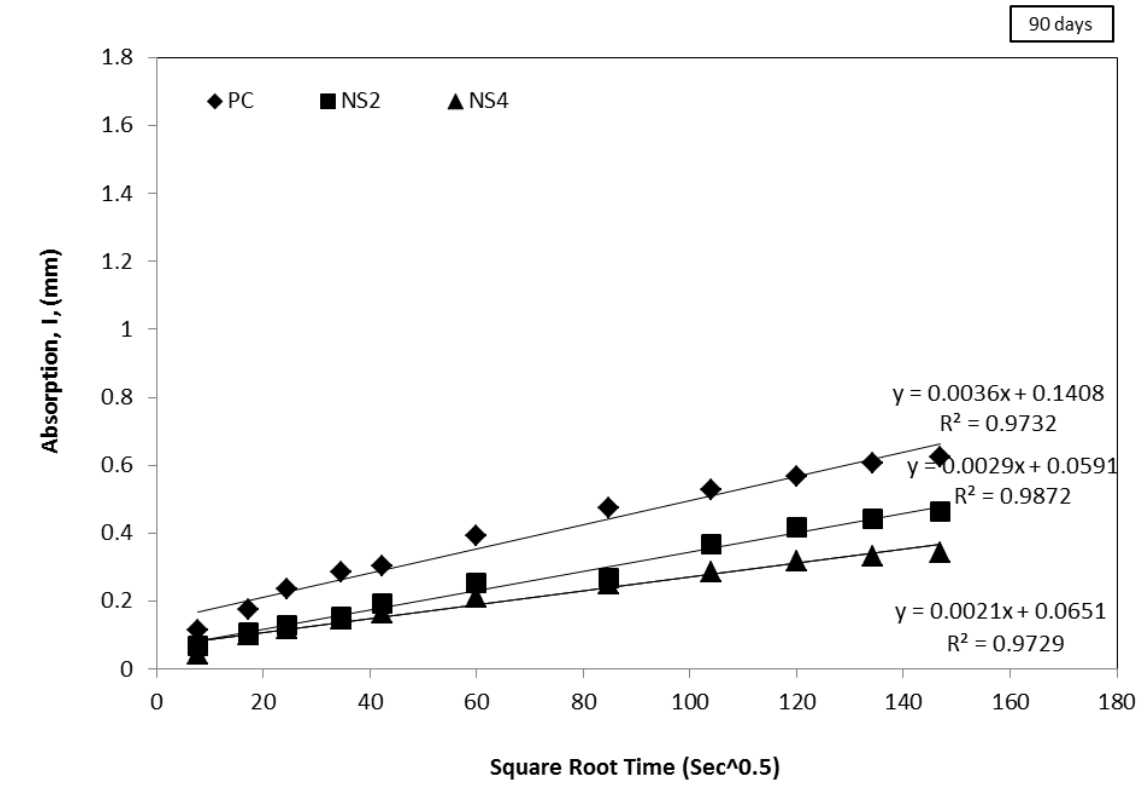

(b)

Figure 4.14 Water absorption of cement concrete mixes containing nano silica at 28 and 90 days

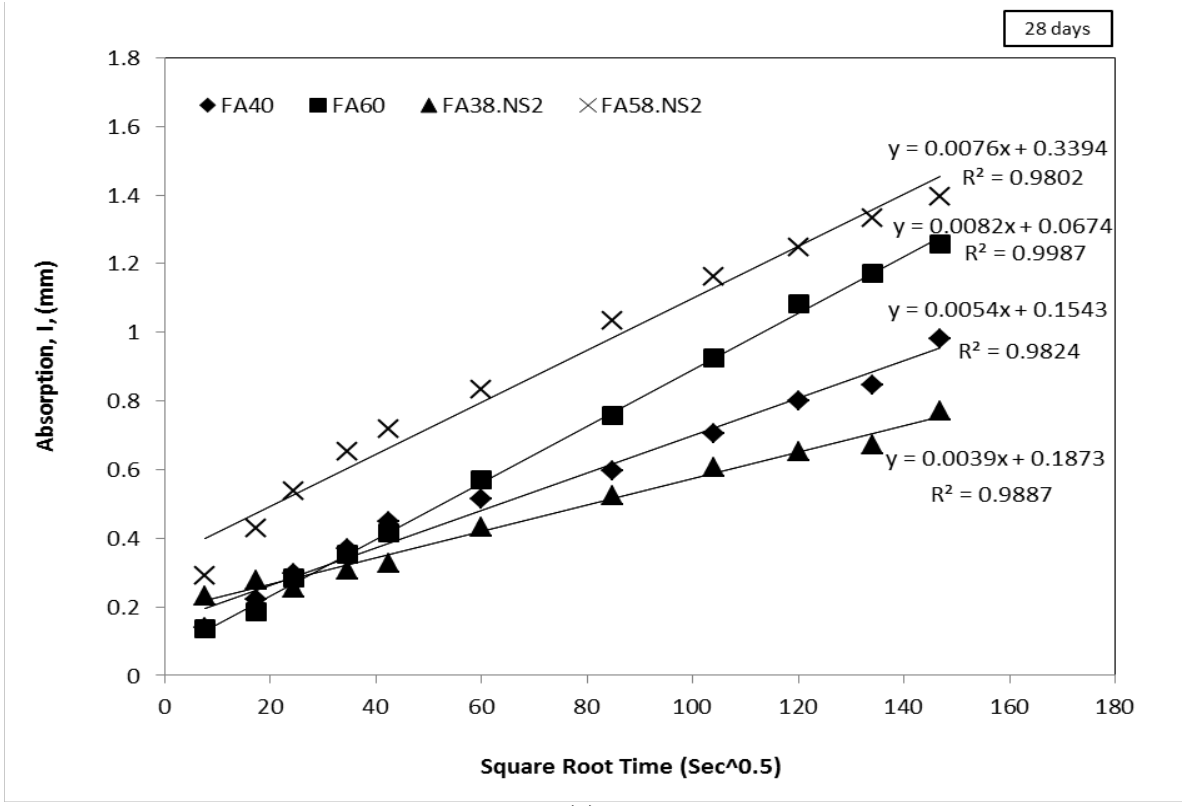

(a)

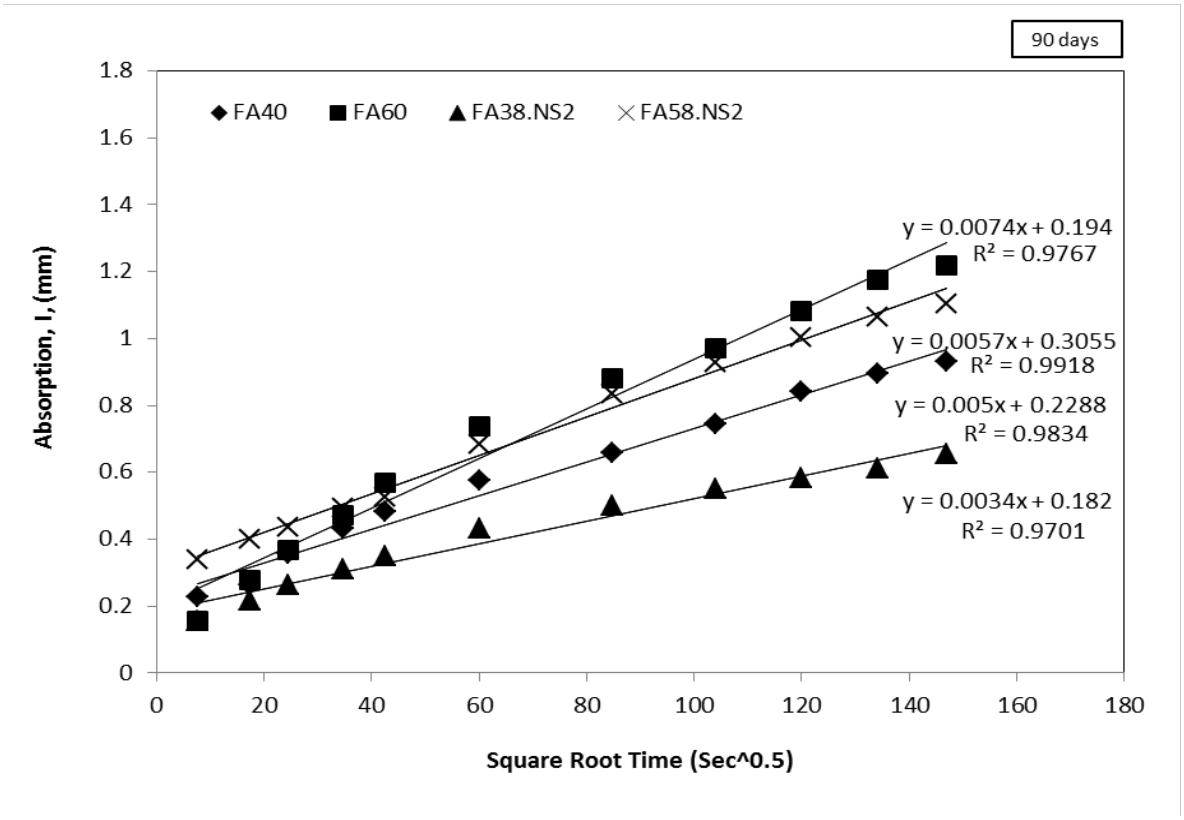

(b)

Figure 4.15 Water absorption of HVFA concrete mixes containing 2% nano silica at 28 and 90 days

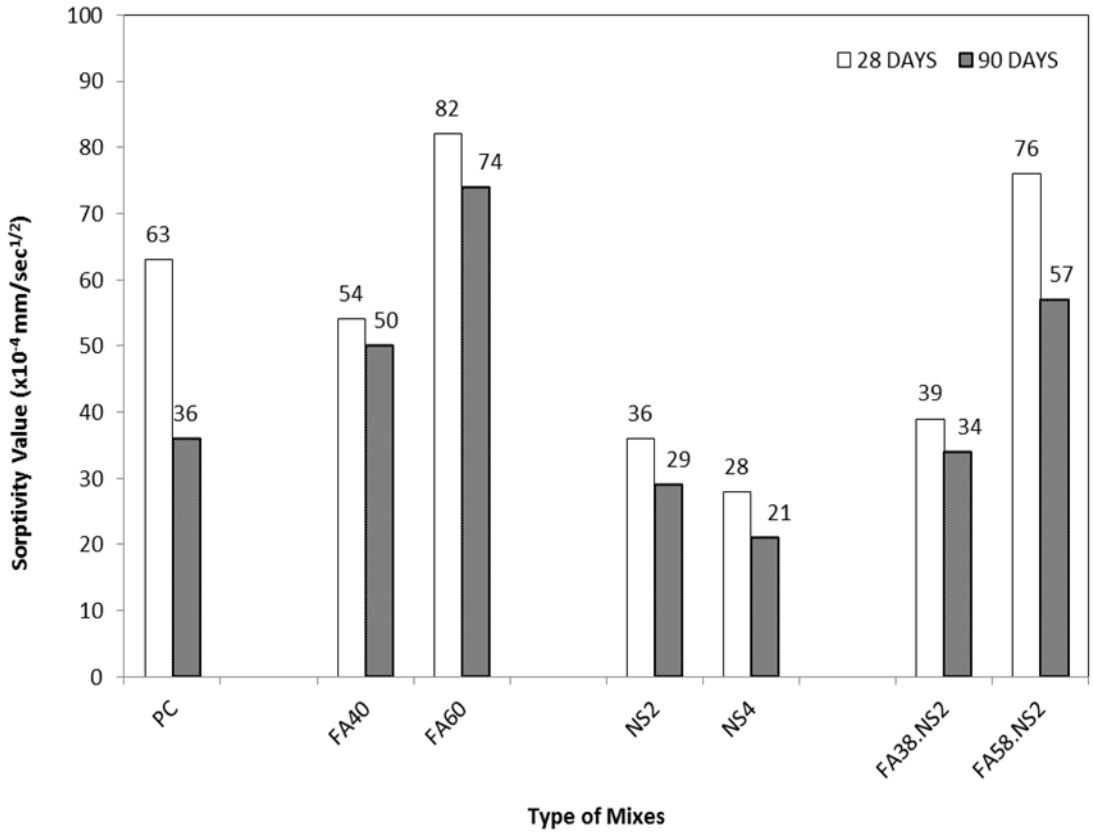

Figure 4.16 Sorptivity value of concretes containing 2% nano silica at 28 and 90 days

4.5.1.2 Effect of nano-$CaCO_3$ on water sorptivity of ordinary concrete and HVFA concretes

The effects of nano-$CaCO_3$ on sorptivity of 28 and 90 days cured ordinary cement concrete and HVFA concretes are shown in Figure 4.17. It clearly shows the decrease in water absorption at 28 and 90 days in the concrete containing nano-$CaCO_3$. By comparing Figures 4.17a and b, it can be seen that the addition of 1% nano-$CaCO_3$ performed better than 2% at both 28 and 90 days. Water sorptivity of NC1 concrete is 19% and 60% lower than the control concrete (PC) at 28 and 90 days, respectively (see Figures 4.19). This result shows that the rate of water absorption is reduced in concrete containing nano-$CaCO_3$ due to formation of C-S-H gels which filled the water-filled spaced and reduced the capillary pores. The reduction of pore volumes of NC1 and NC2 concretes is also evidenced in this study through mercury porosimetry test results as discussed in the following section.

The sorptivity test results also show that the use of 1% nano-$CaCO_3$ in HVFA concretes significantly reduced the rate of water absorption (see Figures. 4.18a and b). As can be seen in Figure 4.19 that the water sorptivity values of FA39.NC1 concrete at 28 and 90 days were 52 and 46 ($x10^{-4}$ $mm/min^{1/2}$), respectively, which is lower than the concrete containing 40% fly ash (FA40). It can also be seen that at longer curing time (90 days) the water sorptivity of FA39.NC1 concrete is lower than 28 days curing. The effect of longer curing can also be seen in FA59.NC1 concrete where the sorptivity value is reduced from 82 to 57 ($x10^{-4}$ $mm/sec^{1/2}$) due to 90 days wet curing. This is an indication that the addition of 1% nano-$CaCO_3$ in HVFA paste forms a finer pore structure than HVFA paste alone in longer term. Based on the above results, it can be commented that by combining nano-$CaCO_3$ in HVFA concrete, the hydration process can be intensified due to the consumption of CH and form of new C-S-H gels. In addition, the nano-$CaCO_3$ densified the microstructure and refined the pores and increased the density of concrete, which is confirmed by the results in mercury intrusion porosimetry tests.

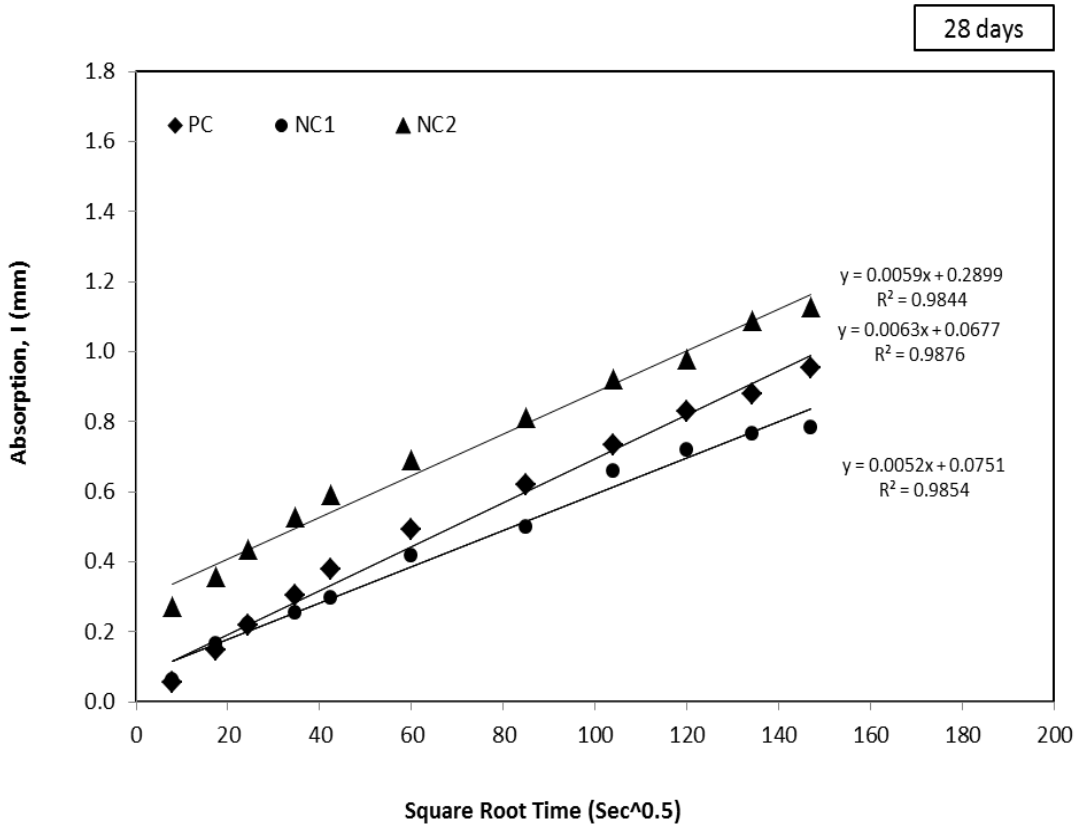

(a)

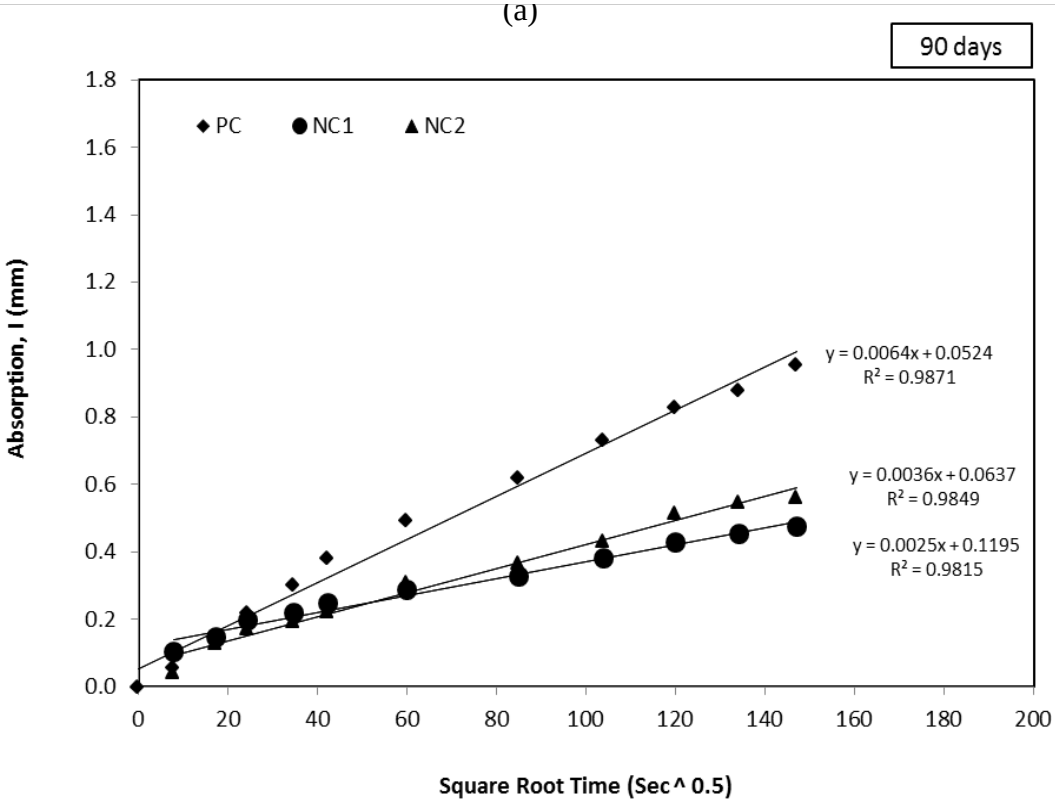

(b)

Figure 4.17 Water absorption of cement concrete mixes containing nano-$CaCO_3$ at 28 days and 90 days

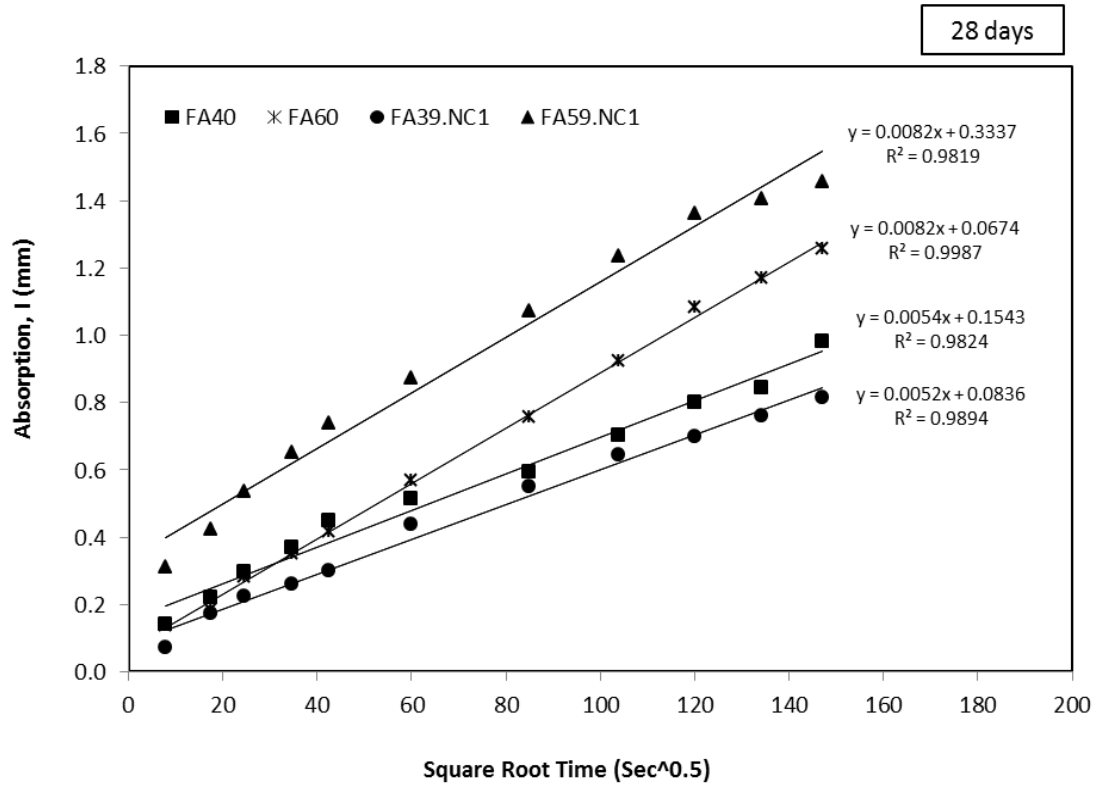

(a)

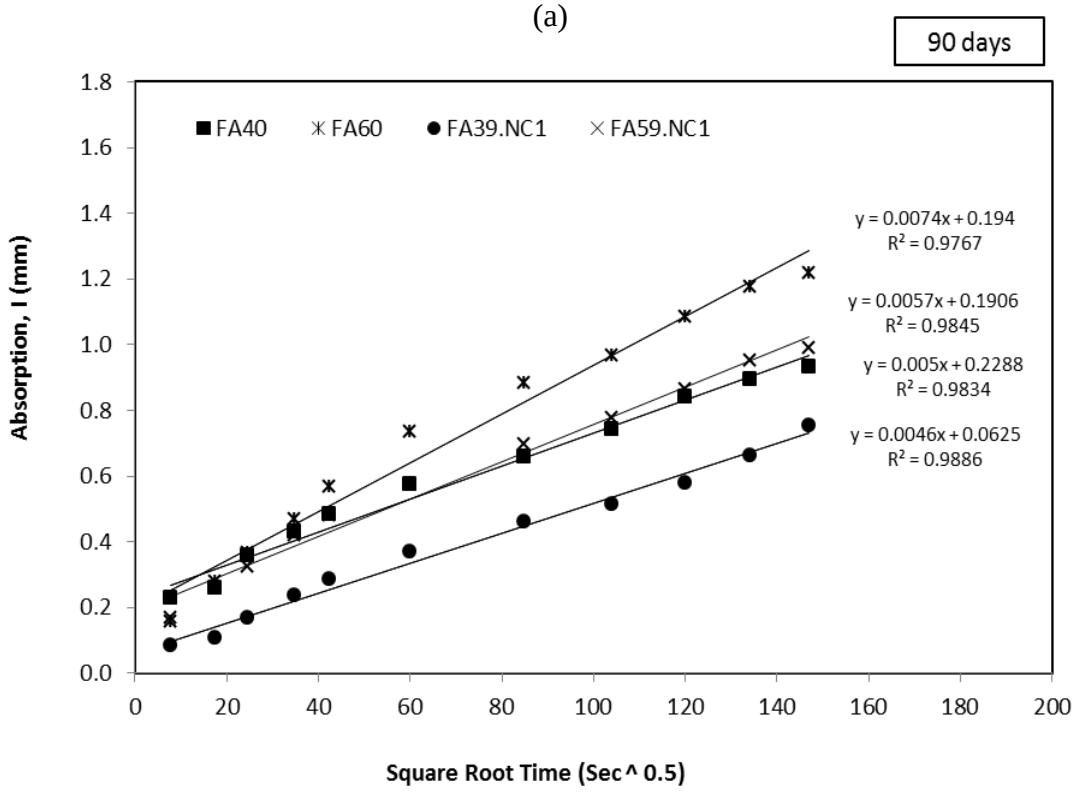

(b)

Figure 4.18 Water absorption of HVFA concrete mixes containing 1% nano-$CaCO_3$ at 28 and 90 days

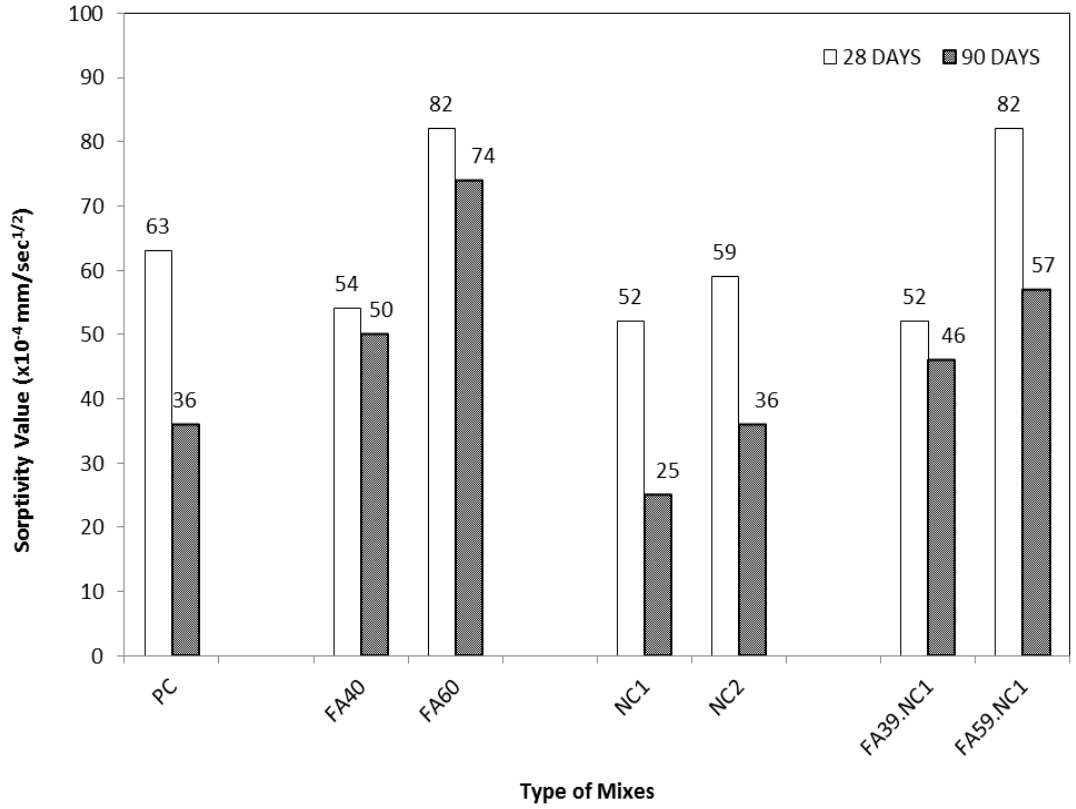

Figure 4.19 Sorptivity value of various concretes containing NC measured after 28 and 90 days of curing

4.5.2 Volume of permeable voids

4.5.2.1 Effect of nano silica on volume of permeable voids of OPC concrete and HVFA concretes

Figure 4.20 presents the volume of permeable voids (VPV) of different concretes at 28 and 90 days. The VPV is recognized as an important property of concrete since it affects the transport mechanism of aggressive fluids through concrete. As expected, the VPV of concrete containing nano silica shows a decreasing tends with increase in curing time. The VPV of NS2 and NS4 concretes at 28 and 90 days are remarkably low and reduced by nearly between 10% and 18% than ordinary concrete. In this case, the NS2 concrete achieves the lowest VPV compared to NS4 concrete, which is consistent with compressive strength results discussed before.

The effect of NS on the VPV of HVFA concretes is also shown in Figure 4.20. The volume of permeable voids is reduced as the nano silica is added in the HVFA concretes. For instance in concrete containing 40% fly ash the incorporation of 2% NS led to about 8% reduction of VPV at both 28 and 90 days. However, no

significant improvement was observed in FA58.NS2 concretes due to addition of 2 % NS.

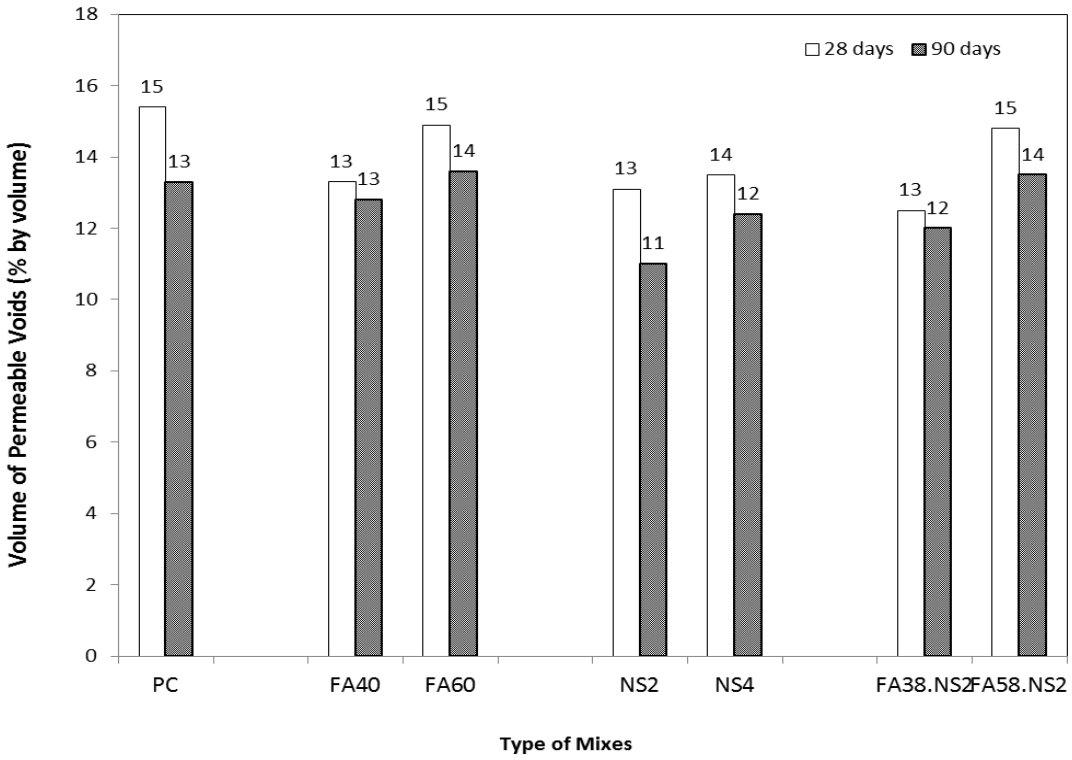

Figure 4.20 Volume of permeable voids of different types of concrete mixtures containing 2% nano silica at 28 and 90 days

4.5.2.2 Effect of nano-$CaCO_3$ on volume of permeable voids of ordinary concrete and HVFA concretes

The effect of nano $CaCO_3$ on VPV of ordinary Portland cement concrete is shown in Figure 4.21. It can be seen in the figure that the percentage of voids in concrete is reduced due to addition of nano-$CaCO_3$ irrespective of curing ages. For example, the concrete containing 1% nano-$CaCO_3$ decreased the VPV significantly up to 46% at 28 days in relation to ordinary cement concrete. As expected, the volume of permeable voids of concrete decreased with increase in curing time. The results showed that the incorporation of 1% nano-$CaCO_3$ in cement concrete increased the packing density of binder due to the distribution of the hydration products hence less pores can be expected.

The effect of 1% nano-$CaCO_3$ on VPV of high volume fly ash concretes is also shown in Figure 4.21. It can be seen that the addition of 1% nano-$CaCO_3$

significantly reduced the VPV of HVFA concretes containing 40% fly ash by 30% and 46% at 28 and 90 days, respectively. However, the reduction of VPV was only 7% and 21% at 28 and 90 days, respectively in FA59.NC1 concrete. This result is consistence with sorptivity and compressive strength results, where the NC1 concrete performed better than the NC2 concrete, presumably due to better dispersion of $CaCO_3$-nanoparticles.

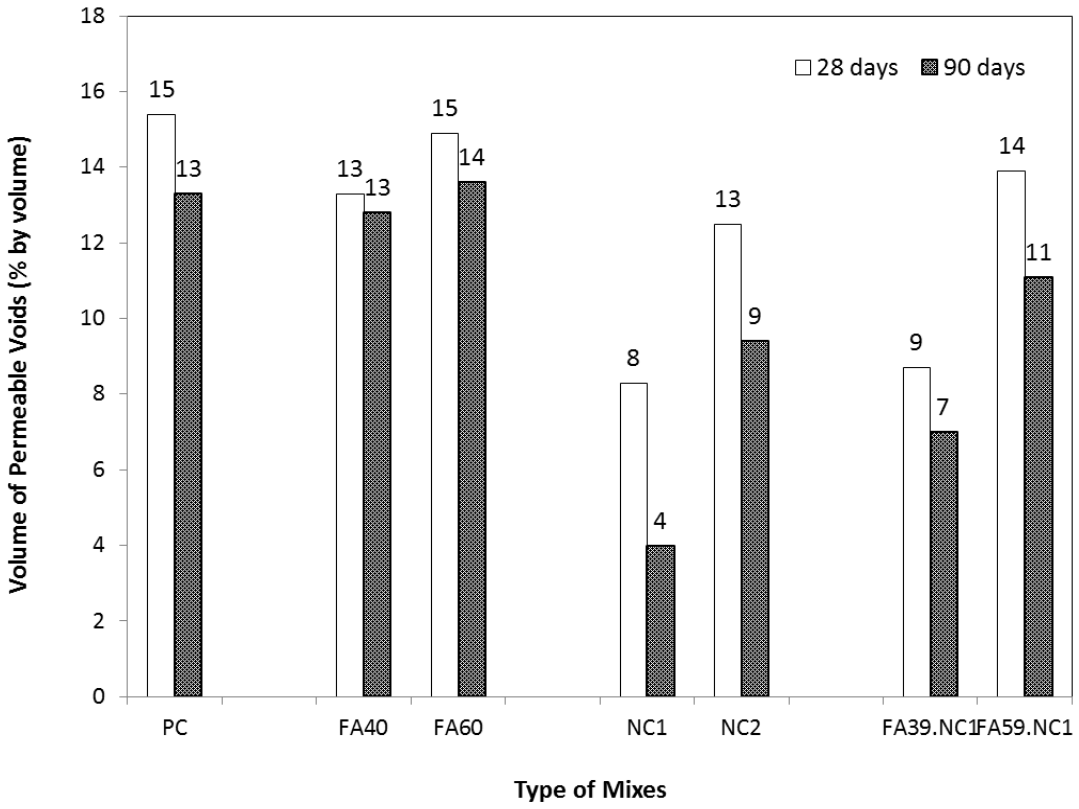

Figure 4.21 Volume of permeable voids of different concretes containing 1% nano-$CaCO_3$ at 28 and 90 days

4.5.3 Mercury intrusion porosimetry (MIP)

Mercury intrusion porosimetry was performed on different cement paste samples containing NS and HVFA after 28 days of curing. This method is widely used to evaluate the total porosity and size distribution of pores in cement matrix. The mercury intrusion porosimetry results of the paste specimens are plotted in Figures 4.22 and 4.23. It shows the relationship between cumulative pore volume and pore diameter in the range of 0.01 to 100µm. Mindess in Zhang and Islam (2012) Classified the pores as large capillary pores, medium capillary pores and gel pores which are in the range of 10-0.05µm, 0.05-0.01 µm and <0.01µm, respectively. Gel

pores form a part of C-S-H and are considered as micro pores. They are not active in water permeability and do not influence the strength. However, they influence shrinkage and creep of the concrete. The capillary pores are partially and completely filled with water and reduce as hydration continues. Capillary pores affect the strength and durability of concrete (Brandt,1995).

4.5.3.1 Porosity of cement and HVFA pastes containing nano silica

The effect of nano silica on the porosity of cement paste and HVFA pastes is shown in Figures 4.22 and 4.23. It is clearly seen in the figure that the total porosity and initial pore entry diameter of NS pastes are about 0.15 cc/g and 0.1 µm, respectively (see Figure 4.22a), where no distinct difference between paste with 2% NS and 4% NS is seen. The initial pore entry diameter is a diameter at first inflection point of volume-diamater curve which indicates the minimum diameter of pores that are continuous through the paste (Winslow and Diamond, 1969; Zhang et al, 2012). The results show that the use of nano silica leads to a more compact paste with a significant reduction of the pores between 0.1 and 10 µm. In addition, it is also observed that all pores especially the large capillary pores of NS pastes are significantly reduced, thus the total porosity of the NS pastes is also decreased.. In comparison to cement paste, the cumulative pore volume of NS pastes is about 25% lower and indicates finer pore structure in the NS pastes. In the case of HVFA pastes, it can be clearly seen that the total pore volume particularly capillary pores of HVFA pastes is higher than pure cement paste and the pastes containing NS. The paste with 60% fly ash has a coarser pore structure with a total porosity of 0.61 cc/g and initial pore entry diameter of 2 µm (see Figure 4.22b). Higher capillary pores of HVFA pastes can be attributed to the less cement and hence, less C-S-H formed during hydration reaction and slow pozzolanic reaction of fly ash in concrete. On the other hand, due to large surface area and higher fineness of NS than fly ash, more C-S-H gel was formed in HVFA pastes containing NS, which contributed to the reduction in capillary volume and gel pores. The results in Figure 4.20b show that all pores of the HVFA pastes were decreased with the addition of 2% NS. These contributed to high resistance of HVFA concretes against water permeability and chloride ion penetration which has been reported in this chapter.

Figures 4.23a and b show the effect of NS on pore size distribution of cement and HVFA pastes. The region under the curve represents the concentration of the pores.

The value of critical diameter corresponds to the peak point of log differential curve from MIP results. Figure 4.23a shows that the maximum concentration of pores in NS pastes tend to be around medium pore sizes and the curve peak become less dominant in comparison to cement and HVFA pastes (see Figures 4.23a and b). The porosity of NS2 and NS4 pastes are concentrated around 0.5 and 0.7 µm, respectively. However, small curve in NS4 paste is observed around large capillary pores (2-20µm) which is assumed to be due to agglomeration of nano silica particles in cement paste matrix. The agglomeration of nano particles will create weak zone and block the surface area from contact with other products (Li et al., 2004). Consequently, the formation of pores can be expected. This explanation supports the results obtained on porosity of concrete containing 4% nano silica particles as described earlier. In addition, the NS paste exhibits not only a lower porosity but also a finer pore structure than cement paste. The NS paste contain mainly pores with diameter < 0.1µm which can restrict the flow of harmful ions into the paste. Since the permeability and penetration of harmful ions into concrete are affected mainly by the large and medium capillary pores, the incorporation of 2% NS is suggested to contribute the improvement of durability properties of concrete.

In the case of HVFA pastes with 2% NS addition, there is also a notable reduction in pore concentration indicating the presence of NS is advantageous for the pores modification. With regard to FA40 paste sample, the result shows that the cumulative pore volume is reduced significantly after adding 2% NS. While the total porosity of FA40 and FA60 are 0.39 and 0.60 cc/g, the FA38.NS2 and FA58.NS2 paste samples have total porosity of 0.31 and 0.28 cc/g, respectively. The graph in Figure 4.23b shows that the porosity of FA38.NS2 is concentrated around 0.0.1-0.10 µm which is lower than the concentration of the pores in FA40 paste. Similar trend is also observed in FA58.NS2 paste. It is noted that NS has a significant influence in the reduction of the total capillary porosities and pores diameter of HVFA pastes. This suggests that the presence of NS with high amorphous silica content can overcome the negative effect of high volume fly ash by increasing the reaction degree, filling spaces between cement and fly ash particles, and increasing the density of microstructure. These results confirm a dense microstructure of the cement and HVFA pastes matrix containing nano silica according to the observation obtained from SEM analysis (see section 4.6.1) and provide a reasonable relationship among

the results gained from water absorption, porosity and rapid chloride permeability test. In conclusion, the reaction between nano silica particles and CH crystals produced more compact matrix, blocked the capillary and gel pores and increased the water and chloride ions permeability resistance.

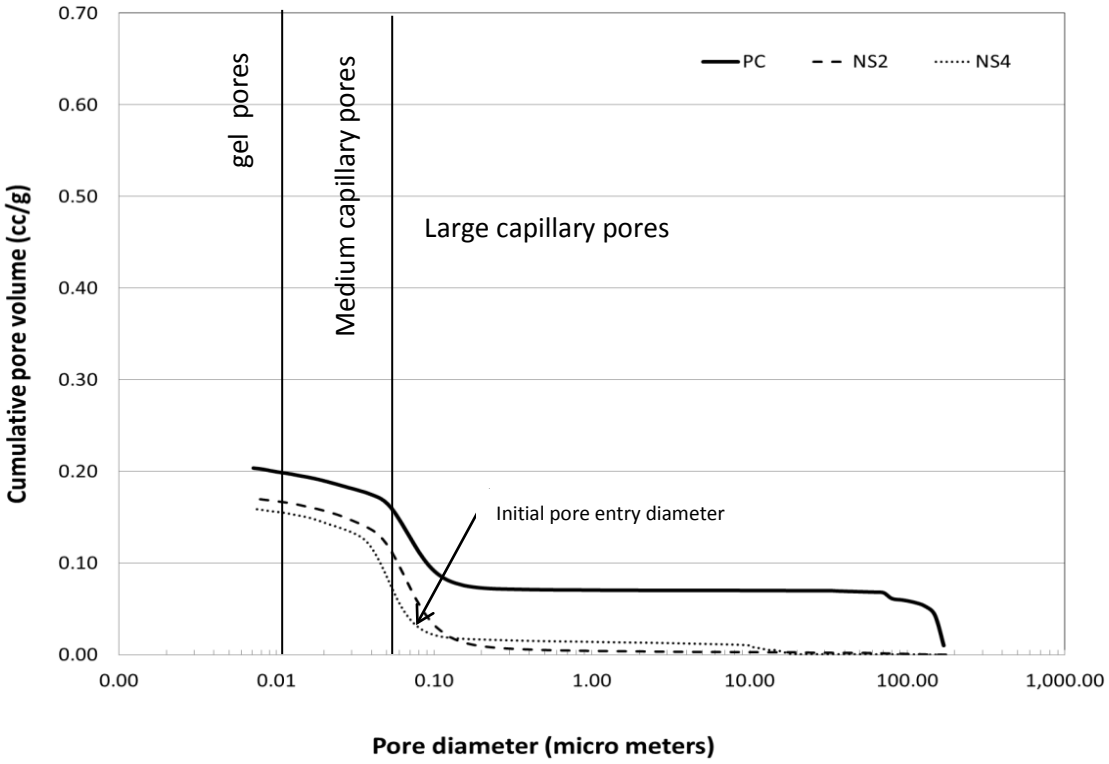

(a)

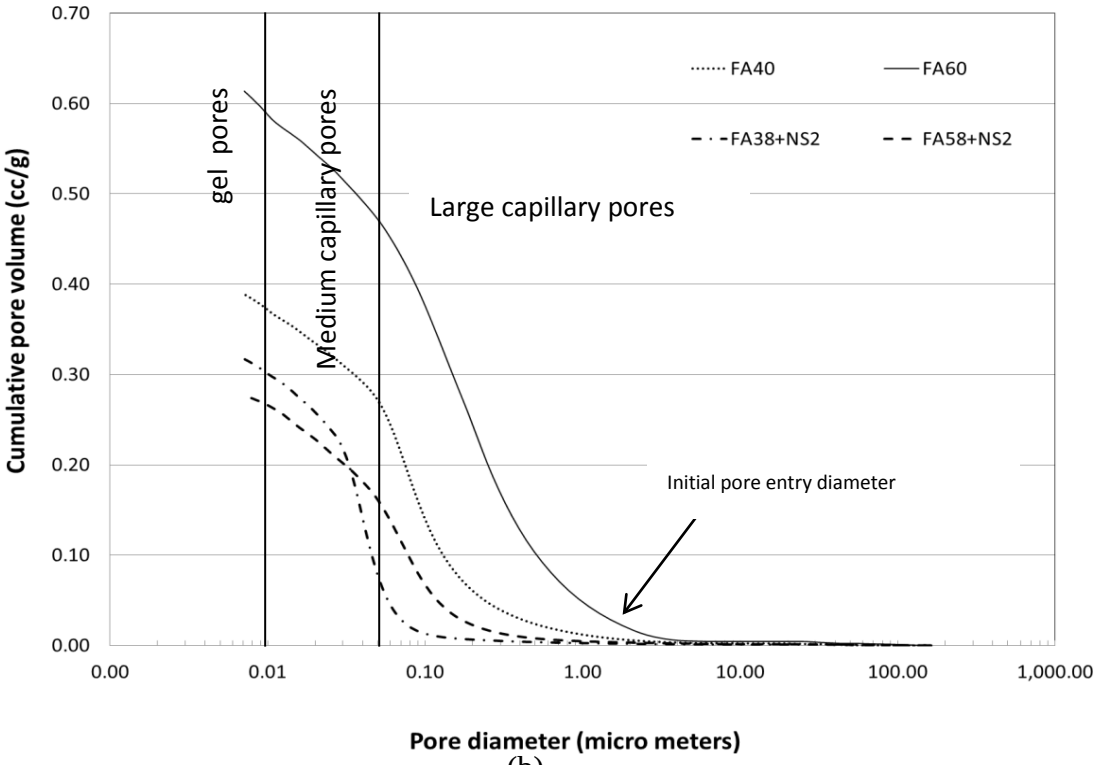

(b)

Figure 4.22 Cumulative pore volume of cement and HVFA pastes containing 2% nano silica

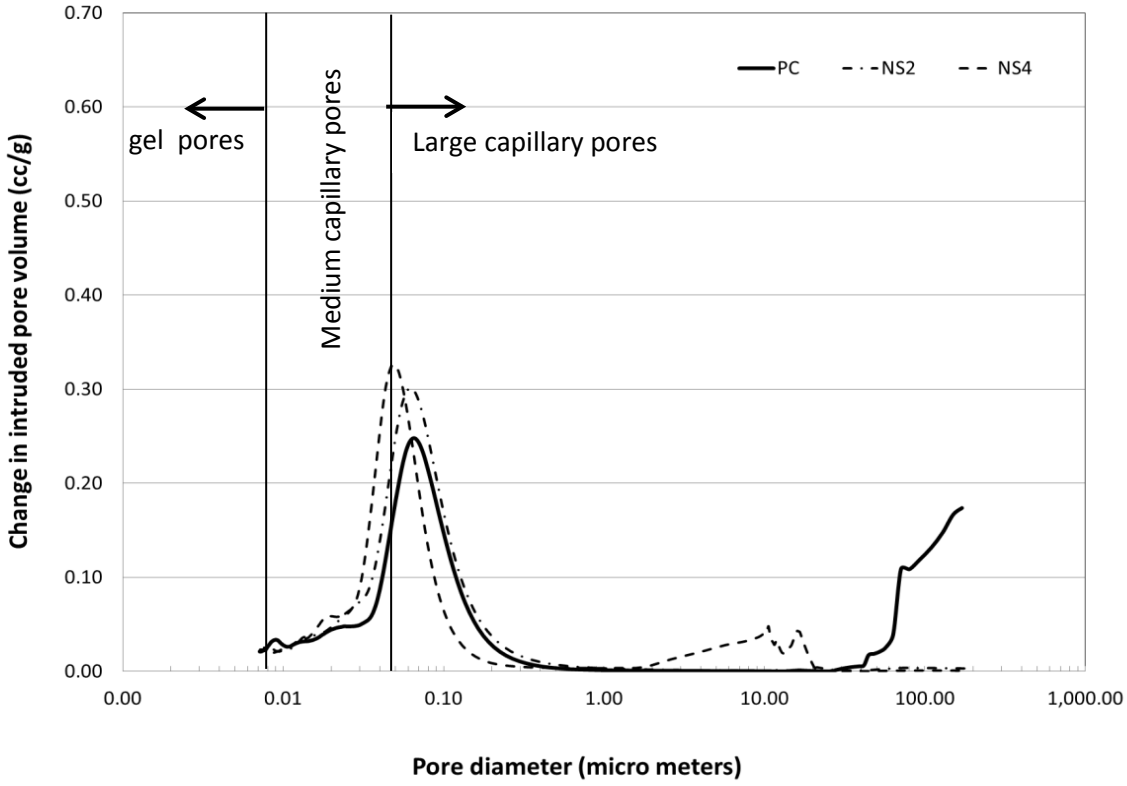

(a)

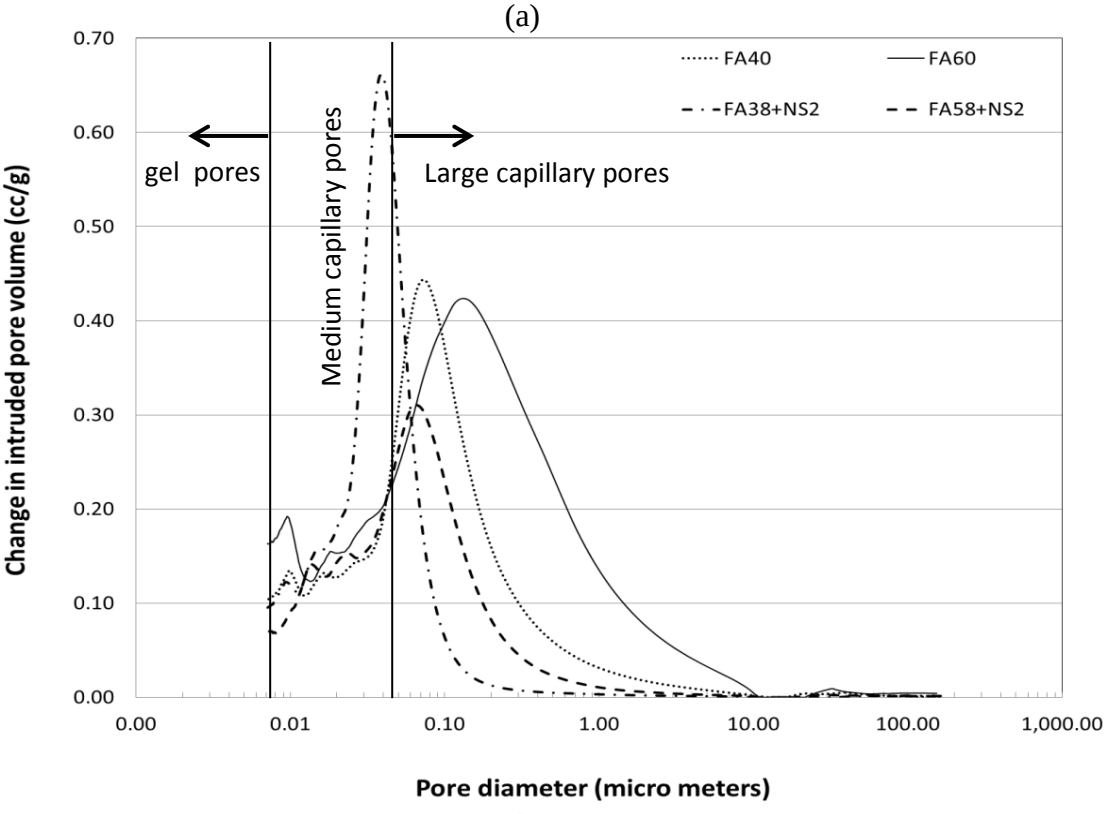

(b)

Figure 4.23 Change in intruded pore volume of cement and HVFA pastes containing 2% nano silica

4.5.3.2 Porosity of cement and HVFA pastes containing nano-$CaCO_3$

The effect of nano-$CaCO_3$ on porosity of the cement and HVFA pastes after 28 days of curing are shown in Figures 4.24 and 4.25. Figure 4.24 shows the relationship between the cumulative pore volume and pore diameter in the range of 0.01-100μm. From Figure 4.24 it can be seen that the pore size distribution of control cement paste has the same general shape as those of cement with $CaCO_3$ nanoparticles. However, the cement paste is more porous than the corresponding cement pastes containing nano-$CaCO_3$. It is clearly seen that the total porosity of pastes containing 1% and 2% $CaCO_3$ nanoparticles is about 0.18 cc/g and 0.27 cc/g, respectively (see Figure 4.24a), where there is no distinct difference on the initial pore entry diameter between paste with 1 wt% and 2wt% of nano-$CaCO_3$. In addition, it is also observed that the large capillary pores of pastes containing $CaCO_3$ nanoparticles are decreased significantly, while medium capillary pores are slightly decreased. In this case, the use of $CaCO_3$ nanoparticles leads to a more compact paste with a significant reduction of the pores between 0.1 and 100 μm.

In the case of HVFA pastes with 1% $CaCO_3$ nanoparticles addition, there is a notable reduction in pore concentration indicating the presence of $CaCO_3$ nanoparticles is advantageous in pores modification. With regard to FA40 paste sample, the result shows that the cumulative pore volume is reduced significantly after adding 1% nano-$CaCO_3$. While the total porosity of FA40 and FA60 are 0.39 and 0.61 cc/g, the FA39.NC1 and FA59.NC1 paste samples have total porosity of 0.20 and 0.32 cc/g, respectively. Both capillary and gel pores are reduced significantly by the addition of nano-$CaCO_3$ in HVFA system. Figure 4.25 shows that the maximum concentration of pores in paste containing 1% $CaCO_3$ nanoparticles tends to be around medium capillary pore sizes. The porosity of paste containing 1wt% nano-$CaCO_3$ is concentrated at 0.05 μm, whereas for pure cement paste it is at 0.07 μm. Figure 4.23b shows that the porosity of FA39.NC1 is concentrated around 0.05 μm which is lower than the concentration of the pores in FA40 paste. Similar trend is also observed in FA59.NC1 paste. It is noted that nano-$CaCO_3$ due to the pozzolanic reaction and the filler effect has a significant influence in decreasing the total capillary porosities of HVFA pastes.

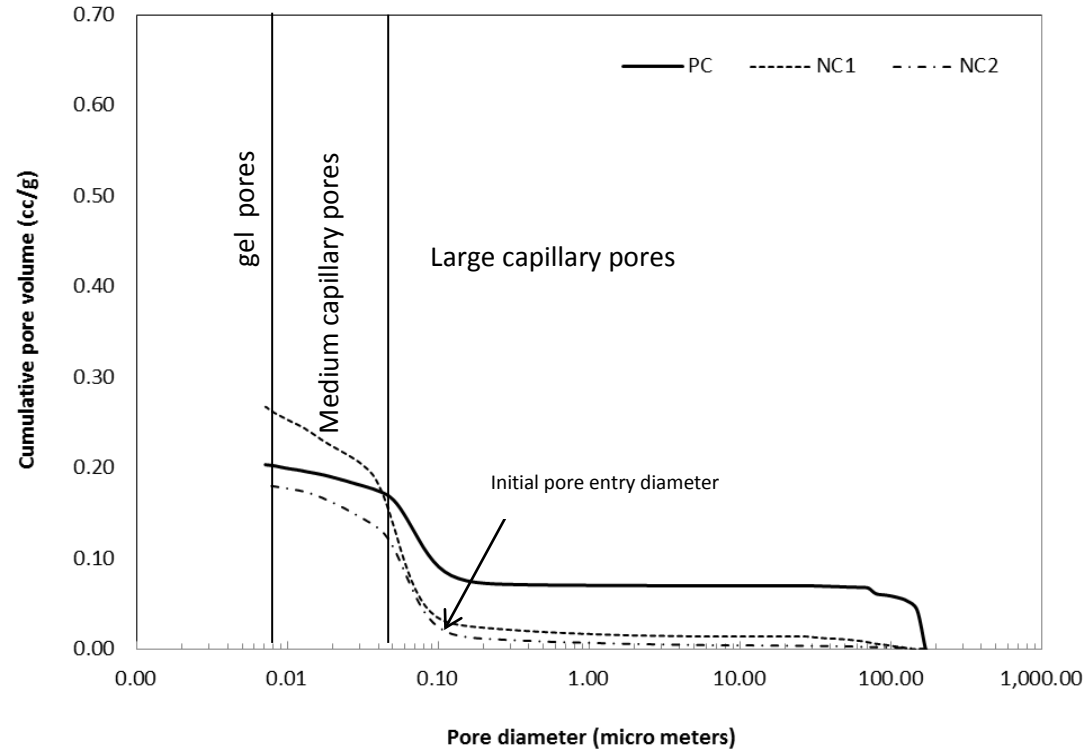

(a)

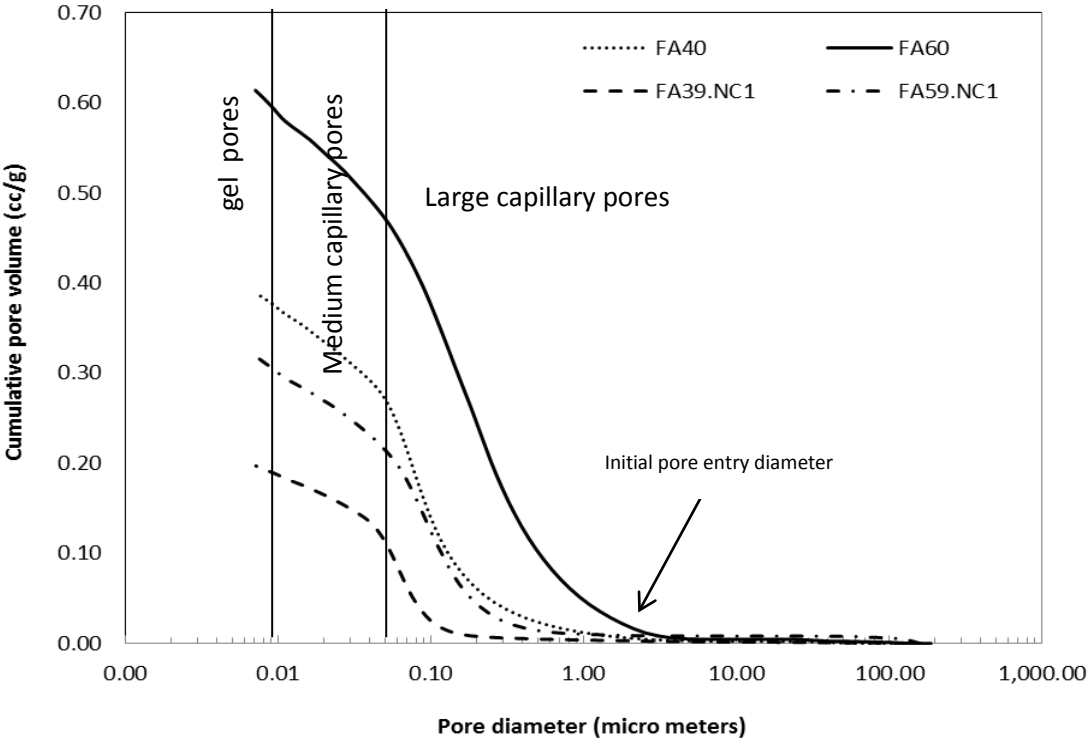

(b)

Figure 4.24 Cumulative pore volume of cement and HVFA pastes containing 1% nano-$CaCO_3$

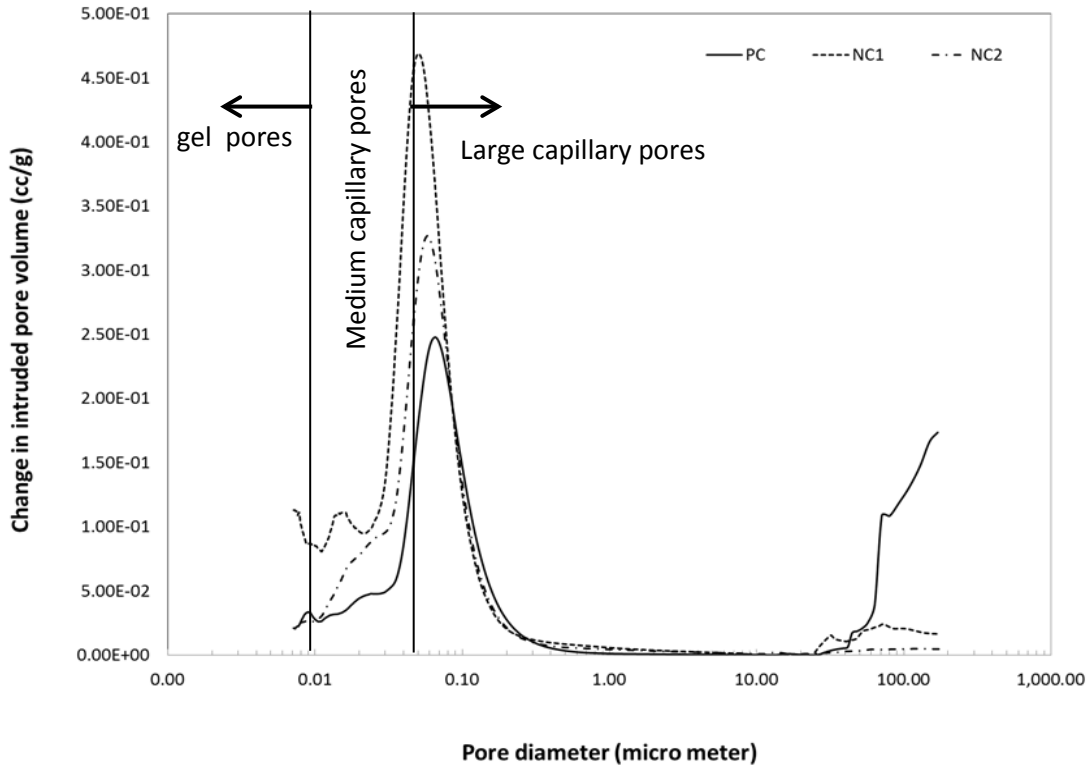

(a)

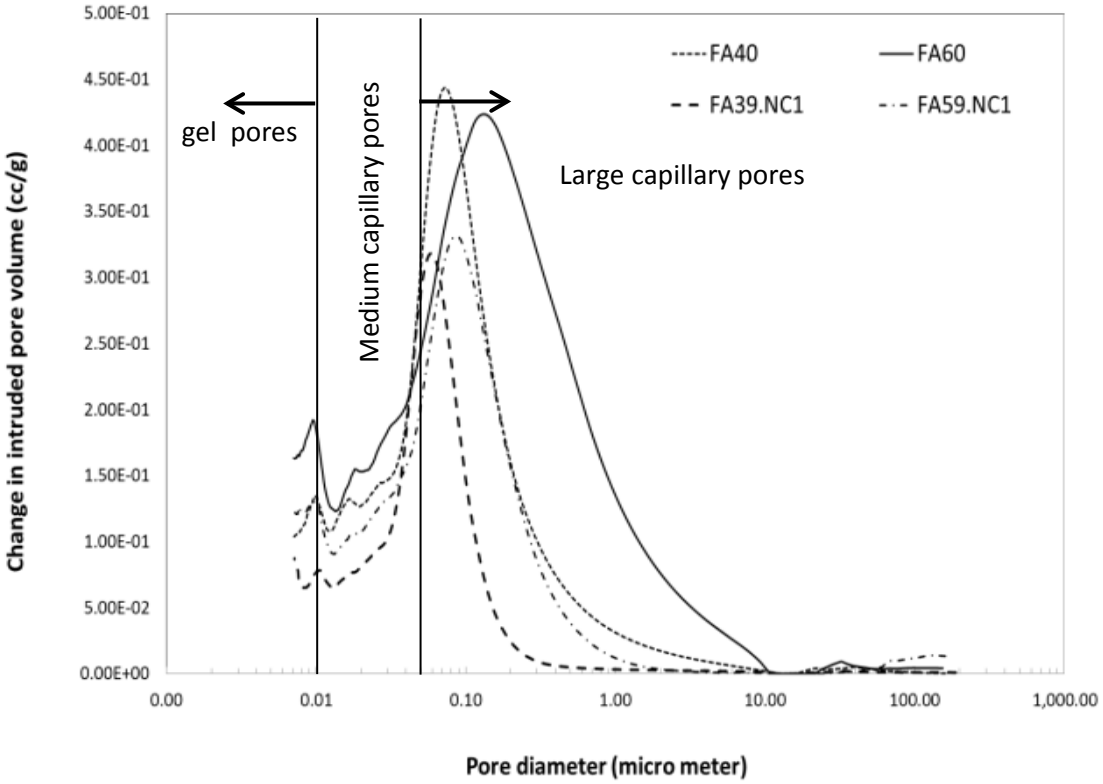

(b)

Figure 4.25 Change in intruded pore volume of cement and HVFA pastes containing 1% nano-$CaCO_3$

4.5.4 Chloride permeability

4.5.4.1 Effect of nano silica on chloride permeability of OPC concrete and HVFA concretes

Figure 4.26 shows the effect of NS as a partial replacement of cement on the resistance to chloride ion penetration in ordinary concrete at 28 and 90 days. A Rapid Chloride Permeability Test (RCPT) value less than 2000 Coulombs is characterized as low chloride permeability, 2000-4000 Coulombs is in medium level while higher than 4000 Coulombs is defined as high chloride permeability (ASTM C1202). Based on the results, it can be seen that by combining 2% nano silica in ordinary concrete a decrease in chloride penetration in terms of total charged passed from 3443 to 2497 Coulombs can be achieved. A similar trend is also observed for concrete containing 4% NS. The total charge passed was 1999 Coulombs at 28 days, which is lower than the result obtained from ordinary concrete and HVFA concretes. Based on the above Classification, the concretes containing NS particles can be Classified as low chloride permeability category indicating the high resistance to chloride ion penetration. At 90 days, the effect of NS on chloride resistance of concrete was even more favourable with total charged passed of 1000 and about 2000 Coulombs for NS contents of 4% and 2%, respectively. This clearly indicates that at later ages the chloride penetration resistance of concrete containing NS is significantly improved.

In the case of HVFA concretes, the results show that the chloride ion penetration is increased at both ages compared to ordinary concrete. The total charge passed of concrete containing 40% fly ash (FA40) was 4996 and 3559 Coulombs and for concrete containing 60% fly ash (FA60) was 6076 and 4937 Coulombs at 28 and 90 days, respectively (see Figure 4.26). In the same Figure, the effect of 2% NS on the chloride ion penetration resistance of HVFA concrete is also shown. The results indicated that when 2% NS was added into 38% fly ash concrete the charge passed decreased significantly from 4996 to 3088 Coulombs at 28 days, a drop of about 38% when compared to the reference FA40 concrete without NS. The lower values of the charge passed found on RCPT can be attributed to the change of concrete microstructure and refinement in the pore system due to the use of NS in HVFA concretes. However, based on the coulomb value, the concrete containing 58% fly ash and 2% nano silica achieves high chloride permeability and indicates that the pore structure is more connected. It is also interesting to see that by incorporation of

2% NS in HVFA concrete containing 38% fly ash the chloride ion penetration can be reduced below ordinary concrete level at both ages. Furthermore, when concrete mixes are properly designed in terms of the amount of NS as cement replacement in HVFA concretes, it is possible to achieve medium chloride ion penetration level as standardized in ASTM C1202 and at later ages this chloride ion resistance is expected to increase.

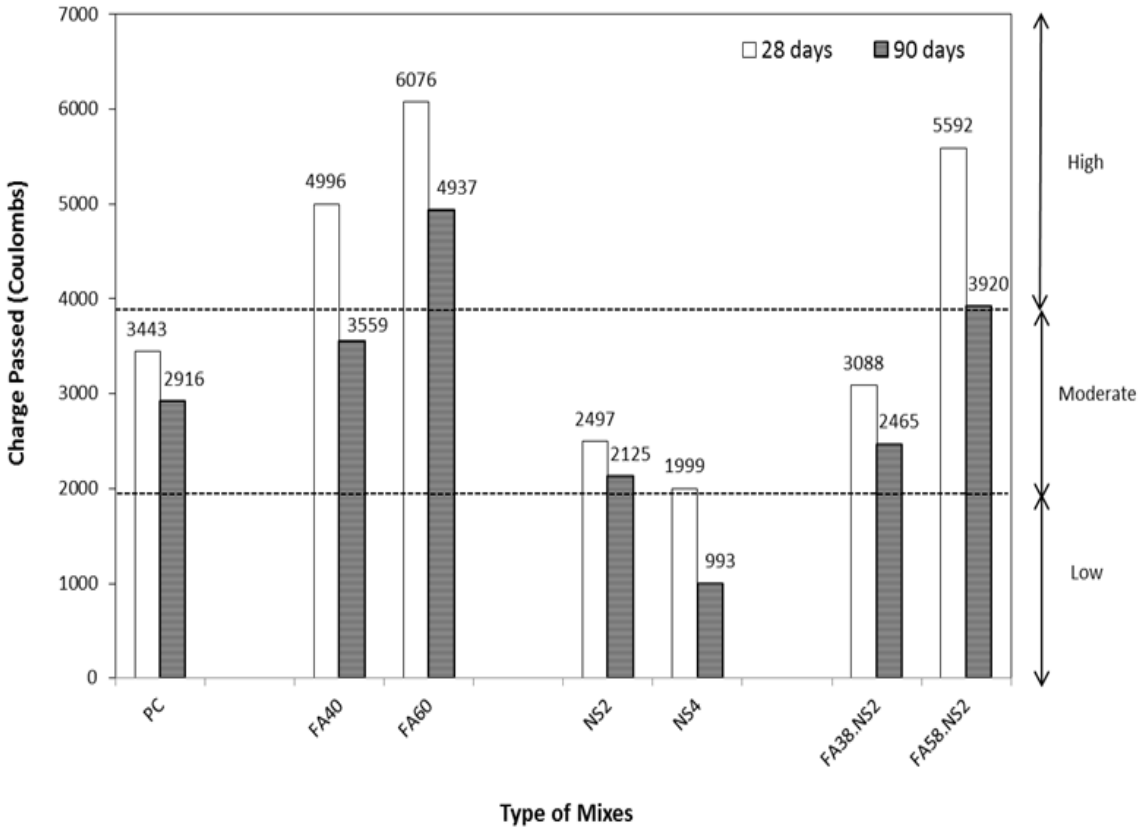

Figure 4.26 Charge passed in concretes containing 2% nano silica measured after 28 and 90 days of curing

4.5.4.2 Effect of nano-CaCO3 on chloride permeability of ordinary concrete and HVFA concretes

Figure 4.27 shows the effect of nano-$CaCO_3$ on resistance against chloride ions penetration of ordinary concrete and HVFA concretes. Based on the obtained results, it can be seen that a replacement of 1% OPC with $CaCO_3$ nanoparticles increased the resistance against chloride ion penetration of ordinary cement concrete by 20% and 50% at 28 and 90 days, respectively. At 90 days, the charge decreased from 2916 Coulombs to 1475 Coulombs (i.e changed from moderate to low chloride permeability rating). When the replacement of cement was increased to 2% nano-

$CaCO_3$, the Coulombs values were not significantly different from 28 days values and decreased by only 20% at 90 days.

With regard to the effect of 1% nano-$CaCO_3$ on chloride permeability of HVFA concretes, it is observed that the charge passed at 28 days decreased from 4996 Coulombs to 4057 Coulombs (approximately 18%) in FA39.NC1 concrete and from 6075 to 5360 Coulombs (approximately 11%) in FA59.NC1concrete (see Figure 4.27). Considering specimens cured at 90 days, the total charge passed of high volume fly ash containing 1% nano-$CaCO_3$ ranged from 3465 to 4556 Coulombs. For all concrete specimens tested, the total charge passed decreased with increase in curing age. It can be concluded that the extension of the curing period from 28 to 90 days resulted in a reduction of the total charge passed through the concrete specimens due to hydration and pozzolanic reactions.

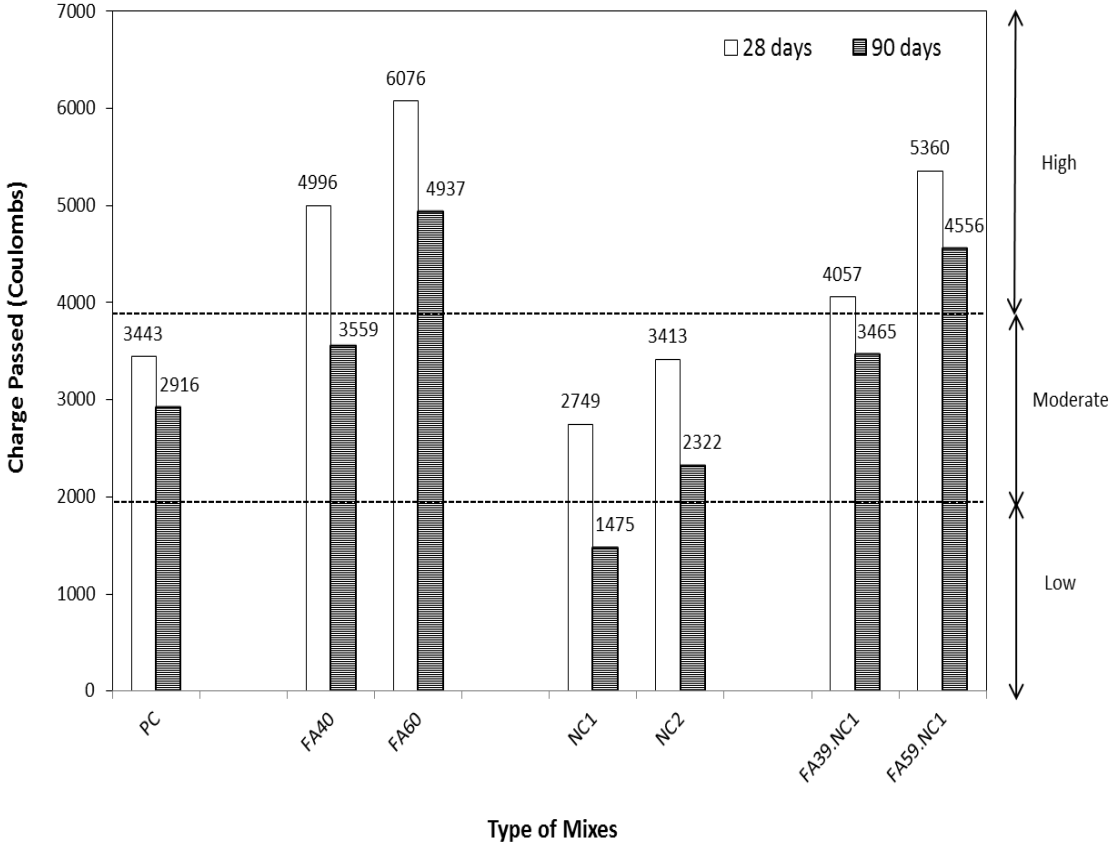

Figure 4.27 Charge passed in concretes containing 1% nano-$CaCO_3$ measured after 28 and 90 days of curing

4.5.5 Chloride diffusion

4.5.5.1 Effect of nano-silica on chloride diffusion of OPC concrete and HVFA concretes

The chloride content profile of different concretes subjected to 60 days exposure in NaCl solution is presented in Figures 4.28a and b. The curve shows the measured acid-soluble chloride ion concentration at different depths inside the concrete by percent of concrete's weight. The chloride penetration profiles were calculated by fitting the data obtained for each concrete in the chloride profile analysis using Fick's second law in equation 2.10. In the acid-soluble chloride ion content profile, the rate of chloride diffusion can be determined from the steepness of the curve. A less steep curve indicates that the concentration of acid-soluble chloride inside the concrete equals to the concentration on the concrete's surface. On the other hand, the steep curve indicates the slow chloride diffusion inside the concrete due to very slow chloride penetration from the concrete's surface. It is also noticed that the fits for each concrete has impressive agreement between the measured data and the model predicted by the Fick's second law.

In Figures 4.28a and b, it is clearly seen that the acid-soluble chloride ion content of the concretes containing nano silica is significantly lower than the acid-soluble chloride ion content of OPC and HVFA concretes. It can be seen that the steepness of the curve is slightly higher in NS2 concrete indicating the influence of nano silica on the reduction of acid-soluble chloride ion content diffusion. By adding nano silica into concretes, the acid-soluble chloride ion decreases with increase in depth indicating the role of nano silica particles appear to be more influential in refining microstructure to enhance the durability properties of cement concretes. Based on the figures, it can be seen that the experimental data are in good agreement with the chloride penetration profiles derived from the Fick's second law that were plotted with actual experimental data after 60 days exposure. The chloride diffusion coefficients of various concretes are presented in Figure 4.29. It can be seen that for the OPC concrete, the chloride diffusion coefficient is 4.1 $x10^{-12}$ m^2/sec while for NS concretes, the chloride diffusion coefficient is 3 $x10^{-12}$ m^2/sec, which is about 26% reduction. Moreover, the high volume fly ash concretes have lower chloride diffusion coefficient than cement concrete but higher when compared to NS concrete. In HVFA concretes, again, such reduction of chloride diffusion coefficient is observed

when nano silica particles are used (see Figure 4.28b). For examples, the chloride diffusion coefficient of the high volume fly ash concretes containing 2% nano silica were about 22% and 14% lower than the FA40 and FA60 concretes, respectively. It indicates that the nano silica particles are very effective in reducing the acid-soluble chloride ion diffusion of concretes containing high volume fly ash.

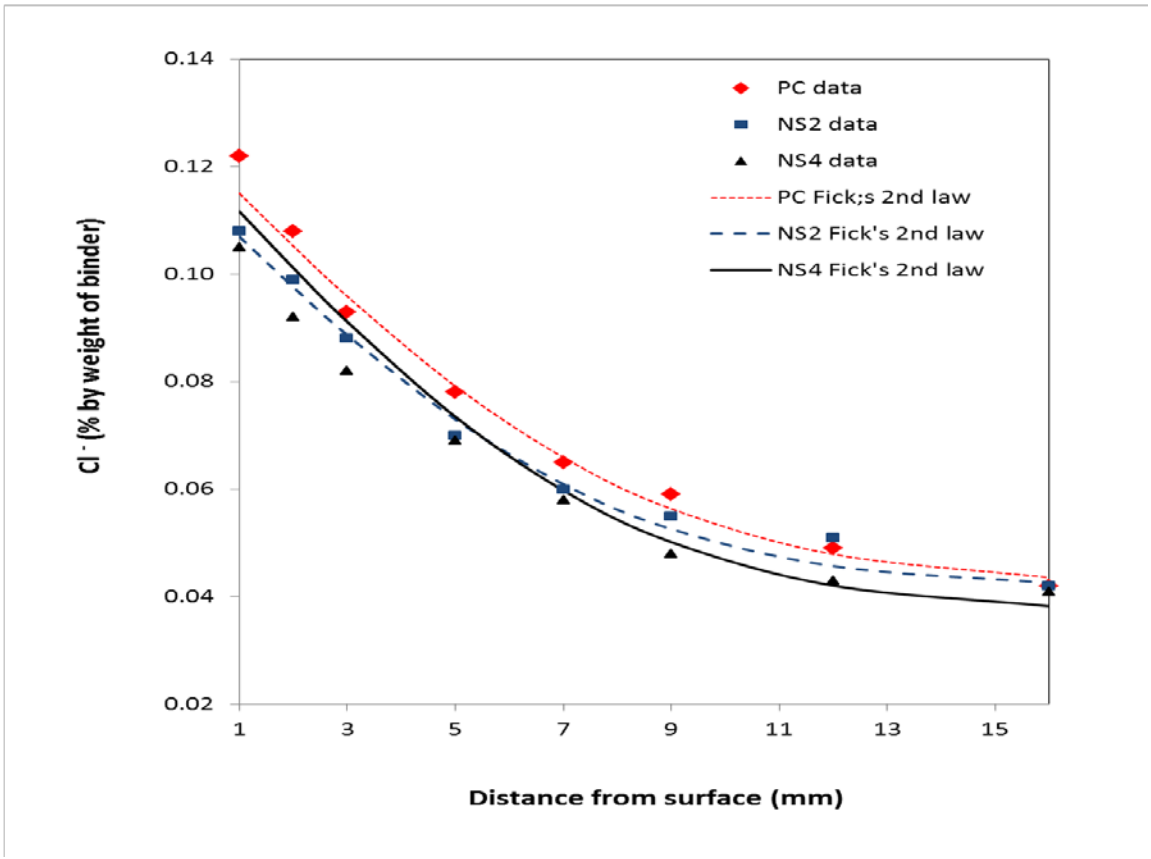

(a)

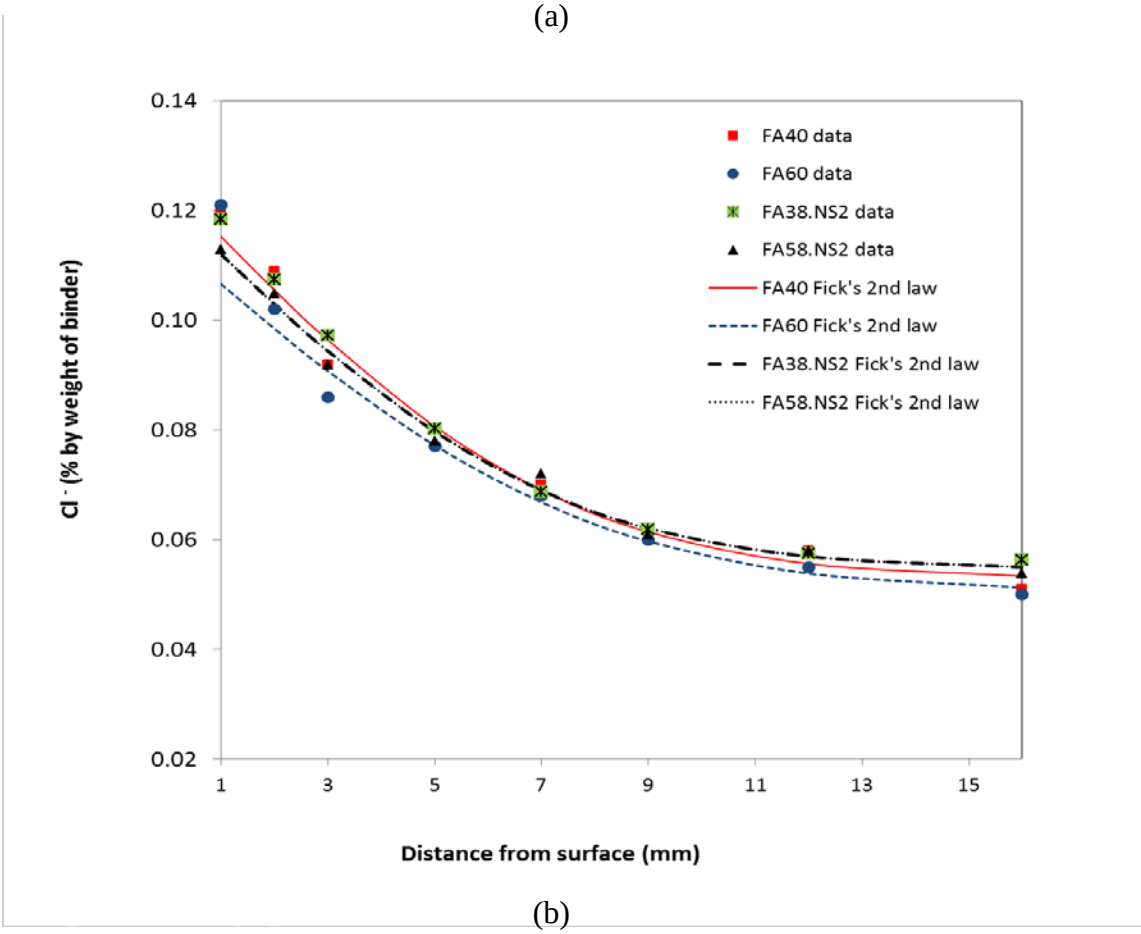

(b)

Figure 4.28 The acid-soluble chloride ion content profile of different mixes of concretes containing 2% nano silica

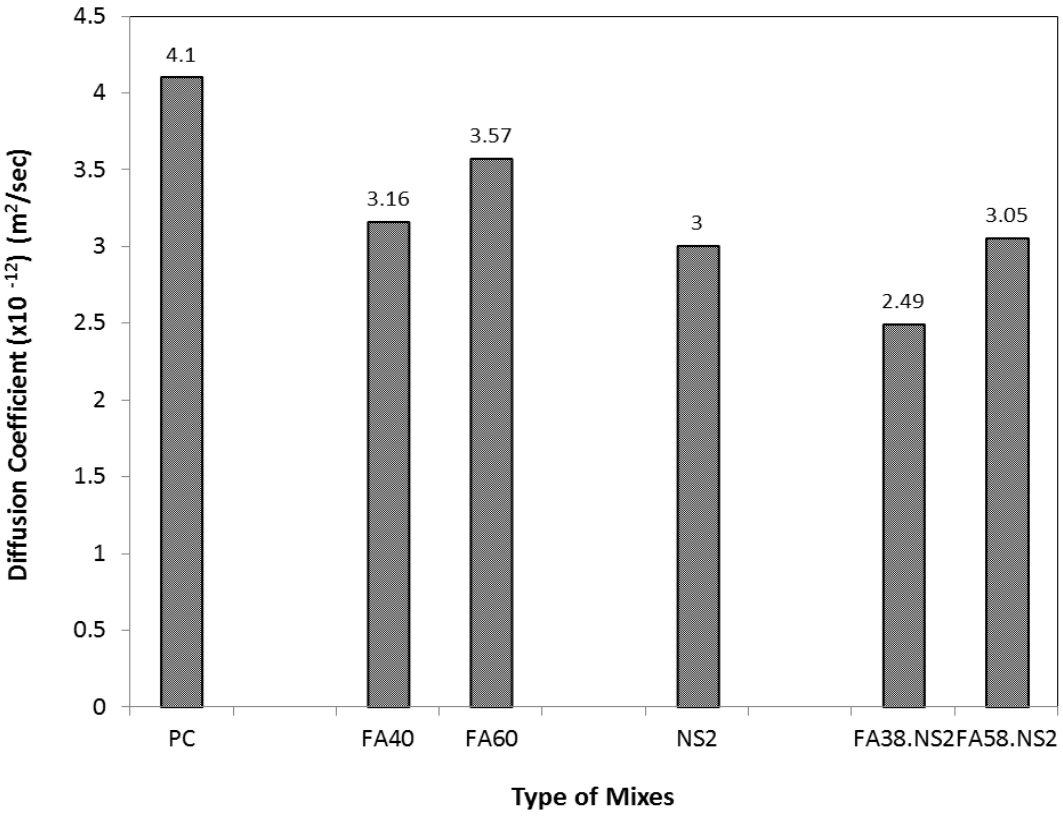

Figure 4.29 Chloride diffusion coefficient of the variation of concrete mixes containing nano silica after 60 days exposure in NaCl solution

4.5.5.2 Effect of nano-$CaCO_3$ on chloride diffusion of OPC concrete and HVFA concretes

The acid-soluble chloride content profile of different concretes of 28 days cured concretes subjected to 60 days exposure to NaCl solution is presented in Figures 4.30a and b. In Figure 4.30a, it is clearly seen than the steepness of the curve is higher in OPC concrete and HVFA concretes containing 1% nano-$CaCO_3$ indicating the influence of $CaCO_3$ nanoparticles on the reduction of chloride diffusivity. For the ordinary concrete, the calculated chloride diffusion coefficient is 4.1 x10^{-12} m^2/sec whilst for concrete containing 1% nano-$CaCO_3$ (NC1), the diffusion coefficient is 3.5 x10^{-12} m^2/sec, which is about 14% lower than the ordinary concrete. In addition, by adding 1% nano-$CaCO_3$ into HVFA concrete mixtures, the acid-soluble chloride ion content decreases with increase in depth (see Figure 4.28b) indicating the role of nano-$CaCO_3$ appear to be more influential in refining microstructure to enhance

durability properties of cement concretes. The calculated chloride diffusion coefficient of concrete mixes is presented in Figure. 4.31.

In HVFA concretes, again, such improvements of chloride diffusion resistance are reported when 1% nano-$CaCO_3$ is added. By adding 1% NC into HVFA concrete mixtures, the chloride diffusion coefficient decreases indicating the role of nano-$CaCO_3$ appear to be more influential in refining microstructure to enhance durability of HVFA concretes. Based on the results, the chloride diffusion coefficient of the high volume fly ash concretes (i.e. FA39.NC1 and FA59.NC1) is decreased by about 11% and 3% due to addition of 1% nano-$CaCO_3$ is added (see Figure 4.31). It indicates that the $CaCO_3$ nanoparticles are very effective in reducing the pore space and its connectivity inside the concrete and therefore the penetration of acid-soluble chloride ions.

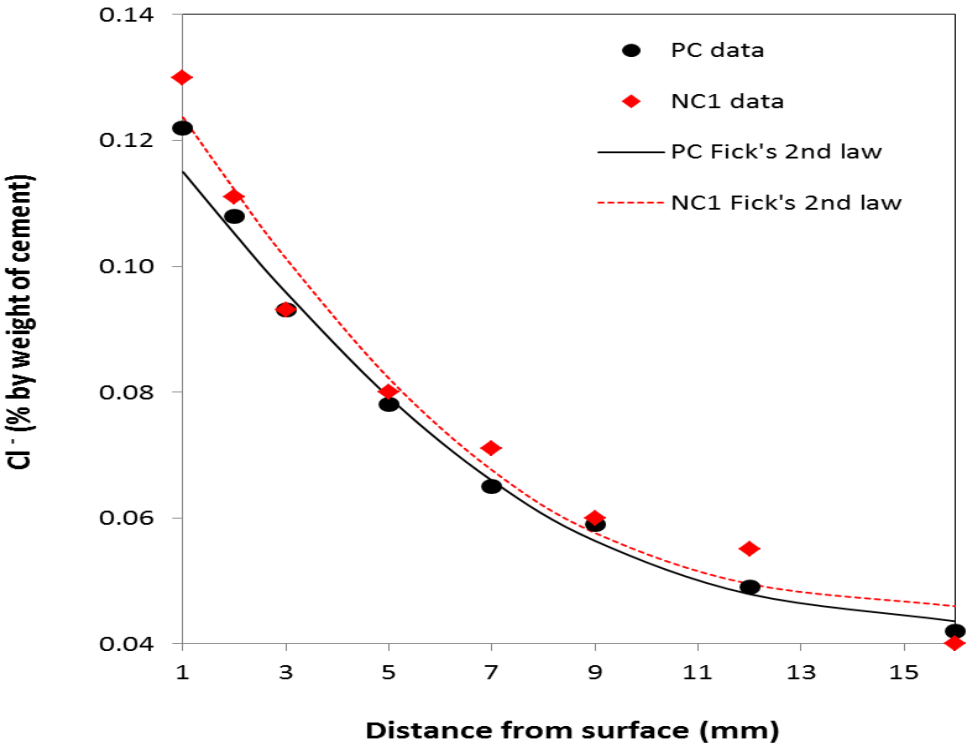

(a)

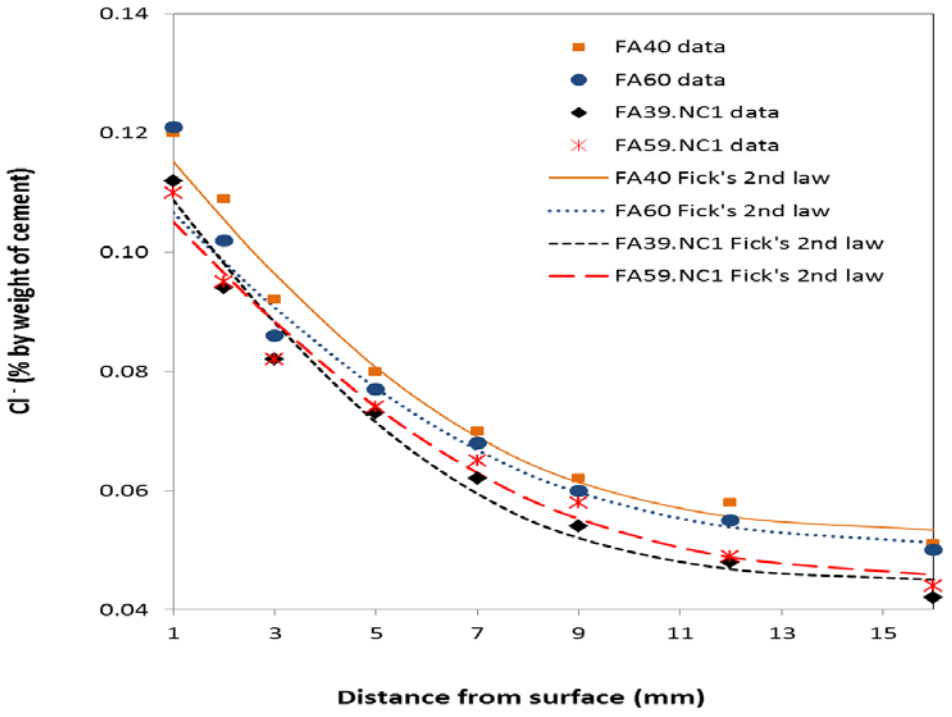

(b)

Figure 4.30 The acid-soluble chloride ion content profile of different mixes of concretes containing nano-$CaCO_3$ after 60 days exposure in NaCl solution

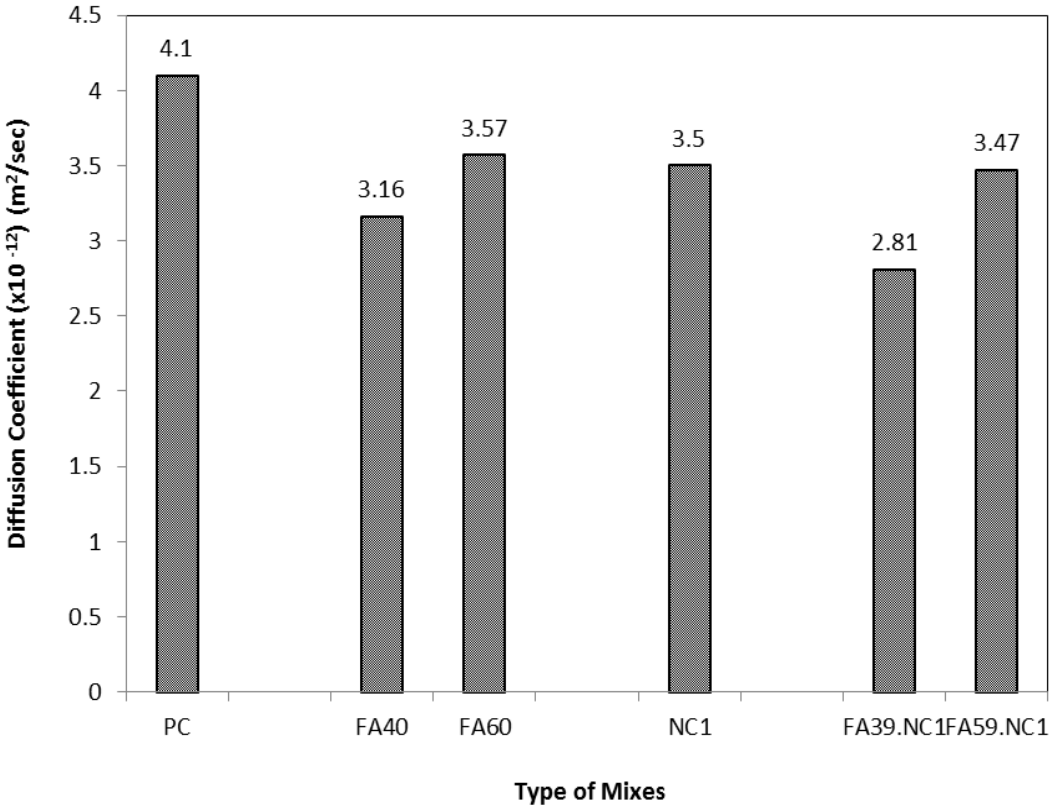

Figure 4.31 Chloride diffusion coefficient of the variation of concrete mixes containing 1% nano-$CaCO_3$

4.5.6 Accelerated corrosion

4.5.6.1 Effect of nano silica on corrosion of steel in ordinary OPC and HVFA concretes

Figures 4.32a and b show the corrosion current-time relationships of concretes containing nano silica subjected to accelerated corrosion regime. The variation of current with time was recorded by data acquisition system until the corrosion cracks appear on the surface of concrete specimens. The figures show that the concretes containing nano silica exhibits lower corrosion currents compared to OPC concrete. In this study, the NS2 concrete took more than 1000 hours for the first corrosion induced crack to appear on the surface. In contrast, the OPC concrete recorded approximately 115 mA current in 700 hours when the crack appeared under the impressed voltage, and then the current shows an increasing trend for the next 1000 hours (see Figure 4.32a). Once the crack appeared, oxygen and chloride ions penetrated through the concrete specimens and accelerated the corrosion of steel that was evident from the high currents reading in OPC concrete. In HVFA concretes, it

can be seen that the time of FA40 and FA60 concretes to crack are around 350 hours, which is shorter than the crack initiation time of approximately > 1000 hours for HVFA concrete containing NS particles (see Figure 4.32b). This indicates that the corrosion resistance of concretes is improved by inclusion of NS in HVFA concretes. The longer time taken by the HVFA concretes containing NS to form crack is probably due to the higher resistance of the NS concretes to chloride penetration as also discussed in section 4.5.4 and 4.5.5.

Figure 4.33 shows the typical deterioration of different types of concretes after the accelerated corrosion test. A very distinguishable difference can be seen in the appearance on the surface of different types of concrete after splitting. It can be clearly seen that there is no large area of corroded surface on the concrete specimens containing nano silica compared to that of typical cement and HVFA concretes. Moreover, the corroded rebars shown in Figure 4.34 are representative examples of corrosion resistance of concretes with and without nanoparticles. The corroded rebars were retrieved from the broken concrete samples and weighted after accelerated corrosion test. It can be identified from the figures that the corrosion and typical pit formation are more visible on the rebar in typical cement concrete (PC). In contrast, the rebars taken from NS2 concrete (see Figure 4.34) have clean surface after removal with less visible corrosion as indicated by a reduction in the weight loss of rebar (see Table 4.4). Similarly, it is also observed that the surface of rebars from HVFA concretes containing 2% NS have also less visible corrosion compared to the typical HVFA concretes (i.e. FA40 and FA 60).

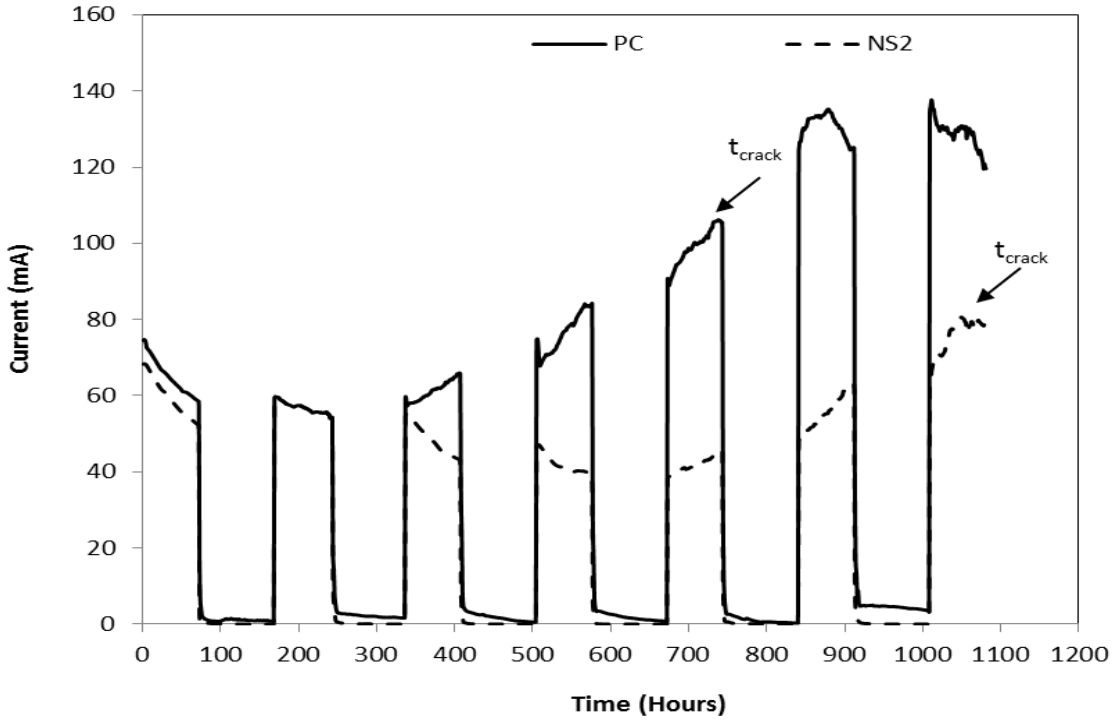

(a)

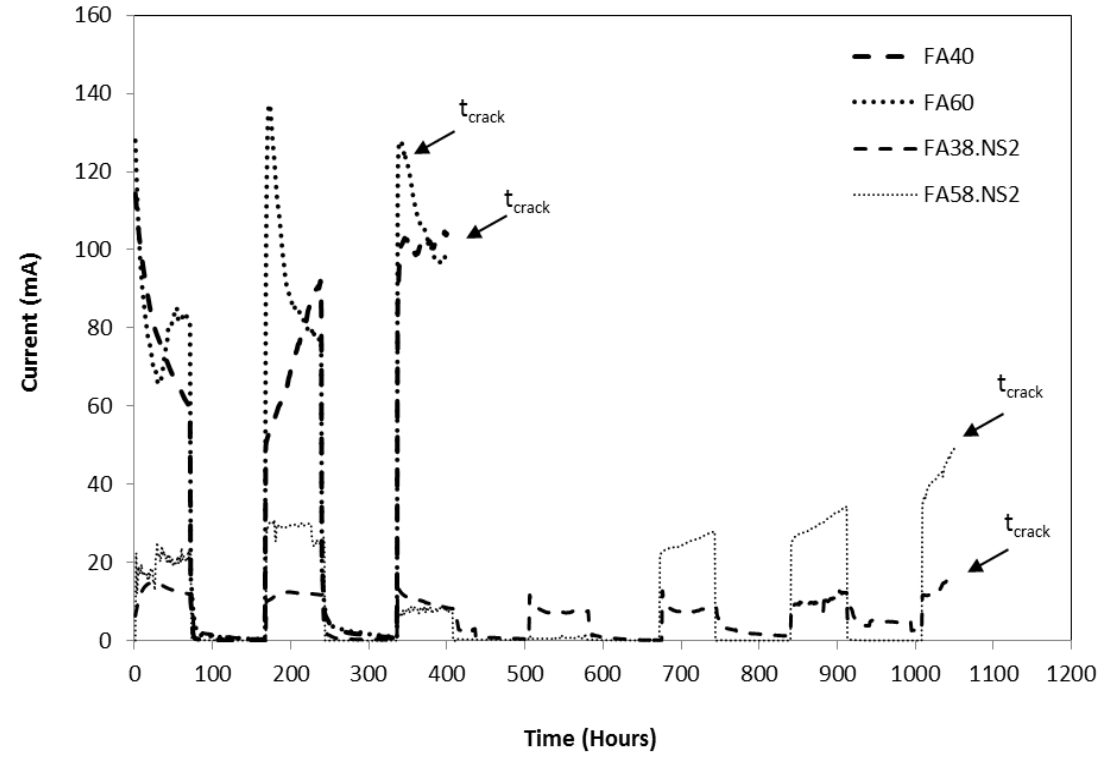

(b)

Figure 4.32 Corrosion current-time relationships of concretes containing nano silica after 28 days of curing

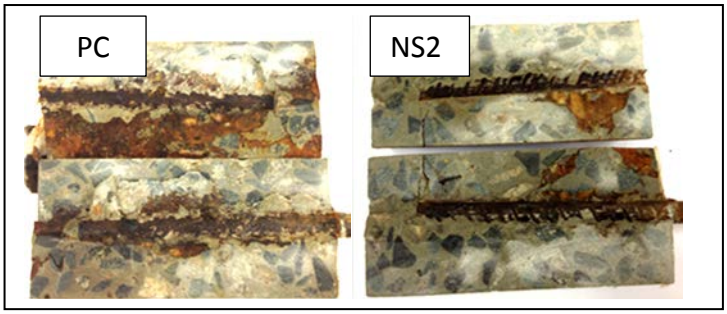

(a)

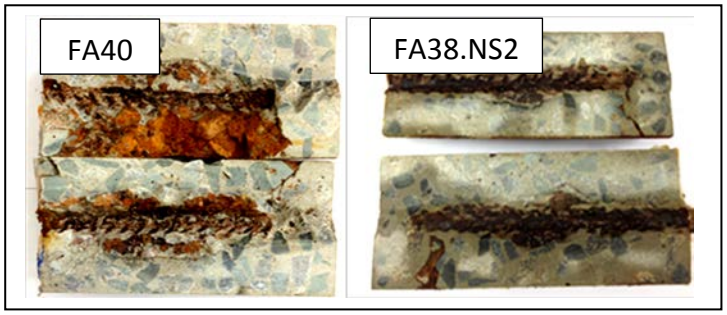

(b)

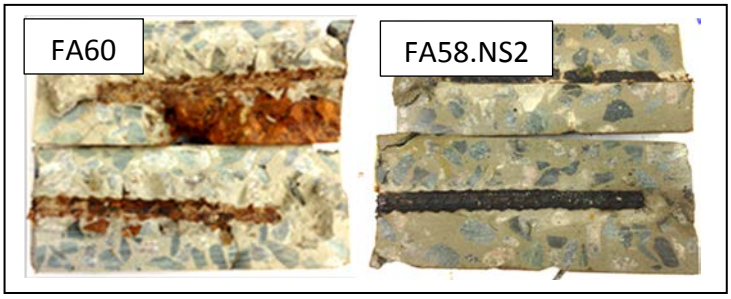

(c)

Figure 4.33 Corroded concrete specimens containing nano silica after accelerated corrosion test

Table 4.4 shows the cumulative theoretical mass loss according to Faraday's law and the actual mass loss of rebar on each sample. The mass loss measurement is known as the most reliable method to investigate the degree of corrosion. Based on the results obtained, the mass loss of the rebar in cement concrete is higher than the mass loss of the rebar in NS2 concrete. It is shown that the typical cement concrete lost an estimated 29.67% of its steel reinforcement whilst in NS2 concrete the lost is about 18.36%. The better corrosion resistance of HVFA concrete specimens containing 2%

NS is also observed where the specimen FA38.NS2 and FA58.NS2 experienced 6.04% and 10.99% steel loss, respectively, (approx. 40% and 11% lower than FA40 and FA60 concretes). It indicates that the presence of silica nanoparticles influenced the mass loss reduction of rebar in HVFA concretes. Furthermore, it can be seen that although the loss of steel take place when corrosion is induced but the presence of nano silica particles in cement and HVFA concretes increased the time to first crack due to the improvement of binding capacity to the steel bar and the enhancement of the pore refinement of the concrete resulting in minimum mass loss of rebar.

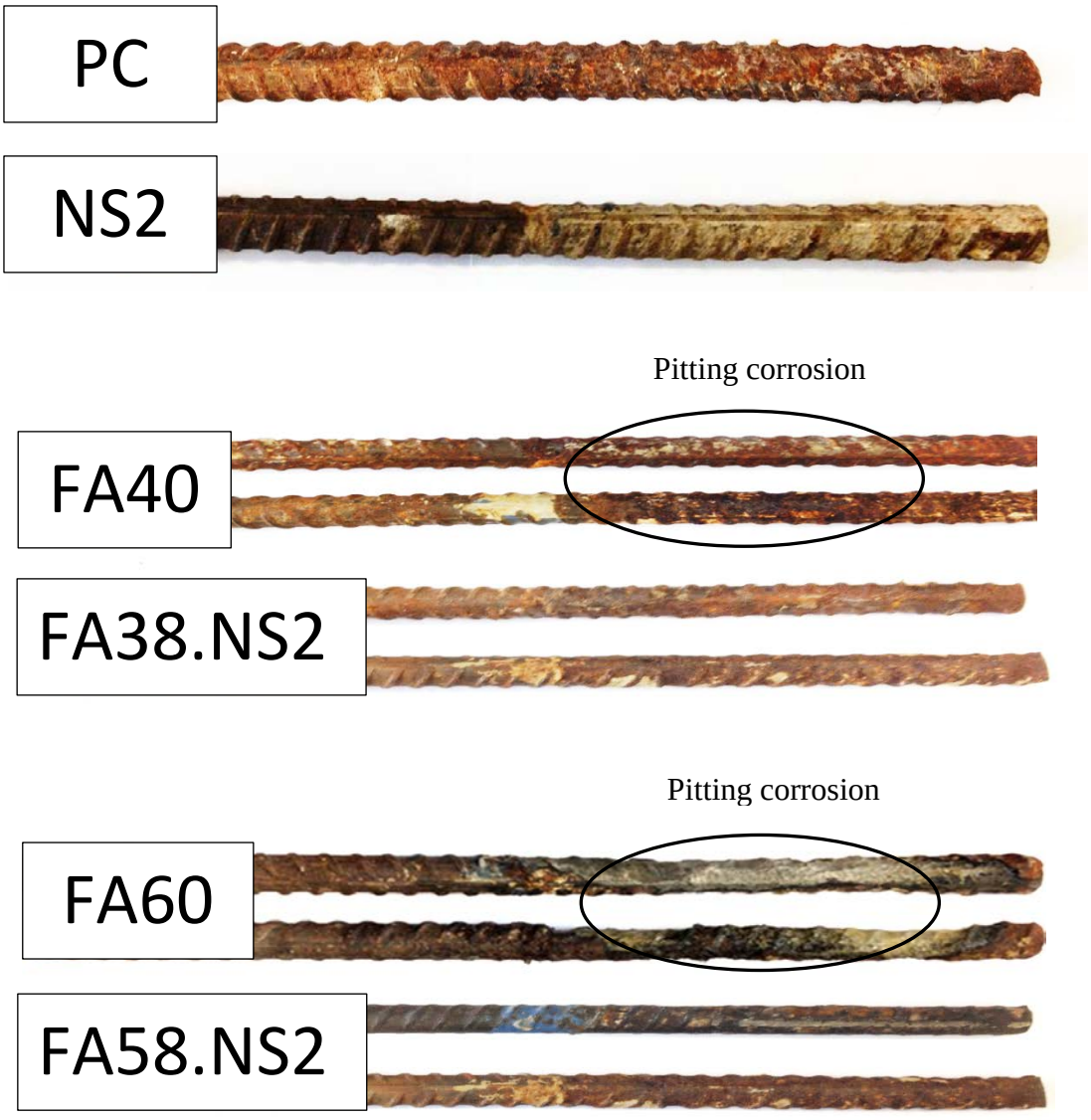

Figure 4.34 Typical deterioration of rebars taken from concretes containing nano silica after accelerated corrosion test

Table 4.4 Weight-loss measurement of rebar from concretes containing nano silica

Mix designation	Initial mass (g)	Final mass (g)	Actual mass loss (g/cm^2)	Theoretical mass loss (g/cm^2)	Percentage of mass loss (%)
PC	536	377	2.11	2.80	29.67
NS2	533	435	1.30	1.83	18.36
FA40	539	485	0.71	0.84	9.99
FA60	532	467	0.87	0.93	12.31
FA38.NS2	539	498	0.43	0.36	6.04
FA58.NS2	534	475	0.77	1.07	10.99

4.5.6.2 Effect of nano-$CaCO_3$ on corrosion of steel in ordinary concrete and HVFA concretes

Figures 4.35a and b show the measured corrosion current from accelerated corrosion test of concrete containing nano calcium carbonate. As can be seen in Figure 4.35a that the rate of increase of corrosion current in concrete containing 1% nano CaCO3 is lower than that of cement concrete. It can also be seen that the NC1 concrete took more than 900 hours for the crack to appear. Time to cracking in FA40 and FA60 concretes were 350 and 400 hours, respectively whereas that in FA39.NC1 and FA59.NC1 concretes were about 1000 hours and 500 hours, respectively, which are much longer than the HVFA concretes. These results support the visual investigation on the deterioration of concrete samples after accelerated corrosion test as shown in Figure 4.36. Distinguishable difference can be seen in the appearance on the surface of the different types of concrete after splitting. It can be seen that the concretes containing nano calcium carbonate seems to show a slightly better performance in terms of corrosion resistance than cement and HVFA concretes. It can be clearly seen that there is no large area of corroded surface on the concrete specimens containing NC compared to ordinary concrete and HVFA concretes specimens. The corroded rebars shown in Figure 4.37 are examples of actual corrosion status of rebars in HVFA concretes with and without nano-$CaCO_3$. It can be identified that the corrosion and typical pit formation are visible on the rebar surfaces of HVFA concretes. In contrast, the rebars taken from HVFA concretes containing NC had almost clean surface after removal with less visible corrosion as indicated by a reduction in the weight loss of rebar. The cumulative theoretical mass loss and the actual mass loss of rebar of each sample are also tabulated in Table 4.5. According to the results, the HVFA concretes with nano calcium carbonate (i.e. FA39.NC1 and

FA59.NC1 concrete mixtures) exhibited about 6.63% and 10.53%, respectively steel loss which is approximately 33% and 14% lower than FA40 and FA60 concretes. It indicates that the presence of nano-$CaCO_3$ reduced the corrosion of rebar in HVFA concretes.

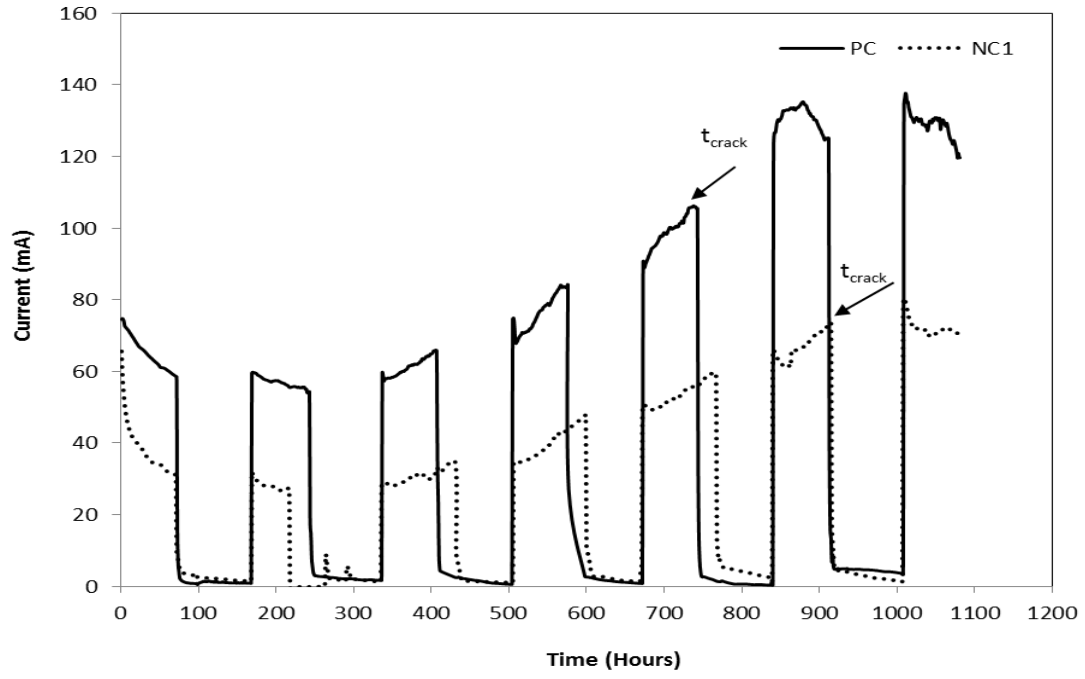

(a)

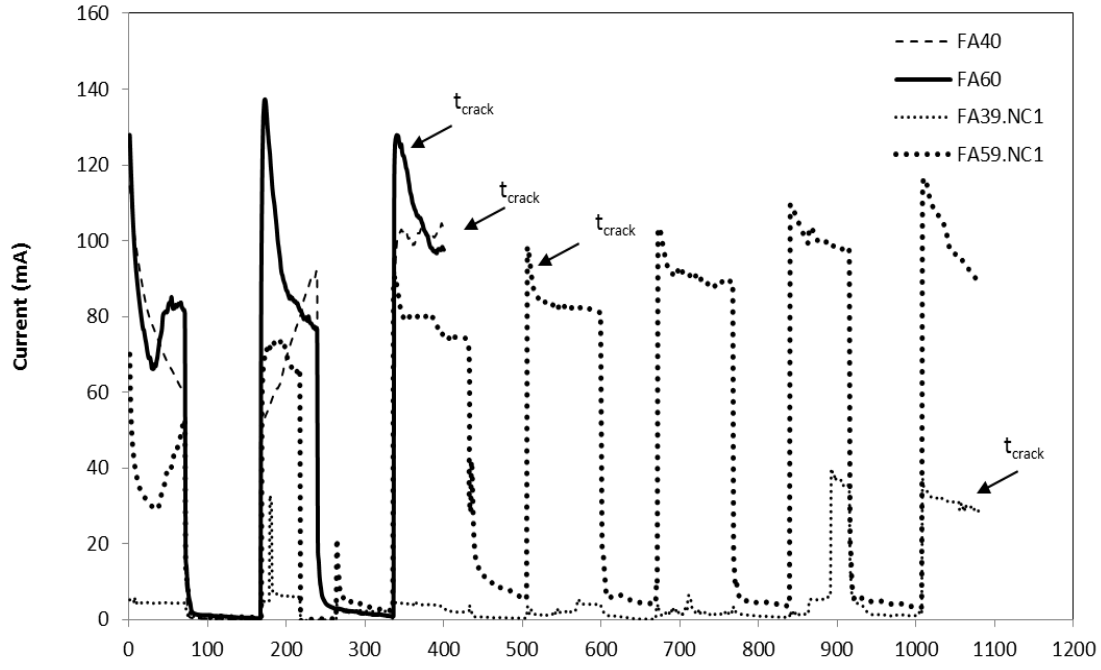

(b)

Figure 4.35 Corrosion current-time relationships of concretes containing nano calcium carbonate after 28 days of curing

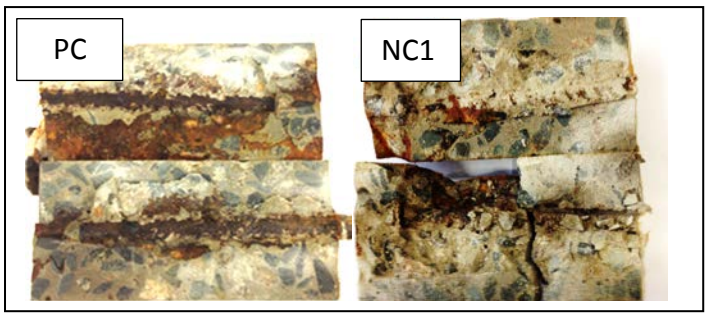

(a)

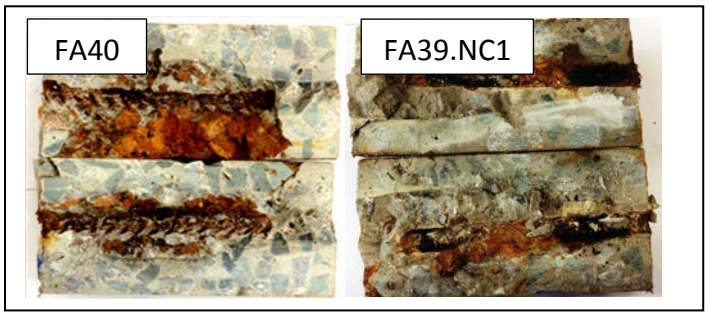

(b)

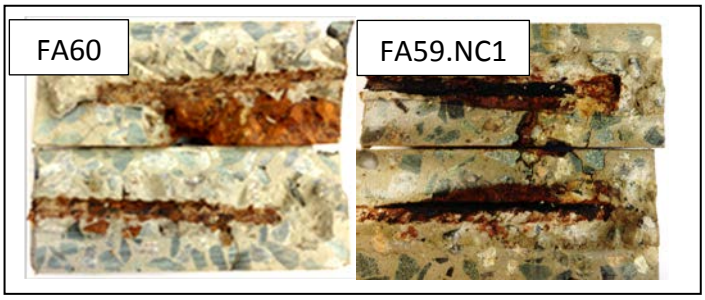

(c)

Figure 4.36 Corroded concrete specimens containing nano calcium carbonate after accelerated corrosion test

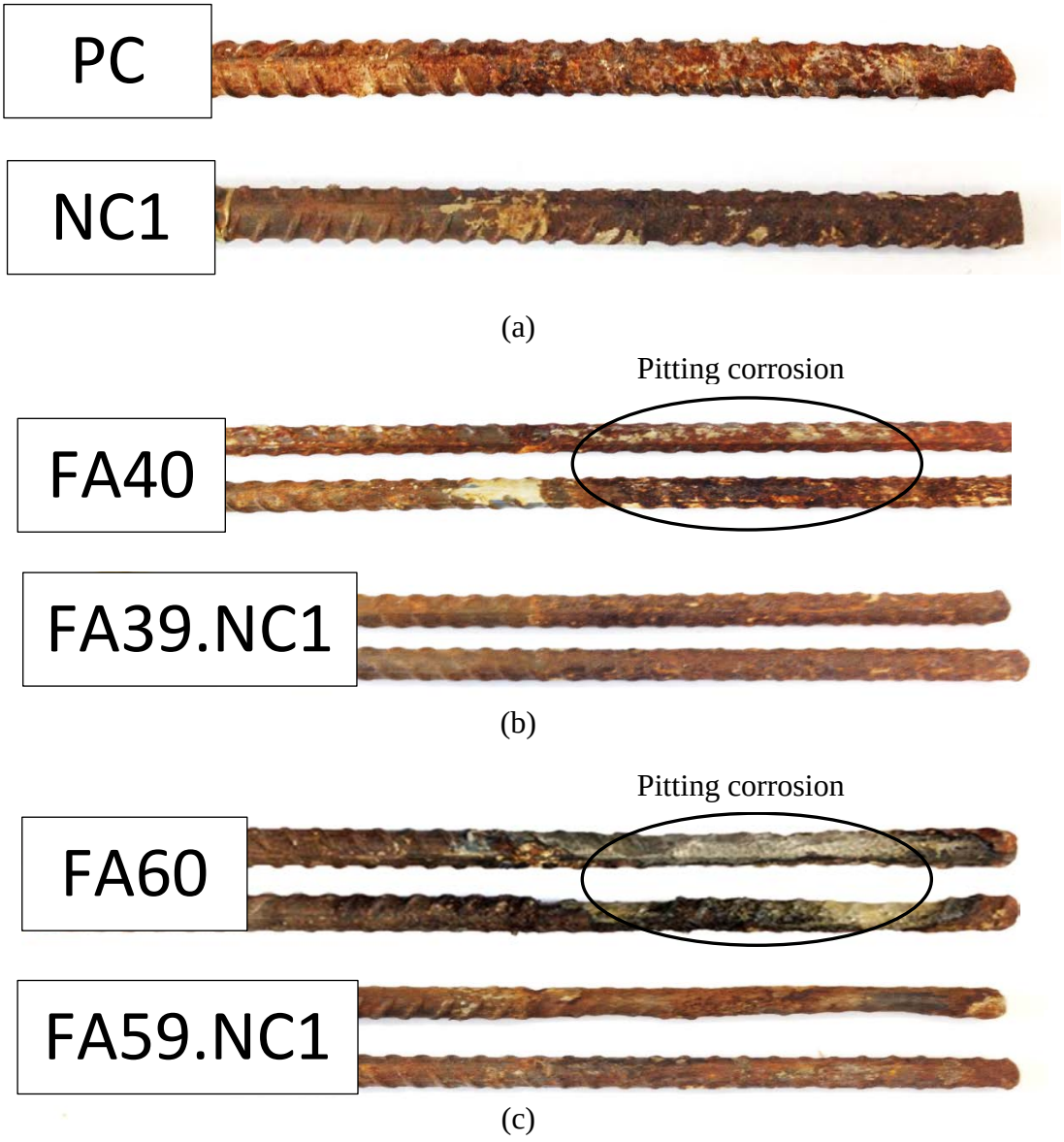

Figure 4.37 Typical deterioration of rebars taken from concretes containing nano calcium carbonate after accelerated corrosion test

Table 4.5 Weight-loss measurement of rebar from different types of concretes

Mix designation	Initial mass (g)	Final mass (g)	Actual mass loss (g/cm^2)	Theoretical mass loss (g/cm^2)	Percentage of mass loss (%)
PC	536	377	2.11	2.80	29.67
NC1	532	412	1.60	2.30	22.63
FA40	539	485	0.71	0.84	9.99
FA60	532	467	0.87	0.93	12.31
FA39.NC1	527	492	0.46	0.16	6.63
FA59.NC1	534	478	0.74	0.66	10.53

4.6 Micro- and nano-structural analysis and phase identification of OPC and HVFA pastes containing nano silica and nano-$CaCO_3$ (Part III)

4.6.1 Scanning electron microscopy

4.6.1.1 Micro- and nano structural analysis of cement and HVFA pastes containing nano silica

Figure 4.38 shows the scanning electron microscopy (SEM) images of pure cement paste and pastes containing 40% fly ash (Figure 4.38b), 2% NS (Figure 4.38c) and combined 38% fly ash and 2%NS (Figure 4.38d) after 28 days of curing. Many spherical shape unreacted fly ash particles together with pores or voids can be seen in Figure 4.38b, whereas very dense microstructures can be observed in the paste containing 2% NS (see Figure 4.38c). No pores or voids are also observed in that sample. This is believed to be due to formation of secondary C-S-H gels through faster pozzolanic reaction of NS with CH in the system. Dense microstructures can also be seen in Figure 4.36d where the effect of addition of 2% NS in HVFA concrete can easily be distinguished from Figure 4.38b.

Backscattered electron (BSE) images of polished samples after 28 days of curing are also shown in Figure 4.39. BSE is useful to identify the constituent phases within cement paste based on their brightness. Therefore, the brightest (or white) parts can be Classified as un-hydrated cement particles, the dark (or black) parts as voids and cracks and grey to dark grey parts can be Classified in the order of CH, other hydration products and C-S-H (Zhao and Darwin, 1992; Scrivener, 2004). The BSE images of paste containing 40% and 60% fly ash are shown in Figures 4.39b and 4.39c, respectively. Many white and black areas can be identified in the images representing un-hydrated cement/fly ash particles and voids/cracks, respectively. The grey to dark grey areas in those images are believed to be those of hydration products. On the other hand, few voids/cracks (limited black areas) and few un-hydrated cement particles (white areas) are noticed in the sample containing 2% NS (see Figure 4.39d). In the same sample large number of grey to dark grey areas representative of hydration products are also observed.

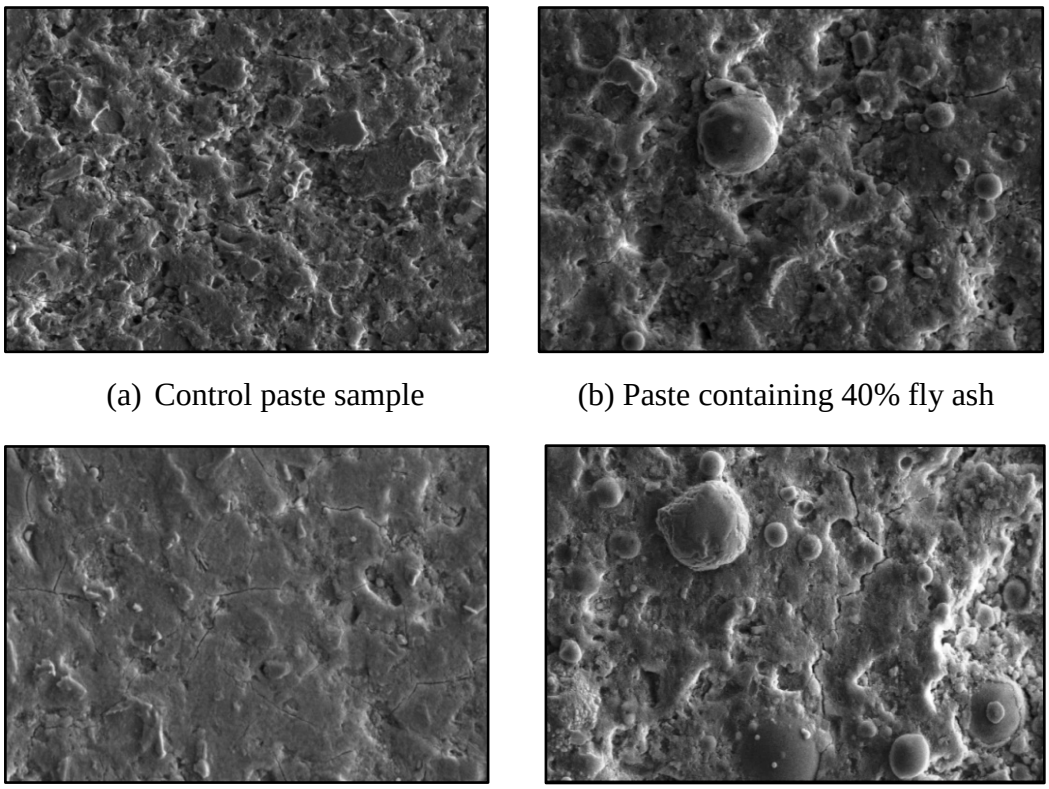

(a) Control paste sample (b) Paste containing 40% fly ash

(c) Paste containing 2% NS (d) Paste containing 38% fly ash and 2% NS

Figure 4.38 Secondary electron (SE) images of paste samples silica after 28 days of curing

The effect of addition of 2% NS in the paste containing 38% and 58% fly ash can also be seen by comparing the BSE images between Figure. 4.39b and Figure 4.39e and between Figure 4.39c and Figure 4.39f. Clear indication of positive effect of NS in HVFA paste can be observed where few black areas and more grey to dark grey areas compared to those of paste containing 40% and 60% fly ash can be clearly seen. Areas with dark grey are also comparably higher than that in the paste containing 40% and 60% fly ash, indicating the consumption of CH by the NS and the formation of C-S-H.

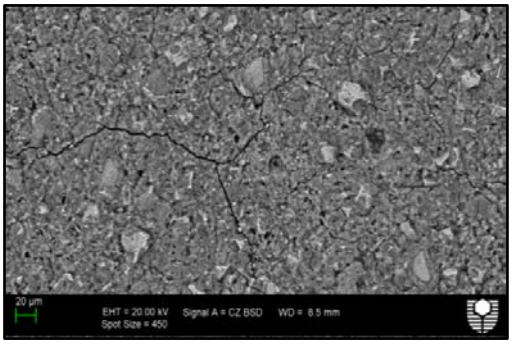

(a) Cement paste

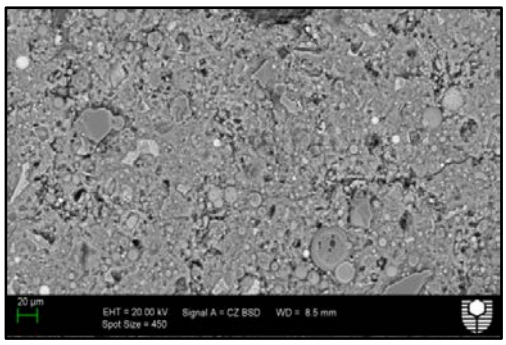

(b) Paste containing 40% fly ash

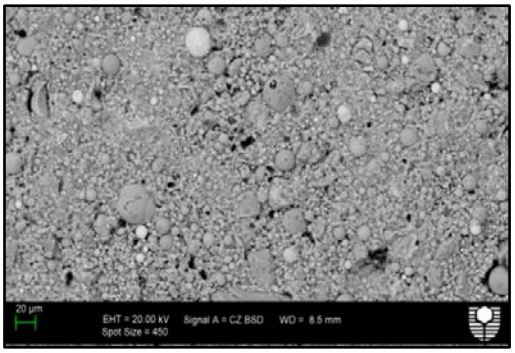

(c) Paste containing 60% fly ash

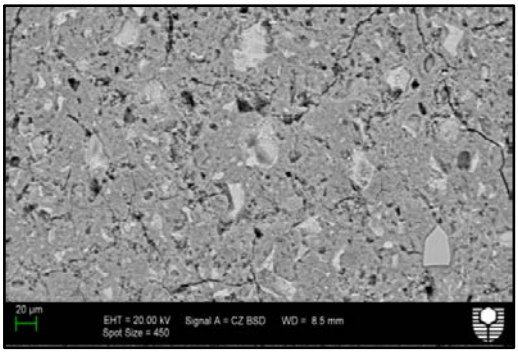

(d) Paste containing 2% NS

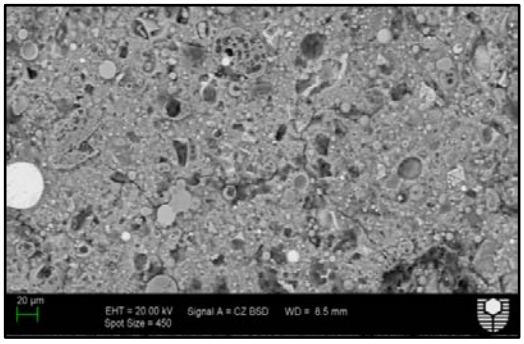

(e) Paste containing 38% fly ash and 2% NS

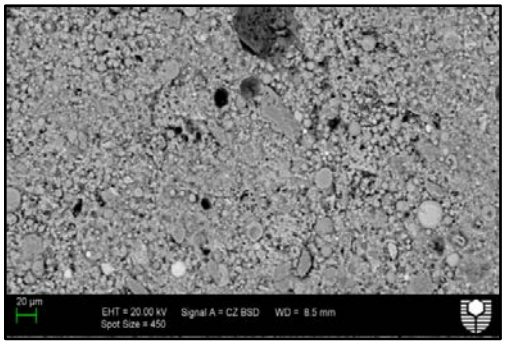

(f) Paste containing 58% fly ash and 2% NS

Figure 4.39 Backscattered electron (BSE) images of polished surface of paste samples after 28 days of curing.

4.6.1.2 Micro- and nano-structural analysis of OPC and HVFA pastes containing nano-$CaCO_3$

The backscatter electron (BSE) microscope observations on a series of HVFA paste samples with nano-$CaCO_3$ addition have also been carried out to observe the microstructure changes. The specimens for SEM analysis were taken from paste samples that had been fractured after 28 days of water curing. The specimens were then cut to expose a new surface, mounted in epoxy, polished and coated with Platinum. BSE images of paste samples are shown in Figures 4.40 and 4.41. In

Figure 4.40b, it is clearly seen that the NC1 sample has very few white and black areas (represents un-hydrated cement particles and voids, respectively) and more grey to dark grey areas than control cement paste sample (see Figure 4.40a), which indicates that the microstructure of NC1 paste is more uniform and dense than that of the cement paste. Similar dense microstructure can also be seen in HVFA paste samples containing 1% nano-$CaCO_3$ in Figures 4.41c and d for FA39.NC1 and FA59.NC1 samples, respectively.

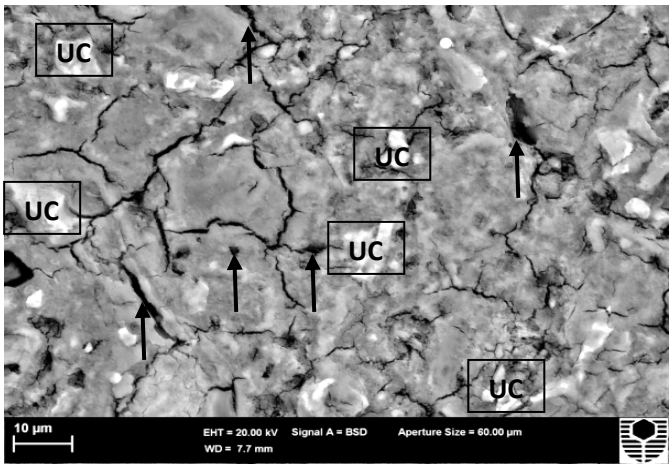

(a)

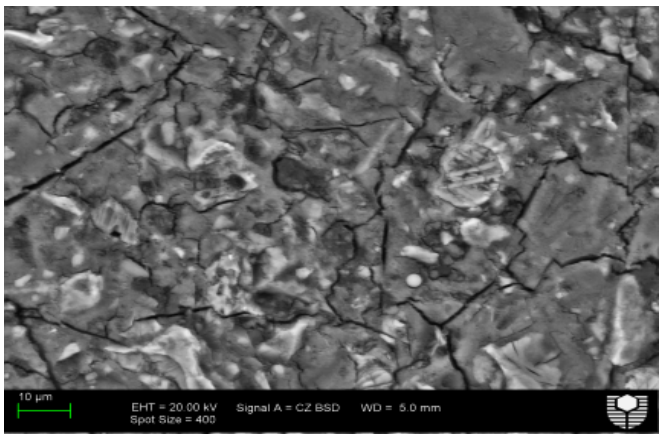

(b)

Figure 4.40 Backscattered electron images of (a) cement pastes (UC represents as unhydrated cement particle, black spots are represented by arrows as voids and (b) NC1 pastes after 28 days of curing

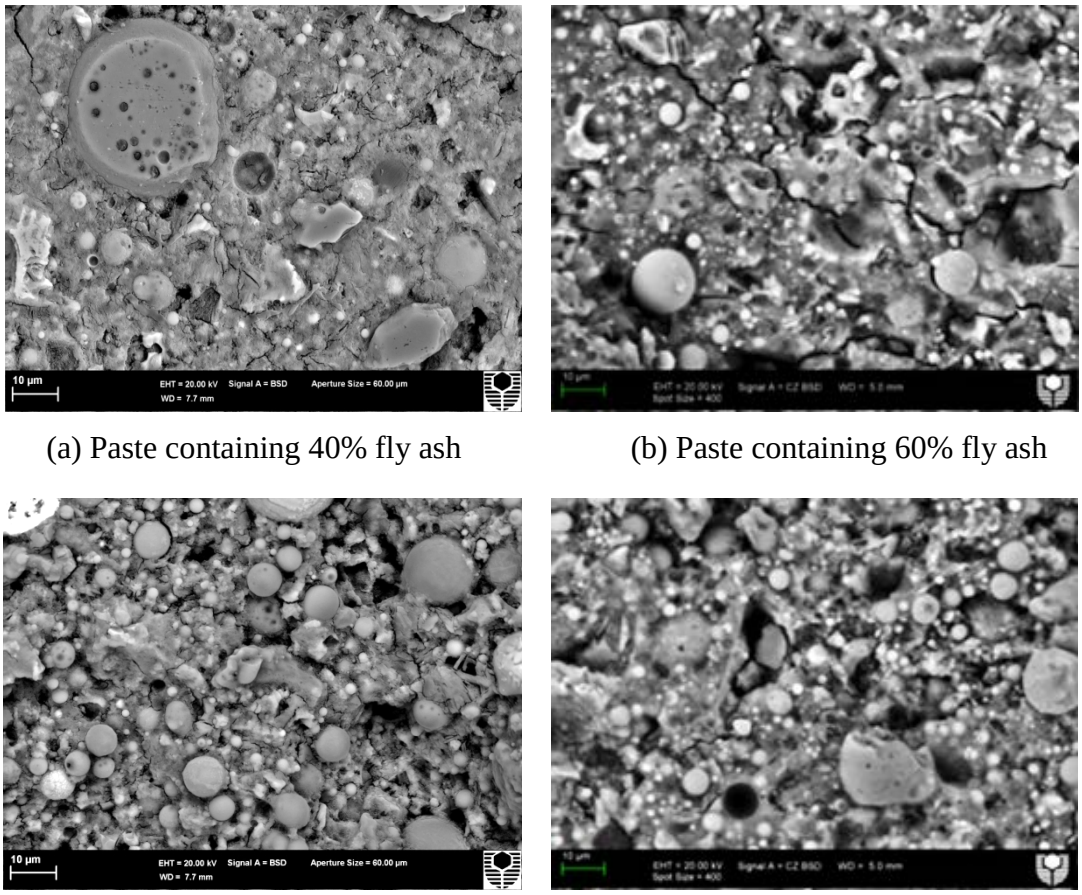

(a) Paste containing 40% fly ash (b) Paste containing 60% fly ash

(c) Paste containing 39% fly ash and 1% NS (d) Paste containing 59% fly ash and 1% NS

Figure 4.41 Backscattered electron images of HVFA and combined HVFA with 1% NC pastes cured at 28 days

4.6.2 X-ray diffraction (XRD)

4.6.2.1 XRD results of OPC and HVFA pastes containing nano silica

The reactions during cement hydration at early age (i.e. 3 days) and 28 days are studied through XRD analysis in a D8 Advance Diffractometer (Bruker-AXS). An analysis of 2θ angle from 7^0 to 70^0 is carried out at a speed of 0.5^0/min. The horizontal scale (diffraction angle) of a typical XRD pattern gives the crystal lattice spacing, and the vertical scale (peak height) gives the intensity of the diffracted ray, measured in pulses/s. XRD patterns of cement pastes with and without 2% NS addition are shown in Figure 4.42. It can be seen that at 28 days the intensity of CH peaks in cement paste containing 2% NS are decreased compared to the intensity in control paste. Analysis indicated the predominance of Portlandite (CH), Calcium Silicate (C2S/C3S) and Quartz (SiO2) where CH is formed in appreciable amount in

all samples. As a product of cement hydration, CH reacts with silica in supplementary cementing system and forms C-S-H resulting in improved mechanical properties of mortars. On the XRD scale, the CH has a strong peak located at 2-theta angle of 18.05^0. The CH peak was considered to be the main indicator of performance in cement past samples. The reduction of CH is the indication of formation of more C-S-H gel that results in improving the mechanical properties and densification of microstructure of mortar and concrete.

The beneficial effect of addition of NS in HVFA pastes is also confirmed in the XRD analysis. Figures 4.43 and 4.44 show the XRD analysis results of various 3 days old pastes samples containing HVFA and NS. The highest CH peak with intensity counts of 5000 and slightly less than 5000 is observed at 2-theta angle of 18.05^0 in the HVFA pastes containing 40% and 60% fly ash, respectively. The slightly reduced CH intensity peak of paste containing 60% fly ash could be attributed to the lesser cement than that containing 40% fly ash. The effect of 2% NS in the above pastes in terms of consumption of CH and hence the formation of C-S-H gel can also be seen in Figures 4.43 and 4.44. It can be seen that the highest CH peak at the same angle in 40% and 60% fly ash pastes is reduced by about 10% and 30%, respectively due to addition of 2% NS. These results also correspond to the compressive strength values measured at 3 days as discussed earlier, where the addition of 2% NS in HVFA concrete containing 60% fly ash exhibited more than 90% increase in compressive strength at 3 days. Larsen (1961) recognized that the CH concentration is inversely related to C-S-H production. If C-S-H is increased, less CH will be available for diffracting X-rays (Belkowitz and Armentrout, 2010). Therefore, the reduction of CH and increase in amorphous contents in XRD analysis results of HVFA pastes containing nano silica indicates, the formation of more C-S-H in the system. In fact the increase in compressive strength is the evidence of C-S-H formation.

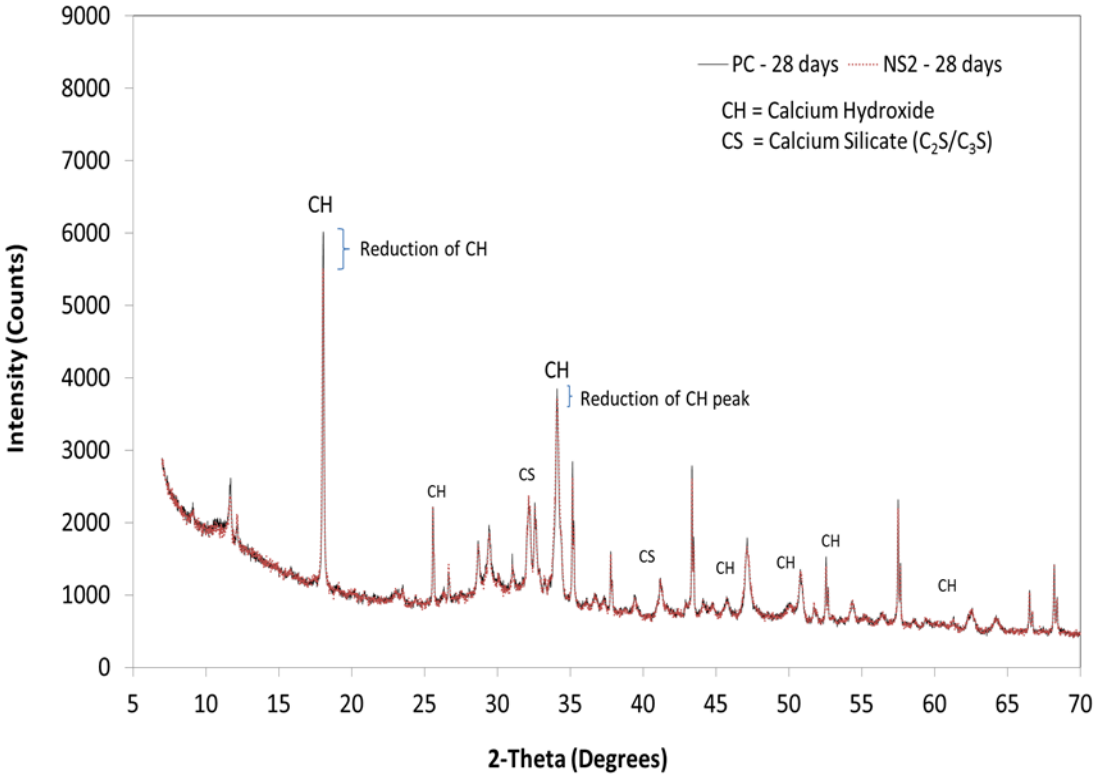

Figure 4.42 XRD analysis of cement paste samples after 28 days of curing

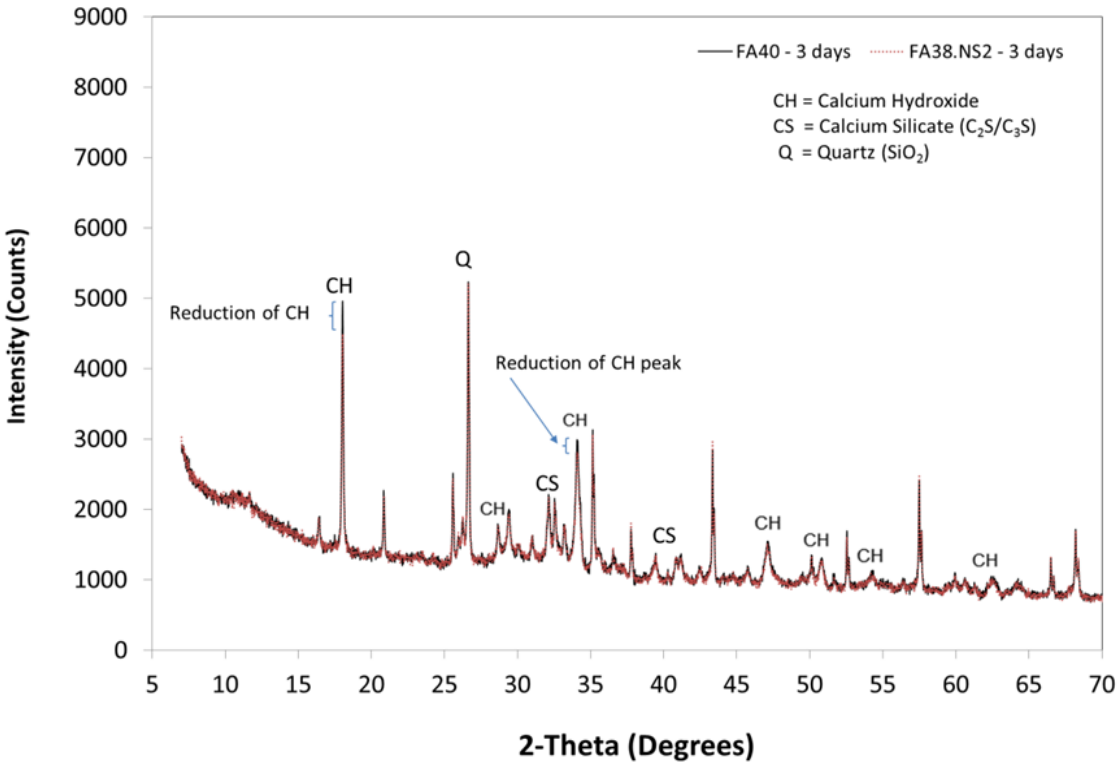

(a)

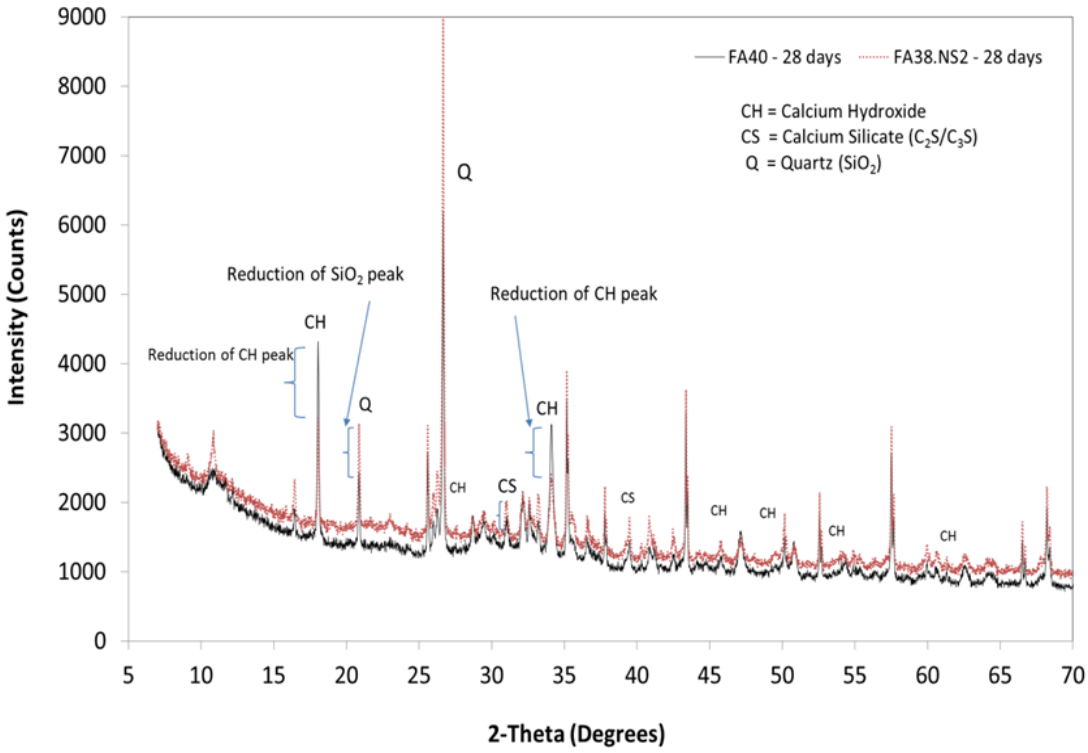

(b)

Figure 4.43 XRD analysis of FA40 paste samples after 3 and 28 days of curing

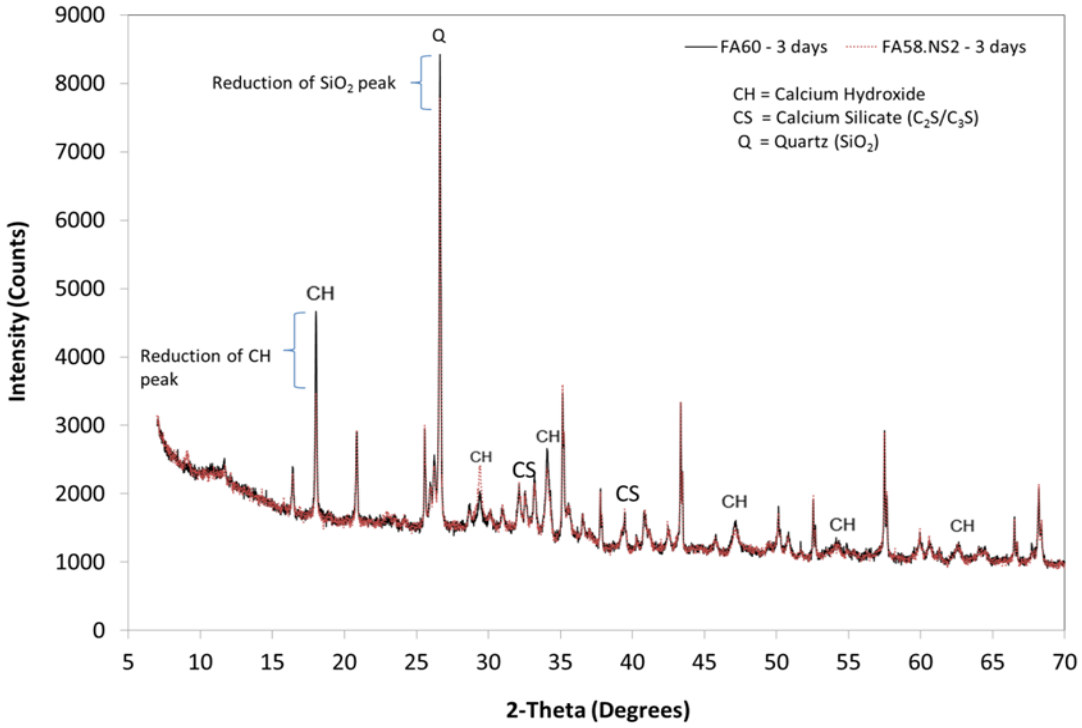

(a)

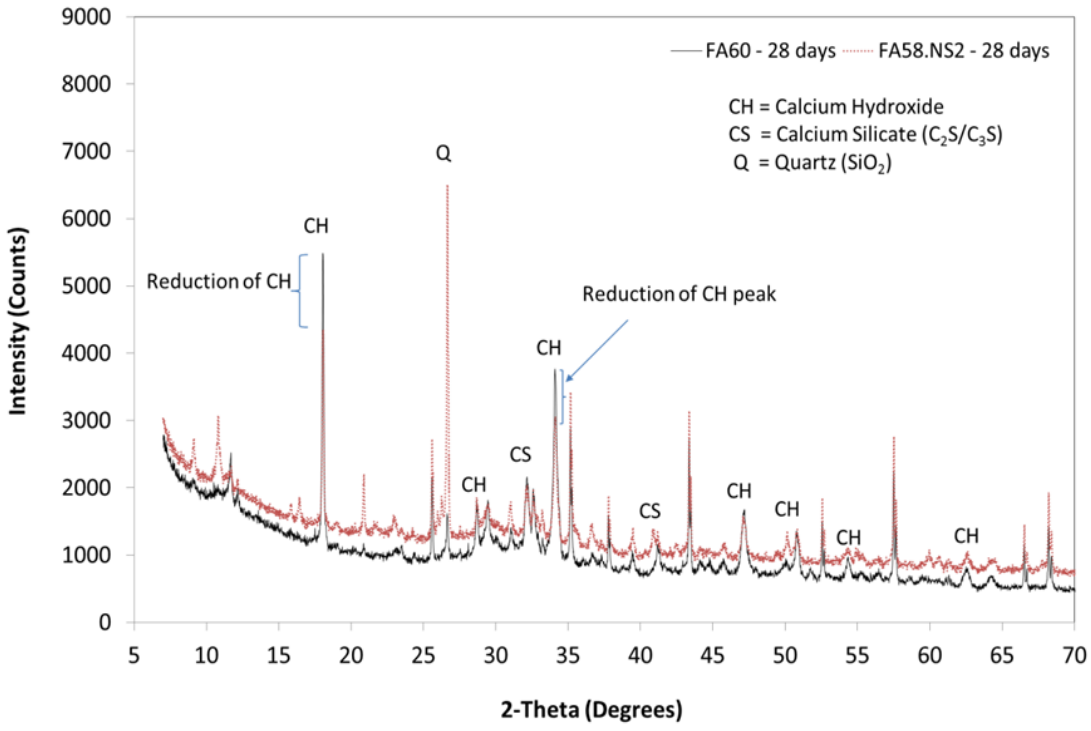

(b)

Figure 4.44 XRD analysis of FA60 paste samples after 28 days of curing

4.6.2.2 XRD results of OPC and HVFA pastes containing nano-$CaCO_3$

Figures 4.45, 4.46 and 4.47 show the XRD patterns of cement pastes containing nano-$CaCO_3$ and combined HVFA with nano-$CaCO_3$. Changes in the mineral phases during hydration were found since ettringite and calcite were present in pastes containing $CaCO_3$ nanoparticles. As can be seen in Figure 4.45, the diffraction spectra of cement paste and that containing 1% nano-$CaCO_3$ do not show any significant difference in different peaks. In HVFA pastes containing 1% $CaCO_3$ nanoparticles, the XRD result show reduction of the CH peak intensity compared to that of HVFA pastes (see Figures 4.46. and 4.47). For instance, after 7 days curing, the intensity peak of CH decreased from 4481 to 4218 at $2\theta = 18.05°$ while at 28 days, the reduction of CH intensity was appeared at $2\theta = 34.09°$. The same trend was also found in paste with 60% replacement of cement with fly ash, where the addition of 1% nano-$CaCO_3$ decreased the intensity of CH from 4840 to 3698 and from 5485 to 4057 at 7 and 28 days, respectively. When combining $CaCO_3$ nanoparticles and high volume fly ash, the fly ash with high silicate and aluminate content reacts with $CaCO_3$ nanoparticles to produce additional hydration products in the system. It is reported that $CaCO_3$ perform as nucleation surface for CH and C-S-H precipitation (Sato and Diallo, 2010).

The XRD results in the figures also showed reduction of calcium silicate (CS) peaks in both HVFA pastes at both curing ages due to addition of 1% nano-$CaCO_3$. The reduction of CS is a clear indication of the formation of hydration products (e.g. C-S-H) in the system. On the other hand, new peaks of ettringite were also present at 7 days sample of HVFA and $CaCO_3$ nanoparticle pastes. Over the time, the etrringite (Aft) was transformed to monosulfate (AFm) and other products, therefore the ettringite peaks were decreased at 28 days. This phenomenon is also found in DTA/TGA analysis as discussed in next section. Furthermore, the results indicate that the consumption of CH and the formation of ettringite contributed to the strength development of HVFA pastes containing $CaCO_3$ nanoparticles.

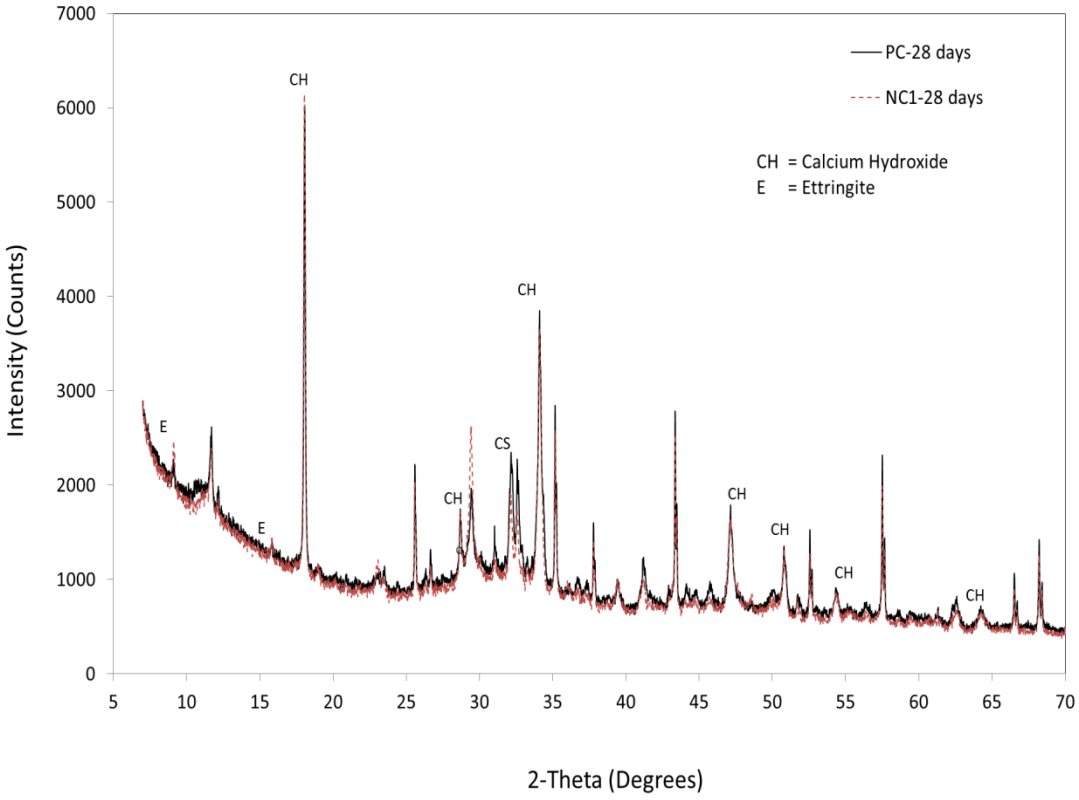

Figure 4.45 XRD analysis of cement and 1% nano-$CaCO_3$ pastes at 28 days

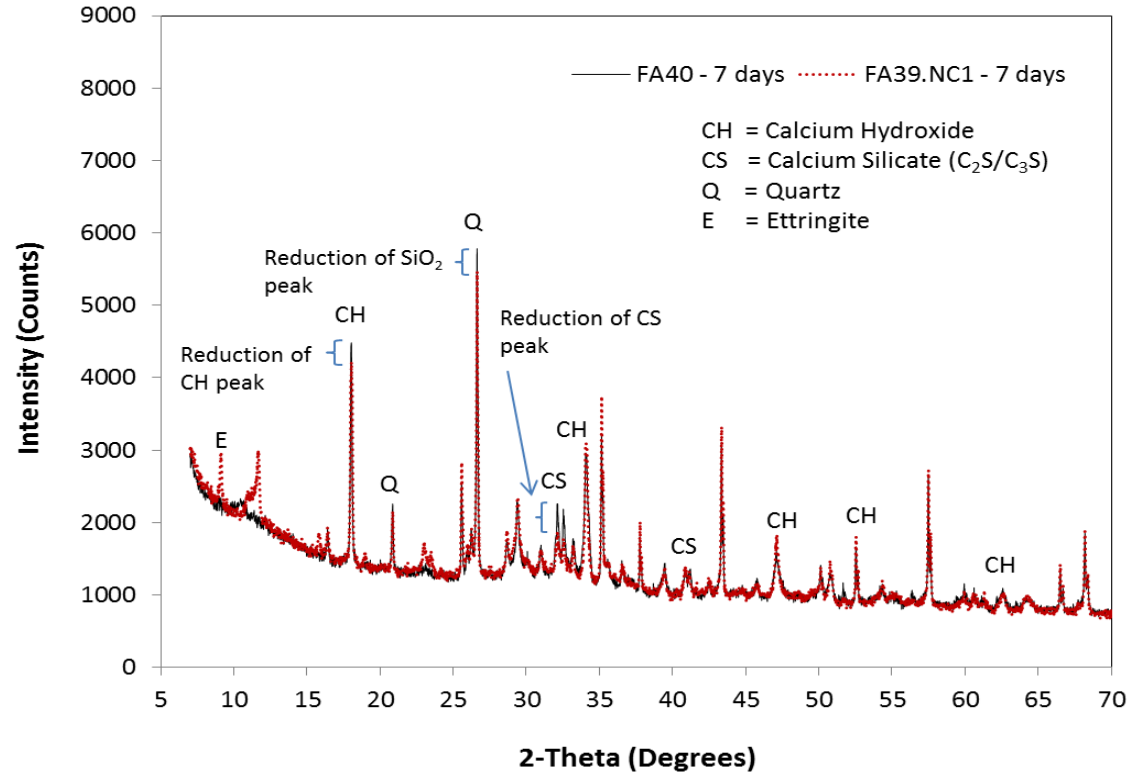

(a)

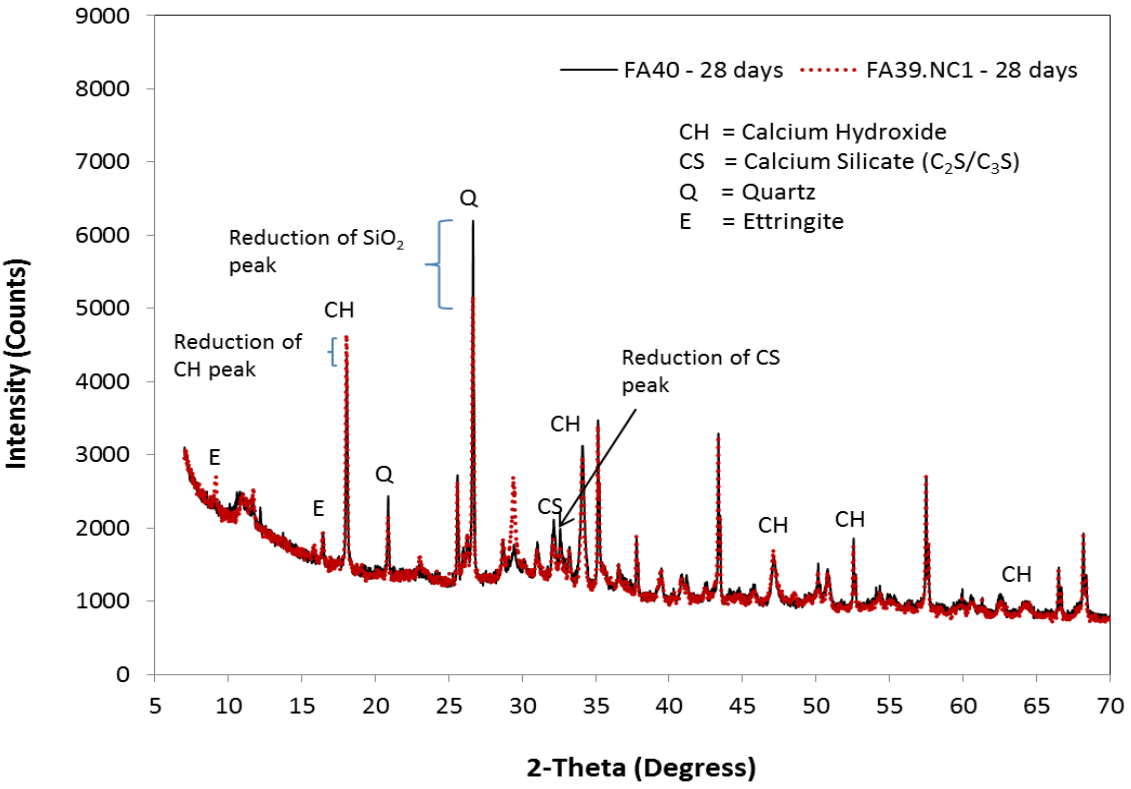

(b)

Figure 4.46 XRD analysis of FA40 pastes with and without nano-$CaCO_3$ at 7 and 28 days

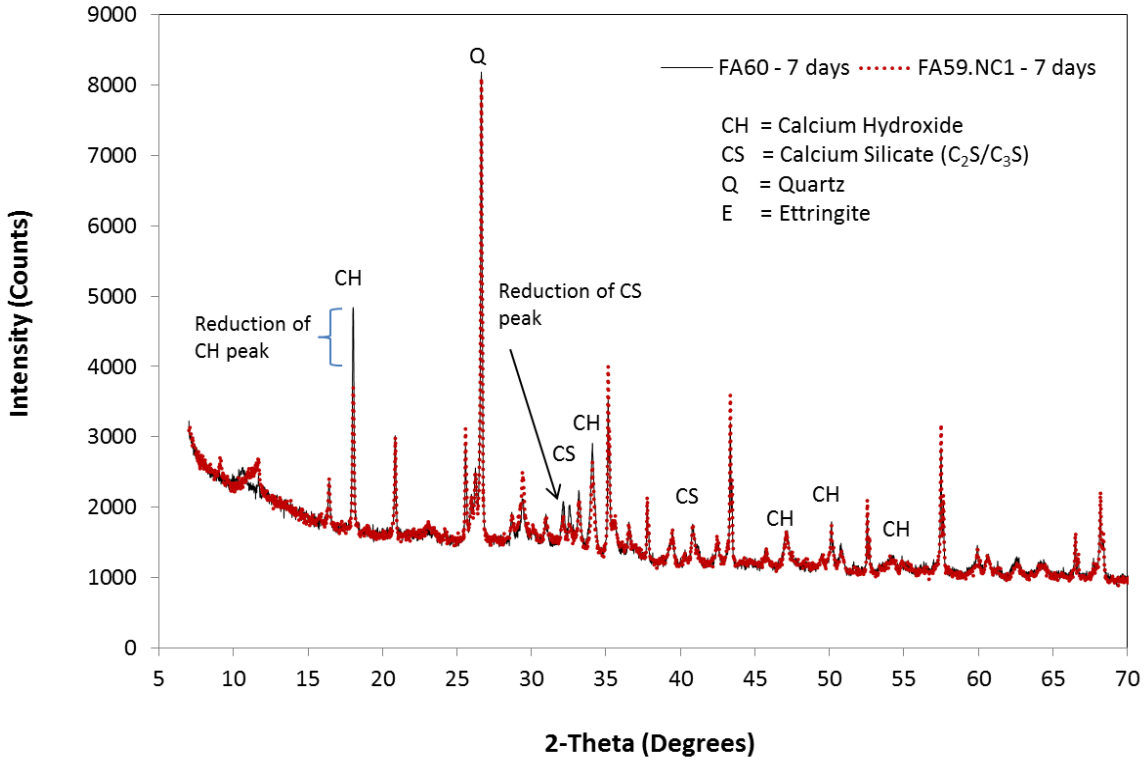

(a)

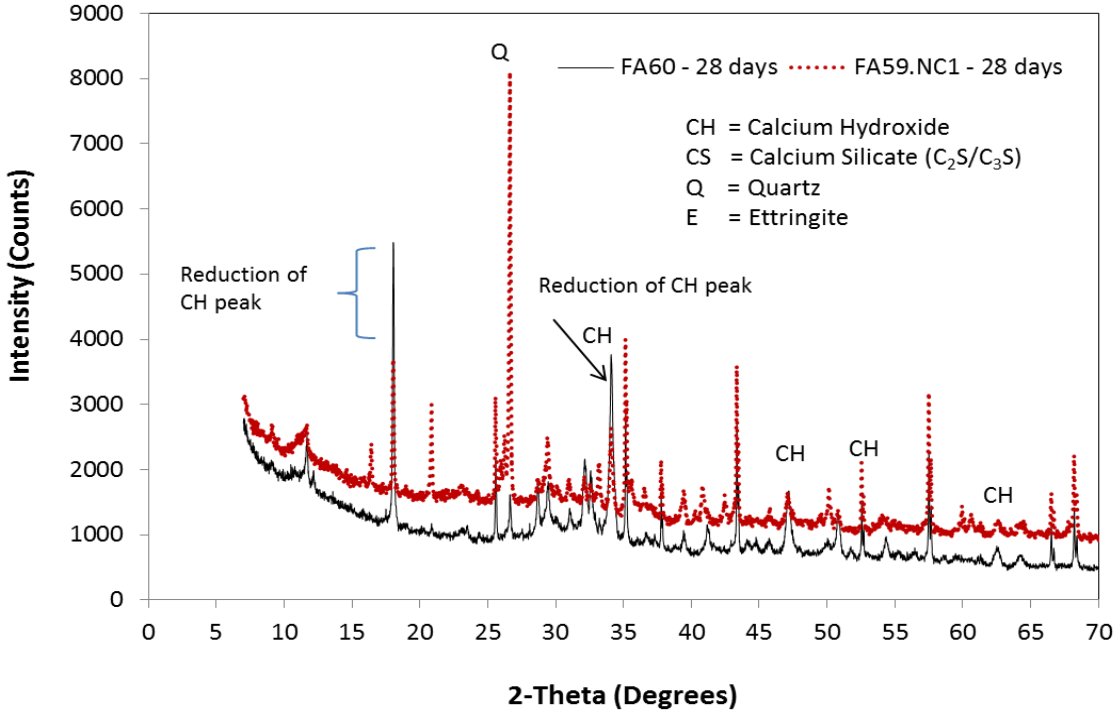

(b)

Figure 4.47 XRD analysis of FA60 pastes with and without nano-$CaCO_3$ at 7 and 28 days

4.6.3 DTA/TGA analysis

4.6.3.1 Thermogravimetric analysis results of OPC and HVFA pastes containing nano silica

The results of DTA/TGA on cement pastes containing 2% NS pastes after 28 days of curing are shown in Figure 4.48. The figure shows the normalized mass loss in percent (current mass divided by initial mass) versus temperature and the temperature difference divided by initial mass versus temperature. From DTA analysis, the U-shaped DTA curve refers to rapid loss of weight followed by rapid gain in the weight under endothermic process. Endothermic process is a process or reaction in which the system absorbs energy from the surroundings in the form of heat (Musa, 2014). Several peaks can be detected in the DTA curves.

In Figures 4.48 and 4.49, the DTA results show two major endothermic peaks at 103°C and 462°C, corresponding to the dehydration of calcium silicate hydrate (C-S-H)/ettringite (AFt) and calcium hydroxide (CH), respectively. In addition, the AFt/C-S-H phases can also be identified by observing the decomposition of hydration products within the temperature range of about 62-157°C. In Figure 4.48, when NS2 paste is compared with cement paste, it can be seen that the amount of CH in NS2 paste decreases in weight loss at 462 ^{0}C indicating the consumption of CH as it either turns into C-S-H or absorb CO_2 to form $CaCO_3$ (calcite). However, since the weight loss from unbound water is lost between 50-200°C, overlapped with the weight loss from C-S-H gel thus it is impossible to accurately determine the amount of C-S-H formed between them. Regarding to the effect of NS in HVFA pastes, it can be seen in Figures 4.49a and b smaller broad peak within the temperature range of 428-495°C indicating the less intensive CH in HVFA pastes with NS than in reference FA40 and FA60 pastes, respectively.

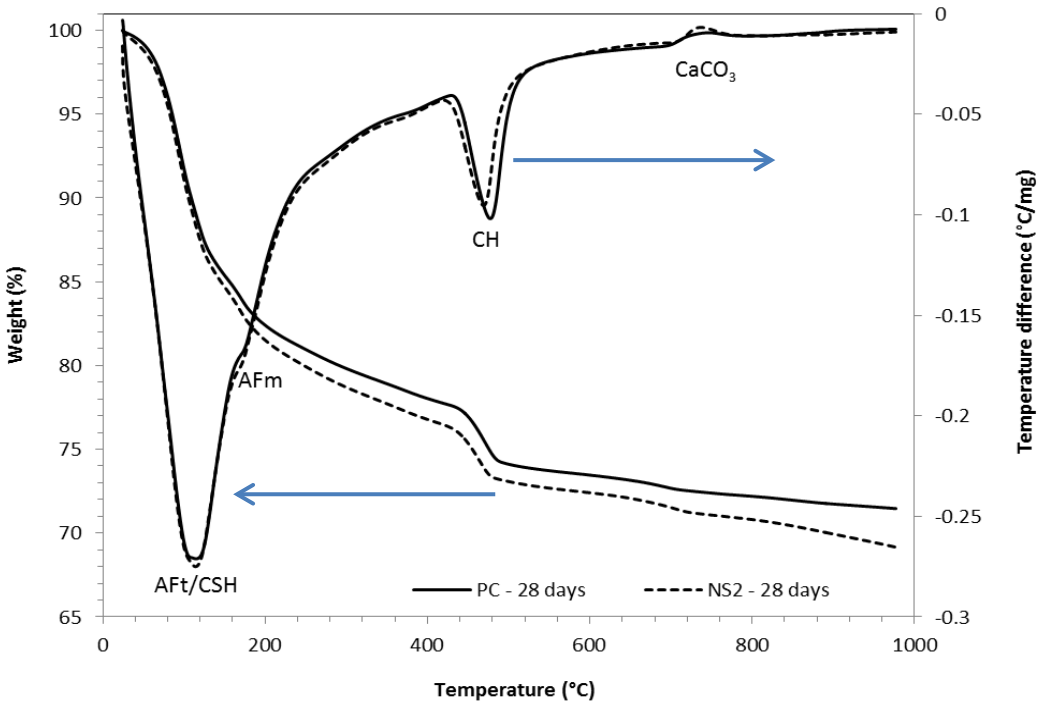

Figure 4.48 DTA/TGA analysis of cement pastes containing NS after 28 days of curing

The TGA curves also show similar pattern to explain that nanoparticles participate in the hydration process of the system. TGA is defined as the technique whereby the mass of a substance in a heated environment is recorded at a controlled rate as a function of time or temperature (Keactch and Dollimore, 1975). In this study, TGA curves indicate the changes in mass of pastes due to heating from room temperature to about 1000°C. Based on the Figures 4.48 and 4.49, the weight loss due to the dehydroxylation of CH can be observed at temperature range between 400 and 500 °C. From Figure 4.50, it can be seen that CH content in approximately 7.5% lower in NS2 paste than PC paste. The estimation of the content of CH is calculated based on Taylor formula as discussed earlier in section 3.5.3. It also can be seen that the amount of CH decreases in HVFA pastes due to the addition of silica nanoparticles. This could be due to the reactivity of NS in HVFA pastes and the consumption of CH by the pozzolanic reaction.

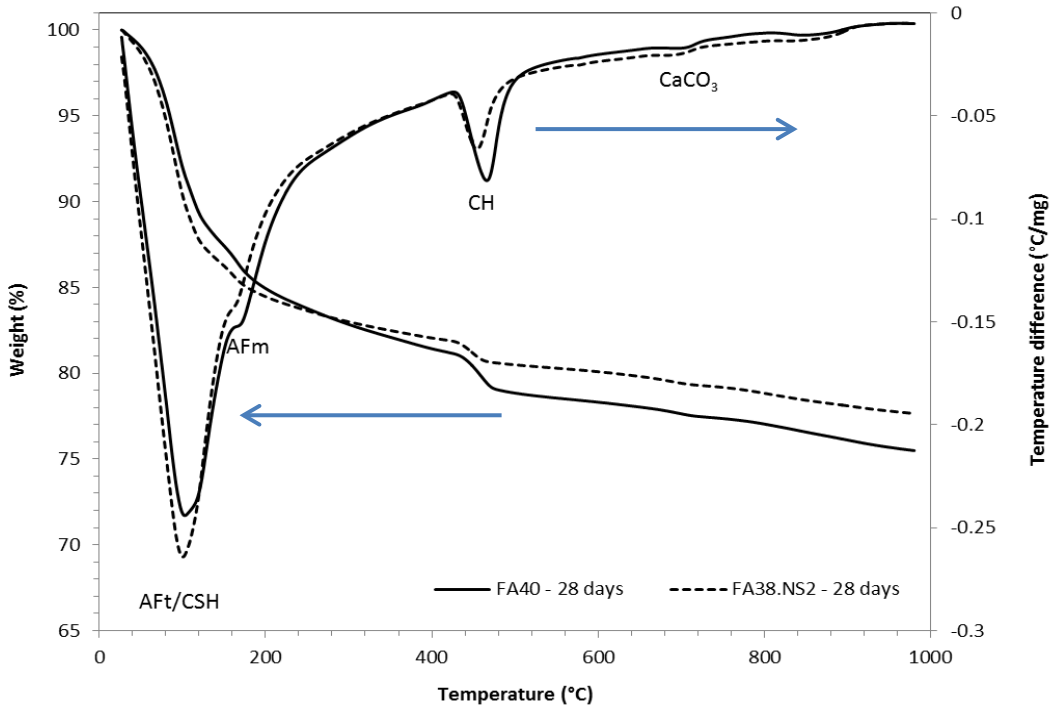

(a)

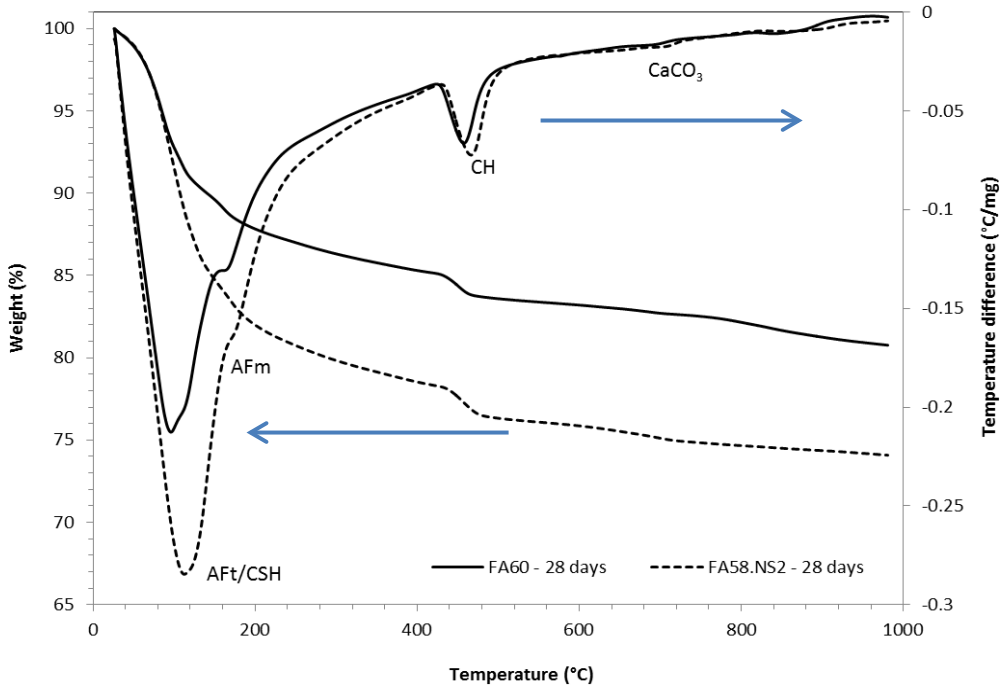

(b)

Figure 4.49 DTA/TGA analysis of cement pastes containing HVFA, NS and HVFA with NS after 28 days of curing

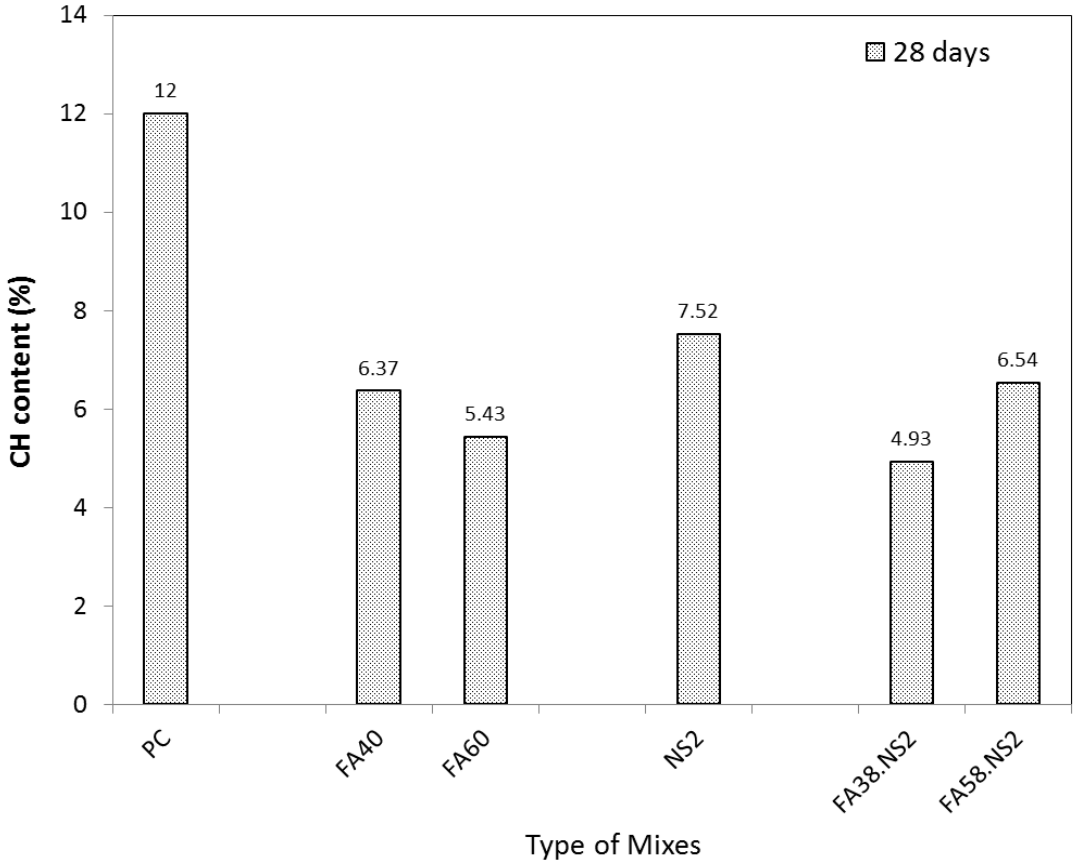

Figure 4.50 Calcium hydroxide content in pastes containing 2% nano silica after 28 days of curing

4.6.3.2 Thermogravimetric analysis results of cement and HVFA pastes containing nano-$CaCO_3$

The thermogravimetric analysis (TGA) and differential thermal analysis (DTA) results of HVFA pastes containing nano-$CaCO_3$ are shown in Figure 4.51. In order to investigate the effectiveness of $CaCO_3$ nanoparticles in reducing the CH at early age, the DTA/TGA measurements have been performed on 7 and 28 days cured HVFA pastes blended mixture with and without 1% $CaCO_3$ nanoparticles.

In Figure 4.52, lower peak of CH within the temperature range of 428-495ºC in HVFA pastes containing $CaCO_3$ nanoparticles can be seen compared to the reference FA40 and FA60 pastes, indicating the consumption of CH by the pozzolanic reaction at 7 days (see Figures 4.52a and b). In addition, the increase in AFt/C-S-H phases can also be identified within the temperature range from 62 to 157 °C, which is an indication of decomposition of more hydration products in HVFA pastes containing 1% nano-$CaCO_3$ than reference fly ash pastes. After 28 days of curing, the FA39.NC1 and FA59.NC1 paste samples also exhibited smaller broad peak of CH

than reference FA40 and FA60 pastes (see Figures 4.53a and b), indicating the mass loss and the reduction of CH content due to the presence of 1 wt% $CaCO_3$ nanoparticles.

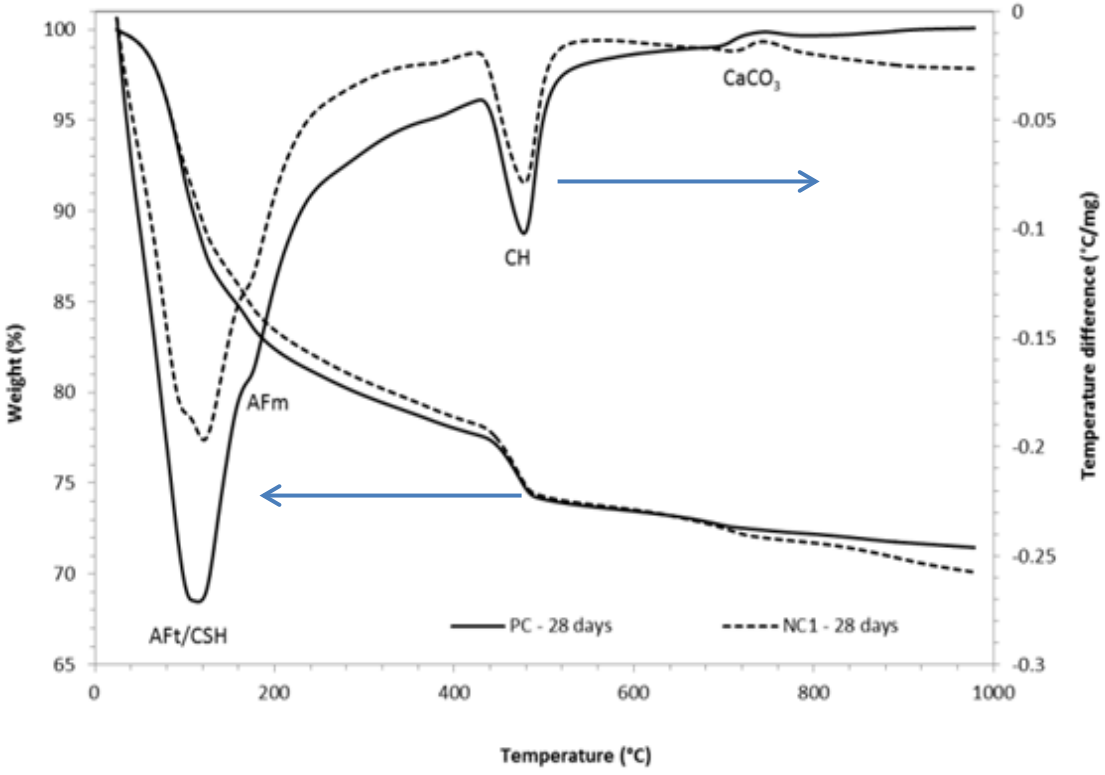

Figure 4.51 DTA/TGA analysis of cement pastes containing NC after 28 days of curing

Figures 4.51, 4.52 and 4.53 show the TGA curves which indicate the changes in mass of pastes due to heating from room temperature to about 1000 °C. It demonstrates the weight loss of all pastes samples. Based on those figures, the weight loss due to the dehydroxylation of CH can be observed at temperature range between 400 and 500 °C. As expected, the weight loss of CH in HVFA containing 1% $CaCO_3$ nanoparticles pastes is decreased at 7 days indicating that the CH is turned into C-S-H (see Figures 4.52). The same trend can also be seen in Figures 4.53a and b where the results from DTA/TGA analysis of HVFA cement pastes containing 1 wt% $CaCO_3$ nanoparticles at 28 days is presented. In addition, the calcium hydroxide (CH) content is also calculated according to Taylor's formula as explained earlier.

From Figure 4.54, it can be seen that the amount of CH is decreased in both HVFA pastes and those containing 1 wt% $CaCO_3$ nanoparticles. It is also be seen that the presence of 1% $CaCO_3$ nanoparticles reduced the CH content in FA39.NC1 and FA59.NC1 pastes compared to FA40 and FA60, respectively. This could be due to the reactivity of $CaCO_3$ nanoparticles in HVFA and the consumption of CH by the pozzolanic reaction. The addition of 1% $CaCO_3$ nanoparticles combined with 39% and 59% of fly ash lead to a reduction of CH by 10% and 15% (at 7 days) and 15% and 59% (at 28 days), respectively. This explains the difference in strength between typical HVFA and HVFA with $CaCO_3$ nanoparticles addition. The TGA results also confirmed the XRD results showing the reactivity of 1 wt% $CaCO_3$ nanoparticles with HVFA in reducing the CH content.

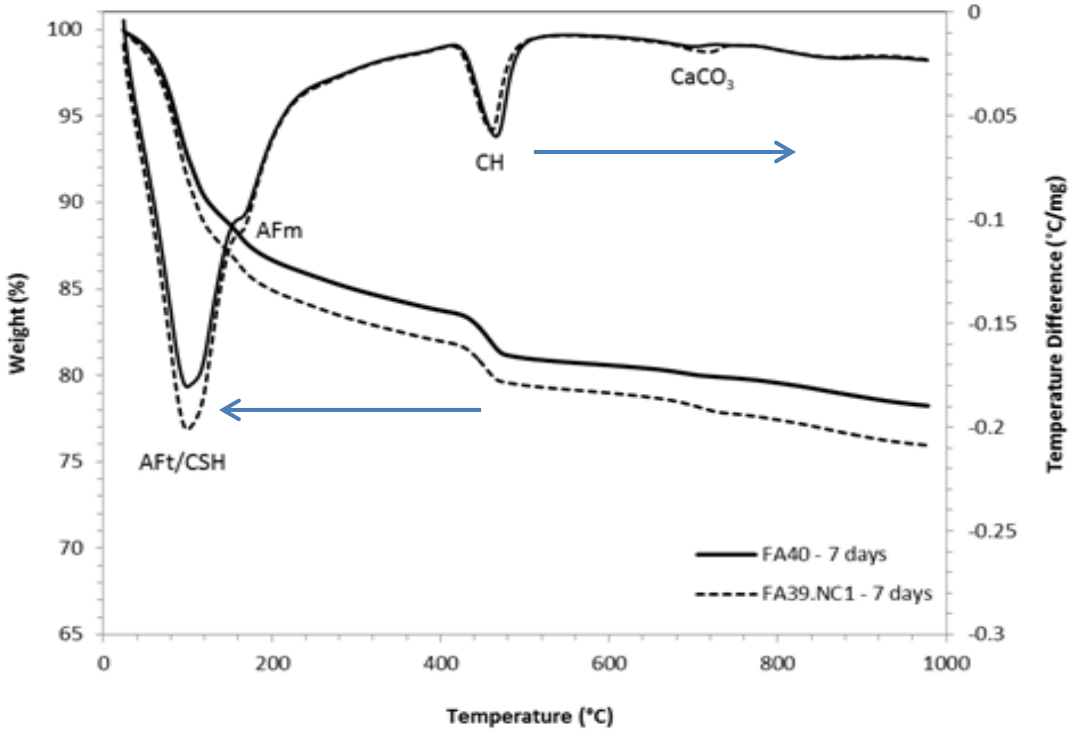

(a)

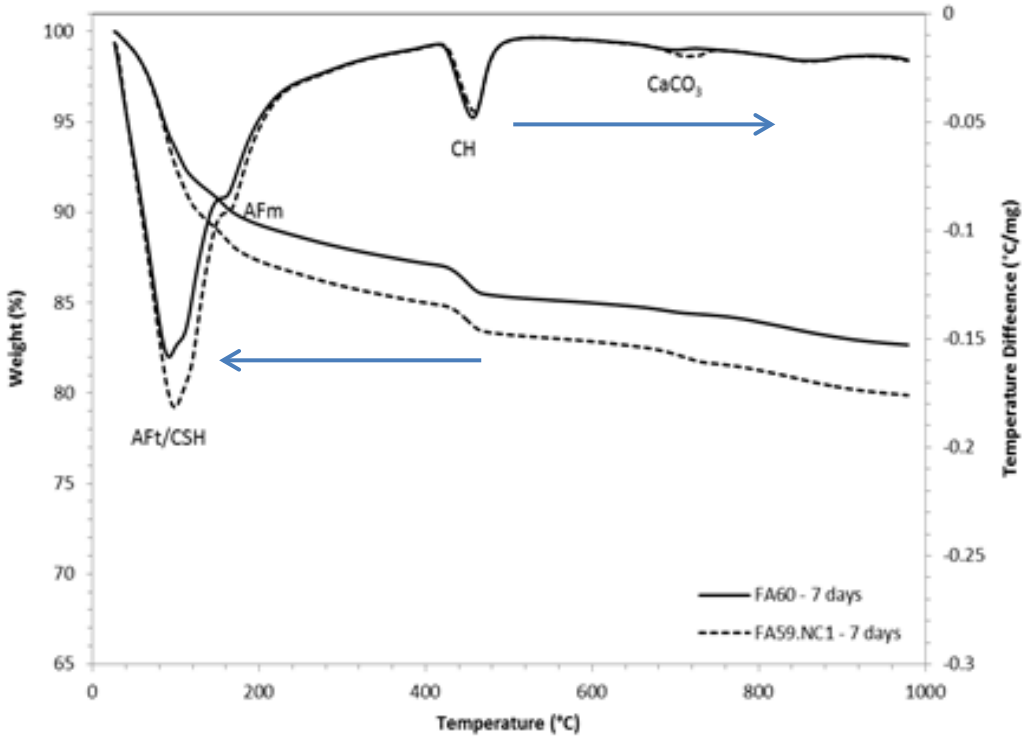

(b)

Figure 4.52 DTA/TGA analysis of HVFA cement pastes containing NC at 7 days

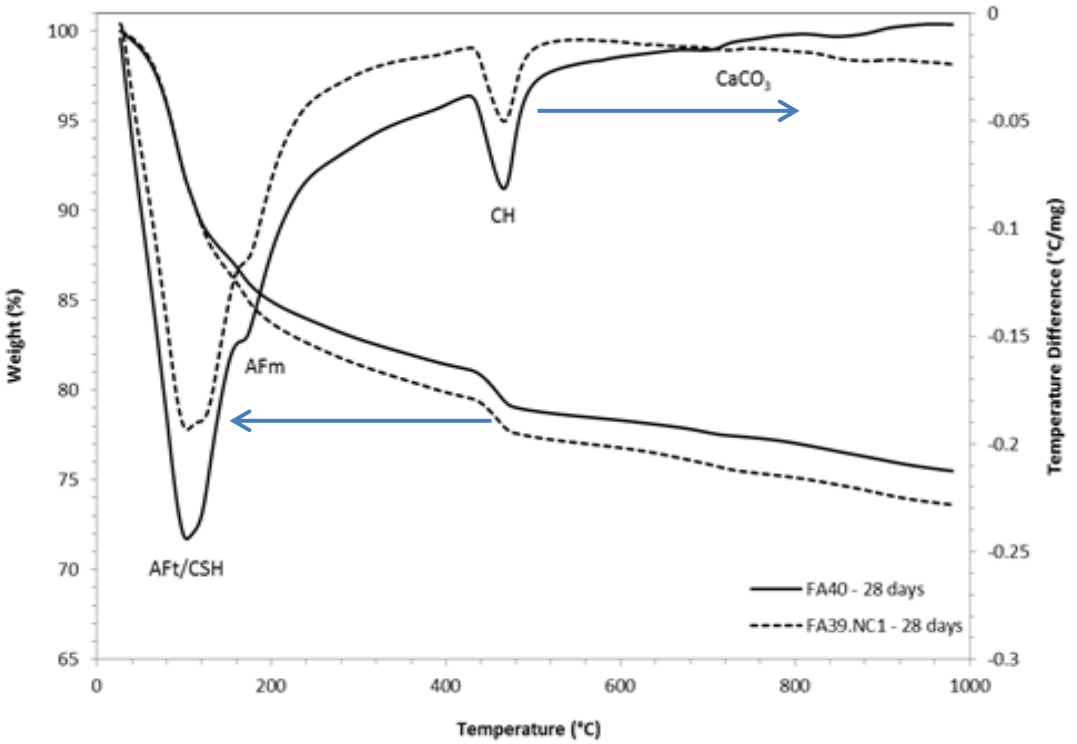

(a)

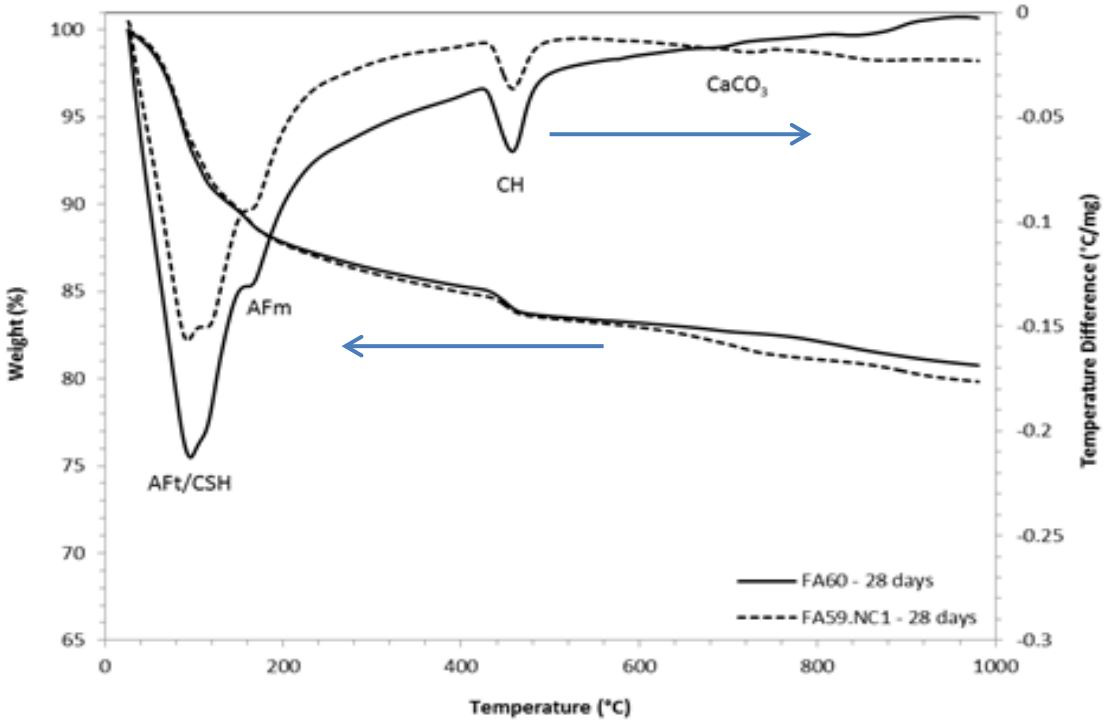

(b)

Figure 4.53 DTA/TGA analysis of HVFA cement pastes containing NC at 28 days

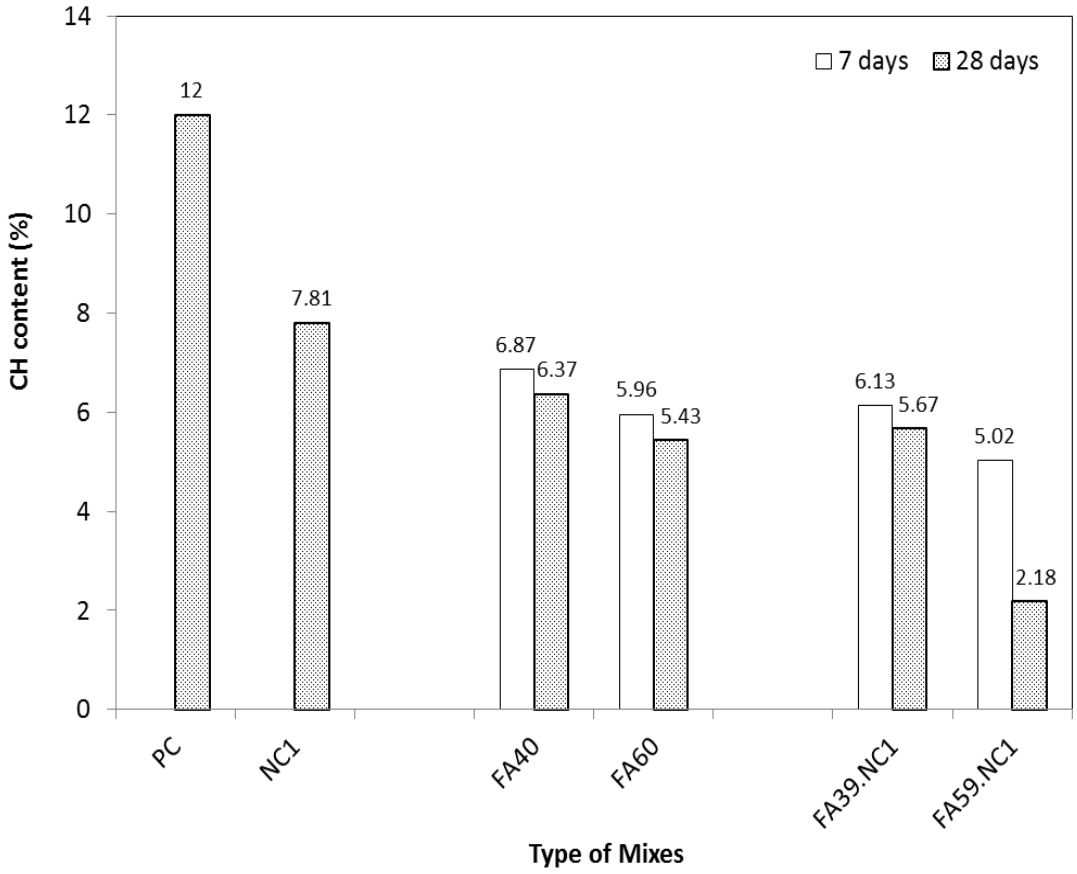

Figure 4.54 Calcium hydroxide content in paste containing 1% nano-$CaCO_3$ after 28 days of curing

4.7 Nano indentation analysis

4.7.1 Nano indentation results of HVFA pastes containing 2% nano silica

Nano indentation of the cement paste also results in identifying any of the cement phases including high and low density CSH, calcium hydroxide (CH), ettringite, pores and unhydrated cement (Taha et al, 2010). In nano indentation technique, the modulus and hardness values of each phase were statistically analysed using hardness frequency distributions with fitted Gaussian distributions to produce a frequency histogram. From each model fit, the mean value (μ) and standard deviation (σ) of the distribution were extracted from the fitting curves to be linked with the individual mineral phases. The area under the normal distribution curve also provide an estimate of the volume fraction of the mineral phases of the sample. In this study, the indentation modulus frequency distribution was used to obtain different phases (Loosed-packed CSH, Outer (Low Density) CSH, Inner (High Density) CSH, and

CH) of HVFA pastes with and without nano particles. These phases are denoted in the figures as model 1, model 2, model 3 and model 4, respectively. The values of elastic modulus higher than 50 GPa were not considered in the analysis as it is assumed as the unreacted cement clinker grains (Nemecek, 2009).

The probability distribution of indentation modulus and hardness of HVFA pastes (i.e. FA40 and FA60) is presented in Figures 4.55 and 4.56. It can be seen that the data of elastic modulus of HVFA pastes was within a range of modulus between 10 GPa and 35 GPa and one peak at 40 GPa corresponding to calcium hydroxide phase. The hardness was found to be within a range of 0.20 to 1.2 GPa, which corresponds to the low and high density phases whereas the hardness of CH was around 1.5 GPa. The modulus lower than 10GPa is a porous phase which is related to the porosity of paste. Furthermore, comparing the current results with those in the literature in Table 2.6 (see Chapter 2), it can be commented that the range of elastic modulus and hardness of HVFA pastes do not show a significant difference when compared to the obtained result for a 28-day hydrated cement specimens.

Table 4.6 shows the elastic modulus and hardness of HVFA pastes containing 2% nano silica. As can be seen in this table, the indentation modulus frequency distribution results show initial relative percentage of LD-CSH and HD-CSH of HVFA pastes containing 2% NS are 39% and 14.40% (FA38.NS2 paste) and 38.90% and 21.80% (FA58.NS2 paste), respectively. The results are higher than the relative volume fractions of LD-CSH and HD-CSH of ordinary HVFA pastes which are about 15.80% and 14.90% (FA40 paste) and 37.50% and 13.80% (FA60 paste), respectively.

Table 4.6 Elastic modulus and hardness of HVFA pastes containing 2% nano silica after 28 days of water curing

Mixes	FA40		FA60		FA38.NS2		FA58.NS2	
	Elastic Modulus	Hardness	Elastic Modulus	Hardness	Elastic Modulus	Hardness	Elastic Modulus	Hardness
Loose-packed C-S-H								
Elastic Modulus (GPa)	10.03	0.24	11.02	0.22	8.00	0.18	7.56	0.15
Volume fraction (%)	55.90	52.90	32.70	35.70	35.40	38.40	27.10	30.10
Outer (LD) C-S-H								
Elastic Modulus (GPa)	21.04	0.50	20.00	0.54	14.25	0.35	14.15	0.35
Volume fraction (%)	15.80	18.80	37.50	34.50	39.00	36.00	38.90	35.90
Inner (HD) C-S-H								
Elastic Modulus (GPa)	30.11	0.88	30.31	0.59	27.82	0.84	28.08	0.71
Volume fraction (%)	14.90	17.90	13.80	16.80	14.40	17.40	21.80	24.80
CH								
Elastic Modulus (GPa)	39.78	1.30	44.75	1.37	42.31	1.53	44.53	1.36
Volume fraction (%)	13.40	10.40	16.00	13.00	11.10	8.10	12.30	9.30

The results indicate that the incorporation of nano silica in high volume fly ash increased the amount of low and high density HVFA pastes. In particular, the low density of CSH phase appears to be more vulnerable to chemical degradation than the high density CSH phase (Constantinides and Ulm, 2004). From the nano indentation results, it can be suggested that HVFA pastes containing 2% nano silica with a higher volumetric proportion of CSH would be less affected by calcium leaching. In addition, it is observed that the probability of elastic modulus of loosed-packed CSH which represents the porous phase is reduced in the HVFA pastes containing nano silica. These results confirm the ability of nano silica in reducing the porosity by filling the gaps between the CSH gels. The reduction of calcium hydroxide is also noticed and confirms the results obtained from XRD and TGA analysis as described in the previous sections of this chapter.

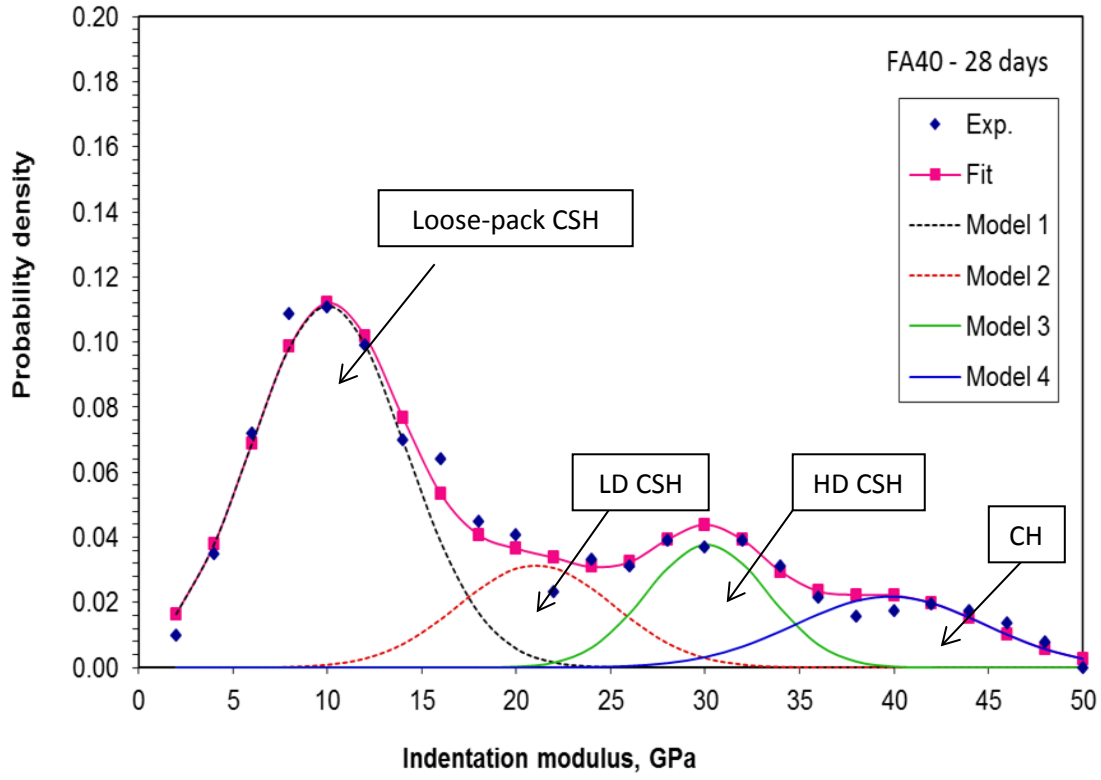

(a)

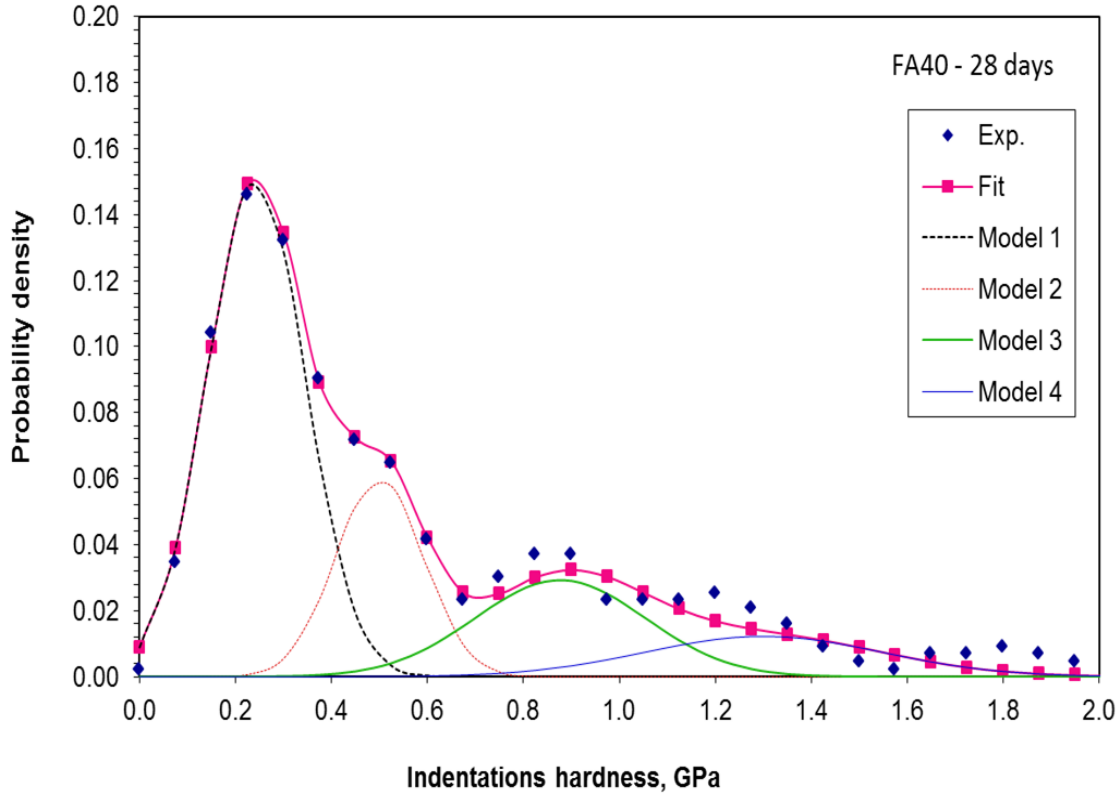

(b)

Figure 4.55 Modulus and hardness of FA40 paste after 28 days of curing

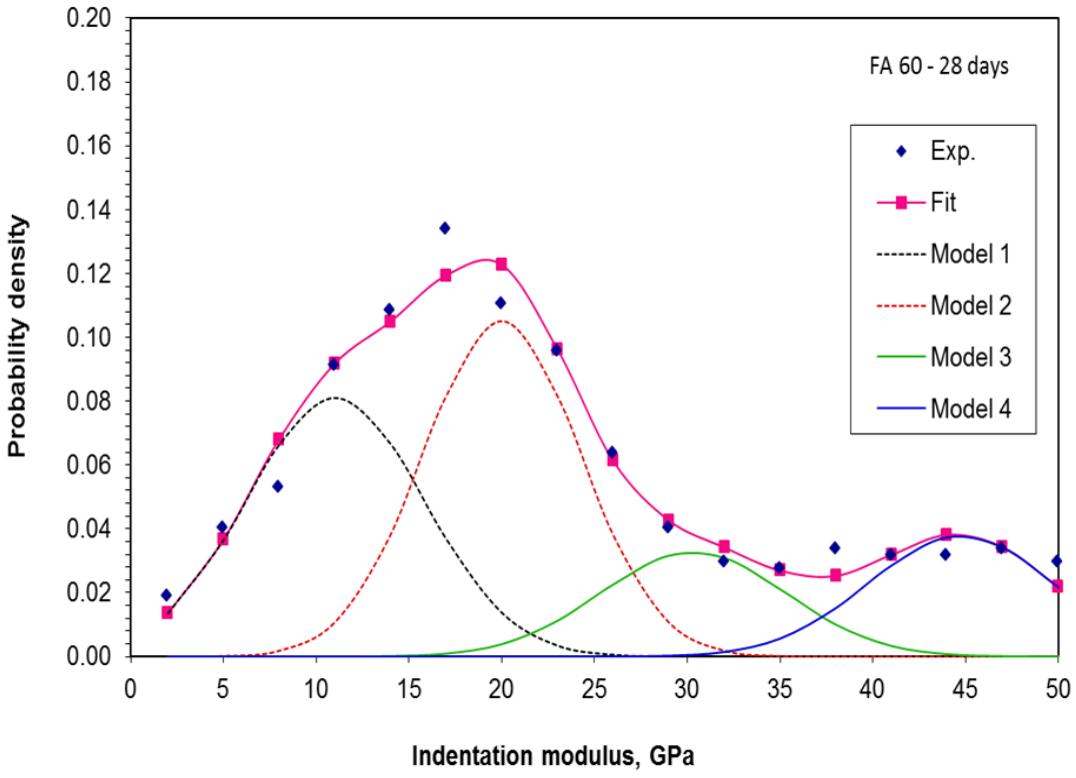

(a)

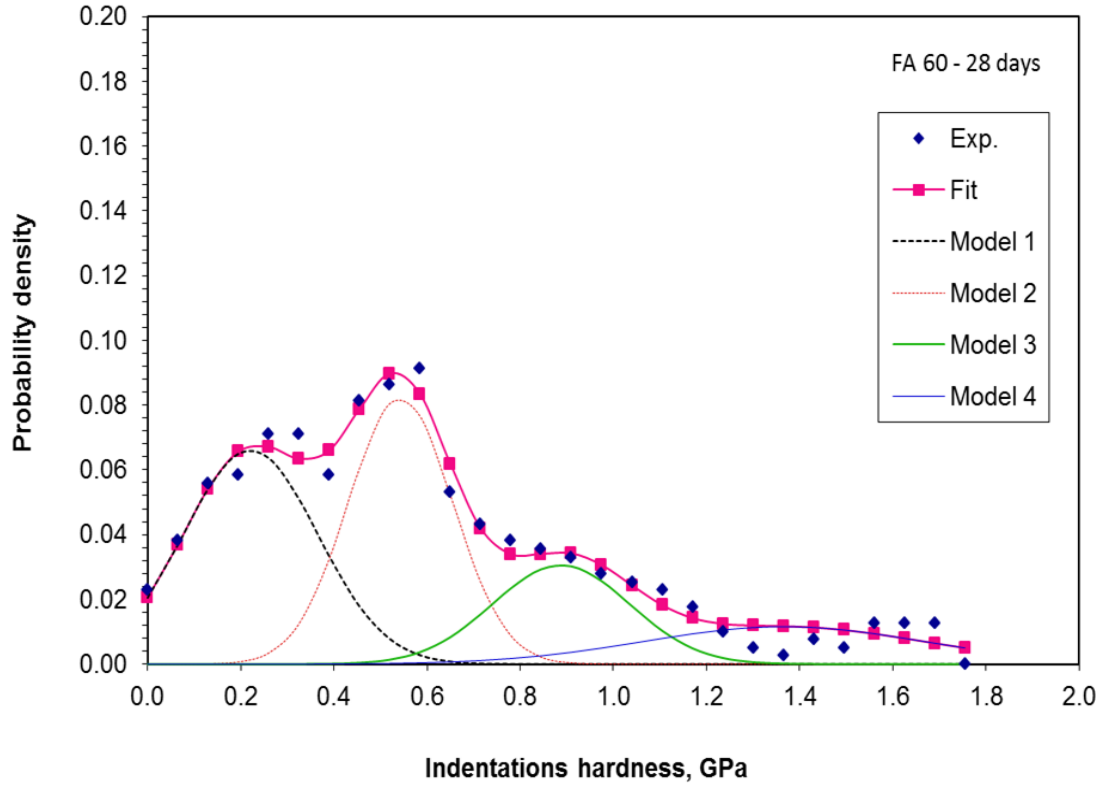

(b)

Figure 4.56 Modulus and hardness of FA60 paste after 28 days of curing

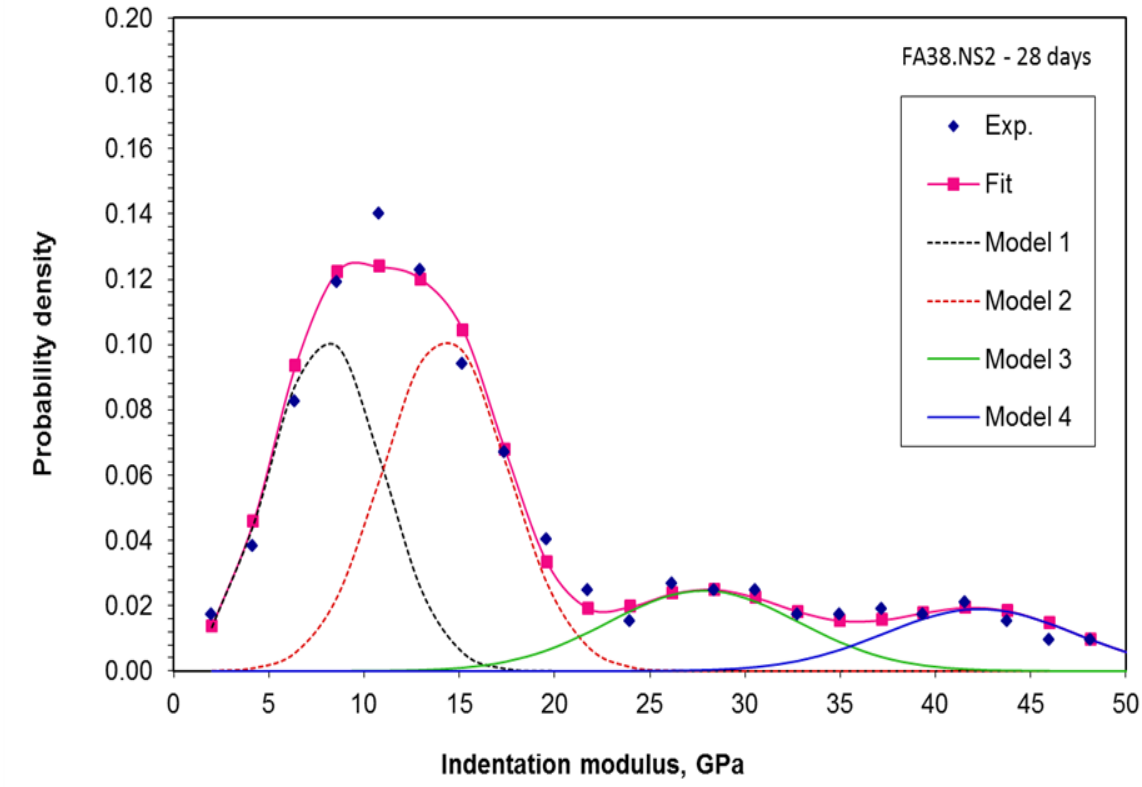

(a)

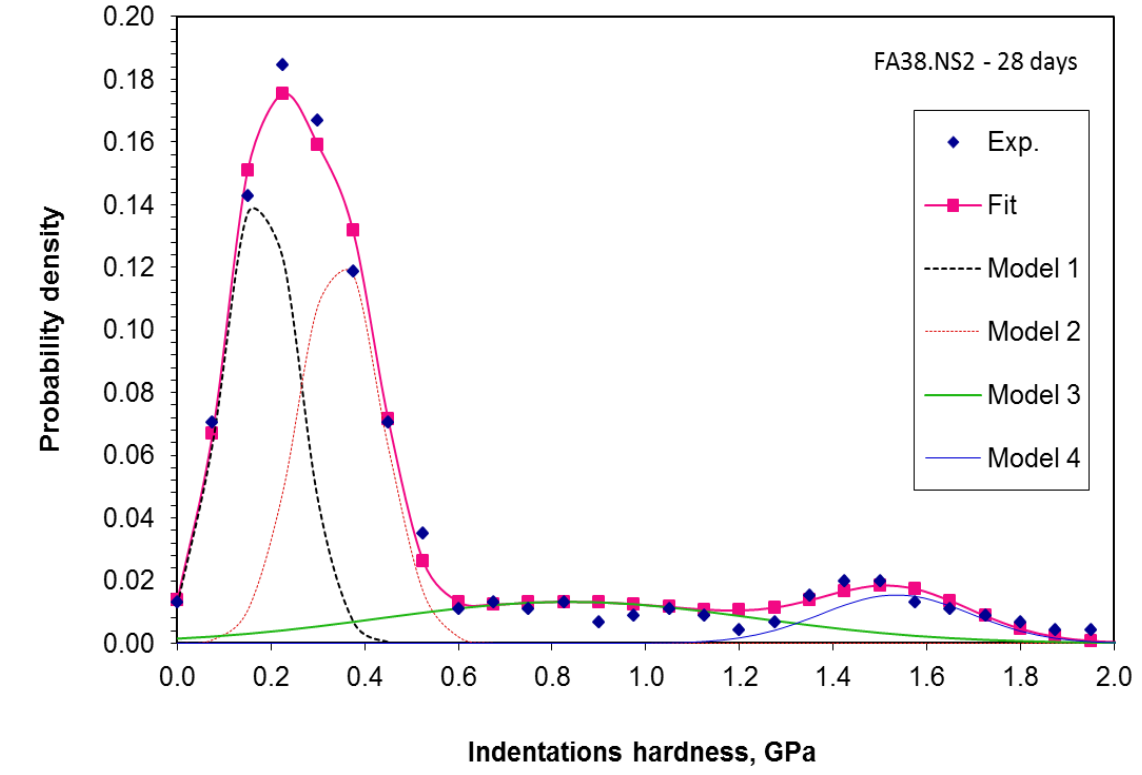

(b)

Figure 4.57 Modulus and hardness of FA38.NS2 paste after 28 days of curing

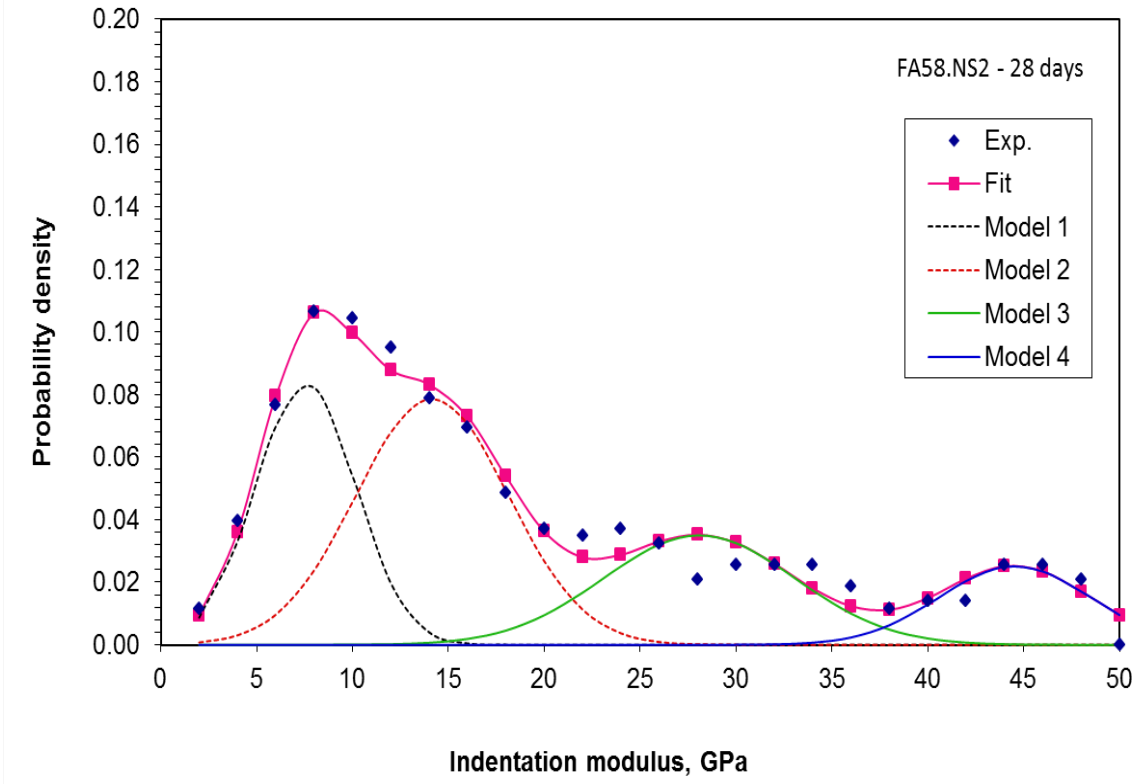

(a)

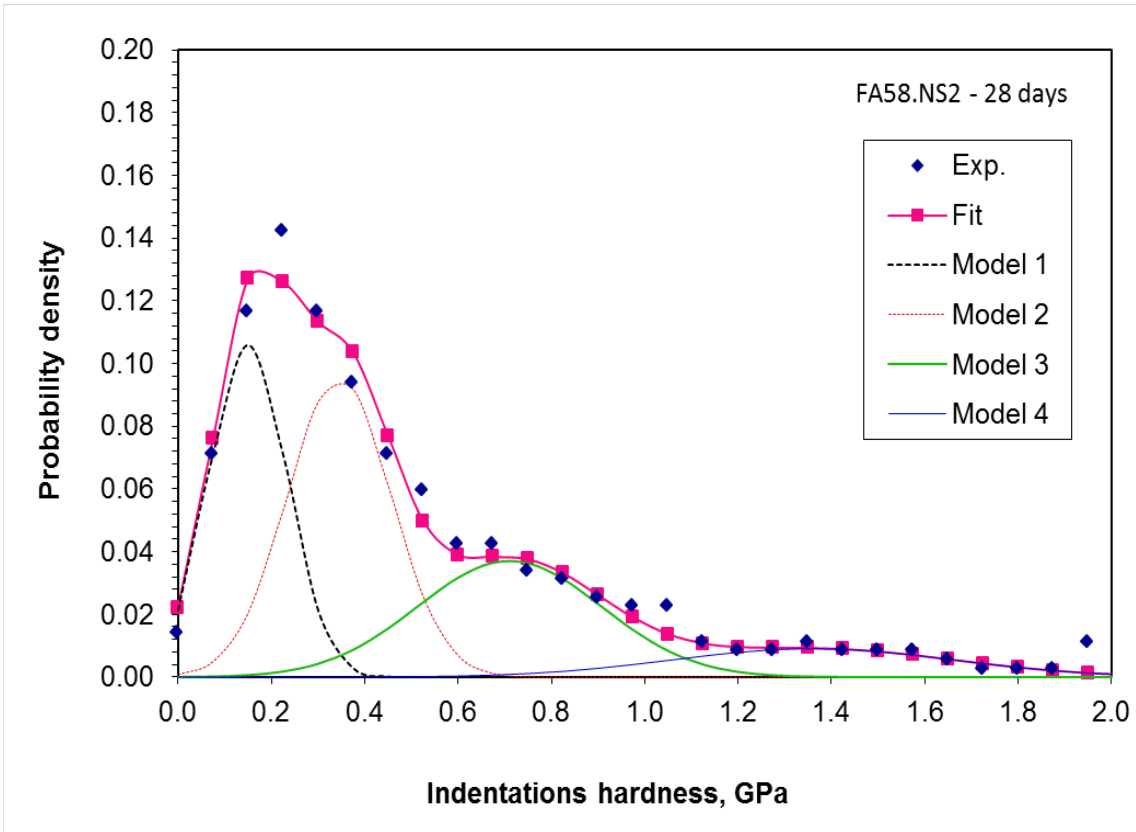

(b)

Figure 4.58 Modulus and hardness of FA58.NS2 paste after 28 days of curing

4.7.2 Nano indentation results of HVFA pastes containing 1% nano-$CaCO_3$

The probability distribution of indentation modulus and hardness of HVFA paste samples are compared with HVFA paste containing 1% nano calcium carbonate (compare Figures 4.55 and 4.56 with Figures 4.59 and 4.60). It is observed that the peak of the distribution of the nano indentation modulus of loose-packed CSH (porous phase) in HVFA pastes is lower than in HVFA pastes containing 1% nano-$CaCO_3$. The peaks of the probability plot of the elastic modulus which corresponds to the low and high stiffness CSH gel for FA39.NC1 and FA59.NC1 were found to be in the range of 10-30 GPa and 20-35 GPa, respectively.

The results of the specific mechanical properties of each hydrate phases of tested HVFA pastes with and without nano calcium carbonate after 28 days of curing are summarised in Table 4.7.

Table 4.7 Elastic modulus and hardness of HVFA pastes containing 1% nano calcium carbonate after 28 days of water curing

Mixes	FA40		FA60		FA39.NC1		FA59.NC1	
	Elastic Modulus	Hardness	Elastic Modulus	Hardness	Elastic Modulus	Hardness	Elastic Modulus	Hardness
Loose-packed C-S-H								
Elastic Modulus (GPa)	10.03	0.24	11.02	0.22	14.34	0.38	8.19	0.15
Volume fraction (%)	55.90	52.90	32.70	35.70	28.20	25.20	34.6	37.60
Outer (LD) C-S-H								
Elastic Modulus (GPa)	21.04	0.50	20.00	0.54	20.82	0.66	19.20	0.50
Volume fraction (%)	15.80	18.80	37.50	34.50	35.40	38.40	27.30	30.30
Inner (HD) C-S-H								
Elastic Modulus (GPa)	30.11	0.88	30.31	0.59	28.00	1.10	19.50	0.94
Volume fraction (%)	14.90	17.90	13.80	16.80	19.40	22.40	30.24	16.50
CH								
Elastic Modulus (GPa)	39.78	1.30	44.75	1.37	41.11	1.71	18.50	1.54
Volume fraction (%)	13.40	10.40	16.00	13.00	17.00	14.00	45.00	15.50

Based on the results presented in Table 4.7, it can be seen that the elastic modulus and hardness probabilities of high density CSH for FA39.NC1 and FA59.NC1 increased from 14.90% to 19.40% and from 13.80% to 30.24 %, respectively, while there is no improvement in the elastic modulus and hardness of low density CSH. However, the nanoindentation results showed evidence of pozzolanic reaction in the sample with nano calcium carbonate where the addition of 1% nano-$CaCO_3$ increased the volume fraction of high-stiffness CSH resulting in a stronger material. Additionally, it is observed that the probability of elastic modulus of porous phase (<10 GPa) is reduced in the HVFA paste samples with 1% nano-$CaCO_3$. These results suggest that the addition of nano calcium carbonate can strongly modify the HVFA pastes matrix by filling the gaps between CSH gel and decreasing the porosity.

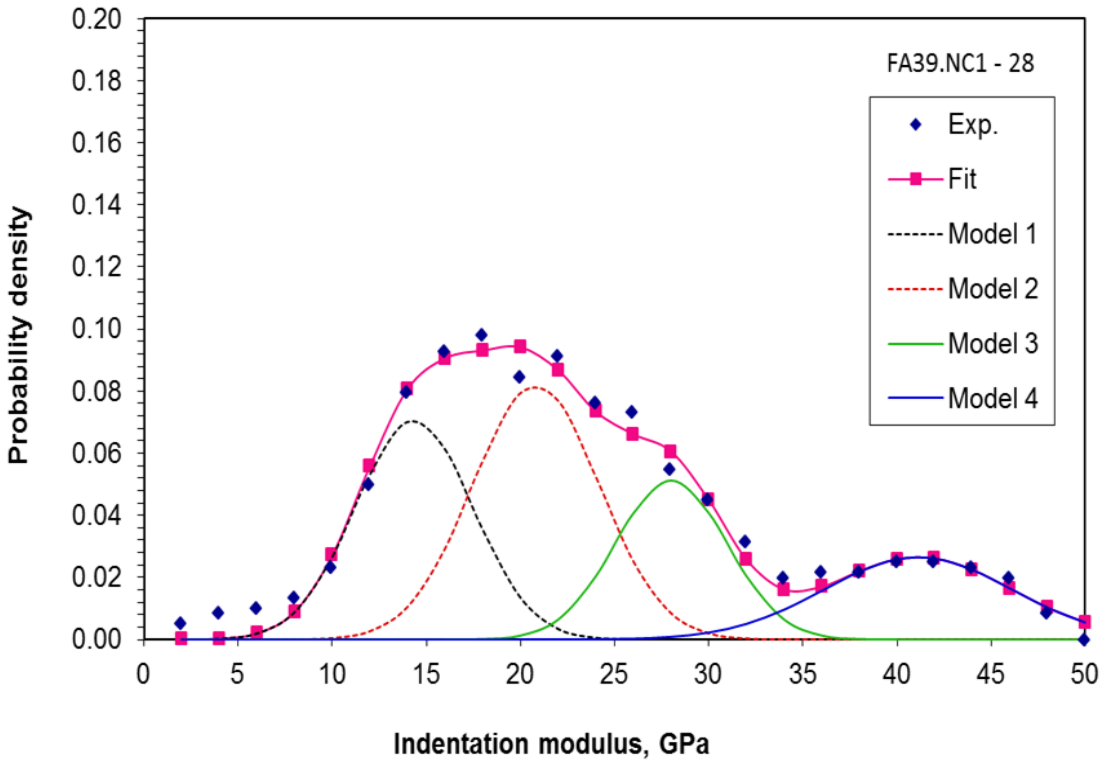

(a)

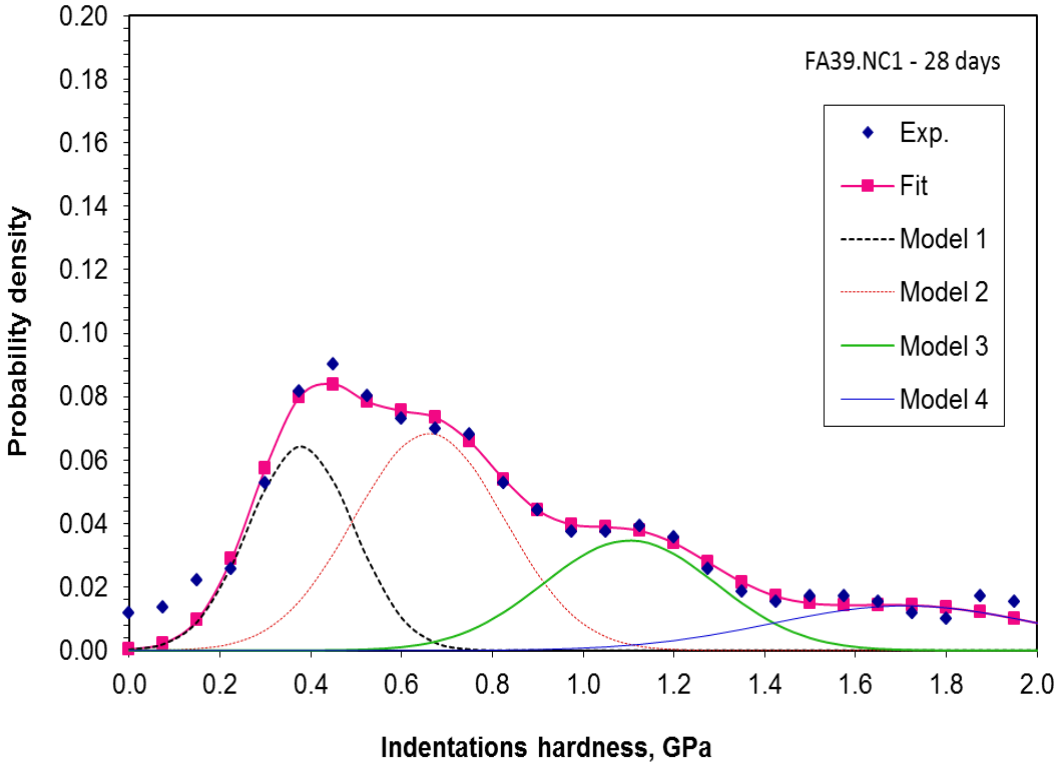

(b)

Figure 4.59 Modulus and hardness of FA39.NC1 paste after 28 days of curing

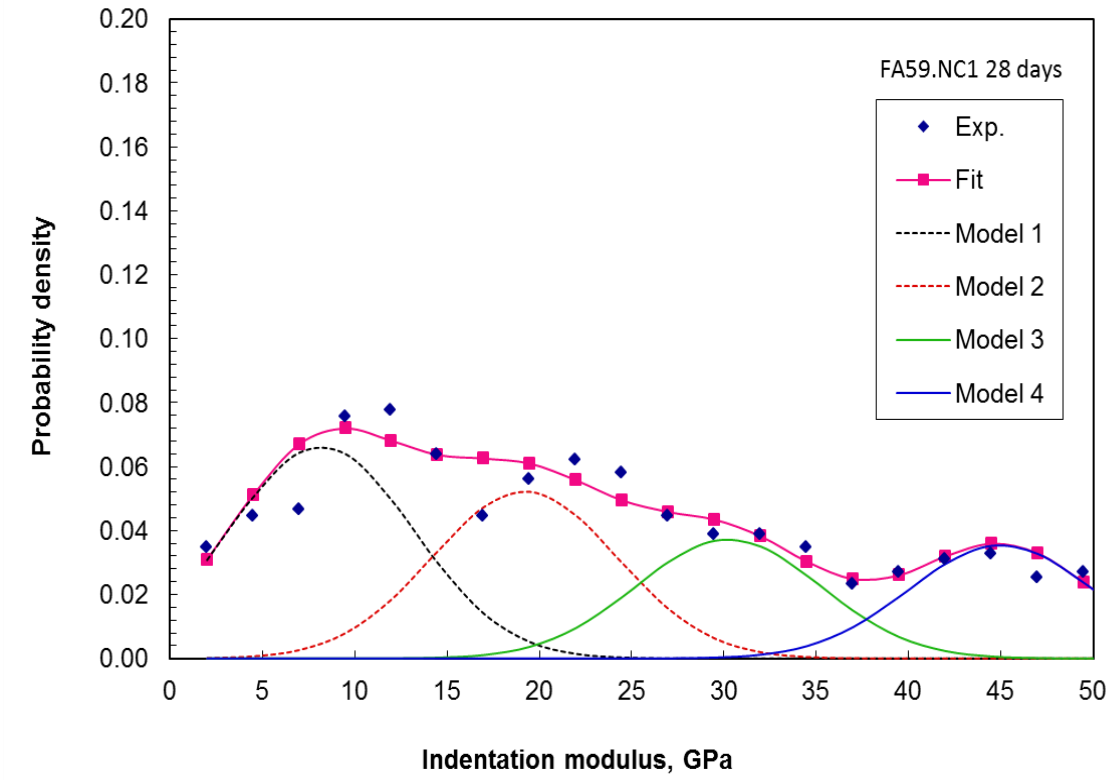

(a)

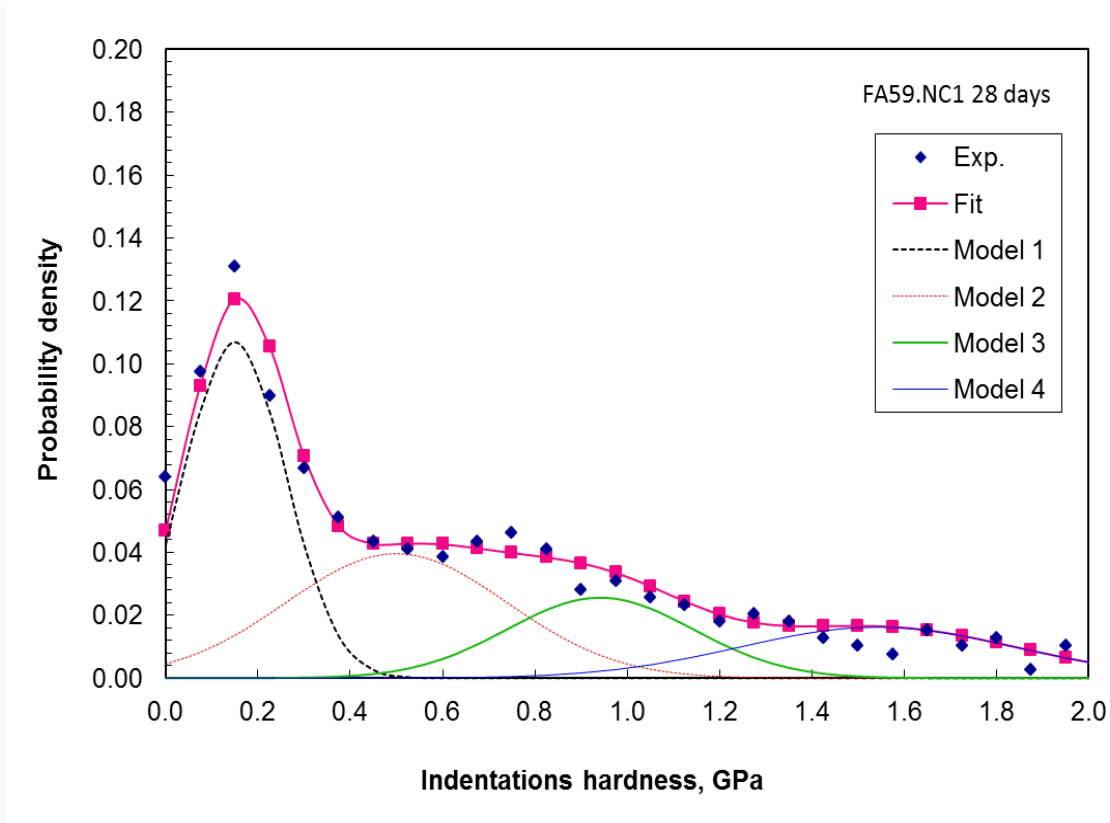

(b)

Figure 4.60 Modulus and hardness of FA59.NC1 paste after 28 days of curing

4.8 Effect of ultrasonic mixing on dispersion of amorphous nano silica

The results on the effect of different mixing times in ultrasonic mixer on the dispersion of nano silica are presented in this section. Figure 4.61 shows the relative strengths of mortars containing 2, 4 and 6% NS, where both mechanical and ultrasonication are used. The effects of three different mixing times of. 30, 60 and 120 minutes represented as U-30, U60, and U120 in Figure 4.61, are also evaluated for above three NS contents. The relative strength presented in Figure 4.61 can be defined as the ratio of compressive strength of mechanically mixed to that of ultrasonically mixed mortar. Based on the results it is found that the 'ultrasonic mixing' method does not demonstrate noteworthy improvement of nano silica particles dispersion used in this study. It can be seen in Figure 4.61 that the compressive strength of mortars after being sonicated are reduced by approximately 10% compared to the compressive strength of mortars prepared under mechanical dry mixing. In addition, when the effect of mixing time is considered, no common trend could be seen due to increase in mixing time. Nevertheless, it could be recognized that one hour sonication recorded higher strength than other mixing times.

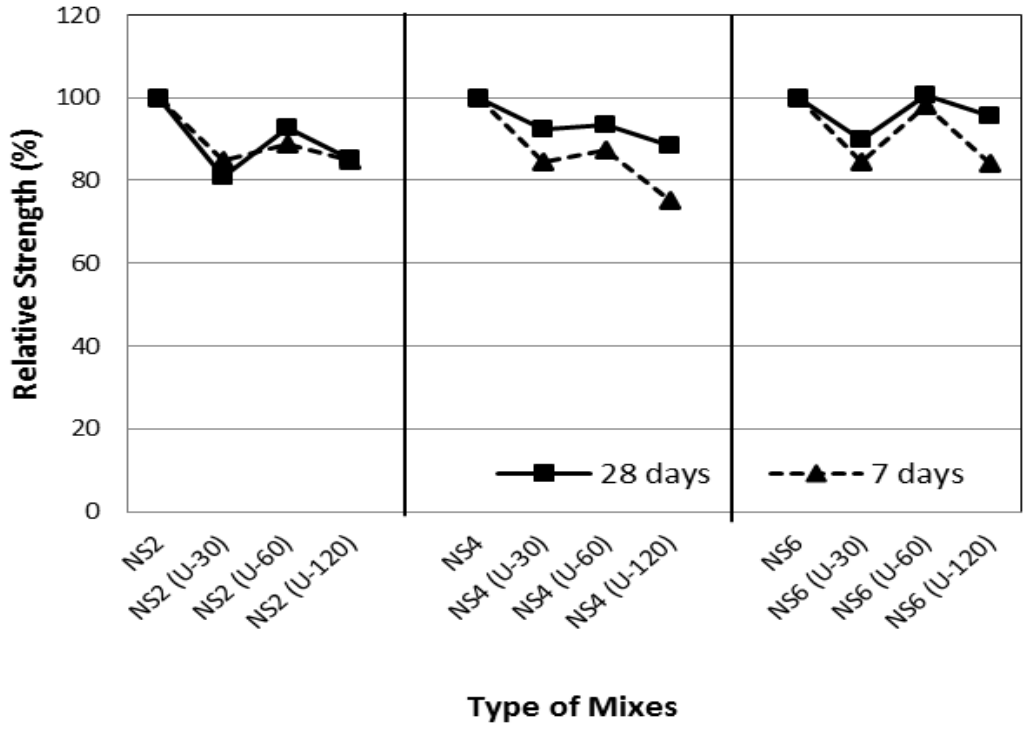

Figure 4.61 Effect of ultrasonic mixing of NS and its time on the strength development of mortars containing different NS contents

4.9 Summary

Improvement of mechanical and durability properties of OPC and HVFA concretes containing nano particles have been confirmed through the overall results presented in this chapter. Compared to the OPC concrete, the compressive strength of concretes containing nano particles is found higher and enhanced the early and later age compressive strength of concretes. From the compressive strength point of view, the optimal replacement percentage of nano silica and nano calcium carbonate is 2% and 1%, respectively. However, there is no significant difference in the compressive strength development of OPC concretes containing 2% NS and 1% NC. In HVFA concretes, the effectiveness of the nano particles in increase in the compressive strength of HVFA concretes is more pronounced in concrete containing 40% replacement of cement. The improvement at early age compressive strength due to addition of 2% NS containing 38% fly ash is about 23% and no improvement is observed in 58% fly ash concrete. On the other hand, the addition of 1% nano-$CaCO_3$ increased the early compressive strength of HVFA concretes containing 39% and 59% fly ash by about 53% and 15%, respectively.

Considering the durability properties, the addition of 2% NS reduced the sorptivity of HVFA concrete (FA40) by about 38 and 47% at 28 and 90 days, respectively than the FA40 concrete while the water sorptivity of FA40 concrete containing 1% $CaCO_3$ nanoparticles was reduced by 4 and 8%, respectively. The volume of permeable voids of HVFA concrete containing 38% fly ash and 2% silica nanoparticles is decreased up to 8% at 28 days compared to FA40 concrete. On the other hand, the addition of 1% $CaCO_3$ nanoparticles in HVFA concrete containing 39% fly ash reduced the VPV significantly by about 30% compared to the FA40 concrete.

The addition of 2% NS also showed significant reduction in chloride ion penetration in HVFA concretes by about 28–38% in concrete containing 40% fly ash and to a lesser extent of 8–20% in concrete containing 60% fly ash. The benefits of adding $CaCO_3$ nanoparticles were also observed in HVFA concretes, where about 18% and 11% reductions in chloride ion penetration of HVFA concretes containing 40% and 60% fly ash, respectively were noticed due to addition of 1% nano-$CaCO_3$ after 28 days of curing. In addition, the chloride diffusion coefficient of the high volume fly ash concretes subjected to 2% nano silica additions (FA38.NS2 and FA58.NS2) were

about 21% and 14% lower than the chloride diffusion coefficient of FA40 and FA60 concretes at 60 days exposure whilst that of the high volume fly ash concretes containing 1% $CaCO_3$ nanoparticles were about 11% and 3% lower than FA40 and FA60 concretes, respectively.

According to the mass loss measurement of rebars, the steel loss of HVFA concrete specimens containing 2% nano silica and 1% NC is found lower where the specimen FA38.NS2 and FA58.NS2 reach 6.04% and 10.99% steel loss whilst in the case of FA39.NC1 and FA59.NC1 concrete samples the weight loss reach 6.63% and 10.53%, respectively. It indicates that the presence of nano particles lowered the corrosion of rebar and deterioration of HVFA concretes.

The indentation modulus frequency distribution results show initial relative percentage of LD-CSH and HD-CSH of HVFA pastes containing 2% NS are 39% and 14.40% (FA38.NS2 paste) and 38.90% and 21.80% (FA58.NS2 paste), respectively. The results are higher than the relative volume fractions of LD-CSH and HD-CSH of ordinary HVFA pastes which are about 15.80% and 14.90% (FA40 paste) and 37.50% and 13.80% (FA60 paste), respectively. On the other hand, the elastic modulus and hardness probabilities of high density CSH for FA39.NC1 and FA59.NC1 increased from 14.90% to 19.40% and 13.80% to 30.24%, respectively, while there is no improvement was observed on the elastic modulus and hardness of low density CSH. These results also confirm the results obtained from XRD and TGA analysis as described in the previous sections of this chapter

According to durability properties results, the use of nano silica and nano-$CaCO_3$ reduced considerably the water sorptivity, VPV, chloride permeability, porosity, chloride diffusion and chloride induced corrosion of HVFA concrete and these values are even lower than ordinary concrete. However, mixed improvements are observed. In this case, the addition of 2% NS is found to be more slightly effective than the 1% NC in accelerating the process of hydration reaction, reducing the pore refinement and improving the microstructures and nano-structures which is directly caused by extremely higher specific surface area and small particle size of the nano silica. The results also show that the blending of nano particles with fly ash in improving the durability properties is more effective in HVFA concrete containing 40% fly ash than that containing 60% fly ash.

CHAPTER 5

CONCLUSIONS AND RECCOMENDATIONS

5.1 Review of the work

This study was conducted to evaluate the effect of nano silica and nano-$CaCO_3$ as partial replacement of cement on the enhancement of early age compressive strength, chloride induced corrosion resistance and related durability properties of HVFA concretes. The first part of this study determined the optimum nano silica and nano-$CaCO_3$ contents based on compressive strength development of ordinary Portland cement (OPC) mortar. The optimum content that exhibited the highest compressive strength in OPC mortar was used in the second part of this study to evaluate the compressive strength development of HVFA concretes containing 40% and 60% Class F fly ash as partial replacement of cement at 3, 7, 28, 56 and 90 days. The durability properties of concrete including chloride permeability, volume of permeable voids, water sorptivity, porosity, chloride diffusivity and chloride induced corrosion of above HVFA concretes containing optimum nano silica and nano-$CaCO_3$ are also evaluated in this part. In the third part, the micro- and nano-structure and the changes in hydration phases of HVFA pastes due to incorporation of nano silica and nano-$CaCO_3$ were investigated through backscattered electron (BSE) microscopy, x-ray diffraction (XRD), thermogravimetric analysis (DTA/TGA) and nano-indentation techniques.

5.2 Summary of findings

The following findings can be summarised on the effect of nano silica and nano $CaCO_3$ on HVFA concretes.

5.2.1 Effect of nano silica addition on mortar and concrete properties

1. The 2% nano silica is found to be the optimum content that exhibited the highest compressive strength among all nano silica contents, where 16% and 14% improvement are noticed at 7 and 28 days, respectively. The addition of 2% NS in high volume fly ash mortars containing 40% and 50% fly ash increased the 7 days compressive strength by 5% and 7%, respectively. However, no improvement is observed when fly ash contents are increased to 60% and 70%.

2. The addition of 2% NS increased the early age compressive strength (i.e. 3 days) of HVFA concrete containing 60% fly ash by about 95%. However, no such improvement is noticed at other ages. In the case of HVFA concrete containing 40% fly ash, the improvement at 3 days compressive strength due to addition of 2% NS is about 24% and also maintained between 15% and 21% improvement in longer term.
3. The addition of 2% NS reduced the sorptivity, porosity and chloride ion penetration of ordinary concrete. In HVFA concretes containing 40% and 60% fly ash the reduction of above durability properties is also significant particularly in longer curing period.
4. The chloride diffusion of NS2 concrete decreased by 26% compared to OPC concrete at 60 days exposure. On the other hand, the chloride diffusion coefficient of the high volume fly ash concretes containing 2% nano silica additions (FA38.NS2 and FA58.NS2) were about 21% and 14% lower than FA40 and FA60 concretes, respectively. The findings support the results on accelerated corrosion test where the steel loss of HVFA concrete specimens containing 2% nano silica is 40% and 11% lower than concretes containing 40% and 60% fly ash, respectively.
5. The mercury porosimetry analysis, XRD analysis, BSE and TGA/DTA results also support this observation where the addition of 2% NS has a significant influence in decreasing the total capillary pores and pores diameter of HVFA pastes. Due to extremely large surface area and small particle size, the NS reacts more quickly with CH in the hydration reaction than the fly ash and produced secondary CSH gel and reduced the capillary pores in the matrix. However, the reactivity of NS is higher in HVFA system containing 38% fly ash than that containing 58% fly ash.
6. The indentation modulus frequency distribution of HVFA pastes containing 2% nano silica is comparatively higher than the relative volume fractions of LD-CSH and HD-CSH of ordinary HVFA pastes. The results indicate that the incorporation of nano silica in high volume fly ash increased the amount of low and high density CSH in HVFA pastes and confirm the ability of nano silica in reducing the porosity of HVFA pastes.
7. The use of mechanical dry mixing of nano silica with cement, fly ash and sand performed better than ultrasonic mixing of NS with water and superplasticizer.

5.2.2 Effect of nano calcium carbonate addition on mortar and concrete properties

1. The 1% nano- $CaCO_3$ is the optimum content that exhibited the highest compressive strength at 7 and 28 days among all nano calcium carbonate contents. Concrete containing 1% nano-$CaCO_3$ as partial replacement of cement exhibited about 140% improvement of early age compressive strength (e.g. at 3 and 7 days) compared to control concrete. At 28 days, the improvement was 62%. In the case of mortars, the improvement at 7 and 28 days compressive strength was only 22% and 18%, respectively.
2. The addition of 1% nano-$CaCO_3$ increased the compressive strength at early ages (e.g. at 3 and 7 days) of HVFA concrete containing 39% fly ash by about 44-46%. At 28 days, the improvement was about 53%. The addition of 1% nano-$CaCO_3$ also improved the long term (90 days) compressive strength of ordinary concrete and that of HVFA concrete containing 39% and 59% fly ash, respectively.
3. The use of 1% $CaCO_3$ nanoparticles in HVFA concrete was found to be significantly effective in reducing the water sorptivity, volume of permeable voids, porosity and chloride ion permeability of ordinary and HVFA concretes. This is an indication that the 1% $CaCO_3$ nanoparticles addition in HVFA system forms a finer pore structure than HVFA paste alone.
4. The chloride diffusion coefficient of cement concrete is reduced by about 73% due to addition of 1% nano-$CaCO_3$. The chloride diffusion coefficient of the high volume fly ash concretes containing 1% $CaCO_3$ nanoparticles were about 60% and 32% lower than FA40 and FA60 concretes, respectively. It indicates that $CaCO_3$ nanoparticles due to its reactivity and filler effect are very effective in reducing the pore space and its connectivity inside the concrete and therefore the penetration of chloride ions. The accelerated corrosion results support the above findings where the mass loss of the rebar in concretes containing 1% nano-$CaCO_3$ is lower than the mass loss of the rebars in cement concrete. The better corrosion resistance of HVFA concretes containing 1% NC is also found in FA39.NC1 and FA59.NC1 concretes where the steel loss reached 6.63% and 10.53%, respectively
5. The backscattered image analysis, XRD, DTA/TGA results further confirmed that the 1% $CaCO_3$ nanoparticles improved the microstructure of HVFA

concretes and thus affected the concrete performance including mechanical and durability properties.

6. The elastic modulus and hardness probabilities of high density CSH of FA39.NC1 and FA59.NC1 pastes increased from 14.90% to 19.40% and from 13.80% to 30.24%, respectively, while there is no improvement in the elastic modulus and hardness of low density CSH. However, the nano-indentation results showed evidence of pozzolanic reaction in the sample with nano calcium carbonate where the addition of 1% nano-$CaCO_3$ increased the volume fraction of high-stiffness CSH resulting in a stronger material.

5.3 Summary of main achievements

Nano silica due to its high surface area reacts with calcium hydroxide to form additional calcium silicate hydrate within the hydration system. On the other hand, nano-$CaCO_3$ has beneficial characteristics in producing higher density of microstructure due to its filler effect. Based on this study, the use of nano particles i.e. nano silica and nano-$CaCO_3$ in ordinary cement concrete and HVFA concretes are effective in increasing the compressive strength at early and later ages. It contributes to the early pozzolanic reaction due to its extremely small particle size and higher surface area than those of Class F fly ash. Additionally, the fly ash with high silicate and aluminate content reacted with nano particles to produce additional hydration products in the system.

According to the chloride induced corrosion resistance results of HVFA concretes and related durability properties affecting chloride induced corrosion, the addition of nanoparticles is found effective in reducing the pore space and its connectivity inside the concrete and therefore lowered the corrosion current and reduced the corrosion of steel in HVFA concretes. In addition, the microstructure and phase identification analysis also confirm that the incorporation of nano particles reduced the calcium hydroxide content and decreased the total capillary porosities and pores diameter which can prevent the harmful chloride ions transport leading to corrosion of rebar and deterioration to the ordinary and HVFA concretes. It is also observed that the early age compressive strength and measured durability properties of HVFA concretes containing 40% fly ash are improved than ordinary concrete due to NS and NC addition.

Finally, the results of this research confirm the potential use of nano particles in the structural application of HVFA concretes particularly in the marine environment. The optimization of the use of HVFA can produce excellent environmental benefits due to reduction of CO_2 associated with ordinary Portland cement production.

5.4 Recommendations for further studies

From the results and conclusions drawn from the analysis, some recommendations for further works are included as follows:

1. The compressive strength results that have been found in this study should be validated by a wider testing scope such as tensile and flexural strength tests.
2. The experimental work done on durability properties of concrete focused on the water sorptivity, porosity, chloride diffusion, chloride permeability and chloride induced corrosion of high volume fly ash concretes containing nano silica and nano calcium carbonate. However, the other durability properties tests such as alkali silica reaction (ASR), sulphate resistance and carbonation are needed to validate the findings on this study based on experimental evidence. The long term testing should be further examined and validated.
3. It is necessary to carry out an experimental study on the effect of colloidal nano particles in the production of high performance concrete containing high volume fly ash. A comparison between the use of colloidal nano particles and powder nano particles in high volume fly ash mortar or concrete can provide a reliable outcome on understanding the behavior of nano particles in mortar or concrete application.
4. Regarding to the use of ultrasonic processor to aid the dispersion of nano particles, it is essential to perform the mechanical mixing using ultrasonic processor at a higher speed of amplitude. On the other hand, the method of dispersing by using surfactants is necessary to be investigated especially in the case of agglomerated nano silica particles. Moreover, continued research is still needed to verify the advantages of using dry mixing compared to sonication methods.
5. Nano indentation analysis provides an effective method of determining the individual phase properties. However, it would be necessary to achieve the standard polishing techniques that provide sufficient surface in order to minimize the error on the evaluation of nano indentation tests.

6. From the outcome the experimental results and the analysis, the challenge for further research on the use of nano materials for building construction and its compatibility in environmental issues and cost are still necessary.

REFERENCES

- ACI Committee 226.4R, (2003) “Guide for selecting proportions for high-strength concrete with Portland cement and fly ash”, *American Concrete Institute,* Detroit, USA.
- ACI Committee 318, (2003) “Building code requirements for structural concrete”, *American Concrete Institute,* Detroit, USA.
- Acker, P., (2001) Micromechanical analysis of creep and shrinkage mechanisms”. In: Ulm, F.J, Bazant, Z.P, Wittmann, F.H, editors. *Creep, shrinkage and duability mechanics of concrete and other quasi-brittle materials*, Cambridge, M.A. oxford, UK: Elsevier.
- Aggarwal, V., Gupta, S. M., and Sachdeva, S. N., (2010) “Concrete durability through high volume fly ash concrete (HVFC) - A literature review”, *International Journal of Engineering Science and Technology*, Vol. 2(9), pp.4473-4477.
- Aitcin, P.C., (1998) *High performance concrete*. E & FN Spon. London and New York, ISBN: 0-203-78327-1.
- Aligizaki, K.K, (2006) Pore structure of cement-based materials – Testing, interpretation and requirements. Taylor and Francis, ISBN: 0-419-22800-4.
- Alizadeh, R., (2009) Nanostructure and engineering properties of basic and modified Calcium-Silicate-Hydrate systems, Phd Thesis, Department of Civil Engineering, University of Ottawa, Canada.
- Ammar, M.M.A.H., (2012) The effect of nano silica on the performance of Portland cement mortar. Master Thesis. The School of Sciences and Engineering. The American University in Cairo.
- Arefi, M.R, Javaheri, R, Mollahmadi, E, Zare, H, Abdollahi, N, and Eskandari, M., (2011) “Silica nanoparticle size effect on mechanical properties and microstructure of cement mortar” *Journal of American Science,* Vol. 7(10).
- ASTM D 3963, (2012) “Standard specification for fabrication and jobsite handling of epoxy-coated steel reinforcing bars”, *American Society for Testing and Materials*, Pennsylvania, USA.

- ASTM C 618, (2012) “Standard Specification for Coal Fly Ash and Raw or Calcined natural Pozzolan for Use in Concrete”, *American Society for Testing and Materials*, Pennsylvania, USA.
- ASTM C 109, (2012) “Standard test method for compressive strength of hydraulic cement mortars (using 50-mm cube specimens)”, *American Society for Testing and Materials*, Pennsylvania, USA.
- ASTM C 1202, (2012) “Standard test method for electrical indication of concrete’s ability to resist chloride ion penetration”, *American Society for Testing and Materials*, Pennsylvania, USA.
- ASTM C 127, (2012) “Standard test method for density, relative density (specific gravity) and absorption of coarse aggregate”, *American Society for Testing and Materials*, Pennsylvania, USA.
- ASTM C 128, (2012) “Standard test method for density, relative density (specific gravity) and absorption of fine aggregate” *American Society for Testing and Materials*, Pennsylvania, USA.
- ASTM C 143, (2012) “Standard test method for slump of hydraulic-cement concrete”, *American Society for Testing and Materials,* Pennsylvania, USA.
- ASTM C 1437, (2012) “Standard test method for flow of hydraulic cement mortar” *American Society for Testing and Materials*, Pennsylvania, USA.
- ASTM C 1556, (2012) “Standard test method for determining the apparent chloride diffusion coefficient of cementitious mixtures by bulk diffusion”, *American Society for Testing and Materials*, Pennsylvania, USA.
- ASTM C 1585, (2012) “Standard test method for measurement of rate of absorption of water by hydraulic-cement concretes”, *American Society for Testing and Materials*, Pennsylvania, USA.
- ASTM C 39, (2012) “Standard test method for compressive strength of cylindrical concrete specimens”, *American Society for Testing and Materials,* Pennsylvania, USA.
- ASTM C 642, (2012) “Standard test method for density, absorption, and voids in hardened concrete”, *American Society for Testing and Materials,* Pennsylvania, USA.

- ASTM C 873, (2012) “Standard Test Method for Compressive Strength of concrete cylinders cast in place in cylindrical moulds”, *American Society for Testing and Materials*, Pennsylvania, USA.
- ASTM G1, (2012) “Standard practice for preparing, cleaning, and evaluation corrosion test specimens”, *American Society for Testing and Materials,* Pennsylvania, USA.
- Babou-Kammoe, R, Hamoudi, S, Larachi, F, and Belkacemi, K., (2012) “Synthesis of $CaCO_3$ nanoparticles by controlled precipitation of saturated carbonate and calcium nitrate aqueous solutions”. *The Canadian Journal of Chemical Engineering,* Vol. 90, pp. 26-33, 2012.
- Bahadori, H, and Hosseini, P., (2013) “Reduction of cement consumption by the aid of silica nano particles (investigation on concrete properties)”. *Journal of Civil Engineering and Management,* Vol, 18(3), pp. 416-425.
- Balakrishnan, B, Awal, A.S.M., (2014) “Durability properties of concrete containing high volume Malaysian fly ash”. *International Journal of Research in Engineering and Technology,* Vol. 03, Issue: 04.
- Barbhuiya, S.A., Gbagbo, J.K., and Russel, M.I., (2009) “Properties of fly ash concrete modified with hydrated lime and silica fume”. *Construction and building materials,* DOI:10.1016/j.conbuildmat.2009.06.001.
- Bazzar, K, Bouatiaoui, M.R, and Alaoui, A.H., (2013) “Performance approach the durability of high volume fly ash concrete”. *International Journal of Engineering Science and Innovative Technology,* Vol.2, ISSN: 2319-5967.
- Behfarnia, K, and Salemi, N., (2013) “The effects of nano silica and nano alumina on frost resistance of normal concrete”. *Construction and Building Materials,* Vol. 48, pp. 580-584.
- Belkowitz, J.S., and Armentrout, D., (2010) “An investigation of nano silica in the cement hydration process”. *2010 Concrete Sustainability Conference,* National Ready Mixed Concrete Association.
- Bendapudi, S.C.K., (2011) “Contribution of fly ash to the properties of mortar and concrete”. *International Journal of earth Sciences and Engineering*, Vol. 04, No 06 SPL, pp 1017-1023.

- Benhalal, E, Zahedi, G, Shamsaei, E., and Bahodori, A., (2012) "Global strategies and potentials to curb CO_2 emissions in cement industry", *Journal of Cleaner Production*,DOI: http://dx.doi.org/10/1016/j.jclepro.2012.10.049.
- Bjornstrom, J, Martinelli, A, Matic, A, Borjesson, L, Panas, I., (2004) "Accelerating effects of colloidal nano-silica for beneficial calcium–silicate–hydrate formation in cement". *Chemical Physics Letters*, 392:242-248.
- Bola, M.M.B, and Newston, C.M., (2000) "Field evaluation of corrosion in reinforced concrete structures in marine environment". *Research Report UHM/CE/00-01*, University of Hawaii, June 200.
- Brandt, M,A., (1995). "Cement-based composites-Materials, mechanical properties and performance". Second edition. Taylor and Francis Group. ISBN: 0-203-88903-7.
- Broomfield, J.P., (1997) "*Corrosion of Steel in Concrete – Understanding, Investigation and Repair"*, E & FN SPON, London and New York. ISBN: -203-78352-2.
- Burden, D., (2003) "The durability of concrete containing high levels of fly ash". Master Thesis. The University of New Brunswick, January 2006.
- Caldarone, M.A., (2009) "High-strength concrete – A practical guide". Taylor and Francis Group, London and New York, ISBN: 0-203-96249-4.
- Camiletti, J., Soliman, A.M. and Nehdi, M.L., (2013) "Effects of nano- and micro-limestone addition on early-age properties of ultra-high-performance concrete", *Materials and Structures,* Vol. 46, pp. 881-898.
- Carette, G., and Malhotra, V.M., (1983) "Early age strength development of concrete incorporating fly ash and condensed silica fume". *ACI SP79-41*, Vol. 79, pp. 765-784.
- Carmichael, J, and Arulraj, P., (2012) "Influence of nano materials on consistency, setting time and compressive strength of cement mortar". *Engineering Science and Technology: An International Journal,* ISSN: 2250-3498, Vol. 2, No.1.
- Chalee, W., Jaturapitakkul, C., and Chindaprasirt, P., (2009) "Predicting the chloride penetration of fly ash concrete in seawater". *Marine structures,* Vol.22, 341-353.

- Chen, S, and Mahadevan, S., (2008) "Chloride-induced reinforcement corrosion and concrete cracking simulation". *Cement and Concrete Composites*, Vol. 30, pp. 227-238.
- Constantinides, G and Ulm, F.-J., (2004) "The nanogranular nature of C-S-H. *Journal of the Physics of Solids"*, Vol. 55, pp. 64-90.
- Constantinides, G, Ulm, F.-J, and Vliet, K.V., (2003) "On the use of nanoindentation for cementitious materials". *Materials and Structures*, Vol. 36, pp. 191-196.
- Cook, R, A, and Hover, K, C., (1999) "Mercury porosimetry of hardened cement pastes". *Cement and Concrete Research*, Vol. 29, pp. 933 – 943.
- De Weerdt, K., Kjellsen, K.O., Sellevoid, E.J. and Justnes, J., (2011) "Synergy between fly ash and lime stone powder in ternary cements". *Cement and Concrete Research*, 41, 279-291.
- Dejong, M., (2005) "Sources of high temperature degradation of cement-based materials: nanoindentation and microporoelastic analysis". Master Thesis. Massachusetts Institute of Technology.
- Detwiller, R.J, Powers, L.J, Jakobsen, U.H, Ahmed, W.U, Scrivener, K.L, and Kjellsen, K.O., (2001) "Preparing specimens for microscopy". *Concrete International*, Vol. 23 (11), American Concrete Institute.
- Elena, J, and Manea, D.L., (2012) "Application of X ray diffraction (XRD) and scanning electron microscopy (SEM) methods to the Portland cement hydration processes". *Journal of Applied Engineering Sciences*, Vol. 2(15), pp. 35-42.
- Elkady, H., and Serag, M.I., (2013) "Effect of nano silica de-agglomeration and methods of adding superplasticizer on the compressive strength and workability of nano silica concrete". *Civil and Environmental Research*, Vol. 3, No.2, ISSN 2222-1719.
- Feynman, R.P., (1960). "There's plenty of room at the bottom". *Engineering and Science*, February 1960, pp. 22-36.
- Fischer-Cripps and C. Anthony, (2002) "*Nanoindentation"*, Springer-Verlag, new York, Secaucus, NJ USA, 2002.
- Fly Ash Utilisation, 2nd annual international summit, 17-18 January 2013, New Delhi, India, http://flyash2012.missionenergy.org/intro.html.

- Gaitero, J.J, Saez de Ibarra, Y, and Campillo, I., (2006) “Silica nanoparticle addition to control the calcium-leaching in cement-based materials”. *Physica Status Solidi.* No. 6, 1313-1318.
- Georgescu, M., and Saca, N., (2009) “Properties of blended cement with limestone filler and fly ash content”. *Scientific Bulletin,* Vol. 71, ISSN 1454-2331.
- Givi, A.N., Rashid, S.A., Aziz, F.N.A., and Salleh, M, A, M., (2010) “Particle size effect on the permeability properties of nano-SiO_2 blended Portland cement concrete”. *Journal of Composite Materials*, 45(11), 1173-1180.
- Goodwin, P.D, Frantz, G.S, and Stephens, J.E., (2000) “Protection of reinforcement with corrosion inhibitors”, *Report No. JHR 00-279*, University of Connecticut, Storrs, CT.
- Guemmadi, Z, Resheidat, M, Chabil, H, and Toumi, B., (2009) “Modeling the influence of limestone filler on concrete: a novel approach for strength and cost”. *Jordan Journal of Civil Engineering*, Vol. 3, No. 2. Pp. 158-171.
- Guneyisi, E, Gesoglu, M, Karaboga, F, and Mermerdas, K., (2013) “Corrosion behaviour of reinforcing steel embedded in chloride contaminated concretes with and without metakaolin”. *Composites: Part B*, Vol. 45, pp. 1288-1295.
- Guo-qiang, X., and Juan-hong, L., (2010) “Experimental study on carbonation and steel corrosion of high volume fly ash concrete”. Power and Energy Engineering Conference (APPEEC), 2010 Asia-Pacific, ID: 10.1109/APPEEC.2010.5448649.
- Guo-qiang, X., and Juan-hong, L., (2010) “Experimental study on carbonation and steel corrosion of high volume fly ash concrete”, *Power and Energy Engineering Conference (APPEEC),* DOI:10.1109/APPEEC.2010.5448649.
- He, X., and Shi, X., (2008) “Chloride permeability and microstructure of Portland cement mortars incorporating nanomaterials”. *Journal of the Transportation Research Board,* No.2070, pp.13-21.

- Hosseini, P, Boosherian, A, Delkash, M, Ghavami, S, and Zanjani, M.K., (2009) "Use of nano-SiO_2 to improve microstructure and compressive strength of recycled aggregate concretes". *Nanotechnology in Construction,* Vol. 3, pp. 215-221.
- Hou, P, Kawashima, S, Wang, K, Corr, D, Qian, J, Shah, S., (2013) "Effects of colloidal nanosilica on rheological and mechanical properties of fly ash-cement mortar". *Cement and Concrete Composite,* Vol, 35, pp, 12-22.
- Howind, T, Hughes, J, and Zhu, W., (2014). Mapping of mechanical properties of cement-based materials at micro/nano-scale. *Journal of Innovative Engineering,* 2(1):2, ISSN: 2347-7504.
- Iler, R.K., (1955) "The colloid chemistry of silica and silicate". Edit. Itchaca, New York, pp.1-250.
- Islam, M.M, and Islam, S.M., (2010). "Strength behaviour of mortar using fly ash as partial replacement of cement", *Concrete Research Letters,* Vol. 1(3) – September 2010.
- Islam, J., (2011) "Use of nano silica to increase early strength and reduce setting time of concretes with high volumes of slag or fly ash". Master Thesis. Department of Civil Engineering, national University of Singapore.
- Jalal, M., Pouladkhan, A.R., Norouzi, H., and Choubdar, G., (2012) "Chloride penetration, water absorption and electrical resistivity of high performance concrete containing nano silica and silica fume". *Journal of American science,* 8(4):278-284.
- Jayapalan, A.R, Lee, B.Y, and Kurtis, K.E., (2009) "Effect of nano-sized titanium dioxide on early age hydration of Portland cement". *Nanotechnology in Construction,* Vol. 3, pp. 267-273.
- Jha, K, Suksawang, N, Lahiri, D, and Agarwal, A., (2012) "Energy-based analysis of nanoindentation curves for cementitious materials". *ACI Materials Journal,* Title no. 109-M09.
- Jha, K.K, Suksawang, N, Lahiri, D, and Agarwal, A., (2012) Energy-based analysis of nanoindentation curve for cementitious materials. *ACI Materials Journal.* Title no.109-M09.

- Ji, T., (2005) "Preliminary study on the water permeability and microstructure of concrete containing nano-SiO_2". *Cement and Concrete Research,* Vol. 35, pp.1943-1947.
- Jiande, H, Ganghua, P, Wei, S, Caihui, W, and Dong, C., (2012) "Application of nanoindentation to investigate chemomechanical properties change of cement paste in the carbonation reaction". *Science China Technology,* Vol. 55, No. 3.
- Jo, B.W., Kim, C.H. and Lim, J.H. (2007) "Characteristics of cement mortar with nano-silica particles". *ACI Materials Journal*, 104(4), 404-407.
- Jozic, D., Zelic, J., and Janjatovuc, I. (2010) "Influence of the coarse fly ash on the mechanical properties of the cement mortars". *Ceramics,* Vol. 54(2), pp. 144-151
- Kawashima, S., Hou, P., Corr, D.J. and Shah, S.P., (2013) "Modification of cement based materials with nanoparticles", *Cement and Concrete Composites*. 36, 8-15.
- Keattch, C.J., Dollimore, D., (1975). *"Introduction to thermogravimetry"*, Heydon, 45.
- Kepler, J.L, Darwin, D, and Locke, C.E., (2000) "Evaluation of corrosion protection methods for reinforced concrete highway structures", *SM Report No. 58*, University of Kansas, Kansas.
- Khanzadi, M., Tadayon, M, Seoehri, H, and Sepehri, M., (2010) "Influence of nano silica particles on mechanical properties and permeability of concrete". *Second international conference on sustainable construction material and technologies,* June 28 – 30, 2010, Italy.
- Konsta-Gdoutos, M., Metaxa, Z., and Shah, S., (2008) "Nanoimaging of highly dispersed carbon nanotube reinforced cement based materials". *Seventh Intnl. RILEM Symp. on Fibre Reinforced Concrete: Design and Applications.*BEFIB-2008 Symposium, Chennai, India, 17^{th}-19^{th} September 2008.
- Kosmatka, S.H, Kerkhoff, B, and Panarese, W.C., (2003) *"Design and control of concrete mixtures - Fourteenth edition"*. Portland Cement Association.

- Krakowiak, K.J, Thomas, J.K, Musso, S, James, S, Akono, A, and Ulm, F. (2015). Nano-chemo-mechanical signature of conventional oil-well cement systems: Effect of elevated temperature and curing time. *Cement and Concrete Research,* Vol. 67, pp. 103-121.
- Larsen, G., (1961) "Microscopic point measuring: a quantitative petrographic method of determining the Ca(OH)2 content of the cement paste of concrete". *Magazine of Concrete Research*, 13(38), 71-76.
- Lazaro, A, and Brouwers, H.J.H., (2010) "Nano-silica production by a sustainable process; application in building materials". *8th Phd symposium in Kgs. Lyngby,* Denmark, June 20-23, 2010.
- LeChatelier, H., (1905) "Experimental researches on the construction of hydraulic mortars". J.L.Mack, McGraw, Publishing Co, New York.
- Li, G., (2004) "Properties of high volume fly ash concrete incorporating nano-silica". *Cement and concrete research*, 34, 1043-1049.
- Li, H., Xiao, H., Yuan, J., & Ou, J., (2004) "Microstructure of cement mortar with nano-particles". *Composites: Part B, 35,* 185-189.
- Lieftink, D.J., (1997) "The preparation and characterization of silica from acid treatment of olivine", Ph.d Thesis, pp. 175. Utrect University, The Netherlands.
- Lisa, K, Spainhour and Wooton, I., (2008) "Corrosion process and abatement in reinforced concrete wraooed by fiber reinforced polymer", *Cement and Concrete Composites Journal,* Vol. 30, No. 6, pp. 535-543.
- Liu, X., Chen, L., Liu, A., and Wang, X., (2012) "Effect of nano-$CaCO_3$ on properties of cement paste". *Energy Procedia,* Vol.16, pp. 991-996.
- Liu, Y., (1996). *"Modelling the time-to-corrosion cracking of the cover concrete in chloride contaminated reinforced concrete structures"*. Phd Thesis. Faculty of the Virginia Polytechnic Institute and State University.
- Luping, T, Nilsson, L, and Basheer, P.A.M., (2012) "Resistance of concrete to chloride ingress – Testing and Modelling". Spon Press. London and New York, ISBN: 978-0-415-48614-9.
- Ma, Y, Hu, J, and Ye, G., (2013) "The pore structure and permeability of alkali activated fly ash", *Fuel*, Vol. 104, pp. 771-780.

- Malhotra, V.M. and Mehta, P.K., (2002) *"High-performance, high-volume fly ash concrete: materials, mixture proportioning, properties, construction practice, and case histories"*. ISBN: 0-9731507-0-X.
- Malvar, L.J., and Lenke, L.R., (2006) "Efficiency of Fly Ash in mitigating alkali silica reaction based on chemical composition", *ACI Material Journal*, Vol. 103, No.5, September-October 2006, pp. 319-326.
- Martinez-Velandia, D, Paya, J, Monzo, J, Borrachero, M.V., (2011) "Effect of sonication on the reactivity of silica fume in Portland cement mortars". *Advances in Cement Research,* Vol. 23, pp. 23-31.
- Medvescek, S., Gabrovsek, R., Kaucic, V. and Meden, A., (2006) "Hydration products in water suspension of Portland cement containing carbonates of various solubility". *Acta Chimica Slovvenica.*, Vol. 53, pp.172-179.
- Mehta, P.K, and Monteiro, P.J.M., (2006) "Concrete: microstructure, properties, and materials". Third edition - The McGraw-Hill Companies, Inc.
- Mehta, P.K., (1991) *"Concrete in the marine environment"*. Elsevier applied science, London and New York, ISBN: 0-203-49825-9.
- Mehta, P.K., (2004) "High performance, high volume fly ash concrete for sustainable development". *Proceedings of the International Workshop on Sustainable Development and Concrete Technology*, Iowa State University, USA, ISBN 0-9652310-7-0.
- Mehta, P.K., and Gjorv, O.E., (1982) "Properties of Portland cement concrete containing fly ash and condensed silica fume". *Cement and Concrete Research.* Ol. 12, pp. 587-595.
- Miller, M, Bobko, C, Vandamme, M, and Ulm, F-J., (2008) "Surface roughness criteria for cement paste nanoindentation". *Cement and Concrete Research*, Vol. 38. Pp. 467-476.
- Mindess, S., Young, J.F. and Darwin, D., (2003). *"Concrete"*, 2nd edition, Prentice Hall, Upper Saddle River, U.S.
- Mondal, P, Surendra, S. Marks, L, and Gaitero, J., (2010) "Comparative study of the effect of microsilica and nanosilica in concrete". *Transportation*

Research Record: Journal of the Transportation Research Board, No. 2141, pp. 6-9.

- Mondal, P., (2008) "Nanomechanical properties of cementitious materials". Phd thesis, Northwestern University.
- Morsy, M.S, Alsayed, S.H, and Aqel, M., (2010) "Effect of nano-clay on mechanical properties and microstructure of ordinary Portland cement mortar". *International Journal of Civil and Environmental Engineering,* Vol.10, No.01.
- Murali, G, Vasanth, R, Balasubramaniam, A.M, and Karikalan, E., (2012) "Experimental study on compressive strength of high volume fly ash concrete". *International Journal of Emerging trends in Engineering and Development,* Issue, Vol. 4, ISSN 2249-6149.
- Musa, N.M., (2014) "Thermal analysis of cement paste partially replaced with Neem Seed Husk Ash". *International Journal of Scientific and Engineering Research,* Vol. 5, ISSN 2229-5518.
- Naik, T.R., Singh, S.S. and Hossain, M.M., (1994) "Permeability of concrete containing large amounts of fly ash". *Cement and Concrete Research* 24 (5): 913–922.
- Němeček, J. (2009). Creep effects in nanoindentation of hydrated phases of cement pastes, Materials Characterization 60 (9), pp. 1028–1034.
- Newman, J, and Choo, B, S., (2003) *"Advanced concrete technology – constituent materials"*, Elsevier, Ltd, ISBN: 0750651032.
- Nik, A.S, Bahari, A, Nik, A.S., (2011) "Investigation of nano structural properties of cement-based materials". *American Journal of Scientific Research,* Vol. 25, pp, 104-111.
- Nili, M., Ehsani, A., and Shabani, K., (2010) "Influence of nano-SiO_2 and microsilica on concrete performance". *Second international conference on sustainable construction materials and technologies,* June 28-30, 2010, Italy.
- Nochaiya, T, Wongkeo, W, Chaipanich, A., (2010) "Utilization of fly ash with silica fume and properties of Portland cement-fly ash-silica fume concrete". *Fuel*. Vol. 89(3), pp.768-774.

- Oliver, W.C, and Pharr, G.M., (2003) “Measurement of hardness and elastic modulus by instrumented indentation: Advances in understanding and refinement to methodology”. *Journal of Materials Research,* Vol. 19, No.1.
- Page C.L, and Page, M.M., (2007) “Durability of concrete and cement composites”. Woodhead Publishing Limited, Cambridge England.
- Pera, J., Husson, S., and Guilhot, B., (1999) “Influence of finely ground limestone on cement hydration”. *Cement and Concrete Composites,* 21, 99-105.
- Poon, J., and Wong, L.Y.L., (2000). A studi pn high strength concrete prepared with large volumes of low calcium fly ash. *Cement and Concrete Research,* Vol. 30, pp. 447-455.
- Popovics, S. (1992). *“Concrete materials – properties, specifications and testing”*, Second edition, Noyes publications, USA. ISBN: 0-8155-1308-9.
- Poulsen. E, and Mejlbro, L., (2006). “Diffusion of chloride in concrete – Theory and application”. Modern concrete technology 14, Taylor and Francis, USA.
- Prasad, J, Jain, D.K., and Ahuja, A.K., (2006) “Factors influencing the sulphate resistance of cement concrete and mortar”. *Asian Journal of Civil Engineering (Building and Housing),* Vol. 7, No.3, pp. 259-268.
- Qing, Y, Zenan, Z, Deyu, K, and Rongshen, C., (2007) “Influence of nano-SiO_2 addition on properties of hardened cement paste as compared with silica fume. *Construction and Building Materials*, Vol. 21. Pp. 539-545.
- Quercia, G, Huske, G, and Brouwers, H.J.H., (2012) “Water demand of amorphous nano silica and its impact on the workability of cement paste”. *Cement and Concrete Research,* Vol, 42, pp. 344-357.
- Rahman, I.A, and Padabettan, V., (2012) “Synthesis of silica nanoparticles by sol-gel: size-dependent properties, surface modification, and applications in silica-polymer nanocomposites - A review”. *Journal of nanomaterials,* Article ID 132424, doi:10.1155/2012/132424.
- Ramachandran, V.S., (1995) “*Concrete admixtures handbook – Properties, science, and technology”*, Second edition, Noyes publications, ISBN: 0815513739.

- Robertson, B., (2013) “Preliminary chemical shrinkage analysis of nano slica cementitious binders”. *Materials Engineering and Research Laboratory Research Report*, No. MERL-2013-53.
- Russel, H.G., (2002) “Mineral admixtures for high performance concrete”, *Concrete Products*, Penton Media, Inc., April.
- Sadrmomtazi, A, and Fasihi, A., (2011) “The role of nano-SiO_2 in the mechanical properties of RHA composite cement mortars”. *Nanotechnology and Nanoscience.* Vol.2, pp. 42-45.
- Said, A.M, Zeidan, M.S, Bassuoni, M.T and Tian, Y., (2012) “Properties of concrete incorporating nano-silica”. *Construction and Building Materials*, Vo. 36, pp. 838-844.
- Sanchez, F, and Sobolev, K., (2010) “Nanotechnology in concrete – A review”. *Construction and Building Materials*, Vol. 24, pp. 2060-2071.
- Saraswathy, V., and Song, H., (2006) “Corrosion performance of fly ash blended cement concrete”. *Corrosion Reviews*, Vol. 24, Issue.1-2.
- Sarath, C.K., and Saha, P., (2011). “Contribution of fly ash to the properties of mortar and concrete”. *International Journal of Earth Sciences and Engineering*. ISSN: 0974-5904, Vol.04, No 06 SPL, October 2011, pp 1017-1023.
- Sato, T. and Beaudoin, J.J., (2011) “Effect of nano-$CaCO_3$ on hydration of cement containing supplementary cementitious materials”, *Advances in Cement Research*, Vol.23, pp. 33-43.
- Sato, T. and Diallo, F., (2010) “Seeding effect of nano-$CaCO_3$ on the hydration of tricalcium silicate”, *Journal of the Transportation Research Board*, No.2141, pp.61-67.
- Schuh, C.A., (2006) “Nanoindentation studies of materials” *Materialstoday*, Vol. 9, pp. 32-40.
- Scrivener, K.L., (2004) “Blackscattered electron imaging of cementitious microstructures: understanding and quantification”. *Cement and Concrete Composites*. 26, 935-945.
- Senff, L, Hotza, D, Repette, W.L, Ferreira, V.M, Labrincha, J.A., (2010) “Mortars with nano-SiO2 and micro-SiO2 investigated by experimental design’’. *Construction Building Materials*, Vol. 24(8), pp. 1432–1437

- Shah, S.P, Konsta-Gdoutuos, M.S, Metaxa, Z.S, and Modal, P., (2009) "Nanoscale modification of cementitious materials". *Nanotechnology in Construction 3,* pp. 125-130.
- Shetty, M.S., (1982) *"Concrete technology – theory and practice"*. S. Chand & Company LTD, New Delhi. ISBN: 81-219-0003-4.
- Shi, C, and Shao, Y., (2002) "What is the most efficient way to activate the reactivity of fly ashes". *2nd Material Specialty Conference of the Canadian Society for Civil Engineering,* June 5-8, 2002.
- Shi, X, Yang, Z, Liu, Y, and Cross, D., (2011) "Strength and corrosion properties of Portland cement mortar and concrete mineral admixtures". *Construction and Building Materials.* Vol. 25. pp. 3245-3256.
- Shrivastava, Y, and Bajaj, K., (2012) "Performance of fly ash and high volume fly ash concrete in pavement design". *IACSIT Coimbatore Conferences,* Vol. 28, Singapore.
- Siddique, R, and Khan, M.I., (2011) "Supplementary cementitious materials". *Engineering Materials,* Springer-Verlag, Berlin Heidelberg, DOI: 10.1007/978-3-642-17866-5_2.
- Siddique, R., (2004) "Performance characteristics of high-volume Class F fly ash concrete". *Cement and Concrete Research,* 34(3): 487-493.
- Singh, L.P, Bhattacharyya, S.K, and Ahalawat. S., (2012) "Preparation of size controlled silica nano particles and its functional role in cementitious system". *Journal of Advanced Concrete Technology,* Vol.10, pp. 345-352.
- Sobolev, K., Flores, I., Hermosillo, R., and Torres-Martines, L., (2006) "Nanomaterials and nanotechnology for high performance cement composites". *Proceedings of ACI Session on "Nanotechnology of concrete: Recent developments and future perspectives"*, November 7, 2006, USA.
- Soman, M, and Sobha, K., (2014) "Strength and behaviour of high volume fly ash concrete". *International Journal of Innovative Research in Science, Engineering and Technology,* Vol. 3, Issue 5, ISN: 2319-8753.
- Song, G, and Shayan.A., (1998) "Corrosion of steel in concrete: causes, detection and prediction". ARRB Transport research Ltd, Review report 4, July 1998.

- Soni, D.K, and Saini, J., (2014) “Mechanical properties of high volume fly ash and concrete subjected to evaluated 120°C temperature”. *International Journal of Civil Engineering Research*, Vol. 5, pp.241-248, ISSN: 2278-3652.
- Sorelli, L, Constantinides, G, Ulm, F.-J, and Toutlemonde, F., (2008) “The nano-mechanical signature of ultra-high performance concrete by statistical nanoindentation techniques”. *Cement and Concrete Research,* Vol. 38, pp. 1447-1456.
- Stefanidou, M, and Papayianni, I., (2012) “Influence of nano-SiO_2 on the Portland cement pastes”. *Composites: Part B*, Vol. 43, pp. 2706-2710.
- Stultzman, P., (2004) “Scanning electron microscopy imaging of hydraulic cement microstructure”, *Cement and Concrete Composites*, Vol. 26, No.8, 957-966.
- Tahir, M.A., and Sabir, M., (2005) “A study on durability of fly ash-cement mortars”, *30th conference on “Our world in concrete and structure”: 23-24 August 2005, Singapore*, article online Id: 100030019.
- Tanesi, J., Bentz, P.D., and Ardani, A., (2013) “Enhancing the performance of high volume fly ash concretes using fine limestone powder”. *National Institute of Standards and Technology Publications,* American Concrete Institute Spring Meeting.
- Taylor, H.F.W., (1990) “Cement chemistry”, *Academic Press Limited,* London.
- Thangaraj, R, and Thenmozhi, R., (2013) “Industrial and environmental application of high volume fly ash in concrete production”. *Nature Environment and Pollution Technology, An International Quarterly Scientific Journal*, Vol.12, No. 2, pp.315-320.
- Thomas M.D.A., M.H. Shehata, S.G. Shashiprakash, D.S. Hopkins, K. Cail., (1999) “Use of ternary cementitious systems containing silica fume and fly ash in concrete”. *Cement and Concrete research*, 29:1207-1214.
- Vandamme, M, and Ulm, F.-J., (2009). “Nanogranular origin of concrete creep”. *Proceeding of the National Academy of Sciences,* Vol. 106, pp. 10552-10557.

- Venkataraman, M., (2002) “The effect of colloidal stability on the heat transfer characteristics of nano silica dispersed fluids”. MSc thesis. Departement of Mechanical, Materials and Aerospace Engineering, University of Central Florida.
- Weng, J.K, Langan, B.W and Ward, M.A., (1997) “Pozzolanic reaction in Portland cement, silica fume and fly ash mixtures”. *Civil Engineering*, Vol. 24, pp. 754-760.
- Wesche., K., (1991) “Fly ash in concrete properties and performance”. *Report of technical committee 67-FAB use of fly ash in building.* ISBN: 0 419 15790.
- Winslow, D. and Diamond, S. A., (1969) “Mercury porosimetry study of the evolution of porosity in Portland cement: technical publication”. *Joint transportation research program,* Doi:10.5703/1288284314510.
- Xu, Q., Meng, T., and Huang, M., (2012) “Effect on nano-$CaCO_3$ on the compressive strength and microstructure of high strength concrete in different curing temperature”. *Applied Mechanics and Materials*, Vol. 121-126, pp.126-131.
- Zhang, M.H. and Islam, J., (2012) “Use of nano-silica to reduce setting time and increase early strength of concretes with high volume fly ash or slag”. *Construction and Building Materials*, Vol. 29, pp.573-580.
- Zhao, H. and Darwin, D., (1992) “Quantitative backscattered electron analysis of cement paste”. *Cement and Concrete Research.* 22, 695-706.
- Zhu, W, Bartos, P.J.M, and Porro, A., (2004) “Application of nanotechnology in construction”. *RILEM 197-NCM: Nanotechnology in construction materials,* Vol. 37, pp. 649-658.

“Every reasonable effort has been made to acknowledge the owners of copyright material. I would be pleased to hear from any copyright owner who has been omitted or incorrectly acknowledged”

APPENDIX A

Results of compressive strength and durability properties of concretes

A.1 Compressive strength results of different types of concrete mixtures at 3, 7, 28, 56 and 90 days

A.1.2 Compressive strength of cement concrete

Series	Specimen No.	Age (days)	Weight (gr)	Compressive strength (MPa)	Average strength (MPa)
PC	1	3	3728	13.26	12.73
	2		3739	12.16	
	3		3730	12.76	
	4	7	3731	17.80	17.14
	5		3732	17.49	
	6		3795	16.12	
	7	28	3803	28.18	28.85
	8		3788	29.22	
	9		3742	29.14	
	10	56	3768	35.63	36.90
	11		3776	36.75	
	12		3733	38.31	
	13	90	3829	37.50	37.60
	14		3872	38.44	
	15		3814	36.85	

A.1.3 Compressive strength of cement concrete containing 40% fly ash

Series	Specimen No.	Age (days)	Weight (gr)	Compressive strength (MPa)	Average strength (MPa)
FA40	1	3	3783	13.14	13.40
	2		3744	13.70	
	3		3724	13.35	
	4	7	3815	17.23	17.97
	5		3850	18.04	
	6		3781	18.65	
	7	28	3843	27.06	26.24
	8		3790	25.57	
	9		3833	26.10	
	10	56	3777	33.23	31.81
	11		3822	31.63	
	12		3875	30.57	
	13	90	3824	33.06	33.29
	14		3848	34.02	
	15		3852	32.78	

A.1.4 Compressive strength of concrete containing 60% fly ash

Series	Specimen No.	Age (days)	Weight (gr)	Compressive strength (MPa)	Average strength (MPa)
FA60	1	3	3783	4.86	3.93
	2		3667	2.94	
	3		3747	3.98	
	4	7	3865	13.25	13.95
	5		3861	14.36	
	6		3841	14.25	
	7	28	3880	20.98	20.36
	8		3816	19.70	
	9		3834	20.40	
	10	56	3861	23.21	22.32
	11		3852	21.47	
	12		3825	22.27	
	13	90	3817	23.24	24.39
	14		3816	25.81	
	15		3813	24.13	

A.1.5 Compressive strength of cement concrete containing 2% nano silica

Series	Specimen No.	Age (days)	Weight (gr)	Compressive strength (MPa)	Average strength (MPa)
NS2	1	3	3793	28.21	31.35
	2		3848	30.69	
	3		3859	29.17	
	4	7	3866	30.52	43.58
	5		3839	33.33	
	6		3873	30.21	
	7	28	3816	45.09	52.25
	8		3840	43.61	
	9		3868	42.04	
	10	56	3861	53.36	53.09
	11		3835	52.05	
	12		3826	51.35	
	13	90	3903	53.92	54.40
	14		3882	51.25	
	15		3872	54.10	

A.1.6 Compressive strength of cement concrete containing 4% nano silica

Series	Specimen No.	Age (days)	Weight (gr)	Compressive strength (MPa)	Average strength (MPa)
NS4	1	3	3771	38.28	36.98
	2		3793	33.21	
	3		3819	39.44	
	4	7	3815	45.63	45.04
	5		3759	43.31	
	6		3801	46.19	
	7	28	3822	50.76	51.20
	8		3816	50.93	
	9		3839	51.92	
	10	56	3764	54.88	54.44
	11		3772	54.25	
	12		3821	54.19	
	13	90	3825	55.54	54.89
	14		3793	54.77	
	15		3783	54.35	

A.1.7 Compressive strength of cement concrete containing 1% nano-$CaCO_3$

Series	Specimen No.	Age (days)	Weight (gr)	Compressive strength (MPa)	Average strength (MPa)
NC1	1	3	3745	33.75	32.30
	2		3836	32.43	
	3		3775	30.73	
	4	7	3820	42.94	40.71
	5		3775	39.85	
	6		3802	39.35	
	7	28	3820	44.09	46.51
	8		3849	48.83	
	9		3843	46.61	
	10	56	3844	51.16	51.76
	11		3835	50.18	
	12		3841	53.93	
	13	90	3775	51.13	52.84
	14		3800	53.25	
	15		3802	54.15	

A.1.7 Compressive strength of cement concrete containing 2% nano-$CaCO_3$

Series	Specimen No.	Age (days)	Weight (gr)	Compressive strength (MPa)	Average strength (MPa)
NC2	1	3	3624	22.40	22.09
	2		3635	21.69	
	3		3652	22.18	
	4	7	3628	26.30	25.14
	5		3606	24.32	
	6		3632	25.06	
	7	28	3747	30.14	31.30
	8		3673	32.27	
	9		3669	31.50	
	10	56	3658	39.25	38.87
	11		3685	39.71	
	12		3645	37.65	
	13	90	3674	42.35	44.20
	14		3681	45.57	
	15		3667	44.67	

A.1.8 Compressive strength of fly ash concrete containing 38% fly ash and 2% nano silica

Series	Specimen No.	Age (days)	Weight (gr)	Compressive strength (MPa)	Average strength (MPa)
FA38.NS2	1	3	3737	16.27	16.79
	2		3807	16.41	
	3		3757	17.68	
	4	7	3791	21.64	20.76
	5		3808	20.44	
	6		3832	20.19	
	7	28	3820	32.32	32.10
	8		3865	31.31	
	9		3824	32.66	
	10	56	3825	37.83	36.90
	11		3860	35.72	
	12		3820	37.15	
	13	90	3838	37.47	37.34
	14		3788	36.98	
	15		3813	37.58	

A.1.9 Compressive strength of fly ash concrete containing 58% fly ash and 2% nano silica

Series	Specimen No.	Age (days)	Weight (gr)	Compressive strength (MPa)	Average strength (MPa)
FA58.NS2	1	3	3776	7.93	7.75
	2		3840	8.19	
	3		3767	7.14	
	4	7	3717	13.39	13.57
	5		3742	13.52	
	6		3688	13.80	
	7	28	3766	20.73	20.03
	8		3724	19.74	
	9		3763	19.61	
	10	56	3814	22.03	22.57
	11		3737	23.41	
	12		3797	22.28	
	13	90	3754	24.09	24.06
	14		3751	22.35	
	15		3672	25.75	

A.1.10 Compressive strength of fly ash concrete containing 39% fly ash and 1% nano-$CaCO_3$

Series	Specimen No.	Age (days)	Weight (gr)	Compressive strength (MPa)	Average strength (MPa)
FA39.NC1	1	3	3810	16.27	18.80
	2		3871	16.41	
	3		3844	17.68	
	4	7	3833	20.44	25.62
	5		3824	21.64	
	6		3842	20.19	
	7	28	3901	32.32	39.64
	8		3846	31.31	
	9		3816	32.66	
	10	56	3882	37.83	45.01
	11		3826	35.72	
	12		3852	37.15	
	13	90	3865	37.47	51.76
	14		3835	36.98	
	15		3884	37.58	

A.1.11 Compressive strength of fly ash concrete containing 59% fly ash and 1% nano-$CaCO_3$

Series	Specimen No.	Age (days)	Weight (gr)	Compressive strength (MPa)	Average strength (MPa)
FA59.NC1	1	3	3788	5.29	5.06
	2		3815	4.91	
	3		3790	4.97	
	4	7	3799	13.97	13.64
	5		3770	13.18	
	6		3818	13.76	
	7	28	3775	23.55	23.17
	8		3794	22.48	
	9		3816	23.48	
	10	56	3814	24.25	24.05
	11		3778	23.89	
	12		3732	24.01	
	13	90	3712	25.10	26.25
	14		3798	27.77	
	15		3723	25.89	

A.2. Rate of water absorption of different types of concretes at 28 and 90 days

A.2.1 Rate of water absorption of cement concrete at 28 days

Test time		Mass (gr)		Δ Mass (gr)		I (mm)		Average I
s	s^1/2	1	2	1	2	I1	I2	
0	0	1073.28	1102.51	0.00	0.00	0.0000	0.0000	0.0000
60	8	1074.06	1102.62	0.78	0.11	0.0962	0.0136	0.0549
300	17	1074.86	1103.30	1.58	0.79	0.1949	0.0974	0.1462
600	24	1075.67	1103.64	2.39	1.13	0.2948	0.1394	0.2171
1200	35	1076.36	1104.34	3.08	1.83	0.3799	0.2257	0.3028
1800	42	1077.20	1104.75	3.92	2.24	0.4835	0.2763	0.3799
3600	60	1078.01	1105.76	4.73	3.25	0.5834	0.4009	0.4922
7200	85	1079.38	1106.46	6.10	3.95	0.7524	0.4872	0.6198
10800	104	1079.97	1107.70	6.69	5.19	0.8252	0.6402	0.7327
14400	120	1080.93	1108.29	7.65	5.78	0.9436	0.7130	0.8283
18000	134	1081.37	1108.69	8.09	6.18	0.9979	0.7623	0.8801
21600	147	1082.07	1109.19	8.79	6.68	1.0842	0.8240	0.9541

A.2.2 Rate of water absorption of cement concrete at 90 days

Test time		Mass (gr)		Δ Mass (gr)		I (mm)		Average I
s	s^1/2	1	2	1	2	I1	I2	
0	0	1163.78	1137.40	0.00	0.00	0.0000	0.0000	0.0000
60	8	1164.66	1138.4	0.88	1.00	0.1085	0.1234	0.1159
300	17	1164.98	1139.07	1.20	1.67	0.1480	0.2060	0.1770
600	24	1165.25	1139.73	1.47	2.33	0.1813	0.2874	0.2344
1200	35	1165.98	1139.85	2.20	2.45	0.2714	0.3022	0.2868
1800	42	1166.1	1140.02	2.32	2.62	0.2862	0.3232	0.3047
3600	60	1166.77	1140.75	2.99	3.35	0.3688	0.4132	0.3910
7200	85	1167.45	1141.45	3.67	4.05	0.4527	0.4996	0.4761
10800	104	1167.84	1141.87	4.06	4.47	0.5008	0.5514	0.5261
14400	120	1168.17	1142.2	4.39	4.80	0.5415	0.5921	0.5668
18000	134	1168.35	1142.65	4.57	5.25	0.5637	0.6476	0.6056
21600	147	1168.54	1142.75	4.76	5.35	0.5871	0.6599	0.6235

A.2.3 Rate of water absorption of FA 40 concrete at 28 days

Test time		Mass (gr)		Δ Mass (gr)		I (mm)		Average I
s	s^1/2	1	2	1	2	I1	I2	
0	0	1036.75	1054.24	0.00	0.00	0.0000	0.0000	0.0000
60	8	1037.97	1055.29	1.22	1.05	0.1505	0.1295	0.1400
300	17	1038.70	1055.86	1.95	1.62	0.2405	0.1998	0.2202
600	24	1039.44	1056.38	2.69	2.14	0.3318	0.2640	0.2979
1200	35	1040.00	1056.98	3.25	2.74	0.4009	0.3380	0.3694
1800	42	1040.68	1057.59	3.93	3.35	0.4848	0.4132	0.4490
3600	60	1041.17	1058.18	4.42	3.94	0.5452	0.4860	0.5156
7200	85	1041.25	1059.4	4.5	5.16	0.5551	0.6365	0.5958
10800	104	1042.39	1060.02	5.64	5.78	0.6957	0.7130	0.7043
14400	120	1043.22	1060.75	6.47	6.51	0.7981	0.8030	0.8005
18000	134	1043.62	1061.07	6.87	6.83	0.8474	0.8425	0.8449
21600	147	1044.03	1061.75	7.28	7.51	0.8980	0.9264	0.9810

A.2.4 Rate of water absorption of FA 40 concrete at 90 days

Test time		Mass (gr)		Δ Mass (gr)		I (mm)		Average I
s	s^1/2	1	2	1	2	I1	I2	
0	0	1101.35	1100.00	0.00	0.00	0.0000	0.0000	0.0000
60	8	1103.7	1101.35	2.35	1.35	0.2899	0.1665	0.2282
300	17	1104.19	1101.4	2.84	1.40	0.3503	0.1727	0.2615
600	24	1105.26	1101.88	3.91	1.88	0.4823	0.2319	0.3571
1200	35	1106.25	1102.1	4.90	2.10	0.6044	0.2590	0.4317
1800	42	1106.82	1102.37	5.47	2.37	0.6747	0.2923	0.4835
3600	60	1107.25	1103.42	5.90	3.42	0.7278	0.4219	0.5748
7200	85	1107.89	1104.15	6.54	4.15	0.8067	0.5119	0.6593
10800	104	1108.15	1105.25	6.80	5.25	0.8388	0.6476	0.7432
14400	120	1108.87	1106.15	7.52	6.15	0.9276	0.7586	0.8431
18000	134	1109.02	1106.87	7.67	6.87	0.9461	0.8474	0.8968
21600	147	1109.35	1107.12	8.00	7.12	0.9868	0.8783	0.9325

A.2.5 Rate of water absorption of FA 60 concrete at 28 days

Test time		Mass (gr)		Δ Mass (gr)		I (mm)		Average I
s	s^1/2	1	2	1	2	I1	I2	
0	0	1139.26	1136.62	0.00	0.00	0.0000	0.0000	0.0000
60	8	1140.28	1137.80	1.02	1.18	0.1258	0.1456	0.1357
300	17	1140.66	1138.23	1.4	1.61	0.1727	0.1986	0.1856
600	24	1141.45	1139.03	2.19	2.41	0.2701	0.2973	0.2837
1200	35	1142.01	1139.58	2.75	2.96	0.3392	0.3651	0.3522
1800	42	1142.53	1140.08	3.27	3.46	0.4034	0.4268	0.4151
3600	60	1143.76	1141.34	4.5	4.72	0.5551	0.5822	0.5686
7200	85	1145.23	1142.93	5.97	6.31	0.7364	0.7783	0.7574
10800	104	1146.62	1144.25	7.36	7.63	0.9079	0.9412	0.9245
14400	120	1147.6	1145.85	8.34	9.23	1.0287	1.1385	1.0836
18000	134	1148.31	1146.55	9.05	9.93	1.1163	1.2249	1.1706
21600	147	1148.98	1146.76	9.72	10.14	1.1990	1.2508	1.2566

A.2.6 Rate of water absorption of FA 60 concrete at 90 days

Test time		Mass (gr)		Δ Mass (gr)		I (mm)		Average I
s	s^1/2	1	2	1	2	I1	I2	
0	0	1073.36	1029.31	0.00	0.00	0.0000	0.0000	0.0000
60	8	1074.67	1030.53	1.31	1.22	0.1616	0.1505	0.1560
300	17	1075.60	1031.60	2.24	2.29	0.2763	0.2825	0.2794
600	24	1076.29	1032.31	2.93	3.00	0.3614	0.3701	0.3657
1200	35	1077.25	1033.04	3.89	3.73	0.4798	0.4601	0.4700
1800	42	1078.25	1033.65	4.89	4.34	0.6032	0.5353	0.5693
3600	60	1079.15	1035.46	5.79	6.15	0.7142	0.7586	0.7364
7200	85	1080.25	1036.72	6.89	7.41	0.8499	0.9140	0.8820
10800	104	1080.58	1037.80	7.22	8.49	0.8906	1.0472	0.9689
14400	120	1081.36	1038.88	8.00	9.57	0.9868	1.1805	1.0836
18000	134	1081.98	1039.74	8.62	10.43	1.0633	1.2865	1.1749
21600	147	1082.35	1040.07	8.99	10.76	1.1089	1.3272	1.2181

A.2.7 Rate of water absorption of NS2 concrete at 28 days

Test time		Mass (gr)		Δ Mass (gr)		I (mm)		Average I
s	s^1/2	1	2	1	2	I1	I2	
0	0	1092.95	1099.60	0.00	0.00	0.0000	0.0000	0.0000
60	8	1094.04	1100.35	1.09	0.75	0.1345	0.0925	0.1135
300	17	1094.50	1100.75	1.55	1.15	0.1912	0.1419	0.1665
600	24	1094.90	1101.11	1.95	1.51	0.2405	0.1863	0.2134
1200	35	1095.19	1101.38	2.24	1.78	0.2763	0.2196	0.2479
1800	42	1095.52	1101.68	2.57	2.08	0.3170	0.2566	0.2868
3600	60	1096.17	1102.39	3.22	2.79	0.3972	0.3441	0.3707
7200	85	1096.79	1103.04	3.84	3.44	0.4737	0.4243	0.4490
10800	104	1097.20	1103.43	4.25	3.83	0.5242	0.4724	0.4983
14400	120	1097.63	1103.85	4.68	4.25	0.5773	0.5242	0.5508
18000	134	1097.87	1104.16	4.92	4.56	0.6069	0.5625	0.5847
21600	147	1098.18	1104.52	5.23	4.92	0.6451	0.6069	0.6260

A.2.8 Rate of water absorption of NS2 concrete at 90 days

Test time		Mass (gr)		Δ Mass (gr)		I (mm)		Average I
s	s^1/2	1	2	1	2	I1	I2	
0	0	1111.29	1092.28	0.00	0.00	0.0000	0.0000	0.0000
60	8	1111.75	1092.92	0.46	0.64	0.0567	0.0789	0.0678
300	17	1112.12	1093.21	0.83	0.93	0.1024	0.1147	0.1085
600	24	1112.28	1093.36	0.99	1.08	0.1221	0.1332	0.1277
1200	35	1112.48	1093.57	1.19	1.29	0.1468	0.1591	0.1530
1800	42	1112.83	1093.89	1.54	1.61	0.1900	0.1986	0.1943
3600	60	1113.25	1094.46	1.96	2.18	0.2418	0.2689	0.2553
7200	85	1113.35	1094.59	2.06	2.31	0.2541	0.2849	0.2695
10800	104	1114.18	1095.35	2.89	3.07	0.3565	0.3787	0.3676
14400	120	1114.57	1095.75	3.28	3.47	0.4046	0.4280	0.4163
18000	134	1114.76	1095.98	3.47	3.70	0.4280	0.4564	0.4422
21600	147	1114.96	1096.13	3.67	3.85	0.4527	0.4749	0.4638

A.2.9 Rate of water absorption of NS4 concrete at 28 days

Test time		Mass (gr)		Δ Mass (gr)		I (mm)		Average I
s	s^1/2	1	2	1	2	I1	I2	
0	0	1098.2	1096.00	0.00	0.00	0.0000	0.0000	0.0000
60	8	1102.08	1097.82	3.88	1.82	0.4786	0.2245	0.3515
300	17	1102.40	1097.55	4.2	1.55	0.5181	0.1912	0.3546
600	24	1102.53	1098.0	4.33	2.00	0.5341	0.2467	0.3904
1200	35	1102.68	1098.4	4.48	2.40	0.5526	0.2960	0.4243
1800	42	1102.87	1098.56	4.67	2.56	0.5760	0.3158	0.4459
3600	60	1103.54	1099.03	5.34	3.03	0.6587	0.3738	0.5162
7200	85	1104.04	1099.61	5.84	3.61	0.7204	0.4453	0.5828
10800	104	1104.42	1099.99	6.22	3.99	0.7672	0.4922	0.6297
14400	120	1104.87	1100.21	6.67	4.21	0.8227	0.5193	0.6710
18000	134	1104.98	1100.38	6.78	4.38	0.8363	0.5403	0.6883
21600	147	1105.26	1100.51	7.06	4.51	0.8709	0.5563	0.7136

A.2.10 Rate of water absorption of NS4 concrete at 90 days

Test time		Mass (g)		Δ Mass (g)		I (mm)		Average I
s	s^1/2	1	2	1	2	I1	I2	
0	0	1051.85	1084.51	0.00	0.00	0.0000	0.0000	0.0000
60	8	1052.25	1084.81	0.40	0.30	0.0493	0.0370	0.0432
300	17	1052.80	1085.16	0.95	0.65	0.1172	0.0802	0.0987
600	24	1053.06	1085.22	1.21	0.71	0.1493	0.0876	0.1184
1200	35	1053.34	1085.39	1.49	0.88	0.1838	0.1085	0.1462
1800	42	1053.45	1085.55	1.60	1.04	0.1974	0.1283	0.1628
3600	60	1053.92	1085.84	2.07	1.33	0.2553	0.1641	0.2097
7200	85	1054.19	1086.21	2.34	1.70	0.2886	0.2097	0.2492
10800	104	1054.56	1086.42	2.71	1.91	0.3343	0.2356	0.2849
14400	120	1054.94	1086.60	3.09	2.09	0.3812	0.2578	0.3195
18000	134	1055.03	1086.72	3.18	2.21	0.3923	0.2726	0.3324
21600	147	1055.13	1086.81	3.28	2.30	0.4046	0.2837	0.3441

A.2.11 Rate of water absorption of NC1 concrete at 28 days

Test time		Mass (gr)		Δ Mass (gr)		I (mm)		Average I
s	s^1/2	1	2	1	2	I1	I2	
0	0	1118.2	1126.03	0.00	0.00	0.0000	0.0000	0.0000
60	8	1118.64	1126.61	0.44	0.58	0.0543	0.0715	0.0629
300	17	1119.46	1127.47	1.26	1.44	0.1554	0.1776	0.1665
600	24	1119.87	1127.96	1.67	1.93	0.2060	0.2381	0.2220
1200	35	1120.14	1128.21	1.94	2.18	0.2393	0.2689	0.2541
1800	42	1120.44	1128.6	2.24	2.57	0.2763	0.3170	0.2967
3600	60	1121.35	1129.67	3.15	3.64	0.3886	0.4490	0.4188
7200	85	1122.15	1130.17	3.95	4.14	0.4872	0.5107	0.4990
10800	104	1123.16	1131.73	4.96	5.70	0.6118	0.7031	0.6575
14400	120	1123.67	1132.23	5.47	6.20	0.6747	0.7648	0.7197
18000	134	1123.92	1132.74	5.72	6.71	0.7056	0.8277	0.7666
21600	147	1124.01	1132.91	5.81	6.88	0.7167	0.8486	0.7827

A.2.12 Rate of water absorption of NC1 concrete at 90 days

Test time		Mass (g)		Δ Mass (g)		I (mm)		Average I
s	s^1/2	1	2	1	2	I1	I2	
0	0	1120.87	1123.25	0.00	0.00	0.0000	0.0000	0.0000
60	8	1121.78	1124.01	0.91	0.76	0.1122	0.0937	0.1030
300	17	1121.87	1124.65	1.00	1.40	0.1234	0.1727	0.1480
600	24	1122.35	1124.98	1.48	1.73	0.1826	0.2134	0.1980
1200	35	1122.68	1125.01	1.81	1.76	0.2233	0.2171	0.2202
1800	42	1122.87	1125.24	2.00	1.99	0.2467	0.2455	0.2461
3600	60	1122.94	1125.84	2.07	2.59	0.2553	0.3195	0.2874
7200	85	1123.35	1126.07	2.48	2.82	0.3059	0.3478	0.3269
10800	104	1123.97	1126.34	3.10	3.09	0.3824	0.3812	0.3818
14400	120	1124.01	1127.02	3.14	3.77	0.3873	0.4650	0.4262
18000	134	1124.35	1127.12	3.48	3.87	0.4293	0.4774	0.4533
21600	147	1124.47	1127.35	3.60	4.10	0.4441	0.5057	0.4749

A.2.13 Rate of water absorption of NC2 concrete at 28 days

Test time		Mass (gr)		Δ Mass (gr)		I (mm)		Average I
s	s^1/2	1	2	1	2	I1	I2	
0	0	1035.94	1044.67	0.00	0.00	0.0000	0.0000	0.0000
60	8	1038.12	1046.87	2.18	2.20	0.2689	0.2714	0.2701
300	17	1038.95	1047.42	3.01	2.75	0.3713	0.3392	0.3552
600	24	1039.64	1048.05	3.70	3.38	0.4564	0.4169	0.4367
1200	35	1040.38	1048.76	4.44	4.09	0.5477	0.5045	0.5261
1800	42	1040.87	1049.35	4.93	4.68	0.6081	0.5773	0.5927
3600	60	1041.68	1050.15	5.74	5.48	0.7080	0.6760	0.6920
7200	85	1042.54	1051.25	6.60	6.58	0.8141	0.8116	0.8129
10800	104	1043.25	1052.31	7.31	7.64	0.9017	0.9424	0.9220
14400	120	1043.87	1052.58	7.93	7.91	0.9782	0.9757	0.9769
18000	134	1044.01	1054.25	8.07	9.58	0.9954	1.1817	1.0886
21600	147	1044.25	1054.65	8.31	9.98	1.0250	1.2310	1.1280

A.2.14 Rate of water absorption of NC2 concrete at 90 days

Test time		Mass (g)		Δ Mass (g)		I (mm)		Average I
s	s^1/2	1	2	1	2	I1	I2	
0	0	1041.25	1037.56	0.00	0.00	0.0000	0.0000	0.0000
60	8	1041.65	1037.85	0.40	0.29	0.0493	0.0358	0.0426
300	17	1042.35	1038.56	1.10	1.00	0.1357	0.1234	0.1295
600	24	1042.87	1038.74	1.62	1.18	0.1998	0.1456	0.1727
1200	35	1042.98	1038.97	1.73	1.41	0.2134	0.1739	0.1937
1800	42	1043.15	1039.25	1.90	1.69	0.2344	0.2085	0.2214
3600	60	1043.67	1040.12	2.42	2.56	0.2985	0.3158	0.3071
7200	85	1043.87	1040.87	2.62	3.31	0.3232	0.4083	0.3657
10800	104	1044.56	1041.25	3.31	3.69	0.4083	0.4552	0.4317
14400	120	1045.25	1041.88	4.00	4.32	0.4934	0.5329	0.5131
18000	134	1045.45	1042.25	4.20	4.69	0.5181	0.5785	0.5483
21600	147	1045.59	1042.35	4.34	4.79	0.5353	0.5908	0.5631

A.2.15 Rate of water absorption of FA38.NS2 concrete at 28 days

Test time		Mass (g)		Δ Mass (g)		I (mm)		Average I
s	s^1/2	1	2	1	2	I1	I2	
0	0	1092.00	1080.00	0.00	0.00	0.0000	0.0000	0.0000
60	8	1093.24	1082.50	1.24	2.5	0.1530	0.3084	0.2307
300	17	1093.95	1082.56	1.95	2.56	0.2405	0.3158	0.2782
600	24	1093.46	1082.7	1.46	2.69	0.1801	0.3318	0.2560
1200	35	1093.88	1083.09	1.88	3.09	0.2319	0.3812	0.3065
1800	42	1094.06	1083.24	2.06	3.24	0.2541	0.3997	0.3269
3600	60	1094.83	1084.19	2.83	4.19	0.3491	0.5168	0.4330
7200	85	1095.54	1084.97	3.54	4.97	0.4367	0.6131	0.5249
10800	104	1095.95	1085.88	3.95	5.88	0.4872	0.7253	0.6063
14400	120	1096.34	1086.22	4.34	6.22	0.5353	0.7672	0.6513
18000	134	1096.67	1086.22	4.67	6.22	0.5760	0.7672	0.6716
21600	147	1097.47	1087.01	5.47	7.01	0.6747	0.8647	0.7697

A.2.16 Rate of water absorption of FA38.NS2 concrete at 90 days

Test time		Mass (g)		Δ Mass (g)		I (mm)		Average I
s	s^1/2	1	2	1	2	I1	I2	
0	0	1140.02	1115.78	0.00	0.00	0.0000	0.0000	0.0000
60	8	1140.92	1117.43	0.90	1.65	0.1110	0.2035	0.1573
300	17	1141.41	1117.92	1.39	2.14	0.1715	0.2640	0.2177
600	24	1141.77	1118.31	1.75	2.53	0.2159	0.3121	0.2640
1200	35	1142.05	1118.79	2.03	3.01	0.2504	0.3713	0.3108
1800	42	1142.33	1119.16	2.31	3.38	0.2849	0.4169	0.3509
3600	60	1142.9	1119.93	2.88	4.15	0.3552	0.5119	0.4336
7200	85	1143.3	1120.62	3.28	4.84	0.4046	0.5970	0.5008
10800	104	1143.83	1120.92	3.81	5.14	0.4700	0.6340	0.5520
14400	120	1143.99	1121.25	3.97	5.47	0.4897	0.6747	0.5822
18000	134	1144.38	1121.36	4.36	5.58	0.5378	0.6883	0.6131
21600	147	1144.55	1121.86	4.53	6.08	0.5588	0.7500	0.6544

A.2.17 Rate of water absorption of FA58.NS2 concrete at 28 days

Test time		Mass (gr)		Δ Mass (gr)		I (mm)		Average I
s	s^1/2	1	2	1	2	I1	I2	
0	0	1069.00	1060.00	0.00	0.00	0.0000	0.0000	0.0000
60	8	1071.35	1062.35	2.35	2.35	0.2899	0.2899	0.2899
300	17	1072.52	1063.45	3.52	3.45	0.4342	0.4256	0.4299
600	24	1073.45	1064.25	4.45	4.25	0.5489	0.5242	0.5366
1200	35	1074.33	1065.27	5.33	5.27	0.6575	0.6501	0.6538
1800	42	1074.25	1066.38	5.25	6.38	0.6476	0.7870	0.7173
3600	60	1075.24	1067.25	6.24	7.25	0.7697	0.8943	0.8320
7200	85	1077.52	1068.25	8.52	8.25	1.0509	1.0176	1.0343
10800	104	1078.68	1069.15	9.68	9.15	1.1940	1.1287	1.1613
14400	120	1079.35	1069.85	10.35	9.85	1.2767	1.2150	1.2458
18000	134	1080.25	1070.35	11.25	10.35	1.3877	1.2767	1.3322
21600	147	1080.92	1070.68	11.92	10.68	1.4703	1.3174	1.3939

A.2.18 Rate of water absorption of FA58.NS2 concrete at 90 days

Test time		Mass (gr)		Δ Mass (gr)		I (mm)		Average I
s	s^1/2	1	2	1	2	I1	I2	
0	0	1054	1089.50	0.00	0.00	0.0000	0.0000	0.0000
60	8	1056.92	1092.07	2.92	2.57	0.3602	0.3170	0.3386
300	17	1057.43	1092.56	3.43	3.06	0.4231	0.3775	0.4003
600	24	1057.67	1092.9	3.67	3.39	0.4527	0.4182	0.4354
1200	35	1058.16	1093.35	4.16	3.85	0.5131	0.4749	0.4940
1800	42	1058.48	1093.56	4.48	4.06	0.5526	0.5008	0.5267
3600	60	1059.76	1094.83	5.76	5.33	0.7105	0.6575	0.6840
7200	85	1061.01	1096.04	7.01	6.54	0.8647	0.8067	0.8357
10800	104	1061.89	1096.67	7.89	7.17	0.9732	0.8844	0.9288
14400	120	1062.56	1097.2	8.56	7.70	1.0559	0.9498	1.0028
18000	134	1063.12	1097.65	9.12	8.15	1.1250	1.0053	1.0651
21600	147	1063.45	1097.96	9.45	8.46	1.1657	1.0435	1.1046

A.2.19 Rate of water absorption of FA39.NC1 concrete at 28 days

Test time		Mass (g)		Δ Mass (g)		I (mm)		Average I
s	s^1/2	1	2	1	2	I1	I2	
0	0	1135.81	1002.97	0.00	0.00	0.0000	0.0000	0.0000
60	8	1136.35	1003.6	0.54	0.63	0.0666	0.0777	0.0722
300	17	1137.18	1004.41	1.37	1.44	0.1690	0.1776	0.1733
600	24	1137.59	1004.81	1.78	1.84	0.2196	0.2270	0.2233
1200	35	1137.91	1005.11	2.10	2.14	0.2590	0.2640	0.2615
1800	42	1138.21	1005.42	2.40	2.45	0.2960	0.3022	0.2991
3600	60	1139.33	1006.53	3.52	3.56	0.4342	0.4391	0.4367
7200	85	1140.35	1007.35	4.54	4.38	0.5600	0.5403	0.5501
10800	104	1141.54	1007.68	5.73	4.71	0.7068	0.5810	0.6439
14400	120	1141.89	1008.23	6.08	5.26	0.7500	0.6488	0.6994
18000	134	1142.03	1009.11	6.22	6.14	0.7672	0.7574	0.7623
21600	147	1142.52	1009.45	6.71	6.48	0.8277	0.7993	0.8135

A.2.20 Rate of water absorption of FA39.NC1 concrete at 90 days

Test time		Mass (g)		Δ Mass (g)		I (mm)		Average I
s	s^1/2	1	2	1	2	I1	I1	
0	0	1128.12	1134.25	0.00	0.00	0.0000	0.0000	0.0000
60	8	1128.76	1134.97	0.64	0.72	0.0789	0.0888	0.0839
300	17	1128.96	1135.15	0.84	0.90	0.1036	0.1110	0.1073
600	24	1129.15	1135.97	1.03	1.72	0.1271	0.2122	0.1696
1200	35	1129.87	1136.35	1.75	2.10	0.2159	0.2590	0.2374
1800	42	1130.15	1136.87	2.03	2.62	0.2504	0.3232	0.2868
3600	60	1130.93	1137.46	2.81	3.21	0.3466	0.3960	0.3713
7200	85	1131.87	1137.98	3.75	3.73	0.4626	0.4601	0.4613
10800	104	1132.15	1138.57	4.03	4.32	0.4971	0.5329	0.5150
14400	120	1132.74	1139.04	4.62	4.79	0.5699	0.5908	0.5804
18000	134	1133.97	1139.15	5.85	4.90	0.7216	0.6044	0.6630
21600	147	1134.87	1139.75	6.75	5.50	0.8326	0.6784	0.7555

A.2.21 Rate of water absorption of FA59.NC1 concrete at 28 days

Test time		Mass (g)		Δ Mass (g)		I (mm)		Average I
s	s^1/2	1	2	1	2	I1	I2	
0	0	1090.06	1064.25	0.00	0.00	0.0000	0.0000	0.0000
60	8	1093.12	1066.25	3.06	2.00	0.3775	0.2467	0.3121
300	17	1094.02	1067.14	3.96	2.89	0.4885	0.3565	0.4225
600	24	1094.67	1068.35	4.61	4.10	0.5686	0.5057	0.5372
1200	35	1095.35	1069.56	5.29	5.31	0.6525	0.6550	0.6538
1800	42	1095.97	1070.35	5.91	6.10	0.7290	0.7524	0.7407
3600	60	1096.89	1071.56	6.83	7.31	0.8425	0.9017	0.8721
7200	85	1099.35	1072.35	9.29	8.10	1.1459	0.9991	1.0725
10800	104	1101.02	1073.35	10.96	9.10	1.3519	1.1225	1.2372
14400	120	1101.56	1074.86	11.50	10.61	1.4185	1.3087	1.3636
18000	134	1101.98	1075.15	11.92	10.90	1.4703	1.3445	1.4074
21600	147	1102.02	1075.89	11.96	11.64	1.4753	1.4358	1.4555

A.2.22 Rate of water absorption of FA59.NC1 concrete at 90 days

Test time		Mass (g)		Δ Mass (g)		I (mm)		Average I
s	s^1/2	1	2	1	2	I1	I1	
0	0	1172.53	1154.25	0.00	0.00	0.0000	0.0000	0.0000
60	8	1173.65	1155.87	1.12	1.62	0.1382	0.1998	0.1690
300	17	1174.85	1156.14	2.32	1.89	0.2862	0.2331	0.2597
600	24	1175.13	1156.89	2.60	2.64	0.3207	0.3256	0.3232
1200	35	1175.97	1157.64	3.44	3.39	0.4243	0.4182	0.4212
1800	42	1176.45	1158.12	3.92	3.87	0.4835	0.4774	0.4804
3600	60	1177.15	1158.96	4.62	4.71	0.5699	0.5810	0.5754
7200	85	1178.65	1159.43	6.12	5.18	0.7549	0.6390	0.6969
10800	104	1179.25	1160.1	6.72	5.85	0.8289	0.7216	0.7753
14400	120	1179.98	1160.84	7.45	6.59	0.9190	0.8129	0.8659
18000	134	1180.87	1161.35	8.34	7.10	1.0287	0.8758	0.9523
21600	147	1180.97	1161.87	8.44	7.62	1.0411	0.9399	0.9905

`

A.3 Volume of permeable voids of different types of concretes at 28 and 90 days

Mixes	Sample	Age (days)	Oven dry mass for 24 hrs (gr)	After immersion for 48 hrs (gr)	After boiling for 5 hrs (gr)	Mass in water (gr)	Absorption after immersion and boiling (%)	Volume of permeable pore space/voids (%)	Average VPV
			A	B	C	D	[(C-A)/A] x 100	[(C-A)/(C-D)] x 100	
PC	1	28	1051.19	1119.93	1120.60	672.35	6.60	15.48	15.4
	2	28	1067.31	1125.25	1142.15	654.60	7.01	15.35	
	1	90	1092.31	1155.33	1159.35	675.48	6.14	13.85	13.3
	2	90	1156.11	1210.54	1226.89	671.52	6.12	12.74	
FA40	1	28	988.44	1057.21	1038.78	538.52	5.09	10.06	13.3
	2	28	930.80	996.92	998.57	588.50	7.28	16.53	
	1	90	1031.51	1088.68	1091.44	610.25	5.81	12.45	12.8
	2	90	1028.35	1093.36	1090.25	620.12	6.02	13.17	
FA60	1	28	1039.22	1106.43	1107.11	647.91	6.53	14.78	14.9
	2	28	1022.14	1086.37	1089.01	641.69	6.54	14.95	
	1	90	1020.55	1060.95	1072.35	632.25	5.08	11.77	13.6
	2	90	1030.22	1089.40	1100.80	642.30	6.85	15.39	
NS2	1	28	1068.63	1133.75	1134.52	610.25	6.17	12.57	13.1
	2	28	1072.33	1136.45	1136.85	665.95	6.02	13.70	
	1	90	1068.25	1121.25	1121.89	658.35	5.02	11.57	11.0
	2	90	1071.32	1125.32	1125.68	600.25	5.07	10.35	
NS4	1	28	1069.40	1136.25	1136.45	634.52	6.27	13.36	13.5
	2	28	1069.86	1133.25	1133.85	664.79	5.98	13.64	
	1	90	1053.75	1102.35	1102.58	630.26	4.63	10.34	12.4
	2	90	1037.41	1108.25	1109.12	614.21	6.91	14.49	

A.3 Volume of permeable voids of different types of concretes at 28 and 90 days (cont'd)

Mixes	Sample	Age (days)	Oven dry mass for 24 hrs (gr)	After immersion for 48 hrs (gr)	After boiling for 5 hrs (gr)	Mass in water (gr)	Absorption after immersion and boiling (%)	Volume of permeable pore space/voids (%)	Average VPV
			A	B	C	D	[(C-A)/A] x 100	[(C-A)/(C-D)] x 100	
NC1	1	28	1104.48	1139.22	1141.07	684.63	3.31	8.02	8.3
	2	28	1095.37	1133.35	1134.73	672.72	3.59	8.52	
	1	90	1128.63	1145.41	1146.53	679.82	1.59	3.84	4.0
	2	90	1118.25	1136.42	1137.10	687.25	1.69	4.19	
NC2	1	28	1020.51	1076.29	1077.58	614.65	5.59	12.33	12.5
	2	28	997.49	1053.85	1054.88	600.20	5.75	12.62	
	1	90	1017.25	1062.25	1064.25	625.32	4.62	10.71	9.4
	2	90	1012.35	1043.35	1044.25	650.25	3.15	8.10	
FA38.NS2	1	28	1020.84	1055.26	1081.25	632.25	5.92	13.45	12.5
	2	28	1030.39	1052.35	1083.52	625.35	5.16	11.60	
	1	90	1045.25	1065.25	1102.32	640.57	5.46	12.36	12.0
	2	90	1055.04	1115.25	1110.25	639.25	5.23	11.72	
FA58.NS2	1	28	1032.25	1070.25	1103.89	610.13	6.94	14.51	14.8
	2	28	1024.25	1063.25	1090.25	652.21	6.44	15.07	
	1	90	1045.80	1087.35	1109.35	655.25	6.08	13.99	13.5
	2	90	1053.90	1092.35	1112.52	658.70	5.56	12.92	
FA39.NC1	1	28	1104.85	1142.73	1143.14	681.16	3.47	8.29	8.7
	2	28	1114.81	1156.21	1157.62	692.85	3.84	9.21	
	1	90	1125.82	1155.35	1157.25	665.14	2.79	6.39	7.0
	2	90	1118.12	1156.35	1158.01	628.14	3.57	7.53	
FA59.NC1	1	28	1048.44	1113.85	1114.01	622.15	6.25	13.33	13.9
	3	28	1108.50	1189.65	1190.02	626.29	7.35	14.46	
	1	90	1054.52	1100.00	1100.21	651.09	4.33	10.17	11.1
	2	90	997.02	1050.57	1052.46	593.98	5.56	12.09	

A.4 Rapid chloride permeability results of different types of concretes at 28 and 90 days

Series	**Spec No.**	**Age** *(day)*	**Current (Amperes)** *Io*	*$2I_{30}$*	*$2I_{60}$*	*$2I_{90}$*	*$2I_{120}$*	*$2I_{150}$*	*$2I_{180}$*	*$2I_{210}$*	*$2I_{240}$*	*$2I_{270}$*	*$2I_{300}$*	*$2I_{330}$*	*I_{360}*	**Charge Passed** (Coulombs)	**Average** (Coulombs)	**Class according to ASTM C 1202**
PC	1	28	0.129	0.286	0.308	0.326	0.338	0.346	0.352	0.356	0.356	0.358	0.356	0.356	0.178	3641	3442.50	Moderate
	2	28	0.096	0.260	0.274	0.290	0.298	0.306	0.312	0.316	0.320	0.322	0.324	0.324	0.163	3245		
	1	90	0.074	0.172	0.220	0.242	0.258	0.282	0.296	0.312	0.322	0.334	0.340	0.344	0.172	3031	2916.45	Moderate
	2	90	0.053	0.220	0.240	0.250	0.260	0.266	0.272	0.276	0.280	0.282	0.284	0.286	0.144	2802		
FA40	1	28	0.137	0.336	0.368	0.394	0.414	0.426	0.436	0.442	0.450	0.456	0.462	0.468	0.236	4523	4995.90	High
	2	28	0.105	0.418	0.444	0.484	0.510	0.534	0.546	0.552	0.552	0.552	0.552	0.552	0.276	5469		
	1	90	0.115	0.240	0.252	0.272	0.288	0.318	0.342	0.366	0.384	0.408	0.418	0.422	0.212	3633	3559.05	Moderate
	2	90	0.118	0.242	0.250	0.264	0.278	0.298	0.316	0.338	0.362	0.390	0.400	0.410	0.206	3485		
FA60	1	28	0.156	0.386	0.452	0.512	0.554	0.606	0.660	0.686	0.720	0.758	0.772	0.800	0.404	6719	6075.90	High
	2	28	0.148	0.382	0.390	0.486	0.494	0.506	0.516	0.538	0.542	0.576	0.578	0.586	0.294	5432		
	1	90	0.122	0.316	0.354	0.396	0.432	0.452	0.488	0.506	0.522	0.536	0.542	0.546	0.274	4937	4937.40	High
	2	90	0.119	0.318	0.358	0.396	0.428	0.448	0.480	0.500	0.518	0.536	0.550	0.556	0.279	4937		

A.4 Rapid chloride permeability results of different types of concretes at 28 and 90 days (Cont'd)

Series	**Spec No.**	**Age** *(day)*	**Current (Amperes)** *Io*	$2I_{30}$	$2I_{60}$	$2I_{90}$	$2I_{120}$	$2I_{150}$	$2I_{180}$	$2I_{210}$	$2I_{240}$	$2I_{270}$	$2I_{300}$	$2I_{330}$	I_{360}	**Charge Passed** (Coulombs)	**Average** (Coulombs)	**Class according to ASTM C 1202**
NS2	1	28	0.081	0.180	0.188	0.192	0.194	0.202	0.216	0.218	0.226	0.232	0.234	0.238	0.121	2270	2497.05	Moderate
	2	28	0.087	0.198	0.216	0.232	0.244	0.254	0.264	0.270	0.276	0.280	0.282	0.282	0.142	2724		
	1	90	0.045	0.100	0.162	0.184	0.194	0.202	0.208	0.210	0.212	0.214	0.214	0.216	0.108	2042	2125.35	Moderate
	2	90	0.076	0.170	0.182	0.192	0.200	0.208	0.212	0.216	0.220	0.220	0.222	0.224	0.112	2209		
NS4	1	28	0.063	0.130	0.146	0.164	0.172	0.178	0.190	0.192	0.198	0.206	0.210	0.214	0.108	1954	1999.35	Low
	2	28	0.073	0.146	0.156	0.166	0.174	0.184	0.186	0.196	0.210	0.216	0.222	0.228	0.115	2045		
	1	90	0.040	0.084	0.088	0.092	0.094	0.096	0.098	0.098	0.100	0.104	0.106	0.106	0.054	1044	992.70	Very Low
	2	90	0.036	0.078	0.080	0.082	0.084	0.086	0.088	0.090	0.092	0.092	0.094	0.096	0.048	941.40		
NC1	1	28	0.100	0.220	0.234	0.244	0.252	0.260	0.266	0.270	0.272	0.272	0.274	0.274	0.137	2768	2749.05	Moderate
	3	28	0.095	0.216	0.228	0.240	0.252	0.258	0.266	0.266	0.268	0.270	0.270	0.270	0.135	2731		
	1	90	0.040	0.084	0.118	0.124	0.136	0.140	0.150	0.158	0.124	0.130	0.138	0.140	0.070	1397	1475.10	Low
	2	90	0.056	0.116	0.120	0.124	0.128	0.138	0.144	0.150	0.156	0.162	0.170	0.174	0.088	1553		

A.4 Rapid chloride permeability results of different types of concretes at 28 and 90 days (Cont'd)

Series	Spec No.	Age (day)	Current (Amperes)													Charge Passed (Coulombs)	Average (Coulombs)	Class according to ASTM C 1202
			Io	$2I_{30}$	$2I_{60}$	$2I_{90}$	$2I_{120}$	$2I_{150}$	$2I_{180}$	$2I_{210}$	$2I_{240}$	$2I_{270}$	$2I_{300}$	$2I_{330}$	I_{360}			
NC2	1	28	0.900	0.204	0.216	0.226	0.238	0.246	0.254	0.260	0.266	0.270	0.274	0.276	0.138	3391	3413.25	Moderate
	2	28	0.850	0.200	0.214	0.232	0.244	0.256	0.264	0.272	0.280	0.284	0.286	0.290	0.145	3435		
	1	90	0.078	0.168	0.184	0.204	0.244	0.256	0.260	0.264	0.270	0.272	0.274	0.276	0.138	2599	2322.00	Moderate
	2	90	0.040	0.084	0.178	0.184	0.196	0.198	0.204	0.210	0.214	0.216	0.218	0.220	0.110	2045		
FA38.NS2	1	28	0.119	0.270	0.286	0.302	0.312	0.322	0.326	0.330	0.332	0.332	0.332	0.332	0.166	3385	3088.35	Moderate
	2	28	0.096	0.224	0.240	0.252	0.260	0.264	0.270	0.272	0.272	0.272	0.272	0.272	0.136	2792		
	1	90	0.074	0.162	0.178	0.186	0.192	0.202	0.206	0.208	0.212	0.214	0.218	0.220	0.110	2144	2465.55	Moderate
	2	90	0.09	0.20	0.23	0.24	0.25	0.26	0.27	0.27	0.28	0.28	0.28	0.28	0.14	2787		
FA58.NS2	1	28	0.139	0.358	0.396	0.440	0.490	0.540	0.590	0.638	0.684	0.708	0.720	0.732	0.368	6123	5592.15	High
	3	28	0.170	0.360	0.390	0.426	0.456	0.480	0.498	0.510	0.518	0.518	0.518	0.520	0.260	5062		
	1	90	0.115	0.260	0.286	0.302	0.320	0.334	0.354	0.370	0.394	0.406	0.422	0.424	0.214	3781	3920.40	Moderate
	2	90	0.118	0.256	0.284	0.308	0.334	0.360	0.390	0.414	0.440	0.450	0.460	0.464	0.233	4060		

A.4 Rapid chloride permeability results of different types of concretes at 28 and 90 days (Cont'd)

Series	Spec No.	Age (day)	Current (Amperes) Io	$2I_{30}$	$2I_{60}$	$2I_{90}$	$2I_{120}$	$2I_{150}$	$2I_{180}$	$2I_{210}$	$2I_{240}$	$2I_{270}$	$2I_{300}$	$2I_{330}$	I_{360}	Charge Passed (Coulombs)	Average (Coulombs)	Class according to ASTM C 1202
FA39.NC1	1	28	0.129	0.270	0.298	0.306	0.344	0.372	0.394	0.404	0.428	0.440	0.476	0.482	0.245	4129	4057.20	High
	2	28	0.118	0.260	0.278	0.286	0.304	0.312	0.394	0.416	0.430	0.460	0.464	0.470	0.236	3985		
	1	90	0.079	0.274	0.298	0.318	0.332	0.342	0.348	0.354	0.356	0.358	0.358	0.358	0.179	3559	3465.90	Moderate
	2	90	0.107	0.246	0.256	0.268	0.274	0.298	0.316	0.332	0.342	0.370	0.372	0.378	0.189	3373		
FA59.NC1	1	28	0.177	0.370	0.384	0.410	0.430	0.464	0.574	0.610	0.634	0.638	0.638	0.638	0.319	5657	5360.40	High
	2	28	0.170	0.360	0.390	0.426	0.456	0.480	0.498	0.510	0.518	0.518	0.520	0.520	0.260	5063		
	1	90	0.117	0.266	0.296	0.308	0.334	0.358	0.376	0.392	0.422	0.450	0.472	0.498	0.252	4087	4556.25	High
	3	90	0.165	0.356	0.364	0.396	0.406	0.446	0.486	0.504	0.542	0.546	0.548	0.550	0.275	5026		

A.5 Chloride content of different types of concretes after 60 days exposure

Depth (mm)	Chloride content (mass %)										
	PC	**FA40**	**FA60**	**NS2**	**NS4**	**NC1**	**NC2**	**FA38.NS2**	**FA58.NS2**	**FA39.NC1**	**FA59.NC1**
1	0.1150	0.1152	0.1066	0.1070	0.1117	0.1237	0.1190	0.1184	0.1120	0.1088	0.1051
2	0.1052	0.1055	0.0984	0.0976	0.1011	0.1122	0.1124	0.1074	0.1029	0.0982	0.0965
3	0.0958	0.0964	0.0907	0.0886	0.0911	0.1012	0.1060	0.0972	0.0944	0.0882	0.0884
5	0.0792	0.0807	0.0772	0.0730	0.0735	0.0822	0.0939	0.0802	0.0797	0.0715	0.0741
7	0.0659	0.0690	0.0668	0.0609	0.0598	0.0676	0.0832	0.0686	0.0690	0.0595	0.0630
9	0.0564	0.0614	0.0597	0.0526	0.0502	0.0576	0.0743	0.0618	0.0621	0.0520	0.0553
12	0.0479	0.0556	0.0539	0.0457	0.0421	0.0495	0.0641	0.0575	0.0569	0.0468	0.0488
16	0.0436	0.0534	0.0513	0.0426	0.0383	0.0460	0.0562	0.0563	0.0550	0.0450	0.0459